David A. Egger

Exploring the Interactions at Metal-Organic Interfaces with Density-Functional Theory

Doctoral Thesis

For obtaining the academic degree of
Doktor der Naturwissenschaften

Doctoral Programme of Natural Sciences
Technical Physics

Graz University of Technology

Supervisor:
Ao.Univ.-Prof. Dipl.-Ing. Dr.techn. Egbert Zojer
Institute of Solid State Physics

Graz, October 2013

Acknowledgments

I express my deepest gratitude to people and institutions who supported me during the 3+ years of my Ph.D., and without whom I could not have finished this work:

Austrian Academy of Sciences, Austrian Science Fund: For financially supporting my Ph.D. thesis.

Bureau of International Relations (TU Graz): For financially supporting my visits to foreign institutes.

ZID (TU Graz): For providing outstanding resources and support for the simulations.

Egbert: For truly excellent supervision, guidance and support throughout my thesis, including the chance to visit research institutes and conferences. Special thanks for having an open ear to any kind of topic and being the constant source of a good atmosphere in our group in Graz.

Georg: Thanks for taking care of me in Berlin, for a most joyful time in and outside the office and for being a friend.

Leeor: For having me twice in Rehovot, being the most caring host one could ever hope for and insight into DFT and middle-eastern culture.

Eli, Sivan, Ofer, Ariel, Ido, Anna, Shira, Baruch, Tobi: For having a good time in Israel during hikes, barbecues, beaches, drinks, food and, of course, during work.

Colin, Sergey, Jerome, Victor, Melanie, Luca: Thanks for introducing me to Belgian food & culture, and caring so much about keeping me busy outside the lab.

Ferdinand, Reini, Simon, Oliver, Stefan, Lukas, Martin, Piet: For being colleagues and friends at the same time, and for many memorable after-work beers! Special thanks to Ferdinand for great team work and insights into philosophy, to Reini for literally hundreds of coffees and Simon for analogies in physics.

Manuel, Iris, Berni, Lisi, Elsi, Gernot, Veronika: Thanks for the support while I was writing my thesis and for good spirit in our renewed group including the occasional Tuesday cooking session.

Fellow co-authors not mentioned in this list: For many interesting discussions, help and insight – it was a pleasure and honor to work with all of you!

Josef, Liliane, Karoline, Philipp: Simply for being a family.

Alexandra: For being my most important support of all.

Abstract

The interfaces that form between extended metallic substrates and organic molecules represent an intriguing and fascinating field of research. From a technological point of view, they are important as integral parts of novel electronic devices that employ organic materials as functional semiconducting units. Establishing a microscopic understanding of the interactions that govern the electronic properties of these interfaces is, however, also a considerable challenge from a more fundamental scientific perspective. In this thesis, interfaces between noble-metal surfaces and organic monolayers are studied by means of atomistic simulations based on density-functional theory. Various material systems relevant in the broader context of organic and molecular electronics – from organic molecules in the gas phase to molecular assemblies and rather complex metal-organic-organic hybrid systems – are investigated with focus on the interactions occurring at the various interfaces and on extending the computational methodology towards quantitatively accurate atomistic simulations. In the former context, we find that collective electrostatic interactions can revert the most fundamental charge-transport properties of molecules once they are assembled into densely-packed monolayers. These collective electrostatic effects are also relevant for the observed dipole-induced level localization and energy shifts, for which we show that they cause an unexpected anticorrelation between the evolution of the monolayer dipole moment and the induced work-function modification. The state-of-the-art theoretical methods tested and employed in this thesis are furthermore shown to cure some of the inherent drawbacks of common approximations in density-functional theory. Our results in this respect show that a quantitative agreement with experiments from efficient *first-principles* simulations is possible, both for the geometric structure of complex hybdrid interfaces as well as for the electronic structure of gas-phase organic molecules.

Kurzfassung

Die Grenzflächen zwischen Metallen und organischen Molekülen sind von besonderer technologischer Relevanz, da organische Materialien in neuartigen elektronischen Bauteilen zum Einsatz kommen. Diese Grenzflächen sind aber auch wissenschaftlich von großer Bedeutung, da ein mikroskopisches Verständnis der elektronischen Eigenschaften von kombinierten metallorganischen Systemen zwingend notwendig ist, um neuartige funktionelle Bauelemente zu realisieren. In dieser Doktorarbeit werden mittels atomistischer Simulationen auf Basis der Dichtefunktionaltheorie die Grenzflächen zwischen Metallen und organischen Monolagen studiert. Verschiedene Materialien – von isolierten organischen Molekülen in der Gasphase bis hin zu molekularen Ensembles und komplexen metallorganischen Hybridsystemen – werden besonders im Hinblick auf die Wechselwirkungen an der Grenzfläche und hinsichtlich einer Verbesserung der angewandten Simulationsmethoden untersucht. Im Kontext metallorganischer Grenzflächen wird gezeigt, dass die kollektive elektrostatische Wechselwirkung zwischen organischen Molekülen die fundamentalen Transporteigenschaften von molekularen Schichten massiv verändern kann. Dieses kollektive Verhalten organischer Moleküle wird im Folgenden für die durch polare Monolagen induzierten Veränderungen der Austrittsarbeit diskutiert, wo wir mittels atomistischer Simulationen eine unerwartete Antikorrelation zwischen dem Dipolmoment der Monolage und der erzielten Veränderung der Austrittsarbeit untersuchen und auf ein durch das molekulare Dipolmoment erzeugtes Lokalisieren und energetisches Verschieben der elektronischen Zustände zurückführen. Unserer Ergebnisse hinsichtlich der Qualität neuartiger Korrekturverfahren innerhalb der Dichtefunktionaltheorie zeigen, dass eine effiziente und akkurate theoretische Beschreibung von neuartigen Materialien auf atomistischer Längenskala möglich ist, sowohl für die strukturellen Eigenschaften komplexer Hybridsysteme als auch für die Vorhersage der elektronischen Struktur von Molekülen in der Gasphase.

Initiatory Statement regarding the Structure of this Thesis

The following work is a so-called cumulative Ph.D. thesis. As such, it is based on peer-reviewed scientific articles to which the author of the thesis has extensively contributed during the scientific work associated with the Ph.D. studies. According to the structure suggested for such a thesis by the "Doctoral School of Physics" at Graz University of Technology, the associated articles should be enclosed in the main part of the thesis in their original and published form. Moreover, an introduction should put this main part into the context of previous work, and a summary should discuss future efforts in the light of the main findings of the thesis.

It is deeply rooted in the nature of a scientific publication that authors of one article have contributed to the underlying scientific content to a different extent. In the light of this fact which is, of course, also reflected in the scientific articles associated to my Ph.D. thesis, I deliberately chose to only enclose those publications to which I have contributed as the leading author. During my Ph.D. thesis, I contributed to four articles as the first author, which are enclosed as original publications in the main part of this thesis. My additional contributions, namely to two articles as second author (to one of them as equally-contributing second author), to one as the third and to one as the fourth author, are not enclosed. In the summary of this thesis, I will discuss the additional findings of these secondary articles in the light of the main articles enclosed in this thesis.

List of enclosed Publications

Paper I (ref. 1)

Polarity Switching of Charge Transport and Thermoelectricity in Self-Assembled Monolayer Devices

D.A. Egger, F. Rissner, E. Zojer, G. Heimel

Advanced Materials **24**, 4403, 2012.

Paper II (ref. 2)

Anticorrelation between the Evolution of Molecular Dipole Moments and Induced Work Function Modifications

D.A. Egger, E. Zojer

Journal of Physical Chemistry Letters, **4**, 3521, 2013.

Paper III (ref. 3)

Understanding Structure and Bonding of Multilayered Metal-Organic Nanostructures

D.A. Egger, V.G. Ruiz, W.A. Al-Saidi, T. Bučko, A. Tkatchenko, E. Zojer

Journal of Physical Chemistry C, **117**, 3055, 2013.

Paper IV

Outer-valence electron spectra of prototypical organic molecules from an optimally-tuned range-separated hybrid functional: A quantitative analysis

D.A. Egger, S. Weissman, S. Refaely-Abramson, S. Sharifzadeh, M. Dauth, R. Baer, S. Kümmel,J.B. Neaton, E.Zojer, L. Kronik

in preparation.

Author Contributions

Paper I

E. Zojer conceived the idea to investigate non-polar molecules with local polar bonds. E. Zojer designed the molecules contained in the main part of the manuscript, and D. A. Egger and G. Heimel the ones contained in the Supporting Information. G. Heimel developed an extension to the `SIESTA` code, which allowed the calculation of transmission functions. For the purpose of this manuscript, this extension was further refined by G. Heimel and D. A. Egger. D. A. Egger performed the calculations and primary analysis of the data. F. Rissner extensively contributed to the analysis and interpretation of the calculated data. D. A. Egger and G. Heimel extended the analysis and interpretation to charge-transport polarity and thermoelectricity. D. A. Egger and G. Heimel designed the storyboard, D. A. Egger wrote the first version of the manuscript and prepared the figures. The manuscript was then improved in close cooperation with G. Heimel, and further improved regarding the presentation of the results with the help of all authors. G. Heimel supervised the project.

Paper II

E. Zojer conceived the idea to investigate donor-acceptor based monolayers. E. Zojer devised one of the two studied systems and D. A. Egger the other. D. A. Egger performed the calculations. For the supporting information, E. Zojer performed additional complete-active-space type calculations. D. A. Egger and E. Zojer interpreted and analyzed the data. D. A. Egger wrote the first version of the manuscript and prepared the figures. The first version of the manuscript was then improved in close cooperation with E. Zojer in several iterations. E. Zojer supervised the project.

Paper III

Stimulated by recent experimental results on this system, E. Zojer conceived the idea to investigate the metal-organic-organic heterostructure contained in the manuscript. D. A. Egger performed the calculations and primary analysis of the data. V. G. Ruiz and A. Tkatchenko developed the vdW$^{\text{surf}}$ scheme and helped with testing it. W. A. Saidi provided the implementation of the vdW$^{\text{surf}}$ scheme in the `VASP` code and T. Bučko an improved version of the `GADGET` code, which were both essential for conducting the calculations. D. A. Egger and E. Zojer further analyzed and interpreted the data. D. A. Egger wrote the first version of the manuscript and prepared the figures. The first version of the manuscript was then improved in close cooperation with E. Zojer in several iterations, and then further improved with the help of all authors. E. Zojer supervised the project.

Paper IV

This project was conceived in an extensive collaborative effort by L. Kronik, D. A. Egger and S. Refaely-Abramson, with additional supporting contributions by E. Zojer. Optimally tuned range-separated hybrid, conventional hybrid and GGA calculations were performed by D. A. Egger, S. Weissman and S. Refaely-Abramson. S. Refaely-Abramson provided additional guidance for the calculations performed by D. A. Egger and S. Weissman. S. Sharifzadeh performed GW calculations under the guidance of J. B. Neaton, and M. Dauth performed SIC and OEP calculations under the guidance of S. Kümmel. R. Baer was involved in developing the theory for optimal tuning. S. Refaely-Abramson, D. A. Egger, L. Kronik and S. Weissmann performed the primary analysis and interpretation of the data, with additional contributions by all other authors. The storyboard was developed by D. A. Egger, S. Weissman and S. Refaely-Abramson, and further improved with the help of E. Zojer and L. Kronik. D. A. Egger wrote the first version of the manuscript in close cooperation with S. Weissman and S. Refaely-Abramson. D. A. Egger prepared the figures except the ones related to the CuPc molecule (which were prepared by S. Weissman) in close cooperation with S. Refaely-Abramson and L. Kronik. The manuscript was then further improved with the help of all authors. D. A. Egger and S. Weissman equally contributed to this publication. S. Refaely-Abramson and L. Kronik supervised the project.

Contents

List of Acronyms

dft density-functional theory. 1, 9, 11, 12, 17, 19–28, 133, 135, 138, 140–142

gga generalized gradient approximation. 24–28, 138, 141

gks generalized Kohn-Sham. 27

hf Hartree-Fock. 21, 26, 27

homo highest occupied molecular orbital. 9, 25, 137, 140

ipes inverse photoemission spectroscopy. 9, 11

ks Kohn-Sham. 20–28

lda local density approximation. 12, 23–26, 28

leed low-energy electron diffraction. 10

lumo lowest unoccupied molecular orbital. 9, 25, 137

nexafs near-edge X-ray absorption fine structure. 10

ot-rsh optimally-tuned range-separated hybrid. 17, 27, 28, 140, 141

pes photoemission spectroscopy. 7, 9, 11, 13, 21, 24, 26, 140

sam self-assembled monolayer. 5, 6, 10, 12, 14–17, 133–138

si supporting information. 1

sie self-interaction error. 25, 26, 140, 141

stm scanning tunneling microscopy. 10

ups ultraviolet photoemission spectroscopy. 7, 11, 139

vdw van der Waals. 11, 12, 14, 138, 140

xc exchange-correlation. 20, 22–27

xps X-ray photoemission spectroscopy. 9, 10

xsw X-ray standing waves. 10

INTERFACES between different substances are ubiquitous in nature. When two fundamentally different materials approach and form one *new*, combined material, the physical and chemical properties can be entirely different from the individual properties of the constituents. Often, these new properties emerge from intriguing *interface phenomena*, whose microscopic understanding led to many different technologically relevant discoveries. Exploring interfaces – especially in the context of materials science – is of both fundamental and technological importance.

Out of the many different conceivable candidates in the context of studying interfaces, this thesis focuses on interfaces between inorganic metallic materials and organic semiconductors. More specifically, it concentrates on the electronic structure at metal-organic interfaces, and on the effects that can influence them. To establish a microscopic understanding of metal-organic interfaces, I relied on atomistic simulations based on density-functional theory (DFT).

This thesis is organized as follows: Part I serves as an introduction and gives a brief overview of the electronic structure at metal-organic interfaces and reviews the theoretical foundations of the simulations that I performed during my thesis. Part II is the main part of this thesis containing four publications to which I have contributed as a first author during the time of my thesis (see "List of Enclosed Publications" and "Author Contribution" at the beginning of this thesis). These four publications including supporting information (SI) are enclosed as *original publications*. In Part III I will summarize the results and give an outlook for future prospects and challenges in the field.

Part I.

Introduction and Background

1. Electronic Properties of Metal-Organic Interfaces

Interfaces between metals and organic semiconductors[4] received ample scientific attention over the last decades. The interest in this particular field is driven by two main aspects: (i) unrevealing the microscopic origin of the effects that lead to the structural and electronic properties of metal-organic interfaces is of fundamental importance to the fields of surface science[5–7] and solid-state physics.[8,9] (ii) employing organic materials as semiconductors[10] in *organic & molecular electronics* requires a detailed understanding of the contact between metals (acting as source for an electric current) and organic materials (acting as active semiconducting elements).[11,12] The latter was lucidly pointed out in the context of heterostructured inorganic semiconductors by H. Krömer in his Nobel lecture:[13] *"Often, it may be said that the interface is the device."* Studying the interface in the context of metal-organic systems is at the heart of this thesis.

Publication I, II and III enclosed in Part II of this thesis focus on the interactions occurring at metal-organic interfaces and how they affect the properties of metal-organic interfaces. In the following, a brief phenomenological introduction to metal-organic interfaces is given, where the systems of interest to this thesis are presented and important physical quantities are introduced.

1.1. Systems of Interest

In the general context of organic and molecular electronics, this work focuses on interfaces between metallic substrates and *monolayers* of organic molecules. There, one can make the distinction between two related, but nevertheless different classes of metal-organic interfaces, both of which are integral parts of organic and molecular electronic devices: interfaces between a metal and (i) a SAM of upright-standing covalently-bonded molecules (see refs. 14, 15 for recent overviews), and (ii) a monolayer of flat-lying large organic molecules (see ref. 16 for an overview). In Figure 1.1 two prototypical examples are shown, for the (111) surfaces of the noble metals gold and silver: a biphenylthiolate-SAM on Au (panel a) and a monolayer of Cu-phthalocyanine (CuPc) on Ag (panel b). In both types, organic molecules form a 2D-ordered one-molecule thick layer on the metal surface.

In publication I and publication II enclosed in Part II of this thesis, two different metal-SAM interfaces are studied, where the focus lies on understanding rather unex-

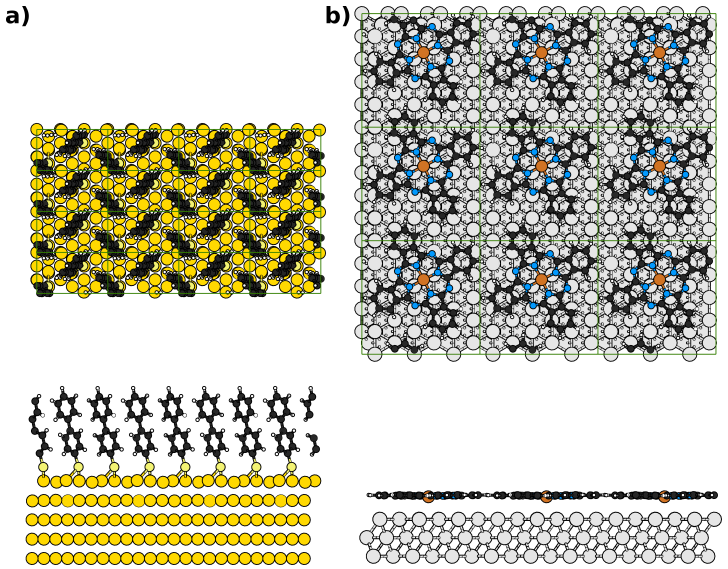

Figure 1.1.: Top view (upper parts) and side view (lower parts) of a) biphenylthiolate-SAM on Au(111) and b) CuPc on Ag(111).

pected trends for the electronic structure of these systems. In publication III we conceptually proceed to the next level of complexity by investigating a metal-organic-organic three-layer system comprising large flat-lying molecules. In the following, the relevant electronic properties of these systems will be introduced.

1.2. Relevant Observables

In the context of metal-organic interfaces, one can conceptually distinguish between *electronic* and *structural* properties. The electronic properties at interfaces are the main focus of this work, but it is stressed that structural and electronic properties are in fact strongly interwoven. In the following, I will introduce important electronic and structural quantities that characterize metal-organic interfaces and briefly sketch how they can be obtained in experiments.

One of the most important electronic quantities in surface science is the *work function* Φ. It is defined as the minimum work (at 0 K) needed to take one electron out of a metal that contains N electrons and place this electron above the sample:[5]

$$\Phi = [E_{\mathrm{vac}} + E(N-1)] - E(N). \tag{1.1}$$

Here, $E(N)$ and $E(N-1)$ is the total energy of the system with N and $N-1$ electrons, respectively, and E_{vac} is the electrostatic energy of an electron above the surface. Eq. 1.1 indicates that the work function is the energy difference between the initial state (crystal with N electrons) and the final state (crystal with $N-1$ electrons and one electron with electrostatic energy E_{vac}).[5] Lang and Kohn[17] have shown that Φ for

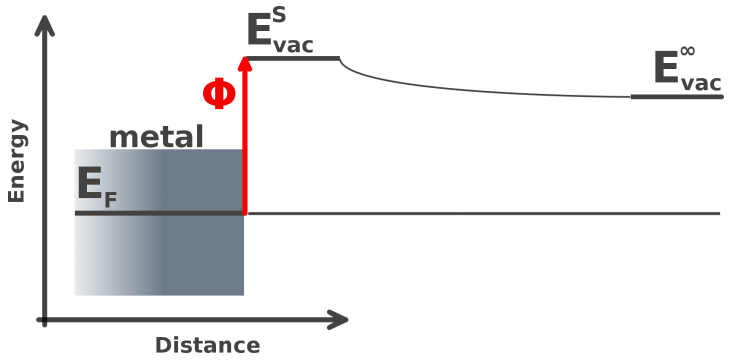

Figure 1.2.: Schematic representation of the difference between the vacuum level right at the surface, $E^{\mathrm{S}}_{\mathrm{vac}}$, and infinitely far away from it, $E^{\infty}_{\mathrm{vac}}$. The work function Φ and the Fermi energy E_{F} are also indicated.

an ideal and clean metal surface has two contributions: (i) the energy difference between the chemical potential of the electrons in the metal and the mean electrostatic energy there; and (ii) the rise in the mean electrostatic energy across a surface due to the spilling out of the electron density at the surface.[17] The latter usually results in a positive energy contribution:[18] Even for a clean and ideal metal surface (*i.e.*, even when assuming that the surface atoms retain their bulk positions), a tail of electrons spills out into the vacuum, which creates a dipole layer with the negative tail sticking out from the surface, hence the electrostatic energy is usually raised across a metal surface. For a metal with finite dimensions, the lateral extent of this dipole layer is also finite. Therefore, the electrostatic energy above the sample, *i.e.*, E_{vac} entering the definition of Φ in Eq. 1.1, depends on the distance to the surface:[18,19] the electrostatic energy just outside the metal surface ("just outside" means large compared to interatomic distances, but small compared to sample dimensions[8,18]) – denoted as $E^{\mathrm{S}}_{\mathrm{vac}}$ – is in general different from the energy infinitely far away from it, which is denoted as $E^{\infty}_{\mathrm{vac}}$ (see Figure 1.2). Due to the above rationalized positive energy contribution that is expected from the surface dipole of a metal, $E^{\mathrm{S}}_{\mathrm{vac}}$ lies usually higher than $E^{\infty}_{\mathrm{vac}}$.[18] Therefore, the term E_{vac} in Eq. 1.1 needs to be further specified. When Φ is measured in an experiment, there is pressing evidence that $E^{\mathrm{S}}_{\mathrm{vac}}$ is the relevant energy level for the measured work function:[19] Φ is known to be different for different crystal faces of one and the same material.[i] Since in thermodynamic equilibrium the chemical potential inside one material is constant and $E^{\infty}_{\mathrm{vac}}$ is invariant by definition, it is the vacuum level right above the surface that determines Φ,[19] as $E^{\mathrm{S}}_{\mathrm{vac}}$ of course depends on the considered crystal face.[19] When Φ is measured in a photoemission spectroscopy (PES)[20] experiment (in the ultraviolet regime (known as ultraviolet photoemission spectroscopy (UPS)) as the cutoff of the tail associated with the secondary electrons, the kinetic energy of the secondary electrons entering the detector is determined by the energy difference between the vacuum energy right at the substrate (*i.e.* $E^{\mathrm{S}}_{\mathrm{vac}}$) and the vacuum level right at the detector.[18] For the electronic structure that appears at the immediate metal-organic interface, it is also $E^{\mathrm{S}}_{\mathrm{vac}}$ that is

[i] As an example, Φ of a tungsten single crystal is 4.63 eV and 5.25 eV for the (100) and (110) surfaces.[19]

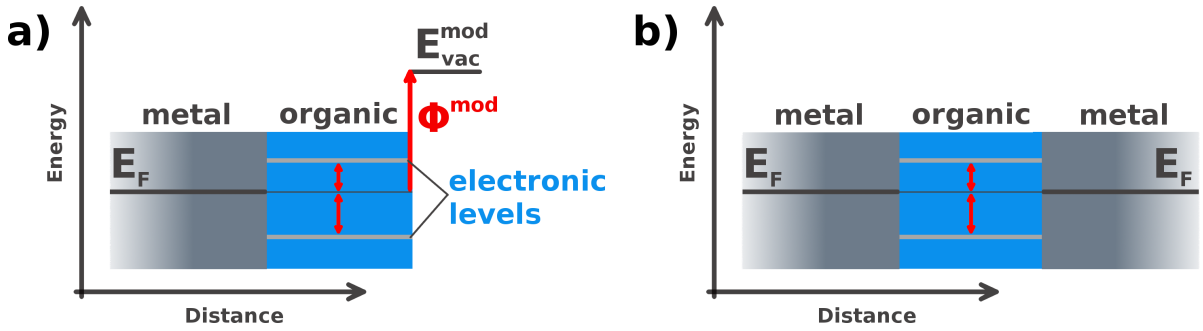

Figure 1.3.: Sketch of important electronic quantities at metal-organic interfaces: In part a), the adsorption-induced modified vacuum energy right at the surface, $E_{\mathrm{vac}}^{\mathrm{mod}}$, the modified work function, Φ^{mod}, and the energy alignment of the electronic levels in organic with the metal Fermi-level are illustrated. In part b), the energy level alignment for a metal-organic-metal system is sketched.

relevant and not $E_{\mathrm{vac}}^{\infty}$. Thus, at 0 K, where the chemical potential equals the Fermi energy E_{F}, the work function is usually denoted as the difference between E_{F} and $E_{\mathrm{vac}}^{\mathrm{S}}$. For a more in-depth discussion of this important aspect, see refs. 17–19, 21 and Chapter 18 of ref. 8. In addition to the above-mentioned electron emission through incoming photons, Φ can also be measured experimentally on the basis of emission by electric fields and thermionic emission, or using Kelvin-probe techniques.[5]

As mentioned above, the work function of a material is determined by two main factors:[5,17] (i) the "internal" electronic structure of the material, which is reflected in its chemical potential and is affected by, *e.g.*, the elements comprised in the material or defects,[22] and (ii) by the surface dipole that, also in the case of a clean and ideal surface, causes the general difference between $E_{\mathrm{vac}}^{\mathrm{S}}$ and $E_{\mathrm{vac}}^{\infty}$.[7,17–19]. The vacuum energy right above the surface can however also be modified by the adsorption of organic species through a variety of effects that will be discussed later. Therefore, the work function of a combined metal-organic system, $\Phi^{\mathrm{mod}} = E_F - E_{\mathrm{vac}}^{\mathrm{mod}}$ (see part a) in Figure 1.3), can be different from the work function of the pristine metallic substrate. The *work-function modification* $\Delta\Phi = \Phi^{\mathrm{mod}} - \Phi$ can thus be positive or negative. Employing deliberately chosen molecules as functional molecular layers could therefore, in principle, serve as a strategy to tune Φ, which is highly interesting for several applications in organic electronics.[23,24]

Significant efforts were geared over the last two decades towards establishing an understanding of the electronic structure at metal-organic interfaces. The phrase *energy level alignment*[19] has become customary in this context (see schematic energy-level diagram shown in in part a) of Figure 1.3) and describes the *"matching of the electrode Fermi-level to the energy level of the charge-transport states in the electroluminescent organic materials"*.[25] This energetic distance is relevant, as the electronic states in the organic semiconductor can serve as channels for charge transport, where the injection

of charge carriers depends exponentially on the energy barrier for it. As such, the energy level alignment is especially important in the context of molecular electronics,[11,26] where individual molecules or monolayers act as the central semiconducting entity in a device, as sketched in part b) of Figure 1.3. From a fundamental point of view, it is important to note that the electronic structure of organic adsorbates arranged in well-ordered layers cannot be represented by discrete energy levels, as the lateral periodicity of the organic semiconductor involves the formation of electronic bands with small but still finite bandwidths. Moreover, the contact with the extended electron reservoir of a metal substrate leads to a broadening and shifting of the electronic states in the organic semiconductor (see Chapter 8 in ref. 27), *i.e.*, the electronic structure in the organic monolayer represents a continuous density of states. Therefore, describing the rather complicated electronic structure of metal-organic interfaces on the basis of single levels (as the term level alignment signifies) can, of course, only serve as an approximation to the "complete picture" (see discussion in ref. 28). From an experimental perspective, information regarding the electronic structure of materials can quite generally be obtained with a combination of PES (again in the ultraviolet regime) and inverse photoemission spectroscopy (IPES). In the process of photoemission, an incoming photon causes the emission of an electron from the N-electron ground state and a "hole" is left behind in the probed system. The intensity measured in PES, therefore, depends (amongst other factors, see ref. 29) on the wave function that represents the N-electron state and the wave function corresponding to the $(N-1)$-electron state.[30,31] In addition to the above-outlined fundamental reasons that indicate the limits of using single-energy levels to identify the metal-organic electronic structure, it is, therefore, also evident that such a strategy can only approximately describe the binding energies as measured in PES experiments. However, it is still customary in the field of organic electronics to describe features in spectra measured with PES and IPES using molecular levels of the N-electron system: The first feature in the occupied part of the spectrum is ascribed as highest occupied molecular orbital (HOMO) and its counterpart on the unoccupied side of the spectrum as lowest unoccupied molecular orbital (LUMO). Under the assumption that the photoemission process occurs on the same time scale as charge transport through the organic semiconductor, the onsets of these HOMO and LUMO peaks represent the onsets where a charge transport through the system can set in (see ref. 32 for further discussion). Accordingly, the gap between these onsets is known as the *transport gap* or *fundamental gap*, and it should be distinguished from the optical gap of a material.[32–34] Note that within the very popular electronic structure method DFT, the identification of the calculated orbital energies with the ionization series measured in PES is not at all straightforward.[31] This issue will be discussed in more depth in Chapter 2, and is the topic of publication IV enclosed in form of a draft in Part II of this thesis. From this phenomenological discussion, the approximate and purely schematic energy-level diagram shown in Figure 1.3 arises for the electronic structure of metal-organic interfaces.

Finally, the energetics of the electronic core levels of materials can be measured employing X-ray photons in PES (known as X-ray photoemission spectroscopy (XPS)). The binding energy of the core electron can reveal the chemical and electrostatic environment

of an atom. XPS is inherently element specific and, thus, allows probing the binding configuration of specific atoms. Interestingly, it can also be used to determine the structural order of thiolate-SAMs through examining the thiolate fingerprint-signal in XPS.[35]

Detailed knowledge regarding the structural properties of metal-organic interfaces, especially concerning the geometry of the molecules within the monolayer and their structural alignment with respect to the metallic substrate, is usually a prerequisite for performing atomistic simulations. This is because optimizing the geometry of the molecules including a *first-principles* determination of the surface unit-cell is in many cases impossible. For the experimental analysis of the structural properties of surfaces, a large variety of different techniques that are based on microscopy-, spectroscopy- and also diffraction can be used.[5]

More specifically, structural information regarding the *order of the molecules* and *surface unit-cell* of metal-supported thin-films can be obtained with low-energy electron diffraction (LEED), which is based on diffraction from the 2D-extended metal-organic system. Experiments based on scanning tunneling microscopy (STM), on the other hand, allow a more locally resolved assessment of the structural order and alignment of the molecules. Furthermore, measurements employing X-ray standing waves (XSW) techniques can give great insight into *vertical distances* of molecules to the surface. These distances are particularly interesting for the case of large flat-lying organic molecules on metals, as they can reveal the *type* of interaction occurring between molecule and metal. For the case of SAMs, an additionally important observable is the molecular *tilt angle* with respect to the surface normal, as it influences the work-function modification induced by a polar SAM. The tilt angle of the SAM molecules can be measured using near-edge X-ray absorption fine structure (NEXAFS) experiments.[36]

1.3. Interactions at Metal-Organic Interfaces

In the following, some of the interactions occurring at metal-organic interfaces are introduced. This discussion focuses on the impact of metal-organic interactions on the *electronic properties*, and serves as a general introduction to publications I, II and III included in Part II of this thesis. It is, however, by far not complete, and the interested reader is referred to the literature for further details, especially to refs. 4, 12, 15, 16, 19, 37, 38.

For the energy level alignment at metal-organic interfaces as introduced above, it has become customary to use the well-known Schottky-Mott limit as a conceptual starting point.[19,39] This model describes the energy barriers for charge-carrier injection exclusively on the basis of the metal work-function, Φ, and the ionization energy and electron affinity of the organic semiconductor.[19] A prerequisite for the Schottky-Mott limit to hold is that the interaction between metal surface and organic layer is negligible (known as *vacuum level alignment*), and especially that the organic adsorbate does not trigger

any additional *interface dipole*.[19] This is because the latter would induce an energy shift between the electronic states of the metal and the organic. It would in this way modify their relative alignment.[19]

An early experimental investigation emphasizing the importance of interface dipoles at metal-organic interfaces is the study by Narioka *et al.*.[40] The authors performed UPS experiments for 5, 10, 15, 20-zinctetraphenylporphyrin (ZnTPP) adsorbed on different metal substrates (Au, Ag, Al, Mg),[40] and concluded that an energy shift occurs at the studied metal-organic interfaces. This finding indicates that the vacuum levels of the metal and the organic monolayer for these particular metal-organic interfaces do not align. Another important implication of the Schottky-Mott limit that can also be tested experimentally is that the charge-carrier injection barrier – estimated experimentally as the onsets of the first features in PES and corresponding IPES spectra (*vide supra*) – depends linearly (with slope $S = 1$) on the substrate work function.[19,39] Interestingly, by using different metals as underlying substrates, Narioka *et al.*.[40] found that this is indeed the case for metal-ZnTPP system, which was interpreted as the occurrence of a constant *substrate-independent* interface dipole.[40]

For a variety of interfaces between metals and large flat-lying organic adsorbates, it was, however, found experimentally that their interfaces rarely align with only a constant interface dipole, see *e.g.*, refs. 19, 41, 42: For charge-carrier injection barriers measured as a function of the substrate work function, strong deviations from a *constant* interface dipole energy shift were found experimentally;[41,42] *i.e.*, the relation between charge-carrier injection barriers and substrate work-function was seen to strongly depend on the specifics of the studied metal-organic system.[41,42] In this context, it is useful to recall that monolayers of flat and large organic molecules can establish bonding to a surface through a variety of interactions. In the literature, the adsorption of large conjugated molecules if often classified using the terms *chemisorption* and *physisorption*.[6,25] These two adsorption mechanisms are usually discussed in regard to their adsorption "strengths",[25] meaning that the adsorption energy in *chemical* adsorption is substantially larger than in *physical* adsorption. A related frequently addressed observation in the discussion of these two mechanisms concerns the electronic structure of the involved species, which is significantly changed in chemisorption, but hardly in physisorption.

An important phenomenon that is often discussed in the context of physisorption is the *instantaneous multipole – induced multipole* interaction, which arises from quantum-mechanical vacuum fluctuations in the charge density and results in an attractive potential. This interaction is known as London dispersion, and is usually the strongest contribution to the van der Waals (VDW) forces.[43] Long-range VDW forces are especially relevant in the context of understanding the interaction of a metal with large π-conjugated molecules, as the latter contain an easily polarizable π-electron system. This also implies an interesting methodological challenge for atomistic simulations, as the workhorse of electronic structure calculations for such large systems – (semi-)local DFT approximations as introduced in the next chapter – does not account for these long-range

VDW interactions. Recently, however, Ruiz *et al.*[44] proposed a remedy to this problem by combining the Tkatchenko-Scheffler scheme[45] with the Lifshitz-Zaremba-Kohn theory[46,47] for the VDW interaction between a surface and one atom. They showed that this approach results in an accurate description of the binding distances for PTCDA on the noble metals.[44] In publication III enclosed in Part II, the application of this approach is taken one step further to the simulation of a rather complex metal-organic-organic three-layer system, which is compared to a recent extensive experimental investigation on this system.[48]

While the consideration of VDW interactions is crucial for a general understanding of the bonding mechanisms relevant for metal-organic interfaces, these interactions alone due not cause additional interface dipoles and, therefore, cannot explain deviations from the Schottky-Mott limit. A different effect that causes an interface dipole and, thus, a deviation from idealized vacuum level alignment at the interface is the so-called "*Push-back*" (or "Pillow" or "Cushion") effect. It describes that electrons tailing from the metal surface into the vacuum (*vide supra*) are "pushed-back" by the approaching electron cloud of the adsorbate, the driving force behind it being the Pauli exclusion-principle. It is by now well-established that this effect naturally arises in the process of adsorption. Historically, the Push-back effect played an important role in understanding $\Delta\Phi$ induced by the adsorption of rare-gas atoms. As noticed by Mignolet already in 1950,[49] it was puzzling that inert rare-gas atoms were found to induce a finite $\Delta\Phi$, as chemical bond-formation was out of the question. Since then, many different models to explain these observations have been put forward such as polarization of the adsorbate,[49] donor-acceptor interaction[50] or charge-transfer effects.[51,52] Already in the early work of Mignolet,[49] the following statement can be found: "*How is it that van der Waals' films of non-polar particles exhibit surface potentials? The effect might be one of compression of the electric double layer at the metal surface by the adsorbed particles, without the latter being polarized, but this is very improbable.*" Interestingly, it was exactly this "improbable" effect of "charge compression" that was later theoretically shown[53] to be able to explain the curious experimental findings for the case of rare-gas adsorption: Already in 1980, Lang in ref. 54 theoretically studied the adsorption of rare-gas atoms on metal surfaces and noticed the *strong interaction* at short substrate-adsorbate distances due to the Pauli exclusion-principle leading to a Push-back of the metal electrons. And yet Lang *concluded* on the basis of DFT calculations in the local density approximation (LDA) (*vide infra*) that a chemical bond-formation is responsible for the finite value of $\Delta\Phi$.[54] Using wave-function based atomistic simulations, more than 20 years later, it was shown that an exchange-based interaction is the most important contribution to the build-up of the dipole at the interface between rare-gas atoms and metal substrates.[53]

The Push-back of metal electron-density will, in general, reduce the original metal surface-dipole. Therefore, it results in an important contribution to a change in work function, $\Delta\Phi$. As such, it has received attention in the forthcoming literature, both for flat-lying organic species[38,55] as well as SAMs.[15] The constant energy shifts reported by Narioka *et al.* for different metal-organic systems[40] (*vide supra*) can be explained

as a manifestation of the Push-back of metal electrons triggered by the adsorption of the organic monolayer. This interpretation, however, would require that the Push-back effect is similar on different metal substrates.

To rationalize the strongly system-dependent deviations from vacuum level alignment already mentioned above (see,*e.g.,* refs. 41, 42), the discussion, however, needs to be extended "*beyond Pauli Pushback*",[56] *i.e.*, to the realm of chemisorption. For the case of flat-lying organic adsorbates, chemical interaction with the substrate is especially strong if the adsorbing molecules are electron-donors or -acceptors. Chemical substitution of molecular backbones with electron-accepting or -donating groups allows to fuel the molecule with strong electron-accepting or -donating character. Such molecules implicate energetically low-lying unoccupied (high-lying occupied) electronic states owing to their accepting (donating) character. Upon adsorption of such strong acceptor molecules (donor molecules) it is, therefore, likely that unoccupied (occupied) molecular electronic states would come to lie below (above) the metal Fermi-level. As such a situation cannot be sustained in thermodynamic equilibrium, a charge transfer between the metal and the molecules sets in to equilibrate the metal-organic interface until the frontier molecular electronic states are aligned with the metal Fermi-level. This phenomenon is known as *Fermi-level pinning*,[25,57] and it naturally involves a significant additional interface dipole due to the charge rearrangements associated with it. Typical examples for electron-acceptors in the context of metal-organic interfaces are the above-mentioned PTCDA,[16,58–61] or 2,3,5,6-tetrafluoro-7,7,8,8 tetracyanoquinodimethane (F4-TCNQ).[38,62,63] Typical molecular donors that have been studied both experimentally and theoretically in the broader context of organic electronics are tetrathiafulvalene,[56,64] viologen[56] and methyl viologen.[65] Indeed, these acceptor and donor molecules were reported to induce charge-transfer effects beyond the Push-back effect when adsorbed on noble metal surfaces.[ii] Moreover, molecular species involved in such charge transfer processes often display significant structural distortions,[58,63,66] *e.g.*, these molecules can significantly bend towards the metal surface.[58,63]. Importantly, the additional interface dipole that is induced by the metal-organic charge transfer can quite generally be expected to have a strong impact on the work function and energy level alignment.[63] Conclusively, the expectations born of the Schottky-Mott rule are entirely violated in the Fermi-level pinning situation: The energy alignment of charge-carrier injection barriers was experimentally shown to be insensitive to a change in substrate work function over a wide range.[42,67] Moreover, Fermi-level pinning implies that the work function of the combined metal-organic system, Φ^{mod}, is also independent of the work function of the metal substrate, as was discussed on the basis of PES experiments in ref. 25.

Publication III contained in Part II explores the interactions occurring at the three-layer system Ag(111)-PTCDA-CuPc. The metal-organic Ag(111)-PTCDA interface involves a partially chemical interaction between substrate and adsorbate (see ref. 16 for an overview). Nevertheless, it was shown that the proper treatment of long-range

[ii] the exception within refs. 16, 56, 58–65 is PTCDA on Au(111)[60]

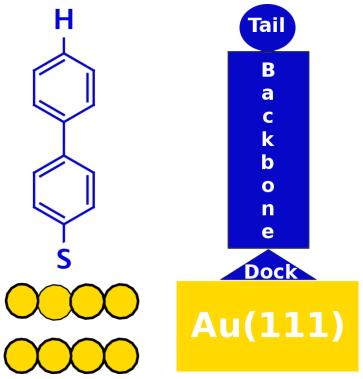

Figure 1.4.: Naming convention for SAMs: docking group, molecular backbone and tail group.

VDW interactions is absolutely crucial for an accurate atomistic simulation of the structural properties of the Ag(111)-PTCDA interface, see ref. 43 for an overview. For organic-organic interfaces such as PTCDA-CuPc, on the other hand, it was argued that the involved vacuum levels can indeed align without establishing an interface dipole, see ref. 68. Therefore, in the absence of chemical interaction at an organic-organic double-layer, VDW interactions can expected to be the dominant bonding mechanism. It is therefore interesting to study a three-layer metal-organic-organic system such as Ag(111)-PTCDA-CuPc, where two interfaces are involved that can be expected to involve somehow different bonding mechanisms.

Publication II enclosed in Part II, on the other hand, focuses on Fermi-level pinning for the case of a self-assembled monolayer (SAM) of donor-acceptor based "push-pull" molecules. Ideally, SAMs are 2D-extended ensembles of molecules that are standing upright on a supporting substrate. The diversity of organic chemistry allows for many different functional docking- and tail-groups (see Figure 1.4 for the here employed naming convention). They can be combined with conjugated or non-conjugated molecular backbones to form SAMs on a variety of substrates[14,69] such as noble metals[35] or inorganic semiconductors.[70,71] In my thesis, I investigated SAMs of conjugated molecular backbones adsorbed on noble-metal surfaces. Bonding of the SAM-molecules to a metal surface is established through a docking group (see Figure 1.4). This bonding mechanism often involves a rather strong covalent bond between SAM and substrate, especially for thiolated SAMs on gold,[72] which are studied in publication I and II contained in this thesis (see Part II). Indeed, metal-SAM systems covalently-linked by a suitable docking group have been classified as strongly chemisorbed systems.[25] Accordingly, for biphenylthiolate SAMs an interface dipole on the order of 1 eV has been predicted theoretically.[73] Note that while the structure of these thiolate-SAMs has been studied intensively in the past,[74] the detailed atomistic structure of the immediate gold-thiol interface is still under dispute, see refs. 37, 72, 75–77 and references therein. Changing the docking group to, *e.g.*, the isocyanide group, can entirely change the metal-SAM bonding process: As was theoretically shown, the resulting charge rearrangements and hence the interface

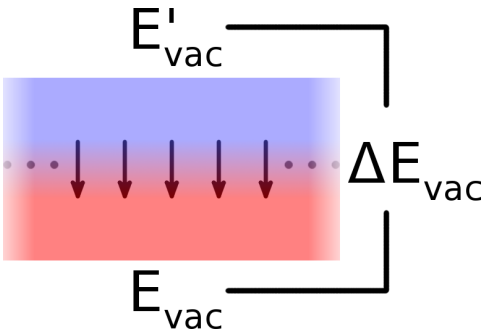

Figure 1.5.: Sketch showing the modification of the electrostatic energy (indicated as a change in color) induced by a an array of dipoles. The step in the energy due to the dipole sheet, ΔE_{vac}, is also indicated.

dipole strongly depend on the involved docking chemistry.[78] Therefore, the details of the docking chemistry impact the level alignment and work function, as has been intensively discussed in the literature.[78–81]

Another "handle" to change the properties of SAMs is to employ different tail-group substituents (see Figure 1.4).[37] Using a polar substituent as tail group allows to change the dipole moment of the SAM molecules. The adsorption of such polar molecules perfectly assembled into monolayers involves various fundamental electrostatic phenomena, which often results in electronic properties of the monolayer that are unexpectedly different from what one would expect from the molecular situation in the gas phase. This is why such effects are often termed "cooperative" or "collective" effects.[82–84] First and foremost, a 2D array of molecular dipoles electrostatically represents a 2D plate-capacitor. As lucidly laid out in a seminal theoretical article by Heimel *et al.*,[73] a polar monolayer involves two *different* vacuum levels on each "side" of it that are energetically separated by a discontinuity in the electrostatic energy ΔE_{vac} (see sketch of an array of dipoles in Figure 1.5). Therefore, the electronic levels within a polar SAM are differently aligned to either "side" of a polar SAM.[73] In this context, Natan *et al.*[85] have emphasized the fundamental electrostatic difference between one dipole and an array of dipoles. They have shown that the electric field decay in space is much faster for an array of dipoles than for a single dipole, *i.e.*, it was calculated that the field decay-length for a sheet of dipoles arranged in a square lattice is by a factor 2π "faster" than the lateral distance of the dipoles contained in the sheet.[85] Therefore, for close-packed polar layers the electric field outside the monolayer rapidly decays to zero and a common electrostatic energy is established.[37,85]

These fundamental electrostatic considerations are especially relevant for metal-organic systems comprising densely-packed molecules, as is often observed for metal-SAM systems. For example, it was theoretically shown for a variety of molecules with different tail-groups that the associated SAMs have essentially the same level alignment with respect to the metal Fermi-level, although the molecules in the gas phase displayed very

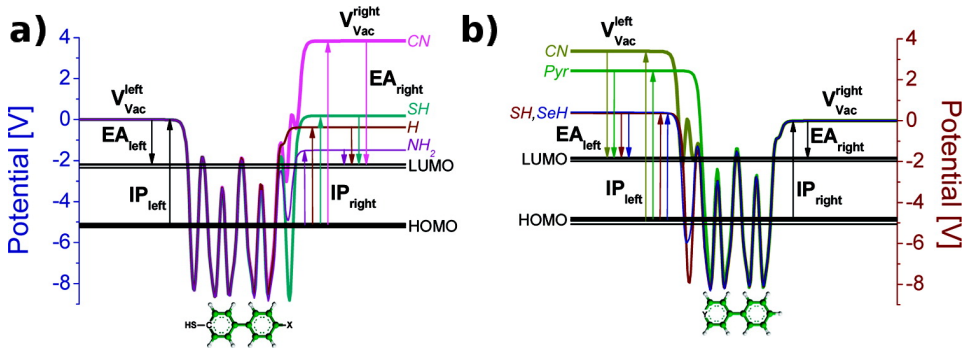

Figure 1.6.: Comparison of the plane-averaged electron potential energy of substituted tail-group (a) and docking-group (b) functionalized biphenyl-SAMs. Adapted with permission from ref. 78. Copyright 2007 American Chemical Society.

different IPs.[73] Interestingly, however, the work function of the combined metal-SAM system was found to strongly depend on the tail-group substituents, because the different tail groups result in different molecular dipole moments of the SAM-forming molecules.[73] On the basis of atomistic simulations it was argued that the modification of the electrostatic landscape due to the tail-group dipoles of the SAM-molecules occurs exclusively at the tail (*i.e.* the vacuum-side) and cannot influence the level alignment, but of course modifies Φ.[73] Note that the entirely different impact of tail-group substituents on the energy level alignment and work function for a metal-SAM interface was later also confirmed experimentally.[86] Conceptually, the effect of polar docking- and tail-groups on the electrostatic energy landscape of a SAM can be investigated in a *Gedankenexperiment*, in which the *free-standing* monolayer (*i.e.*, without supporting substrate) is considered.[73] The effect of docking-group substituents is compared to the effect of tail-group substituents for the case of a free-standing densely-packed biphenyl-SAM in Figure 1.6.[78] As can be seen from the plane-averaged potentials shown in Figure 1.6, the change in the energy landscape along the SAM is confined to the region of the polar substituent.[78]

Another collective electrostatic effect is the mutual depolarization of the neighboring polar molecules in a monolayer:[85,87] Each of the molecules present in a polar monolayer "feels" the electric field generated by the surrounding molecules, which reduces the effective dipole moment of the molecules in the monolayer. The effect is strongly coverage dependent[85] and, in principle, can even result in a saturation of $\Delta\Phi$.[82] Depolarization is especially important in the context of densely-packed SAMs, but has also an impact for $\Delta\Phi$ induced by the adsorption of flat-lying species.[88] In the latter case, the extent of depolarization compared to more densely-packed SAMs is, however, weaker.[87] The interested reader is referred to the reviews refs. 37, 84, 85, 87 and original articles refs. 82, 88–91 that review and discuss the importance of depolarization phenomena for the electronic properties of metal-organic interfaces.

The outlined collective electrostatic effects are especially important in the context of

publication I enclosed in Part II of this thesis. There, the effect of local polar bonds in otherwise non-polar molecules on the charge-transport properties of SAMs is studied. Such local polar bonds can also interact electrostatically and by that alter the energetics in a molecular films, as emphasized already in refs. 92–94. Furthermore, in publication II the limits of exploiting the collective behavior of dipoles to change the work function of a metal substrate are investigated, and discussed in the light of the above-discussed Fermi-level pinning processes and their entailed implications for metal-organic interfaces.

The results presented in publication I, II and III contained in Part II of this thesis were obtained with atomistic simulations based on density-functional theory (DFT). Therefore, in the following chapter I will introduce the basics of DFT with an emphasis on the capabilities of standard approximations for predicting the electronic structure of materials. For organic molecules, the promise of going beyond standard DFT approximations by invoking optimally-tuned range-separated hybrid (OT-RSH) functionals is described in publication IV, which is included as a draft in this thesis.

2. Density-Functional Theory and Methodology

All four publications contained in Part II of this thesis present quantum-mechanical simulations. In the atomistic simulation of materials, one is generally confronted with an intricate many-body problem.[95] The electrons behave in a correlated manner driven by their mutual Coulomb interaction $\hat{V}_{ee}$:

$$\hat{V}_{\mathrm{ee}}(\boldsymbol{r}-\boldsymbol{r'}) = \frac{e^2}{|\boldsymbol{r}-\boldsymbol{r'}|}. \tag{2.1}$$

Moreover, an electron at position $\boldsymbol{r}$ is attracted by a nucleus of atomic number Z at position $\boldsymbol{R}$ as $-Ze^2/|\boldsymbol{r}-\boldsymbol{R}|$, whereas this nucleus repels a second nucleus of atomic number Z' at position $\boldsymbol{R'}$ as $ZZ'e^2/|\boldsymbol{R}-\boldsymbol{R'}|$.[96] Often, we can separately treat the nuclei and electrons (known as the "Born-Oppenheimer" or adiabatic approximation), which allows us to treat the $\boldsymbol{R_i}$ of the nuclei as parameters in the process of solving the *many-electron problem*. The latter is, however, still entirely complicated due to the Coulomb interaction between the electrons and their quantum-mechanical nature. In fact, to calculate the ground state energy E_0 of the N-electron system, one in principle needs to solve the Schrödinger equation (here given in its time-independent form)

$$\hat{H}\psi_0^N = E_0\psi_0^N, \tag{2.2}$$

with $\hat{H}$ being the Hamiltonian and ψ_0^N being the ground-state N-electron wave function

$$\psi_0^N = \psi_0^N(\boldsymbol{x_1}, \boldsymbol{x_1}, ..., \boldsymbol{x_N}). \tag{2.3}$$

The ground state wave function explicitly depends on the coordinates of all N electrons, *i.e.*, ψ_0^N is a complicated mathematical object that is "*not easy to calculate, store, apply or even think about*".[97] In the next chapter, the basic idea of density-functional theory (DFT) will be outlaid.

2.1. Basics of density-functional theory

DFT (refs. 33, 97–100 were especially helpful for the contents presented in this section) is one of the most successful theories for the atomistic simulation of matter. The many-electron problem in the quantum-mechanical simulation of materials as formulated in the last paragraph is fully specified by the positions and types of the nuclei, which for the electrons result in a potential v_{ion}, and the number of electrons in the system.[33] DFT

relies on the fundamental theorem[101] of Hohenberg and Kohn – formulated in 1964 – which states that the ground state electron density of the fully interacting electron system, $n(\boldsymbol{r})$, subject to some external potential $v_{\text{ext}}(\boldsymbol{r})$, determines this external potential uniquely up to a constant.[33,101] Since the effect of the nuclei, *i.e.*, the potential v_{ion}, is external to the electrons and, furthermore, the density also determines (through spatial integration) the number of electrons N subject to v_{ion}, the ground state density $n(\boldsymbol{r})$ completely specifies the full Hamiltonian and allows a complete and unique description of the N (interacting or non-interacting) electron system.[33] Furthermore, Hohenberg and Kohn proofed the existence of the universal density functional $F[n(\boldsymbol{r})]$, which yields the exact ground state energy E_0.[33,101] The power of these theorems is enormous, since they introduced the alternative view of using the density instead of the many-electron wave function as the fundamental variable in the process of calculating the ground state properties of many-electron systems.

DFT is made practically feasible through the ansatz of Kohn & Sham,[102] where a fictitious system of non-interacting electrons is introduced that has the same density as the physical system. This Kohn-Sham (KS) system is, however, subject to the *effective* KS potential v_{KS}:

$$\left(-\frac{\hbar^2\nabla^2}{2m} + v_{\text{KS}}(\boldsymbol{r})\right)\varphi_i(\boldsymbol{r}) = \varepsilon_i\varphi_i(\boldsymbol{r}), \tag{2.4}$$

with the Kohn-Sham potential:

$$v_{\text{KS}}(\boldsymbol{r}) = v_{\text{ext}}(\boldsymbol{r}) + v_{\text{H}}(n;\boldsymbol{r}) + v_{\text{xc}}(n;\boldsymbol{r}). \tag{2.5}$$

v_{H} is the Hartree term of the KS potential: $v_{\text{H}}(n;\boldsymbol{r}) = e^2\int\frac{n(\boldsymbol{r'})}{|\boldsymbol{r}-\boldsymbol{r'}|}d^3r'$, *i.e.* the "classical" Coulomb repulsion of the electrons. All the interaction beyond is comprised in the exchange-correlation (XC) part of the KS potential:

$$v_{\text{xc}}(n;\boldsymbol{r}) = \frac{\delta E_{\text{xc}}[n]}{\delta n(\boldsymbol{r})}, \tag{2.6}$$

i.e. the exchange-correlation energy-density functional $E_{\text{xc}}[n]$ includes all effects that go beyond the non-interacting electron kinetic-energy term in Eq. 2.4 and the Hartree interaction v_{H}. Eq. 2.4 represents a set of single-particle type Schrödinger equations, whose solutions are KS orbitals φ_i with energies ε_i. The ground state density is obtained from the φ_i as: $n(\boldsymbol{r}) = \sum_i|\varphi_i(\boldsymbol{r})|^2$, which allows a self-consistent treatment of the KS equations.[102] Importantly, through the KS scheme an exact mapping from the N-electron problem to N one-electron problems has been established, which enormously reduces the complexity when describing electron systems. Unfortunately, the exact form of v_{xc} is unknown.

2.2. Further details of Kohn-Sham theory

The *physical meaning* of the KS orbitals and energies,[103] especially regarding their interpretation as the ionization series probed in PES (see ref. 31 for details), is of particular interest for the user of KS DFT. Indeed, there is an exact theoretical framework to describe ionization processes in many-electron systems outside the realm of DFT: the solution of the Dyson equation with corresponding Dyson orbitals and quasi-particle energies. However, even the most simple expansion (and, thus, crudest approximation) to it, the so-called G_0W_0 approximation (where G stands for the one-particle Green's function, and W for the screened Coulomb interaction), is a heavily involved and computationally very challenging theory that so far cannot serve as an *efficient* device for calculating the properties of many-electron systems.

Indeed, it would be enormously helpful, if the much more efficient KS theory allowed for a calculation of the ionization series through the KS orbitals and energies, see Eq. 2.4. In Eq. 2.4 the non-interacting kinetic energy term and Hartree term can be readily obtained from the KS orbitals. All the burden of exchange- and correlation is shuffled into v_{xc} which remains, however, unknown. Despite the fact that the exact v_{xc} is unknown, one can still analyze the properties and features of the *exact* v_{xc} to learn what can be expected from KS orbitals and energies *in principle*. No physical meaning was suggested for KS orbitals and energies in the original work of Kohn & Sham,[31,102] and indeed for a longer time the φ_i and ε_i in Eq. 2.4 have been seen as "mere" mathematical devices with no physical meaning at all. However, it was later realized that there is more to it than was initially believed. First and foremost, the *IP theorem*,[i] valid for the *exact* and ultimate KS potential v_{KS}, states that the negative of the calculated KS HOMO energy $\varepsilon_{\text{HOMO}}$ equals the *relaxed* exact IP of the system:[104]

$$IP(N) = E(N-1) - E(N) = -\varepsilon_{\text{HOMO}}(N). \tag{2.7}$$

Note that "relaxed" in this context means that relaxation effects caused by the physical process of ionization are included in this quantity. In contrast, a similar condition in Hartree-Fock (HF) theory known as Koopmans' theorem is only valid for the *unrelaxed* IP and, therefore, does not consider the ionization-induced relaxation of the system. In the following, it is shown that the IP theorem in Eq. 2.7 is valid for the exact KS potential. In the pioneering work of Perdew *et al.*,[105] DFT has been extended to fractional-electron systems, and the piecewise-linearity property of DFT has been established: For a fractionally charged system, the intermediate non-integer electron state (*i.e.* $(N-\alpha)$-electrons) can be described by a statistical mixture of the neutral (*i.e.* N-electrons) and fully-ionized (*i.e.* $(N-1)$-electrons) state. Then, the total energy of the system with $(N-\alpha)$ electrons is:

$$E(N-\alpha) = (1-\alpha)\,E(N) + \alpha E(N-1). \tag{2.8}$$

[i] The proof of the IP theorem follows an outline written by Shira Weissman (Weizmann Institute).

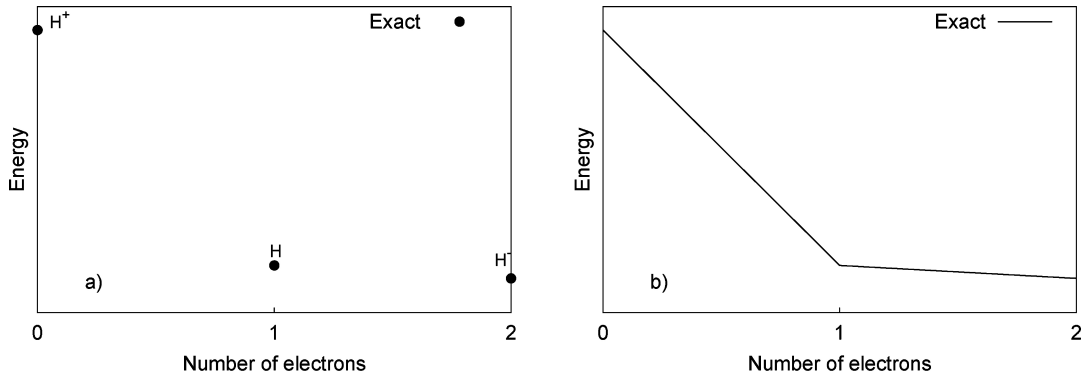

Figure 2.1.: Total energy of hydrogen and its first ionized states (left), and total energy of hydrogen as a function of fractional electron number between integer charges (right). Adapted with permission from ref. 109. Copyright 2012 American Chemical Society.

Hence, the exact total energy versus electron number curve must be a series of linear segments between integer electron numbers, see Fig. 2.1. The piecewise-linearity property of DFT is a feature of the (unknown) *exact* KS potential v_{xc}, but it is grossly disobeyed by commonly used *approximate* KS potentials.[106–109] For the exact functional, one finds from Eq. 2.8 that the slope of each $[N, N-1]$ linear segment is the negative of the exact IP of the system with N electrons:

$$\frac{\delta E(N-\alpha)}{\delta \alpha} = -E(N) + E(N-1) = -IP(N). \tag{2.9}$$

For any system with a non-zero fundamental gap (*vide supra*), the slope of the total energy *vs.* fractional electron curve changes discontinuously at each integer point.[105] Accordingly, the chemical potential, which is the derivative of the energy with respect to the electron number, changes discontinuously at integer points as well.[34] This reflects the fact that the IP depends on the number of electrons present in the system,[34] *i.e.* $IP(N)$ and $EA(N)$ naturally differ for systems with a non-zero fundamental gap. Importantly, in the *exact* KS description of the system with N electrons, this behavior can only be recovered through discontinuities in the potential.[105] Such discontinuities can, in principle, arise from the non-interacting kinetic energy term and the exchange-correlation term of the KS potential in Eq. 2.5.[110] The discontinuity in the XC part of the KS potential is commonly known as the derivative discontinuity, Δ_{xc},[34,110] and it was recently shown that the lack thereof is equivalent to deviation from the piecewise-linearity condition.[111]

Now a different condition valid for *any* KS DFT functional is Janak's theorem,[112] which states that the variation in the total energy with respect to the orbital occupation n_i is equal to the eigenvalue of orbital i: $\frac{\delta E}{\delta n_i} = \varepsilon_i$. Upon the assumption that fractionally charging the N-electron system (to receive the $(N-\alpha)$ electron system) is equivalent to vary the occupation n_i of the HOMO, Janak's theorem can be applied to the *exact*

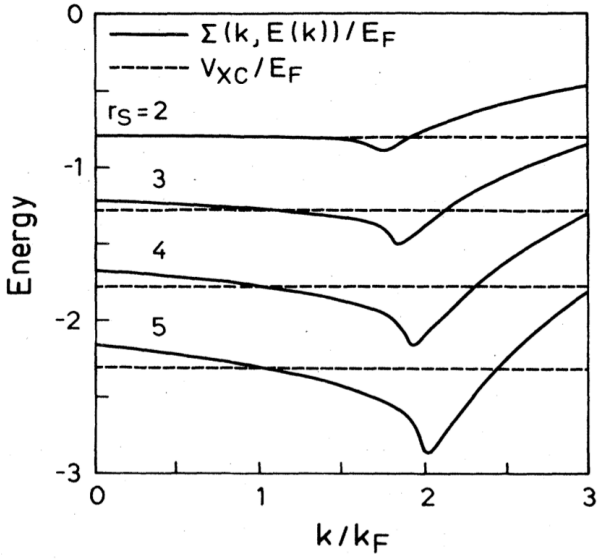

Figure 2.2.: Self-energy, $\Sigma(k, E(k))$, and LDA exchange correlation potential, v_{xc} (in units of the Fermi energy), as a function of electron crystal momentum k, for a homogeneous electron gas of several densities characterized by the Wigner-Seitz radius, r_s. After Jones and Gunnarson, ref. 98. Copyright (1989) by The American Physical Society.

functional. Using Eq. 2.9 valid for the exact functional, one finds:

$$\frac{\delta E(N-\alpha)}{\delta \alpha} = -IP(N) = \varepsilon_{\mathrm{HOMO}}(N), \tag{2.10}$$

which is the IP theorem Eq. 2.7 valid in *exact* DFT schemes. Therefore, one expects that the highest-occupied level, $\varepsilon_{\mathrm{HOMO}}$, exactly predicts the IP of an electron system if the exact $E_{\mathrm{xc}}[n]$ was known.

A different, yet related important physical observable is the fundamental gap between IP and EA. Perdew & Levy[113] and Sham & Schlüter[114] realized that the KS gap, as obtained from HOMO/LUMO orbital-energy differences after solving Eq. 2.4, cannot predict the value of the fundamental gap even if the *exact* KS functional was applied. The reason is the aforementioned necessity for a derivative discontinuity Δ_{xc} in the XC potential upon fractional charge variations: two KS potentials, one accurately predicting the IP and the other one the EA, are expected to exactly differ by the derivative discontinuity.[31] Since all KS orbitals are subject to the same KS potential, and the IP theorem holds, the derivative discontinuity is *inherently* missing in the KS gap as calculated from orbital-energy differences, even if the *exact* KS functional was known (see discussion in chapter IV of ref. 33).

Of equal importance for practical calculations are occupied levels other than the HOMO, *i.e.* valence electron levels deeper in energy. How well does *exact* KS theory perform in this context? It is interesting to remember that the simple LDA represents the exact KS

functional in the case of the homogeneous electron gas. Therefore, for this particular case, it is possible to calculate the *exact* v_{xc} and compare it to the (known) self-energy $\Sigma(k, E(k))$ (yielding accurate quasi-particle excitation energies), as was done by Jones & Gunnarsson.[98] As can be seen in Fig. 2.2, these two quantities are equal at the Fermi energy, reflecting the validity of the IP theorem. Apparently, differences that occur between v_{xc} and $\Sigma(k, E(k))$ (i) depend on the density of the homogeneous electron gas, (ii) are small in the vicinity of the Fermi level, and (iii) build up gradually towards deeper valence electron levels, *i.e.*, to higher PES binding energies. Do these rather "academic" considerations of a model system also provide insight for "real-world" electron systems? Chong and co-workers[115] have calculated highly-accurate *ab-initio* electron densities and back-fitted their results to obtain the exact v_{xc} for small molecules such as CO_2. Their findings are very much in the spirit of the discussed results for the homogeneous electron gas: outer valence electron energies are very accurately ($\approx 0.1\,\mathrm{eV}$ in comparison to experiment) recovered in *exact* KS theory, while lower valence electron energies start to deviate from experiment more significantly (by a few eVs) eventually reaching differences on the order of 20 eVs for the core levels. To summarize: orbital energies calculated from exact KS theory can provide highly accurate approximations to quasi-particle energies, especially for outer valence electrons, including the HOMO. However, to what extent this level of quality holds up to lower valence electron levels indeed depends on the system under study. With the exact version of v_{XC} being generally unknown, one however needs to rely on approximative forms for the exchange-correlation potential in KS DFT.

2.3. Approximations for exchange-correlation in Kohn-Sham theory and their drawbacks

The simplest approximation for the XC functional in DFT calculations is the LDA, here shown in its spin-unpolarized form:

$$E_{\mathrm{xc}}[n] = \int n(\boldsymbol{r}) e_{\mathrm{xc}}(n(\boldsymbol{r})) d^3r, \tag{2.11}$$

with $e_{xc}(n(\boldsymbol{r}))$ being the XC energy per particle of the homogeneous electron gas.[98,100] The exchange part of Eq. 2.11 –*i.e.* the exchange energy of one electron in the uniform electron gas of density n – is known analytically.[33,100] The correlation counterpart is usually obtained from Monte-Carlo simulations of the homogeneous electron gas. Many realistic systems do not exhibit a uniform distribution of their electrons (under this rather crude approximation, the success of the LDA is impressive). An extension to the LDA is the so-called generalized gradient approximation (GGA), again shown here without explicitly denoting its spin-dependence, which treats inhomogeneities in the density by

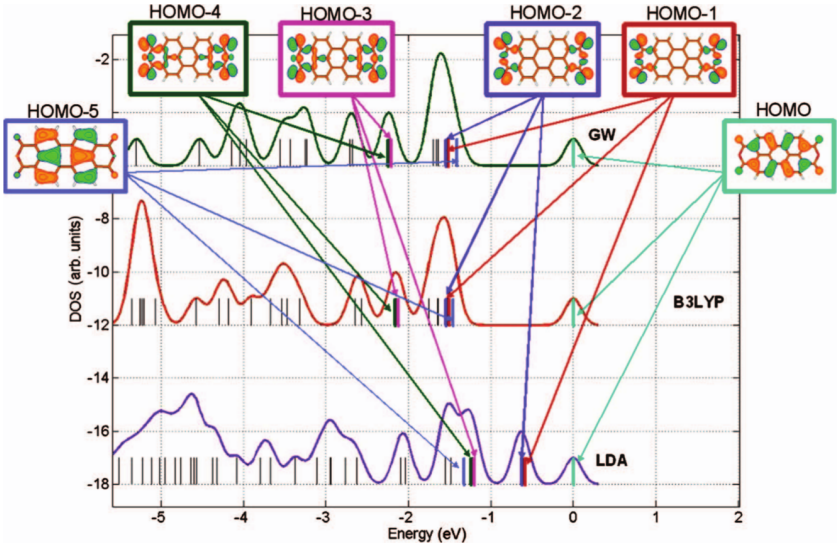

Figure 2.3.: Shifted valence electron spectra (see text of details) for the PTCDA molecule as calculated from *GW*, the conventional hybrid functional B3LYP and LDA. Real-space representations of selected orbitals associated with the energy levels of PTCDA are also shown. After Dori *et al.*, ref. 116. Copyright (2006) by The American Physical Society.

including the gradient of $n(\boldsymbol{r})$ acoording to:[33,97]

$$E_{\mathrm{xc}}[n] = \int n(\boldsymbol{r}) f\left(n(\boldsymbol{r}), \boldsymbol{\nabla} n(\boldsymbol{r})\right) d^3r. \tag{2.12}$$

$f\left(n(\boldsymbol{r}), \boldsymbol{\nabla} n(\boldsymbol{r})\right)$ is often constructed such that certain properties of the exact functional are recovered, and such that it obeys exact results for certain limits (such as the homogeneous electron gas). While the LDA clearly is a local approximation in the density, GGA is also known as a *semilocal* approximation.

Despite its apparent approximative character, (semi-)local KS DFT yields rather accurate predictions of many different physical observables of materials.[33,97] However, there are also some know deficiencies of these approximations, see Figure 2.3. In the following, I will focus on the deficiencies most relevant for *finite* electron systems such as atoms or molecules. First of all, it is by now well established that standard (semi-)local DFT functionals predict a too small HOMO-LUMO gap[33,34] and also fail to obey the above praised IP theorem for finite systems.[117] In this context, it is typically found that $\varepsilon_{\mathrm{HOMO}}^{\mathrm{LDA/GGA}}$ is too close to the vacuum energy compared to the experimental IP. The reason for this is rooted in the incorrect treatment of the asymptotic decay of the potential, which should be $-1/r$, but decays faster in conventional (semi-)local functionals. For example, the potential decays exponentially in the LDA.[118] Hence, the electron can "escape" the rest of the system too easily, as it spuriously interacts with itself as a consequence of the insufficient cancellation of the Hartree self-interaction by the XC energy.[118] This self-interaction error (SIE) manifests itself also in the one-electron energies, *i.e.* the KS

orbital energies, and at the one-electron level can be calculated as[119]

$$e_i = \langle\varphi_i| v_{\mathrm{H}}\left(|\varphi_i|^2\right)|\varphi_i\rangle + \langle\varphi_i| v_{\mathrm{xc}}\left(|\varphi_i|^2, 0\right)|\varphi_i\rangle\,, \tag{2.13}$$

where the e_i are the so-called orbital-SIE. For the exact KS functional, the e_i equal zero because the (unphysical) self-interaction of one electron introduced in v_{H} is exactly canceled by v_{xc}. In Fig. 2.3 the seminal results of Dori *et al.*[116] are shown. It can be seen that for the PTCDA molecule, a mixture of localized and delocalized orbitals occur in the outer valence electron region. Clearly, in the shifted[ii] LDA spectrum the orbitals more localized on the periphery of PTCDA lie too high in energy, while the orbitals more delocalized over the perylene backbone appear more correct in comparison to accurate *GW* calculations (and PES experiments).[116] Hybrid DFT functionals, where a portion of HF exchange is mixed with semilocal GGA exchange, were found to partially correct this error (see the results from the B3LYP functional in Fig. 2.3). Similar failures in the description of differently localized orbitals when (semi-)local KS calculations are used have been reported for phthalocyanine-type molecules.[120,121] For the prototypical PTCDA and 1,4,5,8-naphthalene tetracarboxylic dianhydride (NTCDA) this failure of common KS approximations was traced back to a largely different e_i (*cf.* Eq. 2.13) depending on the degree of spatial localization of the ith orbital:[119] more localized orbitals can be expected to "repel" themselves more strongly than delocalized ones. This electrostatic repulsion is not fully canceled by the one-electron XC energy in common KS approximations (leading to finite e_i), thus shifting more localized states spuriously to higher energies (lower binging energies).[119] Large differences in orbital-SIE can result in qualitatively wrong predictions of PES spectra from orbital energies: while the violation of the IP theorem "only" leads to a *rigid* shift of the orbital-energy spectrum with respect to the experiment, the orbital-SIE can distort the spectrum and even cause orbital-reordering.[119,120]

2.4. Range-separation and generalized Kohn-Sham

There is a fundamental reason why – as mentioned above – a hybrid DFT calculation can result in more accurate *shifted* orbital-energy spectra than calculations using purely (semi-)local functionals. HF is a self-interaction free theory as the one-electron Hartree self-repulsion is exactly canceled by corresponding Fock exchange. The portion of HF exchange "mixed" with GGA semilocal exchange can, thus, be seen as to mitigate the SIE and thus improve the description of differently localized orbitals. (see refs. 33, 116, 119–121 for details). The fact that HF is a SIE-free theory has a second important implication:[31,122,123] it retains the correct asymptotic $-1/r$ form of the potential. Importantly, this does not imply that the HOMO energy calculated from HF is more accurate in predicting the IP than (semi-)local flavors of DFT (except for one-electron systems, where HF theory is exact). In fact, HF theory does not include any correlation, which

[ii] Shifted means that the HOMO energies in different spectra are aligned to compare relative differences.

typically results in a strong overbinding of the HOMO. However, the intrinsic features of HF offer an avenue to correct the above-reviewed drawbacks of conventional (semi-)local functionals: the use of OT-RSH functionals.[34]

I will only very briefly report the basic idea of using OT-RSH functionals because publication IV enclosed in Part II of this thesis extensively discusses the formalism and background of it. Beyond this, the interested reader is referred to the reviews refs. 34, 123 for a very detailed discussion of OT-RSH functionals. The idea of range-separation was introduced by Savin and co-workers,[124] and denotes the separation of the active range of the Coulomb operator into short- and long-range parts. One way to realize this range-separation is through using the error- and complementary error-function to replace the $1/r$ operator in the potential, *i.e.* $r^{-1} = r^{-1}\mathrm{erf}(\gamma \mathrm{r}) + \mathrm{r}^{-1}\mathrm{erfc}(\gamma \mathrm{r})$. From the above discussion of the exact $-1/r$ asymptotical behavior of the potential, it appears reasonable to enforce Fock-exchange in the long-range, as this will guarantee the correct asymptotic decay. In the short-range one, however, wants to maintain compatible exchange and correlation, for example through a semilocal GGA XC potential.[125] The one fundamental parameter determining the properties of the so-obtained functional is the range-separation parameter γ: In the limit of small and large γ values one approaches the full GGA and Fock-like potentials, respectively. The central idea of optimal tuning is to adjust γ such that a physical constraint is fullfilled, *i.e.* until the asymptotic decay of the OT-RSH potential is $-1/r$. Importantly, one can show that a functional fulfilling the IP theorem Eq. 2.7 automatically restores the correct asymptotic decay.[34,104,125] Therefore, in OT-RSH functionals one tunes γ until the calculated HOMO energy $\varepsilon_{\mathrm{HOMO}}$ equals the IP calculated from total-energy differences. Note that OT-RSH is a non-empirical procedure for calculating the electronic properties of finite systems such as atoms and molecules. Even for rather complex molecules such as PTCDA, it has has been shown to yield very accurate HOMO energies and HOMO-LUMO gaps as compared to experimental IPs and fundamental gaps, respectively.[126–128]

The latter is surprising, as according to the discussion in Sect. 2.2 one expects a too shallow HOMO-LUMO gap compared to the exact experimentally obtained fundamental gap. Recall that these findings are valid for KS theory, which involves the mapping from the physical and fully-interacting onto a fictitious non-interacting system. The Fock-exchange operator employed in the OT-RSH-scheme is *orbital dependent*.[33] Formally, this orbital-dependent version of DFT is known as generalized Kohn-Sham (GKS) theory, which in contrast to "traditational" KS theory involves a mapping from the physical system with N interacting electrons onto a system of (partially) interacting electrons which can still be represented by a single Slater-determinant.[129] While there is only one exact KS map, there is a multitude of GKS maps[34] one of which is the exact KS map itself. Using a nonlocal potential in the theoretical description such as introduced by the Fock-exchange operator yields a potential that is different for each orbital.[33,34] Most importantly, such orbital-dependent v_{xc} in principle allow for a derivative discontinuity in the XC potential,[31,33,34] which is absolutely crucial for obtaining a correct fundamental gap from orbital energy differences.[34] One can then seek the GKS map (*i.e.*, the GKS

functional) for which $\varepsilon_{\mathrm{HOMO}}(N)$ and $\varepsilon_{\mathrm{LUMO}}(N)$ correctly predict $IP(N)$ and $EA(N)$.[34] Therefore, one can tune γ until the IP theorem for the neutral (involving $IP(N)$) and for the anion (involving $IP(N+1) = EA(N)$) are fulfilled as closely as possible at the same time.[126] Stein *et al.* showed that a very accurate *simultaneous* identification of $\varepsilon_{\mathrm{HOMO}}(N)$ with $IP(N)$ and $\varepsilon_{\mathrm{LUMO}}(N)$ with $EA(N)$, *i.e.*, the accurate prediction of the fundamental gap from orbital energies calculated in ground state DFT, is possible by using the OT-RSH strategy.[126] This finding clearly renders OT-RSH functionals as a highly interesting candidate for theoretically predicting the electronic structure of finite electron systems such as molecules. Publication IV enclosed in Part II takes this approach to the next level and discusses the reliability of it for predicting the outer-valence electron spectrum of different organic molecules.

One of the central themes that was initially conceived for this thesis was to develop a theoretical scheme that corrects the well-known "level alignment problem" at metal-organic interfaces (see, *e.g.*, ref. 130). This issue describes the fact that the molecular states as calculated from the popular LDA or GGA are energetically too close to the metal Fermi-level, which influences the charge-transport characteristics of molecular devices (see, *e.g.*, ref. 131). Together with G. Heimel (Humboldt-Universität zu Berlin) and Egbert Zojer I started to work on a strategy to realize an appropriate correction. As a first ingredient, the electronic levels of molecules in the gas phase require a correction when calculated with standard approximations in KS theory. Therefore, I joined L. Kronik and S. Refaely-Abramson (Weizmann Institute) in their work on the above-introduced OT-RSH scheme to correct the electronic structure of organic molecules. The latter evolved into an extensive collaborative effort that eventually resulted in publication IV, which is enclosed in its current form as a draft in Part II of this thesis. It contains a thorough quantitative investigation regarding the accuracy of OT-RSH DFT functionals.

Alas, the simple fact that a Ph.D. thesis is limited in time prevented the successful completion of our initial plan to correct the energy levels at metal-organic interfaces, where we have so far completed the correction of the gas-phase molecular levels as the first step. I very much hope that our ideas serve as a starting point for future work.

In parallel I also established the usage of conventional hybrid DFT functionals for treating extended metal-organic systems in our group. These functionals are orbital-dependent and correct some of the drawbacks inherent to LDA and GGA (*vide supra*). However, their reliability for predicting the electronic structure of finite systems is far behind the OT-RSH scheme. In the absence of an OT-RSH scheme for periodic systems, and with the above-mentioned correction scheme not yet developed, the usage of conventional hybrid functionals proofed to be helpful, especially when differently localized states occur in the molecular electronic structure. This strategy was so far applied in two articles, one of which is publication II contained in this thesis.

The next Part represent the main results of my Ph.D. thesis, which are enclosed as original publications.

Part II.

Original Publications

3. Publication I (ref. 1)

3.1. Original Article

Polarity Switching of Charge Transport and Thermoelectricity in Self-Assembled Monolayer Devices

*David A. Egger, Ferdinand Rissner, Egbert Zojer, and Georg Heimel**

Decreasing the size of electronic devices through top-down approaches has its intrinsic limits. Therefore, bottom-up approaches to nanoelectronics based on individual functional molecules constitute an appealing alternative in principle.[1] In practice, however, such devices are challenging to realize because contacts need to be structured down to the molecular scale as well. Compatible with current structuring techniques are devices based on self-assembled monolayers (SAMs) of organic molecules covalently linked to metallic electrodes.[2,3] There, the electrodes are laterally extended *and* charge transport occurs at the desired nanoscale across the SAM. Functionality is introduced to the device through targeted chemical design of the constituting molecules. Such strategies often rely on the individual molecules to maintain their intended function within the completed SAM device. This is, however, not necessarily the case,[4–7] which calls for design criteria that encompass the interrelation between the electrical properties of individual molecules and monolayers.

In the present theoretical work we demonstrate that, through the collective electrostatic action of intramolecular dipoles within the SAM, already the most basic measurable quantity of an electronic device, the current at a given voltage, can be strikingly different for isomeric molecules that exhibit virtually identical frontier-orbital energies as isolated species. More importantly, the same collective electrostatic effect can even reverse the polarity of charge transport across such SAMs, i.e., it can determine whether electronic transport is established *via* occupied (p-type) or unoccupied (n-type) electronic states.[8] Understanding this intriguing effect represents an important step towards establishing viable guidelines for the rational design of functional elements in future molecular electronic devices.

We chose to illustrate the consequences of aligned polar bonds in close-packed self-assembled molecular monolayers on the basis of a prototypical model system in molecular electronics, the so-called 'Tour wire' (**Figure 1**a).[9] Both in single-molecule and SAM devices, Tour wires have been frequently functionalized by chemical substitution at the central ring as indicated in Figure 1b, *e.g.*, dipoles introduced by polar amino and/or nitro groups have been suggested to lead to negative differential resistance,[10] switching,[11] and rectification.[12] However, such side groups might detrimentally affect the close packing and high degree of order observed in SAMs of unsubstituted Tour wires.[13] Therefore, also alternative chemical design strategies have been pursued to imbue molecular wires with electrical dipole moments. For instance, fluorination of one of the terminal phenyl rings in Tour-wire based systems[14,15] or distributing dipoles[16] within the backbone of oligo(*para*-phenylene)s has been seen to trigger molecular-level switching and/or diode behavior in respective single-molecule junctions.[17] Here, we explore a conceptually different approach. Specifically, we built chemical modifications directly into the molecular backbone by *symmetrically* replacing the two outermost phenyl rings of a Tour wire with pyrimidine rings, resulting in the N_{in} molecule (Figure 1c). Note that, other than in the aforementioned strategies for chemical design,[9–12,14–17] N_{in} has no net dipole moment. Rather, polar bonds within the pyrimidine units and on the thiol anchoring groups add up to local dipole moments at both 'ends' of the molecule (arrows in Figure 1c). In contrast to previous studies,[18,19] where changing the anchoring groups from thiols to isocyanines has been observed to reverse the polarity of charge transport through SAMs, we compare N_{in} to its equally thiolated isomer N_{out} (Figure 1d). There, local pyrimidine and S-H dipoles point in opposite directions on both ends of the molecule and, consequently, both the local and the net molecular dipole moments are essentially zero. Importantly, we calculated the highest occupied and lowest unoccupied fully delocalized π-orbitals (see Supporting Information) to be only ~0.1 eV higher in energy for the isolated N_{in} molecule than for N_{out}. As the alignment of these highest occupied (HOTC) and lowest unoccupied end-to-end transport channels (LUTC) with the Fermi level, E_F, of external electrodes has emerged as a dominant parameter controlling current flow through molecular junctions,[2,20] one might expect equally similar electrical characteristics of N_{in} and N_{out}.

To compare the charge-transport properties of these two species, we sandwiched SAMs of N_{in} and N_{out} between two gold electrodes (Figure 1e) and performed density-functional theory (DFT) based electronic structure[21,22] and transport calculations.[23] The result of this procedure is the transmission function, T(E), which describes the 'probability' for an electron impinging on the device from out of one electrode at a certain energy E to be transmitted through the SAM into the other electrode. Current-voltage (*I–V*) characteristics were then evaluated using:[8]

$$I(V) = \frac{2e}{h} \int dE \left[f(E - \mu_{left}) - f(E - \mu_{right}) \right] T(E) \qquad (1)$$

where $f(x)$ is the Fermi-Dirac occupation function (at 300 K unless otherwise noted) and $\mu_{left,right} = E_F \pm e\frac{V}{2}$ with e the

D. A. Egger, Dr. G. Heimel
Institut für Physik
Humboldt-Universität zu Berlin
Brook-Taylor-Strasse 6, 12489 Berlin, Germany
E-mail: georg.heimel@physik.hu-berlin.de
D. A. Egger, Dr. F. Rissner, Prof. E. Zojer
Institute of Solid State Physics
Graz University of Technology
Petersgasse 16, 8010 Graz, Austria

DOI: 10.1002/adma.201200872

ADVANCED MATERIALS
www.advmat.de
www.MaterialsViews.com

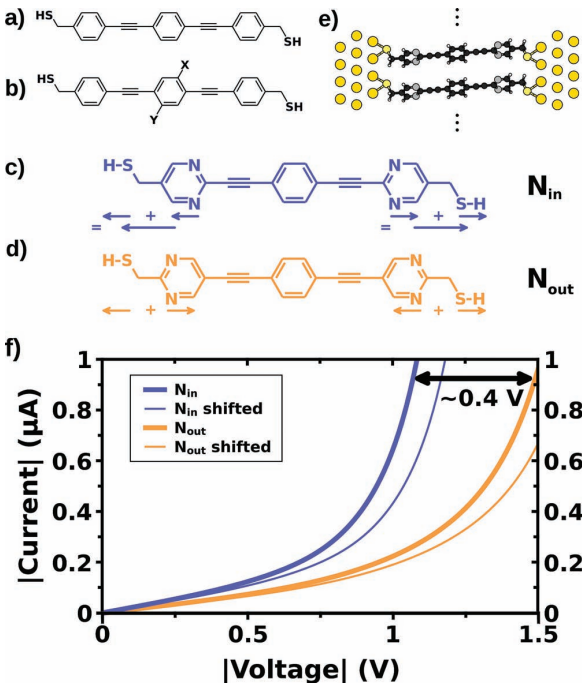

Figure 1. (a) Unsubstituted and (b) substituted Tour wire. (c) N_{in} and (d) N_{out} molecules with arrows indicating local dipoles. (e) Side view of the N_{in} SAM-device structure. (f) Calculated current-voltage characteristics of the SAM devices; thin lines were computed from shifted transmission functions (see text for details). The current is reported per unit cell (area 30.2 Å^2) containing one molecule.

elementary charge. The reader is referred to the Experimental Section for details on the system setup and the computational methodology; a critical assessment of the employed level of theory (briefly summarized also at the end of this communication) is given in the Supporting Information.

The calculated *I–V* curves for the N_{in} and N_{out} SAMs are shown in Figure 1f (thick lines). Despite the fact that the frontier transport-channel energies of the isolated molecules are very similar, we find pronounced differences between the two monolayers: For the N_{in} SAM, the current is up to a factor of 9 (at 1.4 V) higher in the low-bias regime; in fact, the applied bias voltage would have to be ~0.4 V higher to arrive at a comparable current through the N_{out} SAM. Note that this difference is not related to the (small) energy difference between the respective orbitals in the isolated molecules (~0.1 eV). Just to illustrate this, we shifted the transmission curves 0.05 eV down for the N_{in} and 0.05 eV up for the N_{out} SAM and re-calculated the *I–V* curves *via* Equation (1). The difference between the two systems is fully conserved (Figure 1f, thin lines).

However, the fact that the *I–V* curves of N_{in} and N_{out} devices shift in the *same* direction upon shifting the transmission curves in *opposite* directions already presages the fundamentally different nature of charge transport through the SAMs, which becomes more apparent when the current through occupied and unoccupied states is calculated separately; technically, this is achieved by setting T(E) = 0 for E > E_F and T(E) = 0 for E < E_F, respectively, and re-evaluating Equation (1). The results in **Figure 2**a show that N_{in} SAMs primarily conduct *via* occupied (p-type), and N_{out} SAMs primarily *via* unoccupied (n-type) channels. It has been theoretically proposed[8] that such a change in the polarity of charge-transport from p-type to n-type should be experimentally accessible through the thermoelectric properties of the SAMs. This has recently been demonstrated by heating the substrate supporting the molecular monolayers and measuring thermoelectricity with the conductive tip of a scanning-tunneling[18,24,25] or atomic-force microscope.[26] To provide a thusly testable prediction for the present systems, we calculated the thermoelectric current by imposing zero bias voltage, *i.e.*, by setting V = 0 in Equation (1), and continuously varying the temperatures of the two contacts, which enter Equation (1) through the broadening of the respective Fermi functions. Indeed, upon applying a temperature gradient across the SAMs, the direction of charge flow is reversed between N_{in} and N_{out} (Figure 2b). Accordingly, the Seebeck coefficients, extracted from our calculated zero-bias transmission functions as ~+17 μV/K for the N_{in} and ~ −15 μV/K for the N_{out} SAMs, are of opposite sign.

These charge-transport characteristics naturally originate in the relative energetic alignment of the molecular transport channels and E_F in the completed devices. To understand the above-described differences between N_{in} and N_{out}, we thus compare the corresponding transmission functions in **Figure 3**a and realize that, other than in the free molecules, corresponding

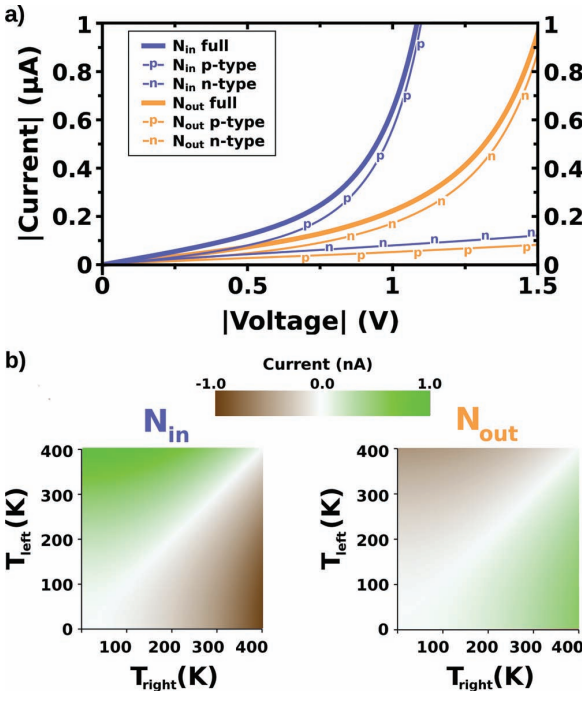

Figure 2. (a) Calculated current through occupied ('p') and unoccupied states ('n'); thick lines indicate the total current from Figure 1f. (b) Thermoelectric current calculated for the N_{in} and N_{out} monolayers (see text for details). A positive current signifies a flow of electrons from right to left.

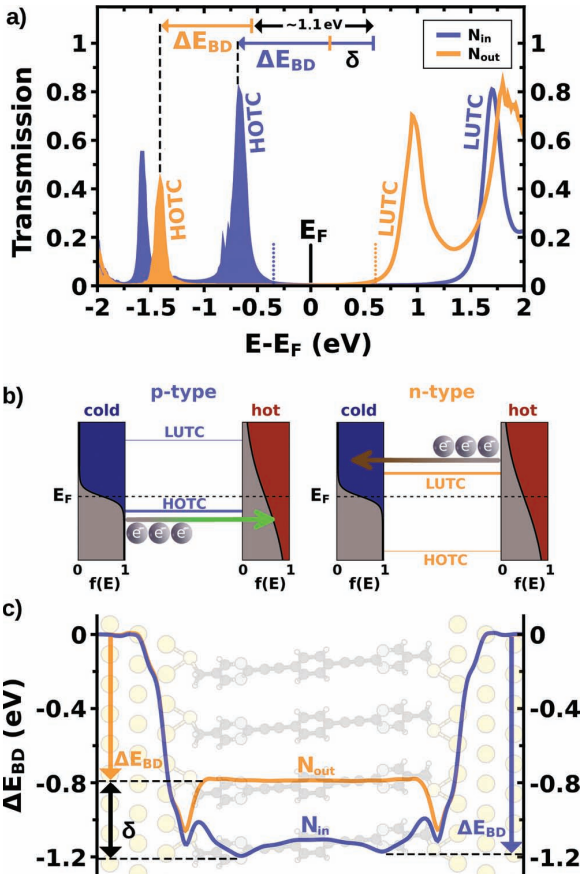

Figure 3. (a) Calculated transmission functions for the N_{in} and N_{out} SAM devices; the Fermi level, E_F, is set as zero. HOTC denotes the highest occupied and LUTC the lowest unoccupied transmission channels; dotted lines indicate the respective onsets. (b) Cartoons showing how contacts of different temperature, due to different Fermi-Dirac occupations, f (E), give rise to thermocurrents of opposite sign through N_{in} (left) and N_{out} (right) SAM devices. (c) Interfacial potential-energy steps, ΔE_{BD}, arising from metal/SAM bonding and the difference, δ, between ΔE_{BD} of N_{in} and N_{out}; these quantities are also indicated in (a).

transport channels of the two SAMs now differ in energy by ~0.7 eV; as T(E) is intimately related to the density of states (see Supporting Information), this relative shift would be experimentally testable by photoelectron spectroscopy on N_{in} and N_{out} SAMs adsorbed on conducting substrates. An important consequence of the difference in energy-level alignment is that the channel closest to E_F, which determines transport polarity, is the HOTC for N_{in} and the LUTC for N_{out}. Moreover, the onset of transmission is ~0.2 eV closer to E_F for N_{in} (dotted lines). As, in the (symmetric) systems considered here, half of the applied voltage drops between the Fermi energy of each electrode and the SAM conduction channels, the bias has to be increased by $\sim 2 \times 0.2 = 0.4$ eV for N_{out} to attain a total current comparable to that through N_{in}, which translates into the voltage difference of ~0.4 V highlighted in Figure 1f.

Furthermore, T(E) dictates[8,18,24–26] the observed sign of the thermocurrent (Figure 3b): Applying different temperatures to the contacts changes the width of their respective Fermi-Dirac electron occupation functions. N_{in} SAMs provide a transport channel (the HOTC) at an energy below E_F, where the concentration of electrons is higher on the cold electrode, thus driving them towards the hot electrode (p-type). In contrast, N_{out} provides a transmission pathway (the LUTC) at an energy above E_F, where electrons are driven from hot to cold (n-type).

In search for the origin of the qualitative differences between the transmission functions of the two systems, we first computed the step in the potential energy, ΔE_{BD}, which arises from the interfacial charge re-arrangements associated with SAM-Au bond formation and which shifts all monolayer electronic states relative to E_F (for details see Ref. [27]). Due to the different positions of the nitrogens, ΔE_{BD} is indeed different for N_{in} and N_{out} (Figure 3c). While the origin of this difference might be a potentially interesting detail by itself, we refer the reader to Ref. [28] for a discussion of these interfacial 'bond dipoles' as well as their impact on energy-level alignment, and focus here on the remarkable fact that, in contrast to Refs. [18,26], it is of the wrong sign to explain the observed differences in the alignment of the frontier conduction channels with E_F: starting from the (almost) identical situation in the free molecules, the electronic states of N_{in} are apparently shifted *down more* in energy (by $\delta \sim 0.4$ eV) relative to E_F than those of N_{out}. And yet, in the SAM device, the transport channels of N_{in} are *higher* in energy (by *ca.* 0.7 eV) with respect to E_F than those of N_{out} (Figure 3a).

This implies that, in contrast to the situation for isolated molecules, the energies of both HOTC and LUTC have to differ substantially between N_{in} and N_{out} SAMs already prior to contact with the metallic leads. To test this hypothesis, we calculated the electronic structure of the respective free-standing monolayers (*i.e.*, without gold electrodes), where sulfurs are saturated with hydrogens. Indeed, we find the transport channels in the N_{in} monolayer to be ~1.1 eV closer to the vacuum level, E_{vac}, than those of N_{out} (see Supporting Information). This appreciable difference can be understood on the basis of the local dipoles indicated in Figures 1c and 1d.[29] For N_{in}, SAM formation corresponds to arranging the local net dipoles at each end of the individual molecules (Figure 1c) into surface dipole layers on both sides of the monolayer.[29] We emphasize that, as they are located entirely on the organic part of the SAM device, they act independently of and in addition to well-understood metal/organic interface effects already captured by ΔE_{BD}.[27,30] These *all-organic surface dipole layers* create steps in the potential energy (**Figure 4**, left center panel), which lift the entire potential-energy landscape around the molecular backbones and, with it, the transport channels towards E_{vac} (compare left top and bottom panels). In contrast, for N_{out}, the local pyrimidine and thiol dipoles almost perfectly cancel on both ends of the molecule (Figure 1d) and, thus, induce only minor modifications to the potential-energy landscape upon SAM formation (right panels in Figure 4). As discussed above, the resulting difference in HOTC and LUTC energies between the free-standing N_{in} and N_{out} monolayers is subsequently mitigated by the binding of the SAMs to the electrodes, where the transport channels of N_{in} are shifted down more with respect to E_F by

ADVANCED MATERIALS
www.advmat.de

Materials Views
www.MaterialsViews.com

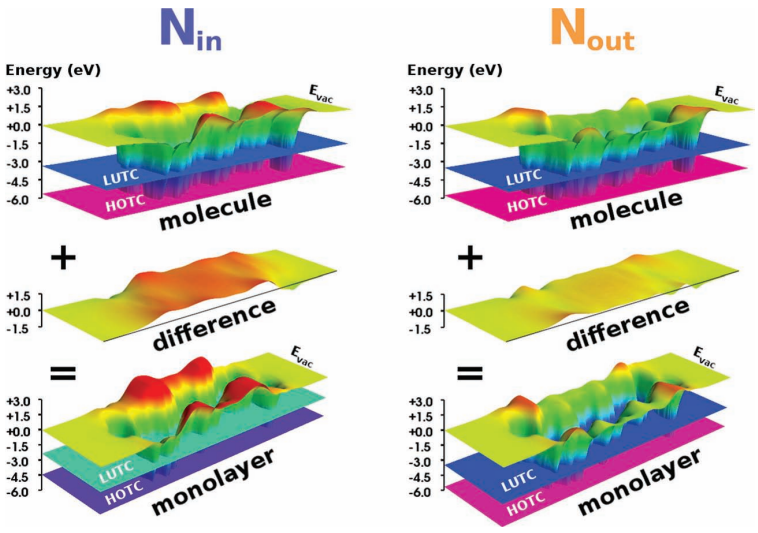

Figure 4. (top) DFT-calculated potential-energy wells and energies of the highest occupied (HOTC) and lowest unoccupied (LUTC) end-to-end delocalized π-orbitals relative to the vacuum level, E_{vac}, for the isolated N_{in} and N_{out} molecules. (center) Potential-energy differences arising upon assembly of the individual molecules into the respective SAMs. (bottom) Potential-energy wells and HOTC/LUTC energies of the respective SAMs.

$\delta \sim 0.4$ eV (Figure 3c). This then results in the final situation (Figure 3a) with the transport channels of N_{in} lying higher in energy by *ca.* $1.1 - 0.4 = 0.7$ eV than those of N_{out}, the HOTC of N_{in} being closer to E_F than the LUTC of N_{out} and, in particular, the different polarity of charge transport and thermoelectric current through the N_{in} and N_{out} SAMs. The purely electrostatic origin of the effect just described underlines its fundamental nature[31] and additional results on systems following the same design principle of local dipoles introduced *via* polar bonds confirm that it is by no means limited to the N_{in}/N_{out} pair of molecules (see Supporting Information Figure S3).

In a final note we remark that, because it originates in polar bonds within the SAMs themselves, the effect just explained should, in principle, be independent of details in the local S-Au docking geometry.[32] Also, we briefly comment on the potential impact of shortcomings in the applied computational methodology: While in the Supporting Information we explicitly show that the choice of the DFT functional is inconsequential, it is well established that the Kohn-Sham gap underestimates the transport gap of (organic) semiconductors and that (semi-)local approximations to the exchange-correlation functional cannot capture polarization-induced reductions of the gap.[33] However, as also demonstrated in the Supporting Information, the observed polarity switch between N_{in} and N_{out} persists as long as potential upwards corrections to the DFT-calculated LUTC energies do not exceed potential downwards corrections to the HOTC energies by more than ~0.6 eV. Even in case they did, however, the collective electrostatic action of intramolecular dipoles would still give rise to an even more pronounced and equally unexpected difference in the total current through N_{in} and N_{out} SAMs.

In summary, two isomeric molecules with essentially identical energies of their frontier delocalized π-orbitals were found to result in two SAM devices with substantially different charge-transport characteristics: The total current in the low-bias regime differs by up to one order of magnitude and the polarity of charge transport through the SAMs switches from p- to n-type, entailing a reversal in the sign of the thermoelectric current and, thereby, of the Seebeck coefficient. These observations are rationalized through the formation of organic surface dipole layers as individual molecules comprising polar bonds are assembled into close-packed SAMs. Our present study thus highlights the collective electrostatic action of deliberately introduced polar bonds on the periphery of otherwise non-polar molecules as a new strategy for controlling device functionality beyond altering molecular dipole moments and anchoring chemistry. It clearly shows that understanding materials properties at the molecular level is of undisputed relevance, but remains far from sufficient for predicting the behavior of more complex systems, such as assemblies of molecules in a monolayer-based electronic device. It is stressed here that considering collective effects is an essential prerequisite for the rational design of functional elements in future molecular electronic circuits.

Experimental Section

To isolate the effect of the molecular chemical structure on charge transport through the SAMs, we exploited the inherent advantages of a computational approach, namely, that extrinsic influences can conveniently be controlled. In particular, we disregarded potential reconstructions of the gold surface[32] and chose a co-facial[34] over a possible herringbone[13] molecular packing; methylene spacers between the thiol and the pyrimidine units (Figures 1c and 1d) are introduced to reduce the electronic coupling between metal contacts and the molecular cores, thus preserving their intrinsic electronic structure in a SAM device and suppressing the potential impact of molecular orientation on transport characteristics.[35] All species were optimized in gas-phase and assembled into 2D-periodic monolayers without further geometry relaxation. The monolayers were then sandwiched between two (111)-terminated gold electrodes with one molecule per $p(2 \times 2)$ surface unit-cell (Figure 1e, area per molecule 30.2 Å^2). Sulfur-gold bonding was assumed to proceed through cleavage of the thiols' hydrogens and the sulfur adsorption site was predetermined in a separate calculation of methylthiolate on Au(111).

Our study relies on DFT using the gradient-corrected exchange-correlation (XC) functional of Perdew, Burke, and Ernzerhof.[36] Geometry optimizations (force cutoff 0.01 eV/Å) of the isolated molecules and electronic-structure calculations of free-standing 2D-periodic monolayers (8×8 $k_{\|}$-points) were performed with the VASP code[21] using the projector augmented-wave method[37] and a plane-wave cutoff of 20 Ryd. To solve the electronic scattering problem, we extracted the Hamiltonian and overlap matrices from a SIESTA[22] calculation on bulk gold in a $(2 \times 2 \times \sqrt{6})$ supercell ($8 \times 8 \times 6$ k-points, double-ζ polarized atomic-orbital basis set). Recursive Green's function techniques[23,38] were then employed to compute the self-energies, $\Sigma_{left,\ right}$, of the leads.[23] The (zero-bias) transmission function T(E) was subsequently obtained as:

$$T(E) = \sum_{k_\parallel} w_{k_\parallel} \cdot \mathrm{Tr}\left[\Gamma_{\mathrm{left}} G_D \Gamma_{\mathrm{right}} G_D^\dagger\right] \quad (2)$$

with

$$\Gamma_{\mathrm{left,right}} = i\left[\Sigma_{\mathrm{left,right}} - \Sigma_{\mathrm{left,right}}^\dagger\right] \quad (3)$$

and G_D the retarded Green's function of the device region (comprising the SAM and 6 layers of gold as shown in Figure 1e) extracted from a second SIESTA calculation (8×8 $k_\parallel$-points with weights $w_{k_\parallel}$).[23] All computational parameters were well converged as benchmarked in Ref. [39].

Finally, current-voltage (I–V) characteristics were evaluated using Equation (1) and Seebeck coefficients, S, were obtained as:[8]

$$S = \frac{-\pi^2 k_B^2 T}{3|e|} \frac{1}{T(E)} \frac{\partial T(E)}{\partial E}\bigg|_{E=E_F} \quad (4)$$

where k_B is the Boltzmann constant, T is the average temperature of the device (300 K) and e is the charge of an electron. Note that, in general, the transmission function $T(E) = T(E,V)$, but neglecting the bias dependence has been shown to have only a minor impact at the relatively low voltages considered here.[40] 3D-representations of the systems were generated with XCrysDen.[41]

Supporting Information

Supporting Information is available from the Wiley Online Library or from the author.

Acknowledgements

The authors thank L. Beverina, A.M. Kelterer, C. Slugovc, and S. Hecht for helpful discussions. D.A.E. is a recipient of a DOC scholarship by the Austrian Academy of Sciences. Financial support by the Austrian Science Fund (FWF): P20972-N20, the Integrative Research Institute for the Sciences (IRIS) Adlershof, and the DFG program SPP 1355 is gratefully acknowledged.

Received: March 1, 2012
Revised: May 9, 2012
Published online: July 16, 2012

[1] H. Song, M. A. Reed, T. Lee, *Adv. Mater.* **2011**, *23*, 1583.
[2] H. B. Akkerman, P. W. M. Blom, D. M. de Leeuw, B. de Boer, *Nature* **2006**, *441*, 69.
[3] A. J. Kronemeijer, H. B. Akkerman, T. Kudernac, B. J. van Wees, B. L. Feringa, P. W. M. Blom, B. de Boer, *Adv. Mater.* **2008**, *20*, 1467.
[4] Y. Selzer, L. Cai, M. A. Cabassi, Y. Yao, J. M. Tour, T. S. Mayer, D. L. Allara, *Nano Lett.* **2005**, *5*, 61.
[5] A. Landau, L. Kronik, A. Nitzan, *J. Comp. Theor. Nanosci.* **2008**, *5*, 535.
[6] M. G. Reuter, G. C. Solomon, T. Hansen, T. Seideman, M. A. Ratner, *J. Phys. Chem. Lett.* **2011**, *2*, 1667.
[7] M. G. Reuter, T. Seideman, M. A. Ratner, *Nano Lett.* **2011**, *11*, 4693.
[8] M. Paulsson, S. Datta, *Phys. Rev. B* **2003**, *67*, 241403R.
[9] L. A. Bumm, J. J. Arnold, M. T. Cygan, T. D. Dunbar, T. P. Burgin, L. Jones, D. L. Allara, J. M. Tour, P. S. Weiss, *Science* **1996**, *271*, 1705.
[10] J. Chen, M. A. Reed, A. M. Rawlett, J. M. Tour, *Science* **1999**, *286*, 1550.
[11] Z. J. Donhauser, B. A. Mantooth, K. F. Kelly, L. A. Bumm, J. D. Monnell, J. J. Stapleton, D. W. Price Jr., A. M. Rawlett, D. L. Allara, J. M. Tour, P. S. Weiss, *Science* **2001**, *292*, 2303.
[12] F.-R. F. Fan, Y. Yao, L. Cai, L. Cheng, J. M. Tour, A. J. Bard, *J. Am. Chem. Soc.* **2004**, *126*, 4035.
[13] A.-A. Dhirani, R. W. Zehner, R. P. Hsung, P. Guyot-Sionnest, L. R. Sita, *J. Am. Chem. Soc.* **1996**, *118*, 3319.
[14] M. Elbing, R. Ochs, M. Koentopp, M. Fischer, C. von Hänisch, F. Weigend, F. Evers, H. B. Weber, M. Mayor, *Proc. Natl. Acad. Sci. USA* **2005**, *102*, 8815.
[15] P. A. Lewis, C. E. Inman, F. Maya, J. M. Tour, J. E. Hutchison, P. S. Weiss, *J. Am. Chem. Soc.* **2005**, *127*, 17421.
[16] D. A. Egger, F. Rissner, G. M. Rangger, O. T. Hofmann, L. Wittwer, G. Heimel, E. Zojer, *Phys. Chem. Chem. Phys.* **2010**, *12*, 4291.
[17] I. Díez-Pérez, J. Hihath, Y. Lee, L. Yu, L. Adamska, M. A. Kozhushner, I. I. Oleynik, N. Tao, *Nat. Chem.* **2009**, *1*, 635.
[18] K. Baheti, J. A. Malen, P. Doak, P. Reddy, S.-Y. Jang, T. D. Tilley, A. Majumdar, R. A. Segalman, *Nano Lett.* **2008**, *8*, 715.
[19] C. D. Zangmeister, J. M. Beebe, J. Naciri, J. G. Kushmerick, R. D. van Zee, *Small* **2008**, *4*, 1143.
[20] Y. Xue, S. Datta, M. A. Ratner, *J. Chem. Phys.* **2001**, *115*, 4292.
[21] G. Kresse, J. Furthmüller, *Phys. Rev. B* **1996**, *54*, 11169.
[22] J. M. Soler, E. Artacho, J. D. Gale, A. García, J. Junquera, P. Ordejón, D. Sánchez-Portal, *J. Phys.: Condens. Matter* **2002**, *14*, 2745.
[23] M. Nardelli, *Phys. Rev. B* **1999**, *60*, 7828.
[24] P. Reddy, S.-Y. Jang, R. A. Segalman, A. Majumdar, *Science* **2007**, *315*, 1568.
[25] J. R. Widawsky, P. Darancet, J. B. Neaton, L. Venkataraman, *Nano Lett.* **2012**, *12*, 354.
[26] A. Tan, J. Balachandran, S. Sadat, V. Gavini, B. D. Dunietz, S.-Y. Jang, P. Reddy, *J. Am. Chem. Soc.* **2011**, *133*, 8838.
[27] G. Heimel, F. Rissner, E. Zojer, *Adv. Mater.* **2010**, *22*, 2494.
[28] G. Heimel, L. Romaner, E. Zojer, J.-L. Brédas, *Nano Lett.* **2007**, *7*, 932.
[29] G. Heimel, I. Salzmann, S. Duhm, N. Koch, *Chem. Mater.* **2011**, *23*, 359.
[30] O. L. A. Monti, M. P. Steele, *Phys. Chem. Chem. Phys.* **2010**, *12*, 12390.
[31] A. Natan, L. Kronik, H. Haick, R. T. Tung, *Adv. Mater.* **2007**, *19*, 4103.
[32] C. Vericat, M. E. Vela, G. Benitez, P. Carro, R. C. Salvarezza, *Chem. Soc. Rev.* **2010**, *39*, 1805.
[33] J. M. Garcia-Lastra, C. Rostgaard, A. Rubio, K. S. Thygesen, *Phys. Rev. B* **2009**, *80*, 245427.
[34] S. Sek, *Langmuir* **2009**, *25*, 13488.
[35] I. Diez-Perez, J. Hihath, T. Hines, Z.-S. Wang, G. Zhou, K. Müllen, N. Tao, *Nat. Nanotechnol.* **2011**, *6*, 226.
[36] J. P. Perdew, K. Burke, M. Ernzerhof, *Phys. Rev. Lett.* **1996**, *77*, 3865.
[37] G. Kresse, D. Joubert, *Phys. Rev. B* **1999**, *59*, 1758.
[38] M. P. L. Sancho, J. M. L. Sancho, J. M. L. Sancho, J. Rubio, *J. Phys. F: Met. Phys.* **1985**, *15*, 851.
[39] M. Strange, I. S. Kristensen, K. S. Thygesen, K. W. Jacobsen, *J. Chem. Phys.* **2008**, *128*, 114714.
[40] Y. Xue, M. Ratner, *Phys. Rev. B* **2003**, *68*, 115406.
[41] A. Kokalj, *Comput. Mater. Sci.* **2003**, *28*, 155.

3.2. Supporting Information

Submitted to ADVANCED MATERIALS

Supporting Information to

Polarity Switching of Charge Transport and Thermoelectricity in Self-Assembled Monolayer Devices

By *David A. Egger, Ferdinand Rissner, Egbert Zojer,* and *Georg Heimel*[*]

[*] Dr. G. Heimel, D.A. Egger
Institut für Physik
Humboldt-Universität zu Berlin
Brook-Taylor-Strasse 6, 12489 Berlin (Germany)
E-mail: georg.heimel@physik.hu-berlin.de
Prof. E. Zojer, D.A. Egger, Dr. F. Rissner
Institute of Solid State Physics
Graz University of Technology
Petersgasse 16, 8010 Graz (Austria)

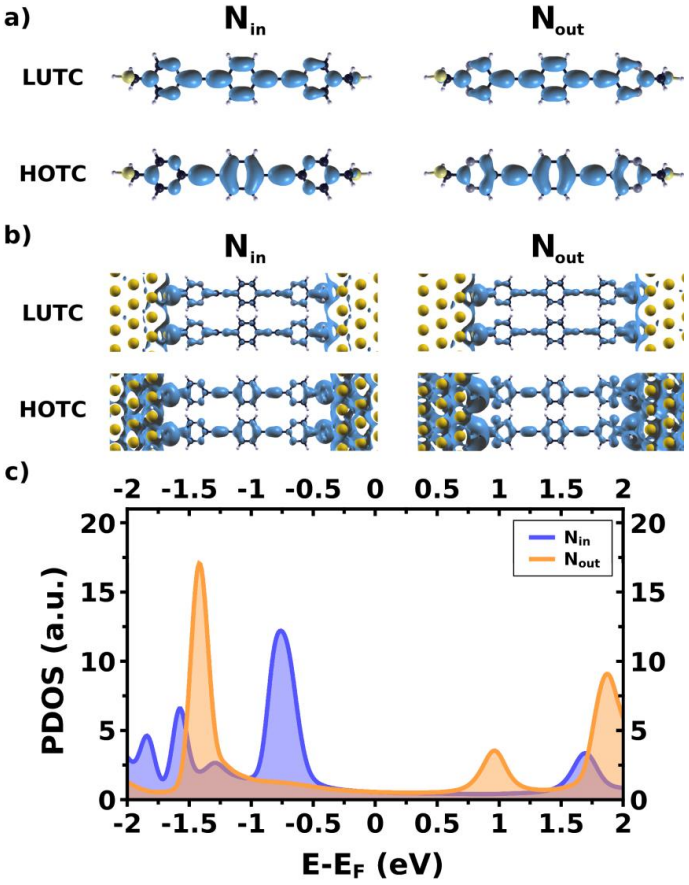

FIGURE S1: (a) Iso-surface representations of the highest occupied (bottom) and lowest unoccupied (top) fully delocalized π-orbitals for N_{in} (left) and N_{out} (right), which represent the highest occupied and lowest unoccupied end-to-end transport channels, HOTC and LUTC, respectively. (b) Iso-surface representation of the local density of states (LDOS) corresponding to the HOTC and LUTC of the respective SAMs in device configuration, *i.e.*, sandwiched between two gold electrodes. (c) The Gaussian-broadened (σ = 0.05 eV) density of states projected onto the molecular part (PDOS) of the SAM device was integrated over a range of 200 meV from the onsets of the peaks closest to the Fermi level (*i.e.*, the origin of the energy scale) to produce the LDOS plots in (b).

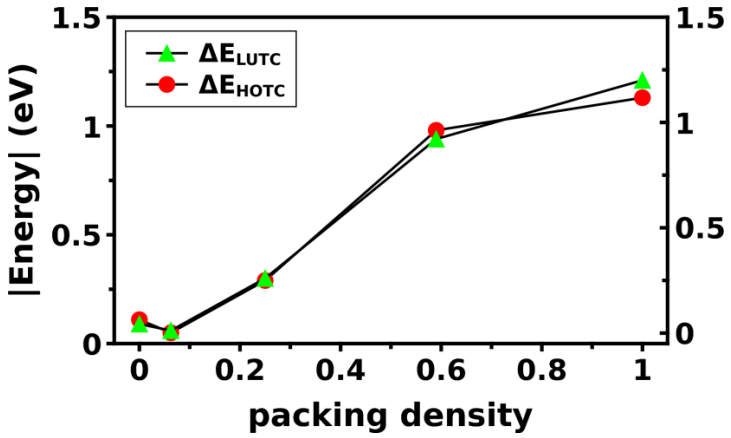

FIGURE S2: (red disks) DFT-calculated difference between the energies of the highest occupied end-to-end transport channels (HOTC) of a free-standing N_{in} monolayer and the HOTC of the corresponding N_{out} monolayer as a function of the SAM packing density. (green triangles) Same difference for the lowest unoccupied end-to-end transport channels (LUTC). A packing density of zero corresponds to the isolated molecules in gas phase and a packing density of one to the close-packed free-standing SAMs discussed in the main text.

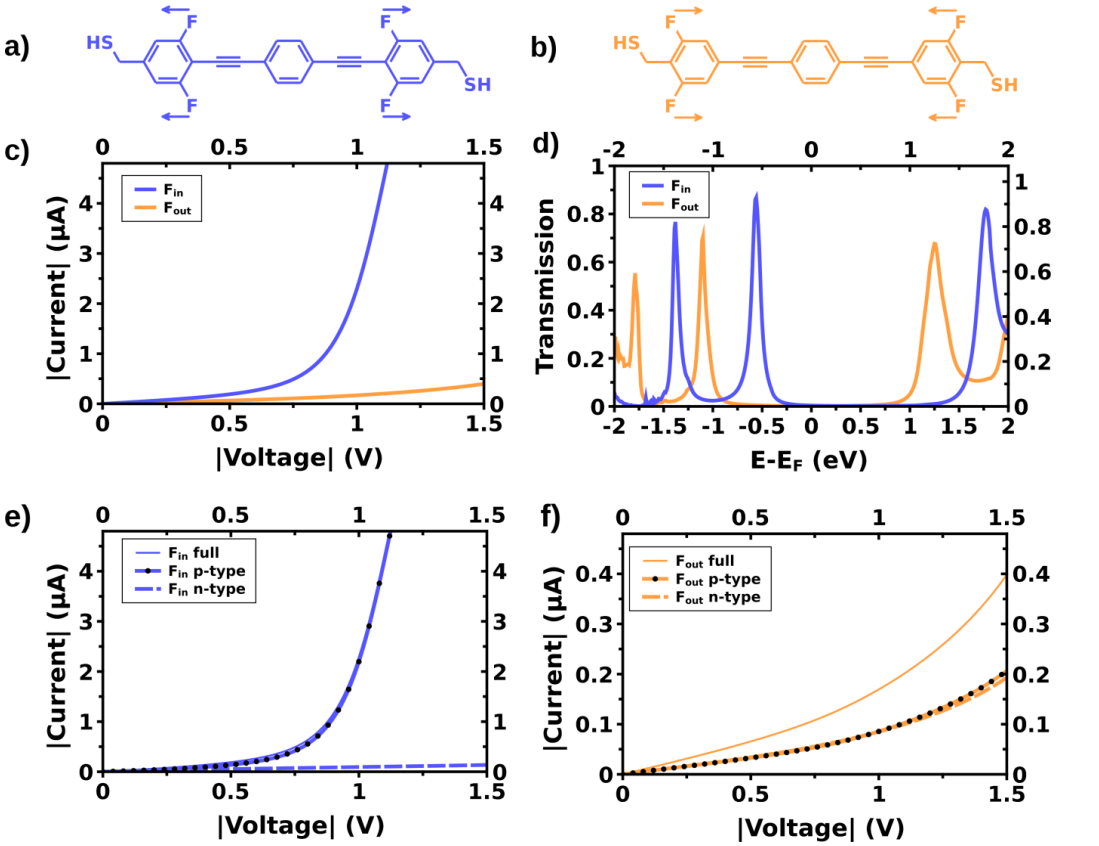

FIGURE S3: Chemical structures of fluorine-substituted Tour wires with projections of local dipoles onto the long molecular axes indicated: (a) F_{in} and (b) F_{out}. Panels (c) and (d) show the calculated current-voltage characteristics and transmission functions of F_{in} and F_{out} SAM-devices. The current through the F_{in} SAM is found to be higher by a factor of up to 29 in the low-bias regime (at V ≈ 1.3 V). The transmission function of F_{in} is shifted to higher energies, which results in an occupied transport channel closer to the metal Fermi-level, E_F, than any of the transport channels of F_{out}. Current-voltage curves calculated separately from occupied (p-type) and unoccupied (n-type) electronic states only are shown in (e) for F_{in} and in (f) for F_{out}. The charge transport through the F_{in} SAM is almost exclusively p-type, whereas it is equally distributed among occupied and unoccupied channels in the F_{out} SAM.

TABLE S1: DFT-calculated energies with respect to the vacuum level of the highest occupied and lowest unoccupied transport channels, HOTC and LUTC, of F_{in} and F_{out} isolated molecules and densely-packed SAMs. The difference of ~ 0.2 eV between the frontier end-to-end delocalized π-orbitals of the isolated F_{in} and F_{out} molecules is amplified to ~ 1.0 eV upon SAM formation and subsequently reduced to ~ 0.5 eV (*cf.* Fig. S3) upon SAM/metal binding through differences in ΔE_{BD} (see main text).

		Isolated (eV)	SAM (eV)
F_{in}	HOTC	-5.36	-4.34
	LUTC	-3.07	-2.19
F_{out}	HOTC	-5.56	-5.37
	LUTC	-3.25	-3.22

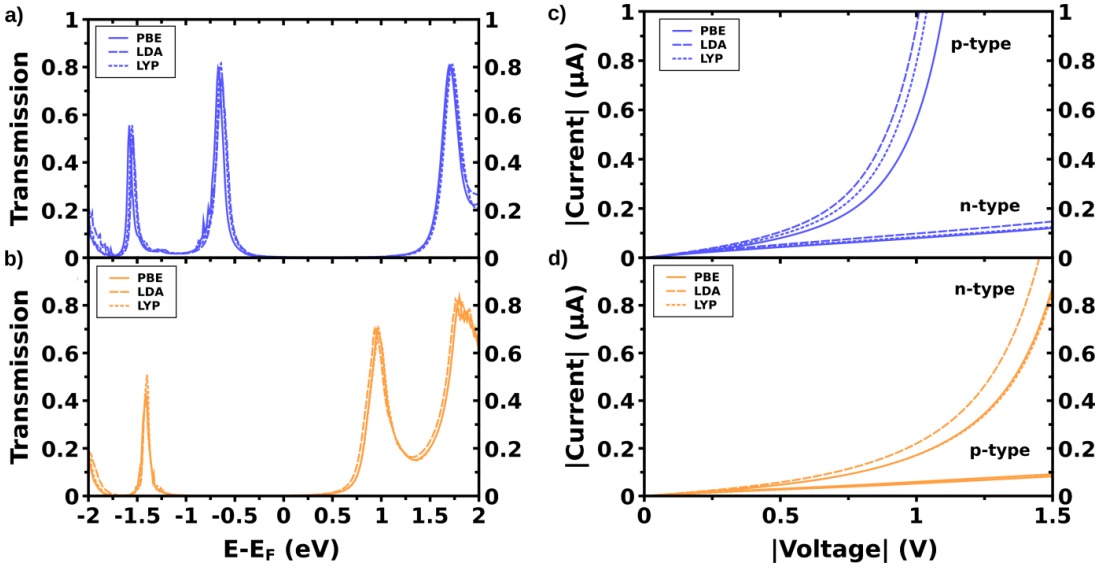

FIGURE S4: Effect of the exchange-correlation (XC) potential on the zero-bias transmission functions (panels a and b) and the polarity of charge transport (panels c and d) through N_{in} (blue) and N_{out} (orange) SAMs. In addition to the generalized gradient approximation (GGA) proposed by Perdew, Burke, and Ernzerhof (PBE; solid lines) considered in the main text [1], we also employed that of Becke and Lee, Yang, and Parr (BLYP; dashed lines) [2-4], as well as the local density approximation (LDA; dotted lines) to the XC functional for comparison [5]. The zero-bias transmission is hardly affected by the choice of the XC-functional and the polarity-change of the current persists.

Robustness of Results towards Methodology

The thermoelectric properties discussed in the main text are calculated using ground-state density-functional theory (DFT). Arguably, thermoelectricity is intrinsically a non-equilibrium phenomenon and, thus, a ground-state theory might not at all be suited to account for the relevant processes [6]. In the light of these severe theoretical restrictions, we stress that our results and conclusions are based on an electrostatic effect, which is an equilibrium phenomenon. As shown in the main text, it is this very effect that determines whether an occupied (p-type, N_{in}) or unoccupied (n-type, N_{out}) channel is closer to the Fermi level. Following Eq. 4 in the main text – valid away from transmission resonances, as it is certainly the case for our systems (see Figure 3a in the main text) – the change in sign of thermoelectric current and Seebeck coefficient then only hinges on the equilibrium electronic structure (and hence the equilibrium transmission function) being adequately described by the underlying theoretical framework.

As already noted briefly in the main text, it is well established that common density-functional approximations notoriously underestimate the transport gap of (organic) semiconductors. In principle, one could employ methods based on many-body perturbation theory (MBPT) [7] to cure the responsible lack of derivative discontinuity (inherent to common DFT) and to treat also non-local electron correlation (necessary to capture the reduction of the free-molecule gap in the vicinity of metal surfaces). However, such

theoretically well-justified schemes are prohibitively demanding on computational resources for systems of the size considered in the present study. Alternatively, one could also resort to (semi-)classical band-gap corrections [8] but, other than MBPT, there are no theoretical means to assess their validity. Moreover, it has been shown [9] that MBPT-based transport calculations yield transmission functions not only with a different gap, but also of a slightly different shape compared to (semi-)classical band-gap corrected DFT (see below).

Here, we argue that the observed polarity switch is, in fact, quite robust towards the level of theory used to describe the electronic structure of the SAM device: Naturally, symmetric corrections to the Kohn-Sham gap, *i.e.*, shifting occupied and unoccupied molecular states in opposite directions by the same amount, will change the absolute values of conductance, current, and Seebeck coefficient but, importantly, cannot affect the observed polarity switch – the HOTC of N_{in} will always stay closer to E_F than its LUTC and *vice versa* for N_{out}. It has been argued, however, that unoccupied levels are more strongly affected by corrections to the Kohn-Sham orbital energies than occupied levels [7, 9]. We first note that shifting the LUTC up in energy more than the HOTC down does, of course, not change the result that N_{in} SAMs are p-type conductors. To also assess the robustness of our conclusions regarding such asymmetric corrections to the Kohn-Sham gap of N_{out}, we shifted $T(E)$ for $E > E_{min}$ up in energy by Δ, with E_{min} denoting the energy (~ -0.3 eV) between HOTC and LUTC where $T(E)$ reaches a minimum (*cf.* Figure 3a in the main text); the resulting gap in the transmission curve was padded with $T(E_{min})$. We find the current through unoccupied states to remain higher than that through occupied states up to $\Delta \approx 0.6$ eV and the total current, *i.e.*, the sum of both contributions, to decrease dramatically upon increasing Δ (Fig. S5). This lead us to the statement towards the end of the main text that the observed polarity reversal of charge transport persist as long as potential upward corrections to the DFT calculated LUTC energies do not exceed potential downward corrections to the HOTC energies by more than ~ 0.6 eV and that, even if they did, an even more pronounced and equally unexpected difference in the total current through N_{in} and N_{out} SAMs would be expected.

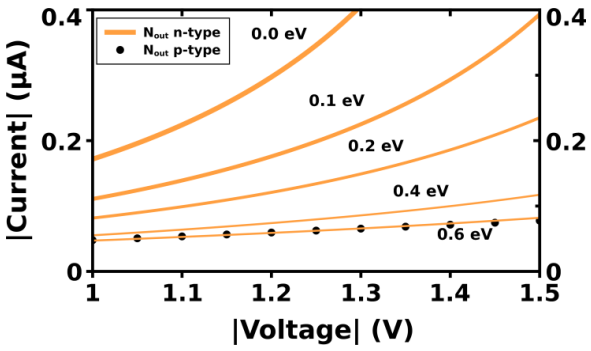

FIGURE S5: Calculated current through the unoccupied states in the N_{out} SAM device upon asymmetrically increasing the molecular Kohn-Sham gap by the indicated amount (solid lines). The black dots correspond to the current through the occupied states. See text for details.

ssess the impact of potential modifications of the conduction-channel shape on our results, we convolved the first-principles transmission functions $T(E)$ of N_{in} and N_{out} SAM devices with a series of Gaussians ($\sigma = 0.1, 0.2, 0.3$) and recalculated the charge-transport properties (Table S2). While I-V characteristics (not shown) strongly depend on the low-bias transmission and thus are, of course, strongly affected by the shape of the channels [9], thermoelectric properties are known to be less sensitive to transmission channel widths (see, *e.g.*, Ref. [10]). The Seebeck coefficients, S, extracted from the broadened transmission functions confirm that the difference between the two systems not only persists, but actually increases.

TABLE S2: Seebeck coefficients, S, extracted from transmission functions $T(E)$, artificially broadened through convolution with a series of Gaussians ($\sigma = 0.1, 0.2, 0.3$), of N_{in} and N_{out} SAM devices.

σ (eV)	S (μV/K)	
	N_{in}	N_{out}
0.0	16.6	-14.9
0.1	19.0	-15.9
0.2	46.0	-21.5
0.3	42.5	-39.7

References

[1] J. P. Perdew *et al.*, Phys. Rev. Lett. **77**, 3865 (1996).
[2] C. Lee *et al.*, Phys. Rev. B **37**, 785 (1988).
[3] A. D. Becke, Phys. Rev. A **38**, 3098 (1988).
[4] B. Mielich *et al.*, Chem. Phys. Lett. **157**, 200 (1989).
[5] J. P. Perdew and A. Zunger, Phys. Rev. B **23**, 5075 (1981).
[6] Y. Dubi and M. Di Ventra, Rev. Mod. Phys. **83**, 131 (2011).
[7] J. M. Garcia-Lastra *et al.*, Phys. Rev. B **80**, 245427 (2009).
[8] S. Y. Quek, *et al.*, Nano. Lett. **7**, 3477 (2007).
[9] M. Strange *et al.*, Phys. Rev. **83**, 115108 (2011).
[10] M. Paulsson and S. Datta, S., Phys. Rev. B **67**, 241403R (2003).

4. Publication II (ref. 2)

4.1. Original Article

THE JOURNAL OF PHYSICAL CHEMISTRY Letters

Letter

pubs.acs.org/JPCL

Anticorrelation between the Evolution of Molecular Dipole Moments and Induced Work Function Modifications

David A. Egger and Egbert Zojer*

Institute of Solid State Physics, Graz University of Technology, Petersgasse 16, A-8010 Graz, Austria

Supporting Information

ABSTRACT: We explore the limits of modifying metal work functions with large molecular dipoles by systematically increasing the dipole moment of archetype donor−acceptor molecules in self-assembled monolayers on gold. Contrary to intuition, we find that enhancing the dipoles leads to a reduction of the adsorption-induced change of the work function. Using atomistic simulations, we show that large dipoles imply electronic localization and level shifts that drive the interface into a thermodynamically unstable situation and trigger compensating charge reorganizations working against the molecular dipoles. Under certain circumstances, these are even found to overcompensate the effect that increasing the dipoles has for the work function.

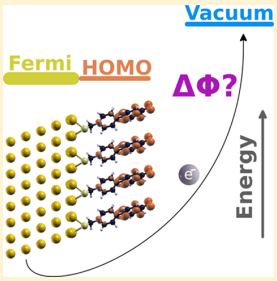

SECTION: Physical Processes in Nanomaterials and Nanostructures

The work function Φ defined as the minimum energy to extract an electron from a solid material is a fundamental physical quantity. When measured by photoemission spectroscopy, it is determined as the difference between the vacuum energy just outside of the material, E_{vac}, and the Fermi Energy, E_F.[1,2] Φ can be altered easily as it is strongly influenced by the detailed atomistic structure of the surface.[1] This triggered the seminal idea of tuning Φ via the adsorption of ordered polar species, which can be exploited to improve the efficiency of charge carrier injection in electronic devices.[3] Organic molecules have been identified as ideal agents for this task as their permanent dipole moments can be efficiently adjusted through chemical substitution. Moreover, they offer the possibility to cover a substrate as a self-assembled monolayer (SAM), this way operating as ideal surface dipole layers.[4−6] While the magnitude of the monolayer dipole moment determines the amount of the work function change ΔΦ, the dipole polarity determines its sign. This correlation between the dipole moment of the SAM molecules and ΔΦ is a well-established concept and has been confirmed experimentally for a number of metal−SAM systems.[1,3,7,8] For "conventional" SAMs, it is recovered also with the methodology used here, as shown for a number of systems contained in the Supporting Information (SI).

Still, a direct correlation between the molecular dipole moment and the SAM-induced ΔΦ can be disturbed by several effects.[9] First, the chemical bonding of the SAM to the substrate is associated with substantial charge rearrangements affecting Φ[10] Their magnitude critically depends on the SAM docking chemistry.[11,12] Also, the possibility of structural reorganizations such as dimerization of the molecules (see ref 13 and references therein) can reduce the monolayer dipole moment and, thus, impede the impact of the molecular dipole onto ΔΦ. Moreover, even in a well-ordered layer, inherent depolarization of the dipoles due to the neighboring polar molecules occurs.[14−20] Such a depolarization causes the dipole moment per molecule to be significantly smaller in the monolayer than that in the gas-phase, effectively limiting the achievable work function change. A saturation of ΔΦ with the molecular dipole has actually been predicted by Vager et al. based on the dielectric breakdown of the layers.[21] For large dipoles and SAMs of low polarizability, also significant charge transfer between the substrate and the SAM has been suggested based on electrostatic total energy arguments.[14]

In this Letter, we show for deliberately chosen donor−acceptor based "push−pull" molecules bonded to Au(111) using state-of-the-art atomistic simulations that under certain circumstances, increasing the molecular dipole moment can, in fact, reduce the change of the work function. This unexpected anticorrelation, which effectively goes beyond the saturation of Φ anticipated from the aforementioned depolarization effect or dielectric breakdown, is rationalized by a dipole-induced localization and renormalization of the electronic levels in the SAM (i.e., traced back to a quantum mechanical origin). These state localization and level shifts, in fact, originate already at the molecular level but are found to prevail in the densely packed monolayer and, thus, withstand competing electrostatic effects such as depolarization. At the metal−organic interface, they lead to charge rearrangements that preserve thermodynamic equilibrium and overcompensate for the increase in dipole moment. The underlying effects are of fundamental nature and

Received: August 12, 2013
Accepted: September 26, 2013

   dx.doi.org/10.1021/jz401721r | J. Phys. Chem. Lett. 2013, 4, 3521−3526

can be expected to apply quite generally for the adsorption of molecules with large, extended dipoles.

We here rely on donor−acceptor (push−pull-type) merocyanine derivatives (MCs), as shown in Figure 1a, because of

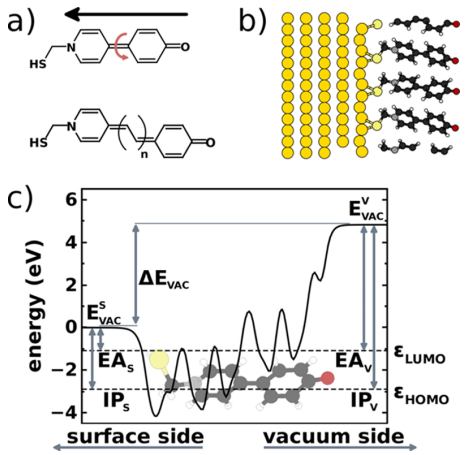

Figure 1. (a) Chemical structures of the investigated MCs. To increase dipole moments, the molecules can be twisted (top) and the separation between the donor and acceptor parts can be increased (bottom). (b) Side view of the Au(111)/MC-SAM interface. (c) Plane-averaged electron electrostatic energy of the planar, free-standing MC-SAM. The vacuum levels (E_{vac}), ionization potentials (IPs), and electron affinities (EAs) are indicated for the side oriented toward the metal surface (s) and toward the vacuum (v). (Structural representations produced using XCrySDen.[22])

their very large molecular dipole moments (ca. −13 D) with the charge separation extending over the molecular backbones. Such systems have been successfully synthesized and employed in the field of nonlinear optics.[23−26] MCs offer exceptionally convenient ways to systematically explore the impact of increasing dipoles as the latter can be tuned by twisting the molecule along the central inter-ring carbon−carbon bond (Figure 1a, top), which drives the molecule into a zwitterionic ground state.[25] Note that such twisting has been achieved experimentally[26] by attaching substituents to the center of the molecule (for a discussion of the possible existence of a biradical state as suggested in ref 27, see the SI). As an alternative strategy for increasing the dipole of MCs, one can elongate the molecules by inserting $-C_2H_2-$ spacers between the donor and acceptor parts (see Figure 1a, bottom).

Experimentally, the assembly of zwitterionic molecules with large dipole moments on inorganic substrates has been realized for several systems.[28,29] For the case of donor−acceptor molecules, it was shown that using chemical linkers to bind the molecules to the substrate results in stable SAMs on Au.[30] Therefore, we functionalized MCs with thiol (−SH) docking groups (cf. Figure 1a and b), allowing for a strong gold−molecule bond, and modeled these MC-SAMs on Au(111) in a $(\sqrt{3} \times 3)$ surface unit cell (Figure 1b). Our simulations and optimizations (for details, see the SI) rely on state-of-the-art density functional theory (DFT) calculations conducted with the electronic structure program VASP[31] and the optimizer GADGET.[32] To obtain the final electronic structure, we performed computationally demanding HSE06 hybrid DFT band structure calculations.[33] This is necessary as it has been shown that hybrid DFT functionals correct some of the errors inherent to standard (semi)local xc functionals,[34] especially for differently localized electronic states.[35]

First, we investigate the unbound molecular layer of MC molecules. In Figure 1c, we show the plane-averaged electron electrostatic energy of the hypothetical, "free-standing", H-saturated MC-SAM (i.e., the system in the absence of the gold substrate; the corresponding plot for the bonded SAM is contained in the SI). The strongly polar MC molecules modify the electrostatic potential energy in a profound way.[10] Arranged in an ordered fashion, they "split space" into two regions with different vacuum levels, E^s_{vac} on the side eventually oriented toward the metallic surface and E^v_{vac} toward the vacuum (see Figure 1c). Due to the strong dipoles, the associated potential energy jump (ΔE_{vac}) is particularly large (ca. 5 eV). Consequently, the monolayer ionization potential IP obtained from the maximum of the band derived from the highest-occupied molecular orbital (HOMO) is largely different for removing an electron to one or the other of the two sides of the monolayer (IP_s versus IP_v; see Figure 1c).[10] Importantly, we find that IP_s is small (ca. −3 eV) compared to the work function of pristine Au(111) calculated to be −5.1 eV. This comparably small IP_s (and large IP_v; cf. Figure 1c) is a direct consequence of the huge ΔE_{vac} as the latter results in a reduction of IP_s and increase of IP_v compared to the molecular situation. Thus, the peculiar alignment of the molecular relative to the metallic levels discussed in detail below, naturally arises from the large molecular dipole moments.

Increasing the dipole moment of the MC molecules in the free-standing SAM by increasing the inter-ring twist angle (see Figure 1a) further amplifies ΔE_{vac} by up to ∼0.7 eV (stars in Figure 2a). Traditionally, one would expect that this tuning of the conformation should boost the SAM-induced change in $\Delta\Phi$ in a similar manner.

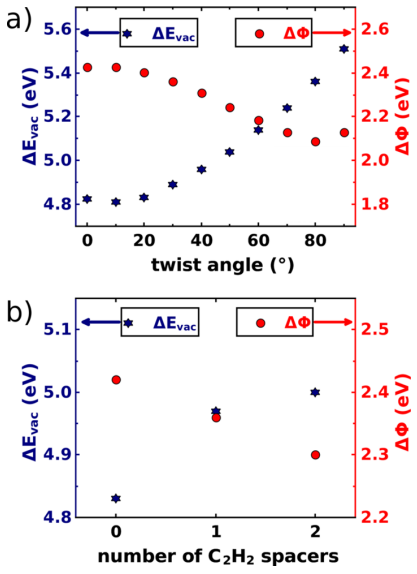

Figure 2. Calculated step in the electrostatic energy for the free-standing SAM, ΔE_{vac}, and induced work function modification, $\Delta\Phi$, for the same SAM adsorbed on gold. Data are plotted both as a function of the inter-ring twist angle (a) and the number of inserted $-C_2H_2-$ spacers (b). Note that for the chosen packing density, 1 eV in energy translates to a dipole moment of −1.2 D per molecule.

dx.doi.org/10.1021/jz401721r | J. Phys. Chem. Lett. 2013, 4, 3521−3526

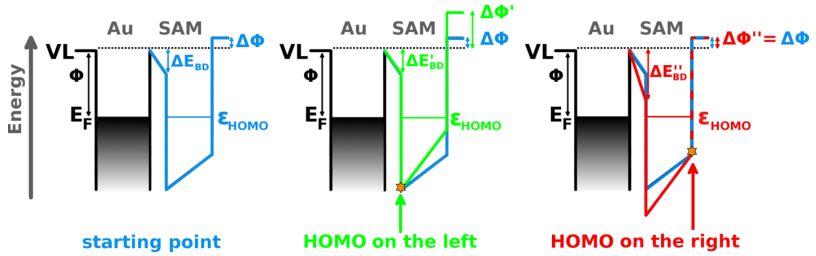

Figure 3. Schematic showing the impact of orbital localization on $\Delta\Phi$ when increasing ΔE_{vac} in the pinning regime. Starting from Fermi-level alignment (left panel and all blue plots), a continuous increase in ΔE_{vac} maps onto an increase in $\Delta\Phi$ when the pinning level is localized close to the metal (green line, center panel) and is diminished by a decrease of ΔE_{BD} when the state is localized toward the vacuum (red line, right panel).

Interestingly, when examining the MC-SAMs bonded to gold via the thiolate group (i.e., when considering $\Delta\Phi$), we find the exact opposite trend (circles in Figure 2a). The twisted MC molecules result in significantly smaller $\Delta\Phi$ values (by ca. 0.3 eV) than their planar (i.e., zero degree twisted) analogues. Note that the slight increase seen for $\Delta\Phi$ when increasing the twist from 80 to 90° is a consequence of a vanishing HOMO−LUMO gap in the MC-SAM. When elongating the MC molecule through inserting $-C_2H_2-$ spacers, thus enlarging the molecular dipoles by increasing the charge-transfer distance between the donor and acceptor groups (cf., Figure 1a), the same trends are found (Figure 2b); ΔE_{vac} increases by 0.2 eV (stars in Figure 2b), while $\Delta\Phi$ decreases by −0.1 eV (circles in Figure 2b). As discussed above, this anticorrelation between trends in ΔE_{vac} and $\Delta\Phi$ (i.e., between the dipolar layer in vacuum and adsorbed on a surface) is entirely unexpected from a purely electrostatic perspective and somehow reminiscent of the anomalous work function shifts reported for atomic species adsorbed on metal surfaces, where negatively charged atoms were shown to result in an unexpected adsorption-induced work function decrease.[36,37]

The origin of this unusual behavior must be rooted in the metal−organic interaction and the potential energy shift arising from the charge rearrangements upon SAM−gold bond formation. This "bond dipole", ΔE_{BD}, electrostatically shifts all molecular states with respect to E_F; with ΔE_{vac}, it adds up to $\Delta\Phi$ ($\Delta\Phi = \Delta E_{vac} + \Delta E_{BD}$).[10] For thiol-bonded SAMs on Au(111), the expected ΔE_{BD} is, however, only on the order of ∼−1 eV,[10] which is much smaller than the relatively large ΔE_{BD} = −2.4 eV calculated from $\Delta\Phi$ and ΔE_{vac} for the planar MC-SAMs on Au(111). Remarkably, we obtain a pronounced amplification of ΔE_{BD} by ∼−1 eV from the planar to the perpendicular configuration, with ΔE_{BD} eventually reaching a value of −3.4 eV (see Figure S4 in the SI). As a consequence, ΔE_{BD} not only counteracts the twisting-induced effect of 0.7 eV in ΔE_{vac}, it even overshoots it in magnitude by 0.3 eV. To appreciate the general relevance of this behavior, it is necessary to understand its microscopic origin. Interfacial charge rearrangements comparable in magnitude to the present ones have previously been shown to occur as a consequence of Fermi level pinning.[38] This mechanism manifests itself in a strong response in the interfacial charge density, which ensures that equilibrium is maintained by preventing occupied states in the organic from lying above (or unoccupied below) the Fermi level.[39,40] Typically, the energy of the frontier electronic states in the organic is then found to be close to E_F of the substrate.[41−44] Recalling that IP_s of the planar free-standing MC-SAM is only ∼−3 eV (see Figure 1c) and Φ of the bare Au(111) substrate is −5.1 eV in the calculations, Fermi level pinning is to be expected here (and also for less noble substrates such as the Ag(111) surface). Indeed, our calculations confirm that the highest-occupied band aligns with E_F for all studied systems.

The evolution of Φ in the case of Fermi level pinning has been shown to depend on the spatial localization of the molecular pinning level.[45] We illustrate this in a *Gedankenexperiment*, where we start from a pinned situation representative of the MC-SAM on gold (Figure 3, blue curves) and then gradually increase ΔE_{vac} across the monolayer (green and red curves in Figure 3, central and right panels). When the pinning level, which for the present situation is the HOMO, is spatially close to the interface region (Figure 3, green curve in central panel), a change in ΔE_{vac} will hardly affect their relative energetic distance to E_F. Then, no further charge rearrangements are needed to maintain equilibrium at the interface (i.e., to align the pinning level with E_F), ΔE_{BD} will remain essentially constant, and an increase of ΔE_{vac} (and the molecular dipoles) directly maps onto a further increase of $\Delta\Phi$. When, however, the HOMO is localized close to the vacuum side (red curve in right panel), increasing ΔE_{vac} would shift it up in energy with respect to E_F and, consequently, trigger further charge rearrangements, keeping the HOMO and E_F aligned, which results in a larger ΔE_{BD}. In that case, an increase in ΔE_{vac} will be diminished by the amplified ΔE_{BD}, and $\Delta\Phi$ remains constant. This saturation of $\Delta\Phi$ due to orbital localization holds for layers with opposite dipole polarity as well. Large molecular dipoles pointing away from the metal surface decrease Φ until pinning of the lowest-unoccupied molecular orbital (LUMO) at E_F occurs. Then, the localization of the LUMO determines the further evolution of Φ.

The localization of the pinned states can be determined by the plane-averaged charge density corresponding to the HOMO-derived band best shown for the free-standing (i.e., nonbonded) MC monolayer (see Figure 4a). It is found to be localized toward the vacuum side of the SAM already at 0° twist (see the SI for the full real space representation of the associated electronic bands). This notion is supported by the center of the HOMO-related charge being shifted relative to that of the (positive) nuclear charge by 2 Å toward the vacuum (vertical lines in Figure 4a). Upon twisting the SAM (and thereby increasing the dipole), the localization of the HOMO even slightly increases. This (partial) localization of the HOMO on the donor side is exactly what one expects for a push−pull molecule, while the LUMO tends to be localized more on the acceptor side (molecular orbital localization). In the densely packed MC-SAM, the "molecular" situation is modified by two collective effects. As mentioned above, a parallel alignment of polar molecules results in a reduction of the individual

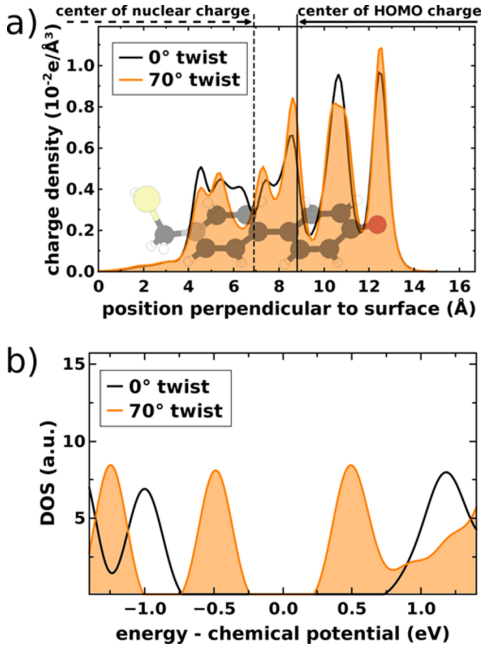

Figure 4. (a) Plane-averaged charge density corresponding to the HOMO-derived band for 0 and 70° twists; (b) corresponding densities of states for the free-standing MC-SAM. In (a), the vertical lines denote the center of the (positive) molecular nuclear charge (dashed) and the center of the charge corresponding to the HOMO (solid) for the planar MC.

molecular dipole due to depolarization effects,[9,14−21] which generally decreases the degree of the aforementioned charge localization (collective orbital delocalization).[35] Concomitantly, the extended dipole moments in the SAM cause a spatially continuous modification of the electrostatic potential along the monolayer (see Figure 1c), which results in a collective orbital localization.[35,46] We, however, do not observe profound changes in the localization of the frontier levels due to these collective effects.

The localization of the relevant states has two important consequences for Φ: (i) Monolayers with particularly large, delocalized dipoles will typically comprise pinning levels more localized toward the vacuum, which in itself poses a natural obstacle for increasing Φ, and for strong localization, even a natural limit for ΔΦ achievable with ordered dipolar layers (see Figure 3, right panel). This rationale prevails when reversing the dipole direction as the change in sign of ΔE_{vac} entails pinning to occur at the LUMO, which then, due to the change in dipole polarity, is again localized close to the vacuum side. (ii) The localization of the frontier states together with the potential gradient within the SAM (see Figure 1c) results in a particularly small IP_s for dipoles pointing toward the surface and particularly large EA_s for dipoles pointing away from it, creating a situation prone to Fermi level pinning independent of the specific nature of the molecules in the SAM. Of course, whether Fermi level pinning is ultimately observed depends on the electronic structure of the substrate (Φ in particular), the electronic levels within the adsorbate, and the amplitude of the molecular dipole moment.

The remaining question is why in the case of the MC-based SAMs on gold one goes beyond the above described saturation of Φ, that is, why does increasing the dipoles result in a decrease of ΔΦ. Indeed, a saturation of ΔΦ can also be inferred from electrostatic models, as explicitly shown in ref 21. To explain the anticorrelation observed here, one however needs to dig deeper and analyze how strategies for increasing dipoles typically affect the molecular electronic structure. Comparing the density of states (DOS) of the MC-SAM at planar and twisted geometries (Figure 4b; see the SI for the complete data set), we find that increasing the dipole by twisting the molecular segments leads to a strong energetic upshift (destabilization) of the HOMO and a downshift (stabilization) of the LUMO; the band gap is reduced significantly (see Figure 4b). For the MC-SAM on the Au(111) substrate (see Figure S7 in the SI), we find a comparable band gap reduction. As the HOMO is aligned with E_F due to Fermi level pinning, this results in a reduced energetic difference between E_F and the vacuum level (i.e., the work function is decreased). This eventually causes the observed anticorrelation between the molecular dipole and ΔΦ. Similar effects are observed when increasing the charge-transfer distance by inserting $-C_2H_2-$ spacers. As the conjugation length of the molecules in the SAM is extended, its band gap is reduced, and thus, Fermi level pinning involving the HOMO-related band becomes more effective. The net effect can also be explained through the impact of the reduced gap on interfacial charge rearrangements. To maintain equilibrium and retain the alignment of the HOMO with E_F, the destabilization of the HOMO that occurs already in the free-standing SAM has to be compensated for by additional charge rearrangements when the layer is brought into contact with the metal, which further boosts ΔE_{BD}. Consequently, the total ΔE_{BD} not only compensates for increases in ΔE_{vac}, it even overshoots it in magnitude and causes the observed anticorrelation (see Figures 2a and b).

In summary, we have shown that, in sharp contrast to intuition, increasing the dipole of SAM-forming molecules attached to a metal substrate does not necessarily result in an increase of ΔΦ. As soon as the dipole moments surpass a certain limit, Fermi level pinning becomes inevitable, which can pose a natural limit to achievable work function modifications, in line with earlier electrostatic considerations.[21] To what extent the charge rearrangements can fully compensate for the dipole increase, however, depends on the localization of the pinned states, that is, their quantum nature. The latter becomes even more relevant for explaining our most unexpected finding, namely, an anticorrelation between the evolutions of the dipole moment and induced work function changes observed here for MC-type SAMs on Au(111). It is found to arise from an energetic shift of the HOMO occurring as a consequence of increasing the dipoles.

■ ASSOCIATED CONTENT

Supporting Information

Additional data, including the calculated step in the electrostatic energy for free-standing tail-group substituted biphenylthiol SAMs, ΔE_{vac}, the induced work function modification for the same SAMs bonded to the Au(111) surface, the plane-averaged electron electrostatic energy of the planar Au(111)/MC-SAM, the bond dipole ΔE_{BD} for the MC-SAMs on Au(111), real-space representations of the electronic states, density of states plots, details of the system setup, additional methodological details, and a discussion of the possible existence of a biradical state for the twisted merocyanine molecule. This material is available free of charge via the Internet at http://pubs.acs.org.

AUTHOR INFORMATION

Corresponding Author
*E-mail: egbert.zojer@tugraz.at.

Notes
The authors declare no competing financial interest.

ACKNOWLEDGMENTS

We thank O. T. Hofmann (Fritz-Haber Institut Berlin) for critically reading the manuscript and G. Heimel (Humboldt-Universität Berlin) for providing the optimized geometries of the tail-group substituted SAMs contained in the SI. D.A.E. is a recipient of a DOC fellowship by the Austrian Academy of Sciences. Financial support by the Austrian Science Fund (FWF), P24666-N20, is gratefully acknowledged. Our calculations have been performed at the icluster (ZID TU Graz) and the VSC-2 (Vienna Scientific Cluster).

REFERENCES

(1) Ishii, H.; Sugiyama, K.; Ito, E.; Seki, K. Energy Level Alignment and Interfacial Electronic Structures at Organic/Metal and Organic/Organic Interfaces. *Adv. Mater.* **1999**, *11*, 605−625.
(2) Cahen, D.; Kahn, A. Electron Energetics at Surfaces and Interfaces: Concepts and Experiments. *Adv. Mater.* **2003**, *15*, 271−277.
(3) Campbell, I.; Rubin, S.; Zawodzinski, T.; Kress, J.; Martin, R.; Smith, D.; Barashkov, N.; Ferraris, J. Controlling Schottky Energy Barriers in Organic Electronic Devices Using Self-Assembled Monolayers. *Phys. Rev. B* **1996**, *54*, R14321−R14324.
(4) Boer, B.; de Hadipour, A.; Mandoc, M. M.; Woudenbergh, T.; van Blom, P. W. M. Tuning of Metal Work Functions with Self-Assembled Monolayers. *Adv. Mater.* **2005**, *17*, 621−625.
(5) Zhou, Y.; Fuentes-Hernandez, C.; Shim, J.; Meyer, J.; Giordano, A. J.; Li, H.; Winget, P.; Papadopoulos, T.; Cheun, H.; Kim, J.; et al. A Universal Method to Produce Low-Work Function Electrodes for Organic Electronics. *Science* **2012**, *336*, 327−332.
(6) Fracasso, D.; Muglali, M. I.; Rohwerder, M.; Terfort, A.; Chiechi, R. C. Influence of an Atom in EGaIn/Ga_2O_3 Tunneling Junctions Comprising Self-Assembled Monolayers. *J. Phys. Chem. C* **2013**, *117*, 11367−11376.
(7) Alloway, D. M.; Hofmann, M.; Smith, D. L.; Gruhn, N. E.; Graham, A. L.; Colorado, R.; Wysocki, V. H.; Lee, T. R.; Lee, P. A.; Armstrong, N. R. Interface Dipoles Arising from Self-Assembled Monolayers on Gold: UV−Photoemission Studies of Alkanethiols and Partially Fluorinated Alkanethiols. *J. Phys. Chem. B* **2003**, *107*, 11690−11699.
(8) Malicki, M.; Guan, Z.; Ha, S. D.; Heimel, G.; Barlow, S.; Rumi, M.; Kahn, A.; Marder, S. R. Preparation and Characterization of 4′-Donor Substituted Stilbene-4-thiolate Monolayers and Their Influence on the Work Function of Gold. *Langmuir* **2009**, *25*, 7967−7975.
(9) Cahen, D.; Naaman, R.; Vager, Z. The Cooperative Molecular Field Effect. *Adv. Funct. Mater.* **2005**, *15*, 1571−1578.
(10) Heimel, G.; Romaner, L.; Brédas, J.-L.; Zojer, E. Interface Energetics and Level Alignment at Covalent Metal−Molecule Junctions: π-Conjugated Thiols on Gold. *Phys. Rev. Lett.* **2006**, *96*, 196806/1−196806/4.
(11) Heimel, G.; Romaner, L.; Zojer, E.; Brédas, J.-L. Toward Control of the Metal−Organic Interfacial Electronic Structure in Molecular Electronics: A First-Principles Study on Self-Assembled Monolayers of π-Conjugated Molecules on Noble Metals. *Nano Lett.* **2007**, *7*, 932−940.
(12) Zangmeister, C. D.; Beebe, J. M.; Naciri, J.; Kushmerick, J. G.; van Zee, R. D. Controlling Charge-Carrier Type in Nanoscale Junctions with Linker Chemistry. *Small* **2008**, *4*, 1143−1147.
(13) Schreiber, F. Structure and Growth of Self-Assembling Monolayers. *Prog. Surf. Sci.* **2000**, *65*, 151−257.
(14) L'vov, V. S.; Naaman, R.; Tiberkevich, V.; Vager, Z. Cooperative Effect in Electron Transfer Between Metal Substrate and Organized Organic Layers. *Chem. Phys. Lett.* **2003**, *381*, 650−653.
(15) Natan, A.; Zidon, Y.; Shapira, Y.; Kronik, L. Cooperative Effects and Dipole Formation at Semiconductor and Self-Assembled-Monolayer Interfaces. *Phys. Rev. B* **2006**, *73*, 193310.
(16) Natan, A.; Kronik, L.; Haick, H.; Tung, R. T. Electrostatic Properties of Ideal and Non-ideal Polar Organic Monolayers: Implications for Electronic Devices. *Adv. Mater.* **2007**, *19*, 4103−4117.
(17) Cornil, D.; Olivier, Y.; Geskin, V.; Cornil, J. Depolarization Effects in Self-Assembled Monolayers: A Quantum-Chemical Insight. *Adv. Funct. Mater.* **2007**, *17*, 1143.
(18) Romaner, L.; Heimel, G.; Ambrosch-Draxl, C.; Zojer, E. The Dielectric Constant of Self-Assembled Monolayers. *Adv. Funct. Mater.* **2008**, *18*, 3999.
(19) Monti, O. L. A. Understanding Interfacial Electronic Structure and Charge Transfer: An Electrostatic Perspective. *J. Phys. Chem. Lett.* **2012**, *3*, 2342−2351.
(20) Regemorter, T.; Van Guillaume, M.; Fuchs, A.; Lennartz, C.; Geskin, V.; Beljonne, D.; Cornil, J. Methodological Aspects of the Quantum-Chemical Description of Interface Dipoles at Tetrathiafulvalene/tetracyanoquinodimethane Interfaces. *J. Chem. Phys.* **2012**, *137*, 174708.
(21) Vager, Z.; Naaman, R. Surprising Electronic−Magnetic Properties of Close-Packed Organized Organic Layers. *Chem. Phys.* **2002**, *281*, 305−309.
(22) Kokalj, A. XCrySDen—a New Program for Displaying Crystalline Structures and Electron Densities. *J. Mol. Graphics Modell.* **2000**, *17*, 176−179.
(23) Albert, I. D. L.; Marks, T. J.; Ratner, M. A. Conformationally-Induced Geometric Electron Localization. Interrupted Conjugation, Very Large Hyperpolarizabilities, and Sizable Infrared Absorption in Simple Twisted Molecular Chromophores. *J. Am. Chem. Soc.* **1997**, *119*, 3155−3156.
(24) Marder, S. R.; Kippelen, B.; Jen, A. K.-Y.; Peyghambarian, N. Design and Synthesis of Chromophores and Polymers for Electro-optic and Photorefractive Applications. *Nature* **1997**, *388*, 845−851.
(25) Keinan, S.; Zojer, E.; Brédas, J.-L.; Ratner, M. A.; Marks, T. J. Twisted Π-System Electro-optic Chromophores. A CIS Vs. MRD-CI Theoretical Investigation. *J. Mol. Struct.: THEOCHEM* **2003**, *633*, 227−235.
(26) Kang, H.; Facchetti, A.; Zhu, P.; Jiang, H.; Yang, Y.; Cariati, E.; Righetto, S.; Ugo, R.; Zuccaccia, C.; Macchioni, A.; et al. Exceptional Molecular Hyperpolarizabilities in Twisted π-Electron System Chromophores. *Angew. Chem., Int. Ed.* **2005**, *44*, 7922−7925.
(27) Isborn, C. M.; Davidson, E. R.; Robinson, B. H. Ab Initio Diradical/Zwitterionic Polarizabilities and Hyperpolarizabilities in Twisted Double Bonds. *J. Phys. Chem. A* **2006**, *110*, 7189−7196.
(28) Makoudi, Y.; Arab, M.; Palmino, F.; Duverger, E.; Ramseyer, C.; Picaud, F.; Chérioux, F. A Stable Room-Temperature Molecular Assembly of Zwitterionic Organic Dipoles Guided by a Si(111)-7 × 7 Template Effect. *Angew. Chem., Int. Ed.* **2007**, *46*, 9287−9290.
(29) Routaboul, L.; Braunstein, P.; Xiao, J.; Zhang, Z.; Dowben, P. A.; Dalmas, G.; Costa, V.; Da Félix, O.; Decher, G.; Rosa, L. G.; et al. Altering the Static Dipole on Surfaces through Chemistry: Molecular Films of Zwitterionic Quinonoids. *J. Am. Chem. Soc.* **2012**, *134*, 8494−8506.
(30) Che, H.-J.; Chia, P.-J.; Chua, L.-L.; Sivaramakrishnan, S.; Tang, J.-C.; Wee, A. T. S.; Chan, H. S. O.; Ho, P. K. H. Robust Reproducible Large-Area Molecular Rectifier Junctions. *Appl. Phys. Lett.* **2008**, *92*, 253503.
(31) Kresse, G.; Furthmüller, J. Efficient Iterative Schemes for Ab Initio Total-Energy Calculations Using a Plane-Wave Basis Set. *Phys. Rev. B* **1996**, *54*, 11169−11186.
(32) Bučko, T.; Hafner, J.; Ángyán, J. G. Geometry Optimization of Periodic Systems Using Internal Coordinates. *J. Chem. Phys.* **2005**, *122*, 124508.
(33) Heyd, J.; Scuseria, G. E.; Ernzerhof, M. Erratum: "Hybrid Functionals Based on a Screened Coulomb Potential". *J. Chem. Phys.* **2003**, *118*, 8207; *J. Chem. Phys.* **2006**, *124*, 219906.

(34) Biller, A.; Tamblyn, I.; Neaton, J. B.; Kronik, L. Electronic Level Alignment at a Metal−Molecule Interface from a Short-Range Hybrid Functional. *J. Chem. Phys.* **2011**, *135*, 164706.
(35) Rissner, F.; Egger, D. A.; Natan, A.; Körzdörfer, T.; Kümmel, S.; Kronik, L.; Zojer, E. Collectively Induced Quantum-Confined Stark Effect in Monolayers of Molecules Consisting of Polar Repeating Units. *J. Am. Chem. Soc.* **2011**, *133*, 18634−18645.
(36) Michaelides, A.; Hu, P.; Lee, M.-H.; Alavi, A.; King, D. Resolution of an Ancient Surface Science Anomaly: Work Function Change Induced by N Adsorption on W{100}. *Phys. Rev. Lett.* **2003**, *90*, 246103/1−246103/4.
(37) Bagus, P.; Käfer, D.; Witte, G.; Wöll, C. Work Function Changes Induced by Charged Adsorbates: Origin of the Polarity Asymmetry. *Phys. Rev. Lett.* **2008**, *100*, 126101.
(38) Egger, D. A.; Rissner, F.; Rangger, G. M.; Hofmann, O. T.; Wittwer, L.; Heimel, G.; Zojer, E. Self-Assembled Monolayers of Polar Molecules on Au(111) Surfaces: Distributing the Dipoles. *Phys. Chem. Chem. Phys.* **2010**, *12*, 4291.
(39) Fukagawa, H.; Kera, S.; Kataoka, T.; Hosoumi, S.; Watanabe, Y.; Kudo, K.; Ueno, N. The Role of the Ionization Potential in Vacuum-Level Alignment at Organic Semiconductor Interfaces. *Adv. Mater.* **2007**, *19*, 665−668.
(40) Braun, S.; Salaneck, W. R.; Fahlman, M. Energy-Level Alignment at Organic/Metal and Organic/Organic Interfaces. *Adv. Mater.* **2009**, *21*, 1450.
(41) Hauschild, A.; Karki, K.; Cowie, B.; Rohlfing, M.; Tautz, F.; Sokolowski, M. Molecular Distortions and Chemical Bonding of a Large π-Conjugated Molecule on a Metal Surface. *Phys. Rev. Lett.* **2005**, *94*, 036106.
(42) Rohlfing, M.; Temirov, R.; Tautz, F. Adsorption Structure and Scanning Tunneling Data of a Prototype Organic−Inorganic Interface: PTCDA on Ag(111). *Phys. Rev. B* **2007**, *76*, 115421.
(43) Greiner, M. T.; Helander, M. G.; Tang, W.-M.; Wang, Z.-B.; Qiu, J.; Lu, Z.-H. Universal Energy-Level Alignment of Molecules on Metal Oxides. *Nat. Mater.* **2011**, *11*, 76−81.
(44) Heimel, G.; Duhm, S.; Salzmann, I.; Gerlach, A.; Strozecka, A.; Niederhausen, J.; Bürker, C.; Hosokai, T.; Fernandez-Torrente, I.; Schulze, G.; et al. Charged and Metallic Molecular Monolayers through Surface-Induced Aromatic Stabilization. *Nat. Chem.* **2013**, *5*, 187−194.
(45) Hofmann, O. T.; Egger, D. A.; Zojer, E. Work-Function Modification Beyond Pinning: When Do Molecular Dipoles Count? *Nano Lett.* **2010**, *10*, 4369−4374.
(46) Miller, D.; Chemla, D.; Damen, T.; Gossard, A.; Wiegmann, W.; Wood, T.; Burrus, C. Band-Edge Electroabsorption in Quantum Well Structures: The Quantum-Confined Stark Effect. *Phys. Rev. Lett.* **1984**, *53*, 2173−2176.

4.2. Supporting Information

Supporting Information for:

"Anti-Correlation between the Evolution of Molecular Dipole Moments and Induced Work-Function Modifications"

David A. Egger and Egbert Zojer

Institute of Solid State Physics, Graz University of Technology,

Petersgasse 16, A-8010 Graz, Austria.

Thiol-SAMs with different tail groups on Au(111)

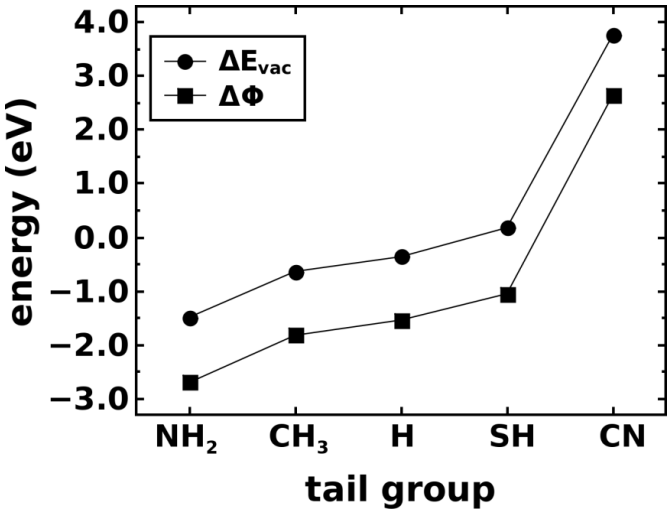

Figure S1: Calculated step in the electrostatic energy for the free-standing biphenylthiol SAMs, ΔE_{vac}, and induced work-function modification, $\Delta\Phi$, for SAMs bonded to the Au(111) surface depending on the tail-group functionalization. One observes a clear correlation between ΔE_{vac} and $\Delta\Phi$. Note that ΔE_{vac} is directly proportional to the perpendicular component of the molecular dipole moment (where depolarization effects are self-consistently included). For computational convenience, we applied the PBE exchange-correlation functional for these test calculations, but no significant variations are expected in these cases when using a conventional hybrid functional such as HSE06 instead.

Discussion of the possible existence of a biradical state for the twisted merocyanine molecule: For the MC-type molecule shown in the top part of Fig. 1 in the main text, the existence of a zwitterionic ground state is controversially discussed in literature. In fact, a second possible ground state for the twisted MC-type molecules is a biradical with a significantly smaller ground-state dipole moment. While the zwitterionic ground states can be accurately described with a single-determinant method (such as the one employed here), it is frequently claimed that the calculation of a biradical state requires multiconfigurational methods (which are, of course, far beyond the reach of computational tools available for studying the interfaces of interest here). To study the effect of multiconfigurational methods on the ground state of MC derivatives, Isborn *et al.* performed a comparative study on MC and smaller molecules using hybrid functionals, Hartree Fock, and complete active space self-consistent field (CASSCF) calculations with different basis sets. While all other calculations predicted a zwitterionic ground-state, the CASSCF calculations with the largest active space used (14,13) suggested a biradical ground state at large twist with a significantly reduced dipole moment.[1] To gain a better insight to what extent the actually chosen active space impacts the result, we also performed CASSCF calculations systematically varying the active space (with the largest spaces somewhat larger than the ones used by Isborne *et al.*). In these studies we also carefully followed the nature of all orbitals to ensure consistent active spaces for all considered tilt angles (0°, 45° & 90° in our case). While the final dipole moment was clearly affected by the chosen active space, we always found the by far largest dipole moment at 90° twist and also never observed an indication for a biradical ground state. This might, however, also be a consequence of the convergence details of the CASSCF calculations: As we were told by Christine M. Isborn in the form of a private communication, she recovered the biradical state only, when using the output densities for smaller twists as inputs for larger twists, but that the final wavefunctions obtained using that strategy were always associated with smaller total energy than when simply starting a CASSCF calculation "from scratch" in analogy to the procedure we had chosen. In this context it should be mentioned that experimental results favor a zwitterionic ground state.[2] This discrepancy with Ref.[1] could be a consequence of solvent effects present in the experiments but not in the calculations, as suggested by Brown *et al.*,[3] who performed state-averaged complete active space self-consistent field (SA-CASSCF) calculations. All these considerations signify that the calculated properties of MC-type dyes do depend on technical details of the employed computational methodology and that there exist high level studies that suggest a biradical ground state at large twist. These complications non-withstanding, it should be stressed that in the present paper we focus on trends arising from fundamental effects, which we expect to be relevant for SAMs consisting of molecules with large delocalized dipoles whatever the origin of

the dipoles is. Consequently, technical details as the ones discussed above can impact the specific results on twisted MC molecules, but do not affect the general conclusions drawn here; this is underlined by the fact that there is no indication for a biradical ground-state for the planar MC-molecules with extended conjugated backbones that we also studied and where we observed exactly the same trends as when increasing the molecular dipoles by twisting (*cf.* Fig. 2b in the main text).

Details on system set-up: The starting point for the structural optimization of the SAMs is a ($\sqrt{3} \times 3$) Au(111) unit cell containing two thiolated merocyanine (MS) molecules (see Fig. 1b in the main text) in a herring-bone arrangement. As the detailed structure of MC SAMs on Au(111) has not been reported before, we adapt a realistic atomistic representation by first performing a full geometry optimization (*vide infra*) of the densely packed monolayers. To allow investigating the impact of the inter-ring twist angle on the electronic structure of the combined metal-organic systems, we removed one of the molecules from the surface unit-cell after the full geometry optimization. We finally varied the twist angle for this setup without further ionic relaxation. While two planar molecules fit into the unit cell, this is no longer the case for twisted ones; in view of the fact that in actual systems twisting is realized by more or less bulky substituents, the achieved packing density also appears more realistic than the full coverage case. For consistency reasons, we also removed one of the molecules from the surface unit-cells of the elongated MC SAMs (see Fig. 1a in the main text) after fully optimizing the structure. Side-views of the obtained structures of the densely-packed and half-coverage MC-SAMs are shown in Fig. S2.

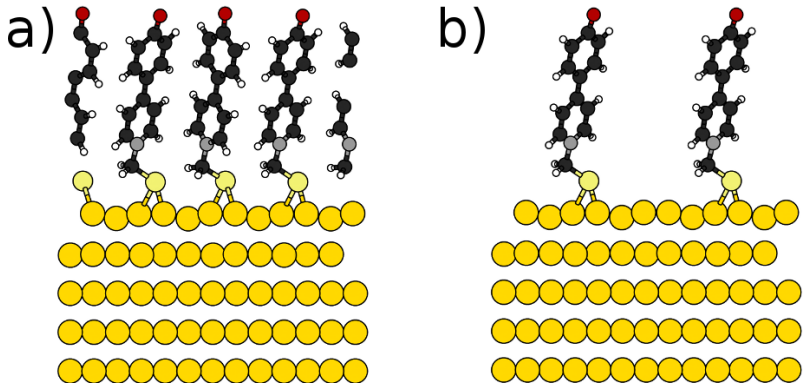

Figure S2: Side-view of the MC-SAMs on Au(111) at full (a) and half coverage (b).

Additional methodological details: Our calculations rely on density-functional theory (DFT) as implemented in the electronic structure program VASP.[4] Valence-core interactions were treated within the projector-augmented-wave[5] (PAW) formalism using soft PAW potentials for all elements, and the resulting valence-electron wavefunctions were expanded in a plane-wave basis (kinetic-energy cutoff of *ca.* 20 Ryd). Along the surface normal, we inserted a vacuum gap of ~20 Å and applied a dipole correction to accommodate the internal 3D-periodicity of the band-structure calculations to the periodicity of our system (extended 2D-periodic surfaces).[6] Our final surface unit-cell was sampled with an (8 × 5) lateral Monkhorst-Pack k-point grid,[7] and we employed a Methfessel-Paxton occupation scheme.[8] To optimize the geometry, we applied GADGET[9] with internal coordinates and relaxed all nuclear degrees of freedom (force cutoff: 10^{-2} eV/Å) keeping the bottom-two Au layers fixed. In these ionic optimizations, we treated exchange and correlation (xc) according to the PBE functional.[10] To improve the reliability of our calculations, we then applied the computationally demanding HSE06 hybrid DFT functional[11] for all subsequent single-point calculations. Hybrid functionals are known to partially correct some of the errors inherent to conventional (semi-) local DFT functionals, especially for organic molecules with differently localized molecular orbitals.[12–14] Periodic band-structure calculations are substantially impeded when hybrid functionals are employed and computational costs rise by nearly two orders of magnitude. To make these calculations feasible and facilitate convergence in the electronic self-consistent cycle, we followed a three-step

process for all HSE06 calculations: (i) We performed a PBE single-point calculation without counter-dipole correction; (ii) we then carried out an HSE06 calculation without counter-dipole correction, where for the evaluation of the Hartree-Fock part in the exchange-correlation potential we reduced the reciprocal grid in the k_x-direction by a factor of two and used the wavefunctions from step (i) as a guess; and (iii) used the wavefunctions from (ii) as a guess for a HSE06 calculation with counter-dipole correction on our standard k-point grid (*vide supra*). For all calculations, where a metallic surface was present, we employed a rather small smearing of 100 K (0.0086 eV) as this was found to improve the convergence. For the present study we have used the vasp.5.2.11 and vasp.5.2.12 releases of the VASP code (transferability was carefully tested) and the following PAW potentials:

Au	PAW_PBE Au 06Sep2000
S	PAW_PBE S 17Jan2003
C	PAW_PBE C_s 06Sep2000
H	PAW_PBE H 15Jun2001
N	PAW_PBE N_s 07Sep2000
O	PAW_PBE O_s 07Sep2000

Additional data

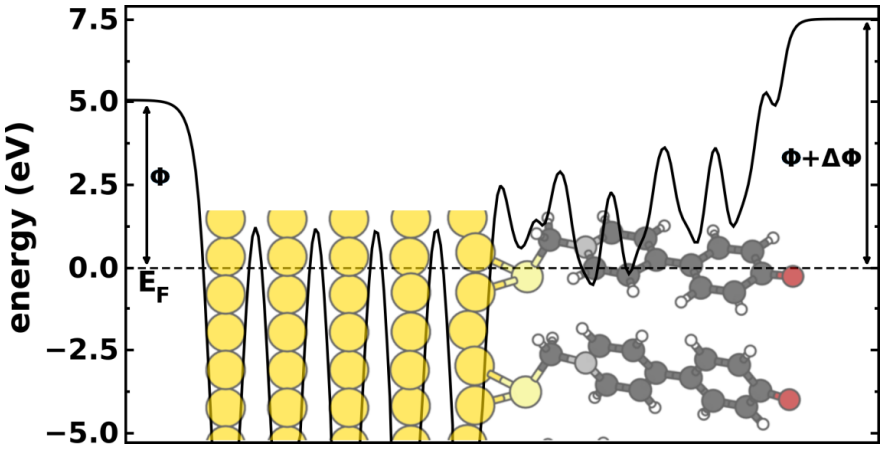

Figure S3: Plane-averaged electron electrostatic energy of the planar Au(111)/MC-SAM plotted along the surface normal. The Fermi-energy E_F and the work function Φ are indicated. The graphical representation of the SAM and substrate are plotted with a proper scaling; note that the distance between the top and bottom Au layers is *ca.* 9.7 Å.

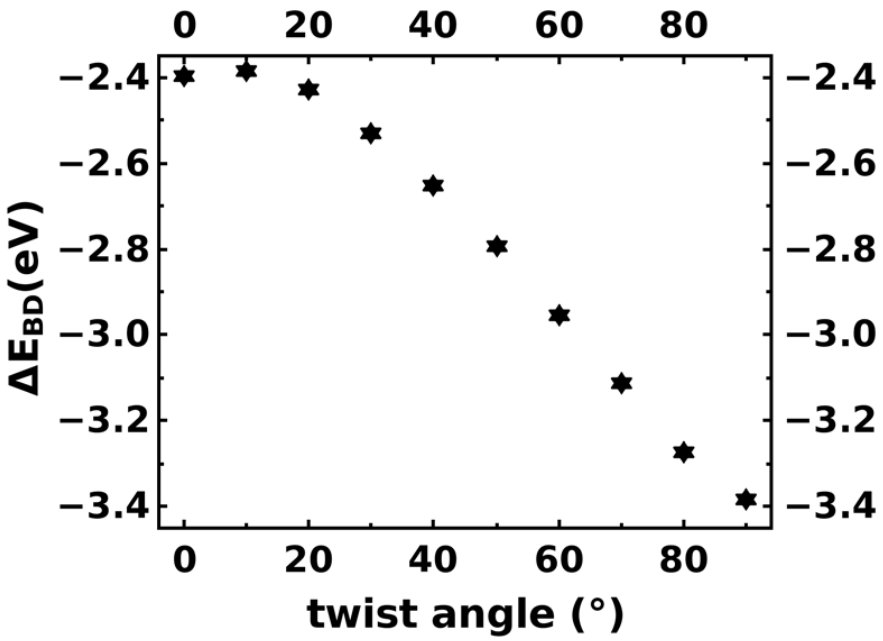

Figure S4: Bond dipole ΔE_{BD} for the MC SAMs on Au(111) as a function of the MC inter-ring twist angle, *cf.* Fig. 2a in the main text.

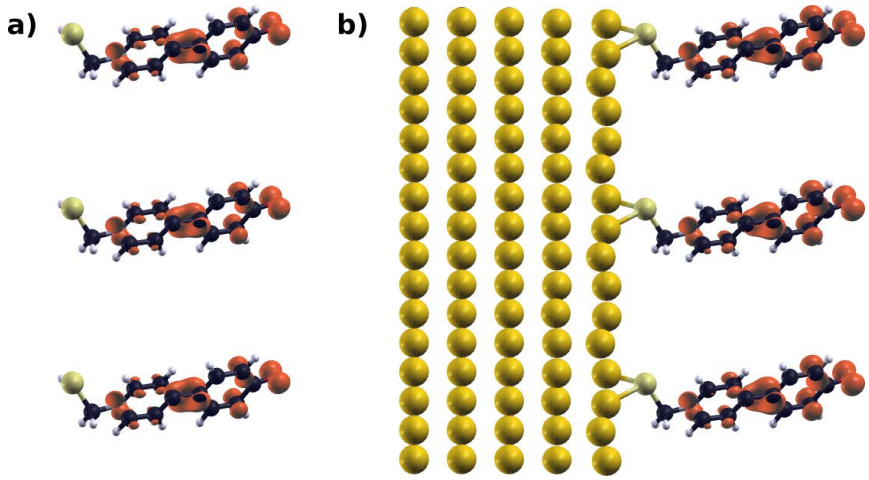

Figure S5: (a) Charge density corresponding to the highest occupied state in the free-standing MC monolayer. (b) Charge density corresponding to the electronic states integrated between E_F and (E_F – 0.1 eV) of the MC SAM on Au(111). Three unit cells are shown for the sake of clarity.

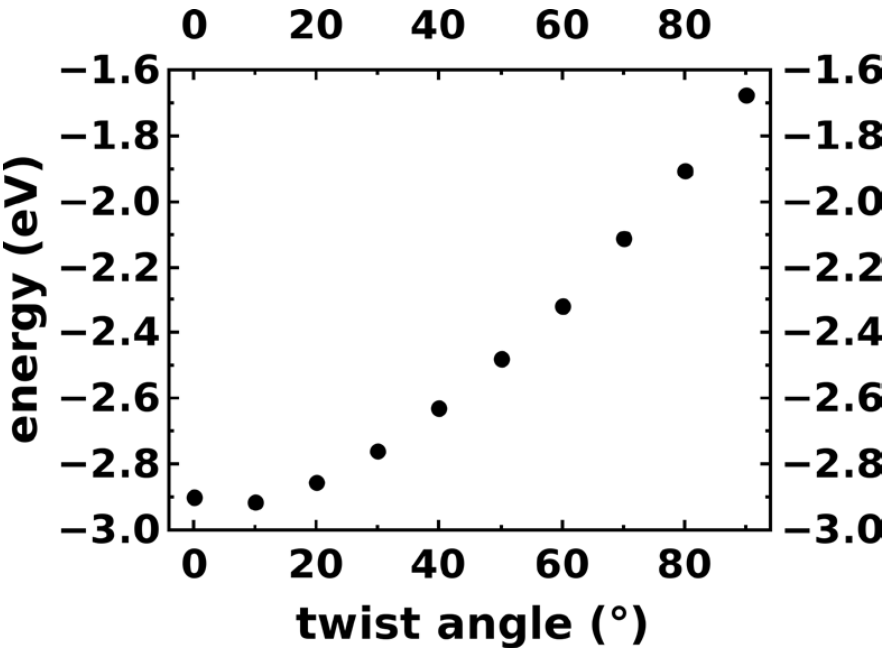

Figure S6: Energy of the onset of the highest-occupied band in the isolated MC SAM with respect to the vacuum level at the surface side (see Fig. 1c in the main text).

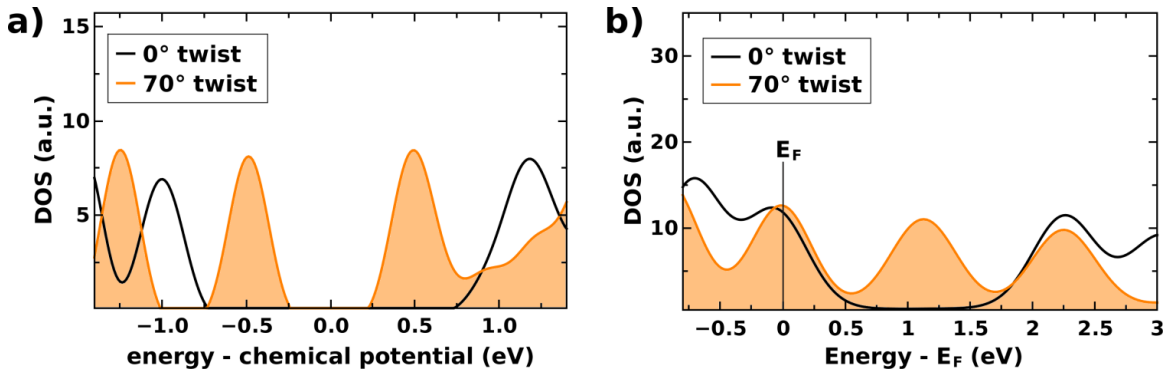

Figure S7: Comparison of the density of states (DOS) (a) for the free-standing MC monolayer and (b) projected onto the organic part of the Au(111)/MC-SAM system, at 0° and 70° inter-ring twist angle.

References

(1) Isborn, C. M.; Davidson, E. R.; Robinson, B. H. Ab Initio Diradical/Zwitterionic Polarizabilities and Hyperpolarizabilities in Twisted Double Bonds. *J. Phys. Chem. A* **2006**, *110*, 7189–7196.

(2) Kang, H.; Facchetti, A.; Jiang, H.; Cariati, E.; Righetto, S.; Ugo, R.; Zuccaccia, C.; Macchioni, A.; Stern, C. L.; Liu, Z.; *et al.* Ultralarge Hyperpolarizability Twisted π-Electron System Electro-Optic Chromophores: Synthesis, Solid-State and Solution-Phase Structural Characteristics, Electronic Structures, Linear and Nonlinear Optical Properties, and Computational Studies. *J. Am. Chem. Soc.* **2007**, *129*, 3267–3286.

(3) Brown, E. C.; Marks, T. J.; Ratner, M. A. Nonlinear Response Properties of Ultralarge Hyperpolarizability Twisted π-System Donor−Acceptor Chromophores. Dramatic Environmental Effects on Response. *J. Phys. Chem. B* **2008**, *112*, 44–50.

(4) Kresse, G.; Furthmüller, J. Efficient Iterative Schemes for Ab Initio Total-energy Calculations Using a Plane-wave Basis Set. *Phys. Rev. B* **1996**, *54*, 11169–11186.

(5) Kresse, G.; Joubert, D. From Ultrasoft Pseudopotentials to the Projector Augmented-wave Method. *Phys. Rev. B* **1999**, *59*, 1758–1775.

(6) Heimel, G.; Romaner, L.; Brédas, J.-L.; Zojer, E. Organic/metal Interfaces in Self-assembled Monolayers of Conjugated Thiols: A First-principles Benchmark Study. *Surf. Sci.* **2006**, *600*, 4548–4562.

(7) Monkhorst, H. J.; Pack, J. D. Special Points for Brillouin-zone Integrations. *Phys. Rev. B* **1976**, *13*, 5188–5192.

(8) Methfessel, M.; Paxton, A. T. High-precision Sampling for Brillouin-zone Integration in Metals. *Phys. Rev. B* **1989**, *40*, 3616–3621.

(9) Bučko, T.; Hafner, J.; Ángyán, J. G. Geometry Optimization of Periodic Systems Using Internal Coordinates. *J. Chem. Phys.* **2005**, *122*, 124508.1–124508.10.

(10) Perdew, J. P.; Burke, K.; Ernzerhof, M. Generalized Gradient Approximation Made Simple. *Phys. Rev. Lett.* **1996**, *77*, 3865–3868.

(11) Heyd, J.; Scuseria, G. E.; Ernzerhof, M. Erratum: “Hybrid Functionals Based on a Screened Coulomb Potential” [J. Chem. Phys. 118, 8207 (2003)]. *J. Chem. Phys.* **2006**, *124*, 219906.

(12) Kümmel, S.; Kronik, L. Orbital-dependent Density Functionals: Theory and Applications. *Rev. Mod. Phys.* **2008**, *80*, 3.

(13) Biller, A.; Tamblyn, I.; Neaton, J. B.; Kronik, L. Electronic Level Alignment at a Metal-molecule Interface from a Short-range Hybrid Functional. *J. Chem. Phys.* **2011**, *135*, 164706.

(14) Rissner, F.; Egger, D. A.; Natan, A.; Körzdörfer, T.; Kümmel, S.; Kronik, L.; Zojer, E. Collectively Induced Quantum-Confined Stark Effect in Monolayers of Molecules Consisting of Polar Repeating Units. *J. Am. Chem. Soc.* **2011**, *133*, 18634–18645.

5. Publication III (ref. 3)

5.1. Original Article

THE JOURNAL OF PHYSICAL CHEMISTRY C

Article

pubs.acs.org/JPCC

Understanding Structure and Bonding of Multilayered Metal–Organic Nanostructures

David A. Egger,[†] Victor G. Ruiz,[‡] Wissam A. Saidi,[§] Tomáš Bučko,[⊥,∥] Alexandre Tkatchenko,[‡] and Egbert Zojer[†,*]

[†]Institute of Solid State Physics, Graz University of Technology, Petersgasse 16, 8010 Graz, Austria

[‡]Fritz-Haber-Institut der Max-Planck-Gesellschaft, Faradayweg 4-6, 14195 Berlin, Germany

[§]Department of Chemical and Petroleum Engineering, University of Pittsburgh, 1249 Benedum Hall, Pittsburgh, Pennsylvania 15261, United States

[⊥]Department of Physical and Theoretical Chemistry, Faculty of Natural Sciences, Comenius University, Mlynska Dolina, SK-84215 Bratislava, Slovakia

[∥]Slovak Academy of Sciences, Institute of Inorganic Chemistry, Dubravska cesta 9, SK-84236 Bratislava, Slovakia

Supporting Information

ABSTRACT: For organic and hybrid electronic devices, the physicochemical properties of the contained interfaces play a dominant role. To disentangle the various interactions occurring at such heterointerfaces, we here model a complex, yet prototypical, three-component system consisting of a Cu–phthalocyanine (CuPc) film on a 3,4,9,10-perylene-tetracarboxylic-dianhydride (PTCDA) monolayer adsorbed on Ag(111). The two encountered interfaces are similar, as in both cases there would be no bonding without van der Waals interactions. Still, they are also distinctly different, as only at the Ag(111)–PTCDA interface do massive charge-rearrangements occur. Using recently developed theoretical tools, we show that it has become possible to provide atomistic insight into the physical and chemical processes in this comparatively complex nanostructure distinguishing between interactions involving local rearrangements of the charge density and long-range van der Waals attraction.

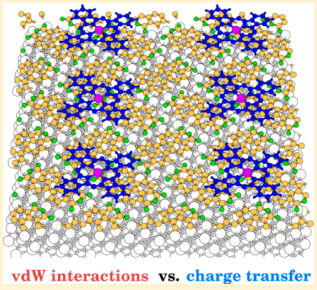

1. INTRODUCTION

When different materials approach each other, the resulting physicochemical properties of the new heterostructures are often dictated by the interfaces. The latter become even more relevant, when the dimensions of the various materials are reduced and one encounters nanoscopic structures (in the present case molecular monolayers). As various types of such heterointerfaces have become integral parts of electronic devices, it is crucial to control their structure and properties for improving device performance. Beyond that it is appealing to design the interfaces' physical and chemical properties to realize novel functionalities.[1]

Understanding the driving forces behind the formation of heterointerfaces and their consequences for the electronic properties[2] of materials is challenging, as simultaneously occurring physical and chemical processes can blur a fully microscopic view on the relevant phenomena. Bonding often occurs due to a superposition of several sources of interaction such as charge-transfer, polarization, Pauli pushback, and van der Waals attraction; consequently, an unambiguous determination of the responsible binding mechanism becomes extremely difficult. This poses a considerable challenge when trying to understand the properties of more complex systems with *several different* interfaces.[3,4] Here, atomistic modeling can aid in achieving an in-depth understanding of the relevant processes, as the latter can be traced back to the atomistic quantum-level and undesired external influences can often be excluded in a well-defined way. In passing we note that this also applies to situations where deviations from ideality such as the roughness of the interface determine the properties of a nanoscopic device, as discussed recently by Aradhya et al.[5]

In the present theoretical study, we focus on the problem of multiple interfaces in the area of organic electronics and study a prototypical multilayered heterostructure consisting of a Ag(111) metallic substrate onto which monolayers of the organic molecules 3,4,9,10-perylene-tetracarboxylic-dianhydride (PTCDA, see Figure 1a, top) and Cu-phthalocyanine (CuPc, see Figure 1a, bottom) are successively adsorbed (Ag(111)–PTCDA–CuPc, Figure 1, parts b and c). The motivation for the choice of this system is 3-fold: (i) It contains two qualitatively different interfaces (one between a metal and an organic semiconductor and one between two organic layers), where different mechanisms can be expected to establish bonding. (ii) The two interfaces are very close (separated only by a PTCDA monolayer) and, thus, can be expected to influence each other.[3] (iii) The Ag(111)–PTCDA–CuPc

Received: October 8, 2012
Revised: December 13, 2012
Published: January 8, 2013

dx.doi.org/10.1021/jp309943k | J. Phys. Chem. C 2013, 117, 3055–3061

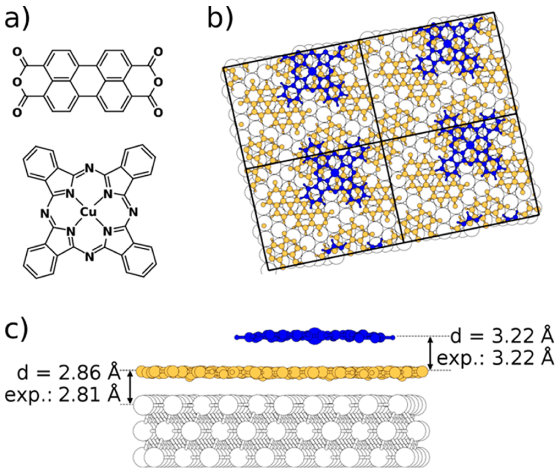

Figure 1. (a) Chemical structures of the studied organic molecules: 3,4,9,10-perylene-tetracarboxylic-dianhydride (PTCDA; top) and Cu–phthalocyanine (CuPc; bottom). Top (b) and side view (c) of CuPc (blue) on PTCDA (yellow) on Ag(111) (white); the considered unit cell is indicated in part b; the calculated and experimental[3] average distances are listed in part c. The former were extracted from a full geometry optimization, see main text.

system is, to the best of our knowledge, the only metal–organic–organic three-layer system for which full experimental information on its geometric structure has been published.[3]

Analyzing the energetic contributions to Ag(111)–PTCDA–CuPc bonding and the resulting charge-transfer at the atomistic quantum-level, we find that for both, the Ag(111)–PTCDA and the PTCDA–CuPc interfaces, no appreciable bonding would occur in the absence of long-range van der Waals (vdW) interactions. The charge-rearrangements are, however, by nearly 2 orders of magnitude larger for the formation of the interface between Ag(111) and PTCDA than for the addition of the CuPc layer, where in the former case the main effect is electron transfer from the metal substrate to the PTCDA monolayer. This hints toward relatively involved binding mechanisms for the Ag(111)–PTCDA–CuPc structure.

2. THEORETICAL METHODS AND SYSTEM SETUP

Modeling complex hybrid metal–organic systems is a sizable challenge and due to system size, atomistic modeling usually relies on density-functional theory (DFT), where long-range vdW contributions to the total energy are missing in common (semi)local approximations.[6] Employing these (semi)local density functionals can, therefore, result in an erroneous description of the binding process and a wrong prediction of the interfacial structure of hybrid metal–organic systems.[6]

Here, we show that this problem can be overcome and a reliable description of the key structural properties of the above-described multilayered heterostructure has now become possible. To this end, we employ the Perdew–Burke–Enzerhof (PBE) exchange-correlation functional[7] and include long-range vdW interactions through the recently developed PBE + vdW^{surf} scheme.[8] The latter seamlessly combines the Lifshitz–Zaremba–Kohn (LZK) theory[9,10] of the vdW interaction between an atom and a solid surface with the dispersion-inclusive PBE + vdW[11] method. Hence, the PBE + vdW^{surf} method simultaneously captures the local hybridization effects within the molecule, surface polarization effects, and the many-body response screening within the metallic bulk. It has so far been successfully applied to binary systems such as Xe, benzene, and PTCDA on transition metals[8] and to 2-pyrrolidone on Ag(111) and Ag(100) surfaces.[12] To describe laterally extended interfaces, slab-type band-structure calculations (plane-wave cutoff: ~270 eV) were employed using a modified version of the VASP code,[13] where PBE + vdW^{surf} has been implemented.[14] Core–valence interactions were treated in the projected augmented wave formalism[15] using soft potentials.[16] 3D representations of the calculated systems were generated with XCrysden.[17]

To model Ag(111)–PTCDA–CuPc, we started from the surface unit-cell observed in STM for PTCDA on Ag(111),[18] whereby the lattice parameter a was set to the value of 4.03 Å that corresponds to the lattice constant of Ag optimized using the PBE + vdW^{surf} method. This unit cell has been found to prevail within the PTCDA layer also in the Ag(111)–PTCDA–CuPc system.[3] We doubled the unit cell in one direction (see Figure 1b), which allowed us to define a structural model with one CuPc molecule per simulation cell. This results in the final unit cell containing one CuPc and four PTCDA molecules, three layers of Ag(111) and altogether more than 400 atoms (Figure 1b and Figure 1c). We note that the experimentally observed unit cell of commensurate Ag(111)–PTCDA–CuPc at full CuPc coverage is even larger by a factor of 2.5 and also contains a larger fraction of CuPc molecules (four CuPc and ten PTCDA molecules per unit cell).[3] Our structural model, however, provides a CuPc coverage close to the packing for which the vertical bonding distances have been reported in ref 3.[19] Further details on the computational methodology and system setup are described in the Supporting Information.

3. RESULTS AND DISCUSSION

3.1. Bonding in the Ag(111)–PTCDA–CuPc Heterostructure. We first analyze the interactions between a CuPc layer and Ag(111)–PTCDA by calculating its binding-energy curve as a function of the vertical distance, d, separating the CuPc layer from Ag(111)–PTCDA. The binding energy $E_B(d)$ is then obtained as

$$E_B(d) = E_{sys}(d) - (E_{sub} + E_{ads}) \quad (1)$$

where E_{sys} is the energy of the complete heterostructure Ag(111)–PTCDA–CuPc, E_{sub} is the energy of the "substrate" (here, the PTCDA layer on silver) and E_{ads} the energy of the adsorbate (here, the CuPc layer, for further details see the Supporting Information). By calculating $E_B(d)$ separately with PBE + vdW^{surf} and pure PBE, i.e., effectively *including and neglecting* vdW interactions, we are capable of assessing their role in the bonding of CuPc to Ag(111)–PTCDA. The results in Figure 2 show that no bonding between CuPc and Ag(111)–PTCDA is predicted in the absence of long-range vdW interactions, revealing their importance in establishing the Ag(111)–PTCDA–CuPc interface. Notably, vdW interactions, which are commonly thought of as being "weak", are in the range of several eV and thus substantially contribute to the relatively large binding energy between Ag(111)–PTCDA and CuPc of ~2.7 eV per CuPc molecule. This is primarily a consequence of the size of the interacting molecules, as the vdW contribution to the overall binding energy of 2.7 eV amount to a quite moderate ~0.1 eV per heavy atom in CuPc.

dx.doi.org/10.1021/jp309943k | J. Phys. Chem. C 2013, 117, 3055–3061

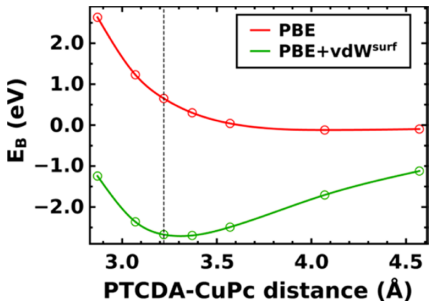

Figure 2. Binding energy E_B between the CuPc layer and Ag(111)−PTCDA as a function of the difference between the average vertical positions of the carbon atoms in the PTCDA and CuPc layers calculated with PBE (red) and PBE + vdW^{surf} (green); the dashed vertical line indicates the experimental distance.[3]

Compared to experiment[3] (dashed vertical line in Figure 2), the equilibrium distance calculated with PBE + vdW^{surf} is already encouraging given that here only a single geometric parameter (the bonding distance) has been "optimized".

For the metal−organic interface between Ag(111) and PTCDA, it is well-known that an equilibrating electron transfer from the silver surface into the band derived from the lowest unoccupied molecular orbital of the PTCDA molecules (former LUMO; F-LUMO) pins that band to the Fermi level.[3,20] Nevertheless, it was repeatedly seen when modeling the Ag(111)−PTCDA structure that only the proper inclusion of vdW interactions yields a realistic binding-energy profile,[6,8,21,22] indicating that a combination of several different binding interactions is responsible for the formation of the Ag(111)−PTCDA interface.

This raises the question, to what extent those interactions are modified by the presence of a CuPc layer (cf., discussion in ref 3). To elucidate this, we compare the binding-energy curves for the PTCDA−CuPc double-layer and the PTCDA single-layer on Ag(111) in Figure 3a (again obtained from calculating the energy difference of the respective combined and separated systems, see Supporting Information for details). As can be seen from the figure, the two binding energy curves are similar, but the PTCDA−CuPc double-layer binds slightly more strongly to Ag(111) than the PTCDA single-layer alone. The origin of this difference can be traced back to the PBE and vdW^{surf} parts of the respective binding-energy curves (see Supporting Information). Calculating the corresponding binding-energy differences (see Figure 3b) allows disentangling the pure long-range vdW contribution (vdW^{surf}) from all other chemical/physical interactions (PBE). The data show that primarily the vdW attraction between PTCDA−CuPc and the silver surface is stronger compared to the PTCDA single-layer on Ag(111). With an energy contribution of ∼0.12 eV at the equilibrium distance, this effect is relatively small compared to the total vdW attractive energy between Ag(111) and PTCDA−CuPc, which amounts to ca. 2.9 eV at the same distance (see Supporting Information). Nevertheless, the other energetic contributions to ΔE_B are clearly less affected by the presence of the CuPc layer. The two main effects contributing to this additional van der Waals interaction can be traced back to (i) the direct vdW attraction between CuPc and the Ag(111) substrate (calculated by removing the PTCDA layer and amounting to 0.07 eV at the equilibrium distance) and (ii) an increased PTCDA−CuPc vdW interaction due to the charge

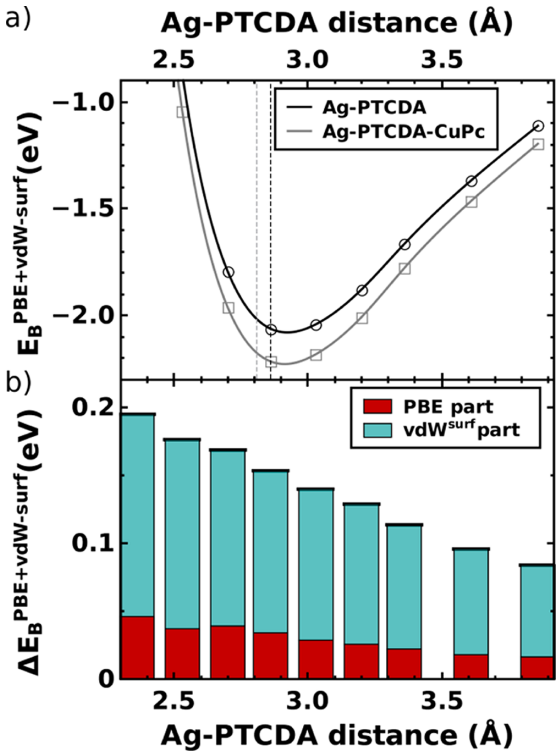

Figure 3. (a) PBE + vdW^{surf} binding-energy curves of a PTCDA single-layer (black) and a PTCDA−CuPc double-layer (gray), adsorbing on Ag(111) as a function of the Ag(111)−PTCDA distance; dashed vertical lines indicate the experimental binding distances for PTCDA[20] (black) and PTCDA−CuPc[3] (gray) on Ag(111). (b) Binding-energy difference ΔE_B of the two curves in part a with the respective PBE (red) and vdW^{surf} (cyan) energy contributions.

transfer between the Ag(111) substrate and the PTCDA layer. The latter occurs because the charge transfer increases the PTCDA's molecular C_6 coefficients by 11% compared to those of the monolayer in the absence of Ag (111) (cf., ref 8). That this effect is accounted for in our calculations is an intrinsic advantage of the applied PBE + vdW^{surf} scheme, where the determination of the C_6 parameters involves a Hirshfeld partitioning of the charge density and, thus, is affected by charge-transfer effects.[11]

The detailed interfacial atomic structure critically affects the electronic properties of interfaces such as the work function, the alignment between electronic levels, and the adsorption-induced charge transfer.[22] To obtain the latter and also to fully benchmark our calculations against experiments in which, naturally, all nuclear degrees of freedom (and not only the interlayer distance) are relaxed, we performed a full geometry relaxation of the Ag(111)−PTCDA−CuPc system (using the GADGET tool;[23] for further details see Supporting Information). This improves the description of equilibrium adsorption distances compared to the approximate value obtained in binding-energy curves (Figure 2 and 3a). The finally obtained adsorption distances (determined by the average carbon positions in the PTCDA and CuPc layers and the hypothetical position of the unrelaxed top Ag layer) are compared to the

dx.doi.org/10.1021/jp309943k | J. Phys. Chem. C 2013, 117, 3055−3061

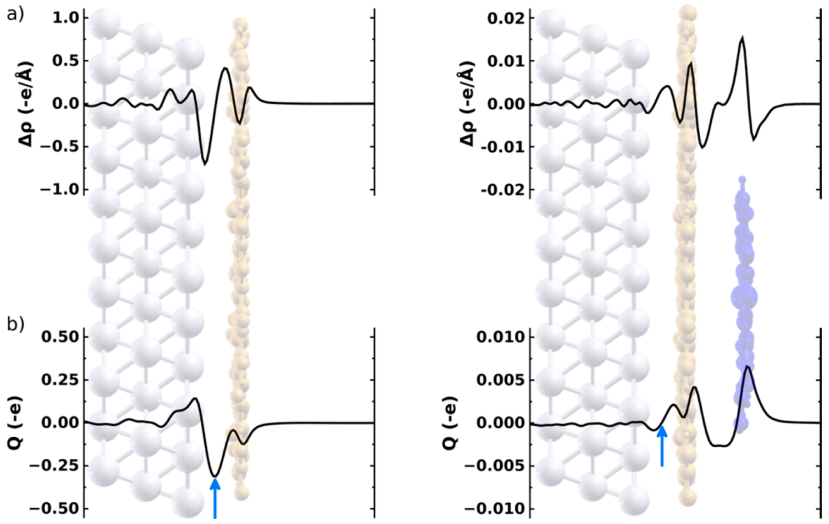

Figure 4. Plane-integrated charge rearrangements $\Delta\rho$ (a) and cumulative charge transfer Q (b) induced upon PTCDA adsorption onto Ag(111) (left) and CuPc adsorption onto Ag(111)−PTCDA (right). These quanitites are calculated from the charge-density differences of the combined systems (left, Ag(111)−PTCDA; right, Ag(111)−PTCDA−CuPc) and the respective subsystems (left, Ag(111) and PTCDA; right, Ag(111)−PTCDA and CuPc). $\Delta\rho$ and Q are reported per PTCDA molecule. Note that the scales in the left and right part differ by a factor of 50. "e" refers to the (positive) elementary charge; consequently, negative values in the $\Delta\rho$-plot correspond to a reduction of the electron density, while positive $\Delta\rho$ are a manifestation of electron accumulation. For the meaning of the sign of Q, see main text.

corresponding experimental result in Figure 1c: Both the metal−organic as well as the organic−organic interlayer distances compare exceptionally well to experimental values.[3] Moreover, we find that the adsorption of CuPc on top of Ag(111)−PTCDA pushes the PTCDA layer toward the silver surface by on average 0.05 Å (2.86 Å vs 2.91 Å), a subtle geometric effect also seen for the average distances in the experiment (2.81 Å vs 2.86 Å).[3] Interestingly, when examining the four inequivalent PTCDA molecules in the unit cell, the calculations reveal variations in the individual adsorption distances between 2.83 and 2.88 Å, depending on how much a PTCDA molecule is "covered" by the CuPc. This effect is not captured by the binding-energy curves, where all layers are assumed to be flat; it is, thus, a possible reason why there the minimum positions are shifted only very slightly (by only 0.01 Å) upon CuPc adsorption (cf., Figure 3a).

3.2. Charge Rearrangements at the Ag(111)−PTCDA and PTCDA−CuPc Interfaces. With a reliable adsorption geometry at hand, assessing the adsorption-induced charge rearrangements, $\Delta\rho$, between the various layers becomes possible. This quantity is interesting as it sheds light onto bonding between CuPc and Ag(111)−PTCDA beyond vdW interactions and provides insight into the extent to which the Ag(111)−PTCDA interaction is modified by CuPc adsorption. Moreover, it directly translates into a work-function change $\Delta\Phi$ via the Poisson equation. The profound charge rearrangements due to Ag(111)−PTCDA interface formation are shown integrated over the *xy*-plane per PTCDA molecule in Figure 4a (left) and as isodensity plots in Figure 5, parts a and b. They hint toward an interaction between PTCDA and Ag(111) far beyond vdW, as discussed in detail in refs 20, 22, 24, and 25. The electron density right above the Ag(111) surface is reduced with the primary reduction occurring below the carboxylic oxygens of the PTCDA layer (see Figure 5a),[25] and some of the charge is redistributed to the region around the top metal layer (as one would expect for Pauli push-back). The main effect, however, is a transfer of electron density to the π-system of PTCDA associated with a filling of the F-LUMO (see Figure 5a)[20,22] that results in Fermi-level pinning. This is accompanied by a somewhat reduced charge density in the σ-orbitals (i.e., in the plane of the molecule) with the largest effect around the carboxylic oxygens. The latter is often observed for the adsorption of acceptor layers and can be related to back-donation processes.[26] To obtain an alternative view of the adsorption-induced charge transfer, we integrate $\Delta\rho$ over distance to obtain the cumulative charge rearrangements Q:[27] A negative value of Q (when plotted in units of $-e$, with e representing the positive elementary charge) at a given position specifies the number of electrons transferred from left-to-right of a plane at that position; correspondingly, a positive value of Q denotes a transfer from right to left and a Q value of zero means that on average no charge is shifted across this plane. For PTCDA adsorbing on Ag(111), Q is indeed substantial (Figure 4b, left) and the (negative) maximum between Ag(111) and PTCDA (indicated by a blue arrow) shows that the net transfer amounts to ca. 0.31 electrons per PTCDA molecule (for more details, see ref 22.).

The adsorption of the CuPc layer impacts the interfacial charge rearrangements only to a very small extent. Overall two effects need to be considered: (i) The PTCDA layer is pushed closer to the substrate, which slightly reduces the distortion of the carboxylic oxygens and, thus, the intrinsic dipole moment of the PTCDA layer. As expected when being in the Fermi-level pinning regime,[28] this decreases the charge-transfer induced dipole between Ag and PTCDA that counteracts the intrinsic molecular dipole. The effect is, however, small (amounting to a reduction of the absolute value of the maximum of Q by 0.02 e) and considering that we do not observe an associated destabilization of the F-LUMO peak, it is attributed to an increase of the above-mentioned back-donation from σ-orbitals.

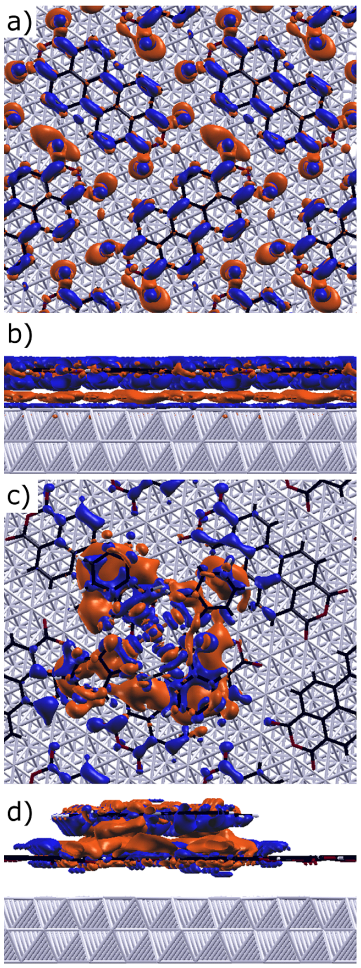

Figure 5. Isodensity plots depicting charge rearrangements upon adsorption of a PTCDA single-layer onto a Ag(111) surface (a, b) and a CuPc layer onto Ag(111)−PTCDA (c, d). Blue (red) regions denote electron accumulation (depletion). Note that due to the much smaller charge rearrangements upon CuPc adsorption, the isodensity value used for parts c and d has been reduced by a factor of 28.

Moreover, the absolute numbers have to be treated with some caution as they are directly related to the positions of the carboxylic oxygens relative to the backbone, which are only quite poorly described when using soft PAW potentials.[16] Our tests described in the Supporting Information however indicate that their impact on the comparison of the situations with and without CuPc layer is only minor.

(ii) The main observation for the additional $\Delta\rho$ when also adding the CuPc layer (Figure 4a, right) is that the magnitude of the calculated peaks is by a factor of ∼50 smaller than the $\Delta\rho$ observed for the interaction between PTCDA and Ag(111). Moreover, the additional $\Delta\rho$ is essentially confined to the organic layers; i.e., there is no further impact on the charge-transfer between Ag(111) and PTCDA as can also be inferred from the corresponding Q in the right part of Figure 4b crossing the zero line between the Ag substrate and the PTCDA layer (indicated by the blue arrow). We find also no clear indications for Pauli push-back between the organic layers (even at the strongly inflated $\Delta\rho$ scale used in Figure 4a). This is ascribed to a — relative to the metal substrate — massively reduced polarizability of the electron cloud in the organic layers and to a stronger spatial confinement of the electrons (i.e., a reduced tailing of the charge density above the PTCDA layer, as plotted in the Supporting Information). The 3D charge-rearrangement pattern for CuPc adsorption shown in Figure 5, parts c and d, is relatively complex and does not allow a clear identification of specific "modes" of interaction. An interesting observation is the electron depletion above the PTCDA layer especially underneath the CuPc molecules. This is accompanied by charge accumulations directly above the PTCDA layer, especially further away from the CuPc molecules, and also in the region directly below the CuPc layer.

The negative values of Q between the PTCDA and CuPc layers indicate a very minor (0.003 electrons per CuPc molecule) electron transfer from PTCDA to CuPc consistent with the isodensity plot in Figure 5, parts c and d. Moreover, both organic layers appear somewhat polarized (*cf.*, Figure 4, right plots) such that electron density is shifted from above the planes of the molecular backbones to below. Regarding this analysis it, however, needs to be kept in mind that the overall magnitude of all rearrangements observed at the PTCDA/CuPc interface are very minor probably reaching the accuracy limit of state of the art calculations.

3.3. Work-Function Changes and the Density of States. The above-described interfacial charge rearrangements together with the possible dipole moment of an adsorbing layer determine the adsorption-induced work-function modification $\Delta\Phi$. For PTCDA adsorption on Ag(111), electron transfer from the metal to the organic adsorbate dominates over the push-back, which together would result in an increase of the work function by $\Delta\Phi_{\Delta_\rho}$ = 0.41 eV. This effect is, however, diminished by the intrinsic dipole of the PTCDA layer (vide infra). The latter originates from the C and O atoms not being in the same plane.[20,22] Regarding the impact of additionally adsorbing the CuPc molecules, a first observation is the only very small intrinsic dipole moment associated with the adsorbed CuPc monolayer amounting to an additional work-function increase on the order of 0.01 eV. Thus, adsorbing CuPc on Ag(111)−PTCDA could induce a significant $\Delta\Phi$ only via charge rearrangements. As discussed in the preceding section, the latter are, however, extremely small. Therefore, it is not surprising that in all cases we studied, $\Delta\Phi$ relative to the bare Ag(111) surface is calculated to lie between 0.04 and 0.05 eV for both the fully optimized Ag(111)−PTCDA and Ag(111)−PTCDA−CuPc system.[29] For Ag(111)−PTCDA, this value is in good agreement with $\Delta\Phi$ = 0.1 eV measured for PTCDA on Ag(111) by Zou et al.[30] A comparative experimental investigation of $\Delta\Phi$ for Ag(111)−PTCDA−CuPc and Ag(111)−PTCDA interfaces, thus, would provide a straightforward way to test the above predictions regarding interfacial charge transfer; to the best of our knowledge, such data on Ag(111)−PTCDA−CuPc are, however, not yet available.

Alternatively, one can compare the valence photoelectron spectra for the two systems as done in ref 3. In the calculations (cf., Supporting Information), we obtain a good qualitative agreement between theoretical and experimental spectra confirming also the assignment in ref 3 of the various peaks to ionization processes within either the PTCDA or CuPc

dx.doi.org/10.1021/jp309943k | J. Phys. Chem. C 2013, 117, 3055−3061

layers; in particular, the association of the highest binding energy feature to the partially filled F-LUMO of PTCDA is supported by the calculations. Associating the measured small (at the maximum 0.12 eV) shift of the PTCDA F-LUMO feature in the valence photoelectron spectrum upon CuPc deposition with charge rearrangements between the Ag(111) substrate and the PTCDA layer (as suggested in ref 3) is, however, potentially complicated by the observation in tunneling spectroscopy experiments that the peak due to the F-LUMO consists of two maxima split by 0.16 eV.[24,25] These arise from the inequivalent molecules in the PTCDA unit cell. As a consequence, an apparent shift of the F-LUMO feature could also be a consequence of cross-section redistributions between the two peaks due to the inequivalent molecules, caused, e.g., by the minor charge rearrangements between PTCDA and CuPc discussed in the previous section or by "shielding" of photoelectrons from the PTCDA layer by CuPc molecules. This effect, however, cannot be captured by our simulations as (i) the calculation of valence photoelectron cross sections would go far beyond the scope of the present paper and (ii) the splitting between the two inequivalent molecules on the Ag(111) surface is not properly recovered by our DFT calculations in analogy to what is described in ref 25. The latter could, indeed, be the explanation, why in the calculations the F-LUMO peak shifts by only 0.01 eV due to the CuPc (note that this value has been obtained at a reduced CuPc coverage as described in section 2). The experimental observation that the position of the former PTCDA HOMO virtually does not shift with increasing CuPc coverage,[3] in fact supports the notion that the electronic states in the PTCDA layer are not rigidly shifted relative to the metal states by some interfacial charge rearrangements induced by CuPc adsorption. (Note that for the former PTCDA HOMO, differences between the two inequivalent molecules in the unit cell are expected to be of only minor relevance, as for the associated feature the above-described tunneling spectroscopy measurements revealed a splitting of only 0.04 eV.[24,25]) These considerations show that a full explanation of all details of the measured valence photoelectron spectra including the presence or absence of small peak shifts by the present calculations remains, however, elusive due to the sheer system size that imposes limitations both on the chosen model unit-cell as well as on the applied computational tools (requiring, e.g., the use of relatively few metal layers to describe the substrate and the application of soft PAW-potentials combined with a relatively sparse *k*-point grid). Further details on the discussion in this paragraph can be found in the Supporting Information together with the calculated density of states.

4. CONCLUSIONS

In summary, we have studied the bonding in a complex three-component system that contains different heterointerfaces. It serves as a prototypical example for portraying the intricate interplay of different processes that determine the interfacial structure in organic nanostructures and also for highlighting the potential of modern computational modeling tools: In Ag(111)−PTCDA−CuPc, the bonding-induced charge transfer is vastly different at the metal−organic (Ag(111)−PTCDA) and the organic−organic (PTCDA−CuPc) interface with very small charge redistributions in the latter case. These coincide with an only very minor additional modification of the system work-function by the adsorbing CuPc layer. While certain ambiguities regarding the interpretation of the calculated density of states and the valence photoelectron spectra in ref 3 remain, it is clearly shown here that bonding for both interfaces is vastly dominated by long-range vdW interactions. Their magnitude is large for both interfaces (ca. 3 eV at the equilibrium distances) rendering a characterization of such interfaces as weakly bonded questionable, even if the dominant interaction strength does not originate from a single, strong bond but from the combined attraction of all atoms that are part of the interacting subsystems. To put the magnitude of the vdW interactions into perspective, it is interesting to remember that the significant charge rearrangements at the Ag(111)/PTCDA interface alone do not result in any appreciable bonding interaction. In passing, we note that such strong binding due to vdW interactions has recently also been extracted from scanning tunneling and atomic force microscope measurements of PTCDA on Au(111).[31]

These results show that a fully quantitative description of metal−organic interfaces without considering vdW interactions is not generally possible and restricted to very few systems that bond, e.g., through suitable anchoring groups. Our data, however, also indicate that by including vdW interactions at surfaces using the recently developed PBE + vdW^{surf} scheme, the necessary reliable description of the geometric structure has become an achievable goal even for large and complex hybrid metal−organic systems. We conclude that with suitable theoretical tools becoming increasingly available, computational modeling can indeed contribute to deriving a detailed microscopic picture of complex hybrid nanostructures.

■ ASSOCIATED CONTENT

Supporting Information

Details on the methodology and system setup, various tests assessing the reliability of our simulations, additional binding-energy curves, calculations of the tailing of the electron clouds, and discussion of the calculated density of states. This material is available free of charge via the Internet at http://pubs.acs.org.

■ AUTHOR INFORMATION

Corresponding Author

*E-mail: egbert.zojer@tugraz.at.

Notes

The authors declare no competing financial interest.

■ ACKNOWLEDGMENTS

The authors thank B. Stadtmüller and C. Kumpf for helpful discussions. D.A.E. is a recipient of a DOC fellowship by the Austrian Academy of Sciences. Financial support by the Austrian Science Fund (FWF), P24666-N20, and from the FP7 Marie Curie Actions of the European Commission, via the Initial Training Network SMALL (MCITN-238804) is gratefully acknowledged. A.T. is supported by a grant from the European Research Council (ERC Starting Grant VDW-CMAT). T.B. receives support by the VASP project and by the Slovak Research and Development Agency under the contract No. APVV-0059-10. Our calculations have been performed at the icluster (ZID TU Graz) and the VSC-2 (Vienna Scientific Cluster).

■ REFERENCES

(1) Koch, N. *ChemPhysChem* **2007**, *8*, 1438−1455.
(2) Ishii, H.; Sugiyama, K.; Ito, E.; Seki, K. *Adv. Mater.* **1999**, *11*, 605−625.

(3) Stadtmüller, B.; Sueyoshi, T.; Kichin, G.; Kröger, I.; Soubatch, S.; Temirov, R.; Tautz, F.; Kumpf, C. *Phys. Rev. Lett.* **2012**, *108*, 106103.
(4) Niederhausen, J.; Amsalem, P.; Wilke, A.; Schlesinger, R.; Winkler, S.; Vollmer, A.; Rabe, J.; Koch, N. *Phys. Rev. B* **2012**, *86*, 081411(R).
(5) Aradhya, S. V.; Frei, M.; Hybertsen, M. S.; Venkataraman, L. *Nat. Mater.* **2012**, *11*, 872−876.
(6) Tkatchenko, A.; Romaner, L.; Hofmann, O. T.; Zojer, E.; Ambrosch-Draxl, C.; Scheffler, M. *MRS Bull.* **2011**, *35*, 435−442.
(7) Perdew, J. P.; Burke, K.; Ernzerhof, M. *Phys. Rev. Lett.* **1996**, *77*, 3865−3868.
(8) Ruiz, V.; Liu, W.; Zojer, E.; Scheffler, M.; Tkatchenko, A. *Phys. Rev. Lett.* **2012**, *108*, 146103.
(9) Lifshits, E. M. *Sov. Phys. JETP* **1956**, *2*, 73.
(10) Zaremba, E.; Kohn, W. *Phys. Rev. B* **1976**, *13*, 2270−2285.
(11) Tkatchenko, A.; Scheffler, M. *Phys. Rev. Lett.* **2009**, *102*, 073005.
(12) Al-Saidi, W. A.; Feng, H.; Fichthorn, K. A. *Nano Lett.* **2012**, *12*, 997−1001.
(13) Kresse, G.; Furthmüller, J. *Phys. Rev. B* **1996**, *54*, 11169−11186.
(14) Al-Saidi, W. A.; Voora, V. K.; Jordan, K. D. *J. Chem. Theory Comput.* **2012**, *8*, 1503−1513.
(15) Kresse, G.; Joubert, D. *Phys. Rev. B* **1999**, *59*, 1758−1775.
(16) For a description of test-calculations using harder potentials, see the Supporting Information.
(17) Kokalj, A. *Comput. Mater. Sci.* **2003**, *28*, 155.
(18) Glöckler, K.; Seidel, C.; Soukopp, A.; Sokolowski, M.; Umbach, E.; Böhringer, M.; Berndt, R.; Schneider, W.-D. *Surf. Sci.* **1998**, *405*, 1−20.
(19) It corresponds to 60% of the experimentally observed full coverage, which is only by a factor of ca. 1.5 larger than the coverage chosen in the calculations. Stadtmüller, B. ; Kumpf, C. Private communication.
(20) Hauschild, A.; Karki, K.; Cowie, B.; Rohlfing, M.; Tautz, F.; Sokolowski, M. *Phys. Rev. Lett.* **2005**, *94*, 036106.
(21) Rohlfing, M.; Bredow, T. *Phys. Rev. Lett.* **2008**, *101*, 266106.
(22) Romaner, L.; Nabok, D.; Puschnig, P.; Zojer, E.; Ambrosch-Draxl, C. *New J. Phys.* **2009**, *11*, 053010.
(23) Bučko, T.; Hafner, J.; Ángyán, J. G. *J. Chem. Phys.* **2005**, *122*, 124508.
(24) Kraft, A.; Temirov, R.; Henze, S. K. M.; Soubatch, S.; Rohlfing, M.; Tautz, F. S. *Phys. Rev. B* **2006**, *74*, 041402(R).
(25) Rohlfing, M.; Temirov, R.; Tautz, F. *Phys. Rev. B* **2007**, *76*, 115421.
(26) Romaner, L.; Heimel, G.; Brédas, J. L.; Gerlach, A.; Schreiber, F.; Johnson, R. L.; Zegenhagen, J.; Duhm, S.; Koch, N.; Zojer, E. *Phys. Rev. Lett.* **2007**, *99*, 256801.
(27) Stadler, R.; Jacobsen, K. W. *Phys. Rev. B* **2006**, *74*, 161405(R).
(28) Hofmann, O. T.; Egger, D. A.; Zojer, E. *Nano Lett.* **2010**, *10*, 4369.
(29) A closer inspection reveals that the impact of the CuPc layer arises not only from its very minor intrinsic dipole, but is also impacted by the small charge rearrangements shown in Figure 4 and by the consequences arising from the modified adsorption distance of the PTCDA layer. All three effects are of comparable magnitude and amount to ∼0.01 eV with the intrinsic dipole and reduced adsorption distance giving rise to a work-function increase that is partially compensated by the charge rearrangements at the PTCDA/CuPc interface. A further analysis of these tiny effects does not appear particularly useful.
(30) Zou, Y.; Kilian, L.; Schöll, A.; Schmidt, T.; Fink, R.; Umbach, E. *Surf. Sci.* **2006**, *600*, 1240−1251.
(31) Wagner, C.; Fournier, N.; Tautz, F.; Temirov, R. *Phys. Rev. Lett.* **2012**, *109*, 076102.

5.2. Supporting Information

Supporting Information to:

"Understanding Structure and Bonding of Multilayered Metal-Organic Nanostructures"

David A. Egger[1], Victor G. Ruiz[2], Wissam. A. Saidi[3], Tomáš Bučko[4,5], Alexandre Tkatchenko[2], and Egbert Zojer[1]

[1] Institute of Solid State Physics, Graz University of Technology, Petersgasse 16, 8010 Graz, Austria.

[2] Fritz-Haber-Institut der Max-Planck-Gesellschaft, Faradayweg 4-6, 14195 Berlin, Germany.

[3] Department of Chemical and Petroleum Engineering, University of Pittsburgh, 1249 Benedum Hall, Pittsburgh, PA 15261, U.S.A.

[4] Department of Phycical and Theoretical Chemistry, Faculty of Natural Sciences, Comenius University, Mlynska Dolina, SK-84215 Bratislava, Slovakia.

[5] Slovak Academy of Sciences, Institute of Inorganic Chemistry, Dubravska cesta 9, SK-84236 Bratislava, Slovakia.

*Corresponding author: egbert.zojer@tugraz.at

Details on the Methodology and System Setup

All results reported in the main text have been obtained with the VASP code[1] and, if not otherwise stated, with an energy convergence criterion for the SCF cycle of 10^{-4} eV and a $\Delta\Phi$ convergence criterion of 10^{-2} eV. Due to the large surface unit-cell, we employed a 2x1x1 Monkhorst-Pack[2] *k*-point grid. We used a Methfessel-Paxton occupation scheme (smearing: 0.2 eV).[3] The unit cell was 3D-periodically repeated, where we inserted a vacuum gap of ~20 Å in the z-direction that is perpendicular to the surface and, whenever necessary, used a counter-dipole correction to prevent spurious interactions. In case of Ag(111)-CuPc-PTCDA, we employed spin-polarized calculations owing to the odd number of electrons in the CuPc molecule. In this context, it is interesting that the results for vertical bonding distances in the fully optimized structure obtained in a spin-unpolarized optimization are similar (deviations <0.05 Å). The PBE+vdW^{surf} method[4] results in screened C_6 coefficients, vdW radii and polarizabilities, which in technical terms means that for the case of Ag(111)-PTCDA-CuPc the free-atom vdW parameters[5] of silver are replaced by the screened ones.[4] The geometry optimization was performed in internal coordinates using the GADGET code,[6] where we kept the bottom two layers of Ag(111) fixed and relaxed the structure until all forces where below 0.01 eV/Å. We note that for Ag(111)-PTCDA-CuPc, GADGET resulted in a *ca.* five-time speed up compared to a damped molecular dynamics scheme.

For calculating the binding-energy curves and performing the full ionic relaxation, a CuPc molecule was placed onto four PTCDA molecules in a surface unit-cell as shown in Fig. 1b in the main text, which corresponds to the adsorption site denoted as "B" in Ref. [7]. There, several other simultaneous adsorption sites and a very large unit cell have been observed, whose calculation is not yet computationally feasible. To test the impact of the adsorption site we also placed the CuPc molecule in the middle of the surface unit-cell and obtained similar results (deviations <0.05 Å) for the adsorption distances.

To calculate the various binding-energy curves (*cf.*, Fig. 2 and Fig. 3 in the main text), several geometric parameters need to remain fixed:
(i) For obtaining the binding-energy curve between CuPc and Ag(111)-PTCDA (*cf.* Fig. 2 in the main text), we used the fully relaxed Ag(111)-PTCDA geometry and optimized an isolated planar CuPc layer. We then placed the CuPc layer on-top of Ag(111)-PTCDA and varied the CuPc-PTCDA distance without allowing any further relaxation; as mentioned in the main text, we report the distance between the average values of the carbon atoms inside CuPc and PTCDA in order to compare the calculated to the experimental results.
(ii) To obtain the binding-energy curves of the PTCDA single-layer and the CuPc-PTCDA double-layer to the Ag(111) substrate (*cf.*, Fig. 3 a & b in the main text), we first relaxed the Ag(111) surface, the isolated PTCDA single-layer and the isolated CuPc-PTCDA double-layer. In those relaxations, the coordinates of the bottom-two Ag(111) layers were kept fixed, the isolated organic layers were forced to remain planar during the relaxations, and the CuPc-PTCDA distance was set to be 3.22 Å (the eventually obtained average equilibrium distance in the full geometry optimization). We then varied the distance between the individually optimized Ag(111) and PTCDA and between the Ag(111) and CuPc-PTCDA sub-systems, respectively, again without further relaxations. Distances between the average values of the carbon atoms inside PTCDA and the hypothetical unrelaxed Ag(111) surface are reported in order to be consistent with the experimental procedure.

We note that the small reduction of the Ag(111)-PTCDA distance seen in experiment[7] and in our fully relaxed structure (see main text) is not reproduced by the binding-energy curve calculations. This might arise from the fact that, as discussed above, in the binding-energy curves many geometric parameters are kept fixed making them only a rough approximation to a full geometry relaxation. Moreover, in the case of Ag(111)-PTCDA-CuPc, we find that the four PTCDA molecules in the relaxed structure are at different vertical distances (up to 0.05 Å) from the underlying Ag(111) depending on whether they are covered by the CuPc layer or not, supporting our interpretation that the CuPc layer "pushes" the PTCDA slightly down towards Ag(111). This effect cannot be entangled in the binding-energy curve, as for its calculation we assumed a flat PTCDA sheet (*vide supra*).

Discussion on the convergence of spin-polarized calculations

Obtaining the correct spin-polarized ground state (with a magnetic moment of $1\mu_B$) is rather difficult as the large number of atoms in the unit cell promotes many different minima with similar energies. For all calculations, we thus ensured that a spin-polarized ground state is obtained and checked that the magnetic moment is largely located at the copper atom and the surrounding nitrogen atoms bound to it. In case of the binding-energy curves, we performed two subsequent calculations: (i) A spin-unpolarized calculation, and (ii) a spin-polarized calculation with an initial magnetic moment of $1.5\mu_B$ for the Cu atom (for all other atoms $0\mu_B$) and the charge density from (i) as starting guess. Despite these precautions, we still experienced convergence issues when calculating the binding-energy curves, as can be seen, for example, in Fig. 3b of the main text (at d = 2.53 Å), where a deviation from a "smooth" curve is observed. We performed several different test calculations to improve the data points, *e.g.*, reduced the smearing for the occupation scheme, increased the convergence criterion in the SCF procedure, increased the number of *k*-points, made slight variations in the bonding distance, and tried several different starting configurations for the spin-polarized calculations. By those measures we could not improve the "smoothness" of the binding-energy curves. This indicates that the reported energy differences for systems of the size discussed here approach the limits of the numerical accuracy we could achieve with our approach. Nevertheless, throughout all tests described above, the general conclusions presented in the manuscript remained valid.

Details on used VASP version and PAW potentials

For the present calculations release 5.2.11 of the VASP code has been used together with the following PAW potentials:

Ag	PAW_PBE Ag 06Sep2000
C	PAW_PBE C_s 06Sep2000
H	PAW_PBE H 15Jun2001
O	PAW_PBE O_s 07Sep2000
Cu	PAW_PBE Cu 05Jan2001
N	PAW_PBE N_s 07Sep2000

Additional binding-energy curves

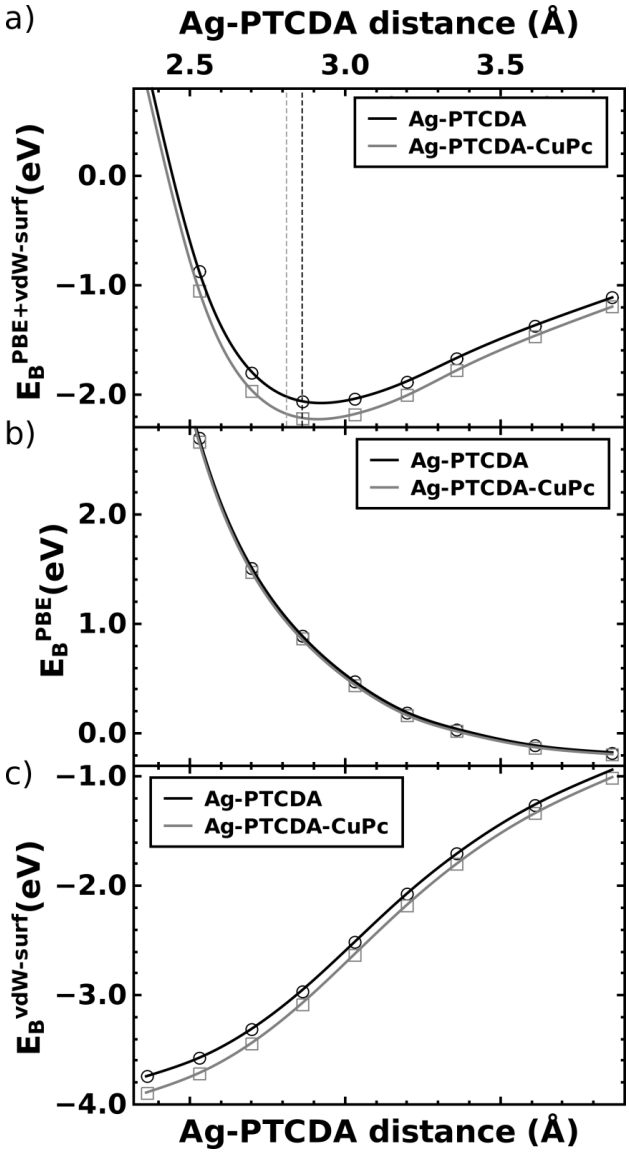

FIGURE S1: PBE+vdW^{surf} binding-energy curves (a) of a PTCDA single-layer (black) and a PTCDA-CuPc double-layer (grey), adsorbing on Ag(111) as a function of the Ag(111)-PTCDA distance; dashed vertical lines indicate the experimental binding distances[7] for PTCDA (black) and PTCDA-CuPc (grey) on Ag(111). PBE (b) and vdW^{surf} (c) energetic contributions to the PBE+vdW^{surf} binding-energy curves in (a). These curves were used to calculate ΔE_B in Fig. 3b in the main text.

Tailing of charge density above the Ag(111) and Ag(111)-PTCDA surfaces

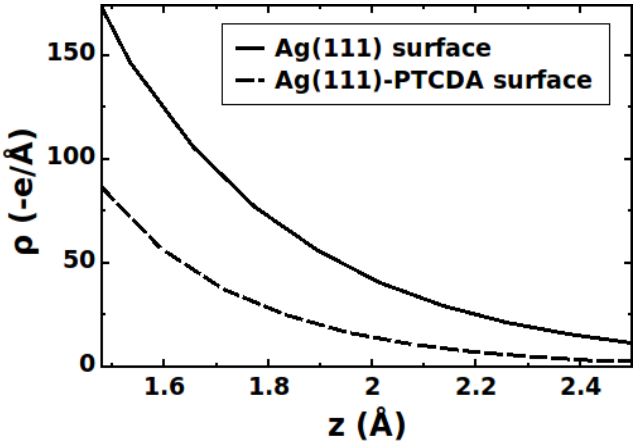

Figure S2: Plane-integrated charge density above the Ag(111) substrate relevant for PTCDA adsorption and the Ag(111)-PTCDA substrate relevant for CuPc adsorption. The reported values correspond to an integration over the area assigned to one PTCDA molecule. The origin of the horizontal axis is set in one case to the averaged positions of the atoms in the top Ag layer and in the other case to the average positions of the C atoms in the PTCDA layer. "*e*" refers to the (positive) elementary charge.

Impact of using soft PAW-potentials and the chosen convergence criteria

In test calculations on Ag(111)-PTCDA we experienced that replacing the "soft" PAW-potentials with "normal" ones and correspondingly increasing the plane-wave cutoff-energy by *ca.* 10 Ryd changes the vertical positions of the oxygen atoms within the PTCDA monolayer. As the interaction between Ag(111) and PTCDA could be influenced by the distance of the silver and carboxylic oxygen atoms, we have performed a non-spin-polarized optimization of Ag(111)-PTCDA-CuPc using the "normal" PAW potentials. Doing such a calculation in a spin-polarized manner appears computationally too demanding, but, as mentioned above, we found that spin-polarization only weakly affected our results. While the average positions of the carbon atoms reported in the main text change by only 0.01 Å, the average position of the carboxylic oxygens changes by 0.10 Å from 2.63 Å to 2.73 Å when replacing "soft" with "normal" PAW potentials. Interestingly, this does not impact the shift of the positions of the carboxylic oxygens induced by CuPc adsorption: Both for "soft" and "normal" potentials, their distance to the Ag(111) surface is increased by 0.05 Å.

Regarding the impact of these structural changes on the electronic structure, we find a small shift of the F-LUMO peak by 0.08 eV to lower binding energies when comparing "soft" and "normal" geometries. Most notably, however, in both sets of geometries the calculated shift of the PTCDA F-LUMO upon CuPc adsorption is only 0.01 eV. Thus, independent of the PAW-potential applied, we cannot reproduce the small shift (0.12 eV) seen in Ref. 7.

As a consequence of exchanging "soft" with "normal" PAW-potentials affecting the vertical positions of the carboxylic oxygens, the calculated work-function modification $\Delta\Phi$ also slightly changes: For both Ag(111)-PTCDA and Ag(111)-PTCDA-CuPc we observe a small lowering of $\Delta\Phi$ by 0.03 eV. As this effect is the same for both systems, it does not affect our conclusions regarding the interfacial electronic structure and the bonding induced charge transfer discussed in the main text.

As mentioned in the main text, the shear system size of Ag(111)-PTCDA-CuPc enforced us to use a rather sparse *k*-point grid. We calculated the effect of increasing the numbers of *k*-points by doubling the numbers of *k*-points in *x*- and *y* direction and, because of the small scale of the effects we are interested in, simultaneously decreased the energy-convergence criterion in the SCF cycle to 10^{-6} eV in a single-point calculation. As a consequence, both for Ag(111)-PTCDA and Ag(111)-PTCDA-CuPc $\Delta\Phi$ is reduced by the same, small value (0.04 eV), which again does not impact our discussion and conclusions in the main text.

Discussion of the calculated density of states (DOS)

As shown in Fig. S2, the overall shape of the valence spectra reported in Ref. 7 is reasonably well reproduced by the calculated DOS (within the well known shortcomings of Kohn-Sham orbital positions caused by self-interaction[9,10] and by the lack of derivative discontinuity[11]). However, similar to Ref. 8, we cannot reliably disentangle the electronic structure of the two inequivalent PTCDA molecules within the monolayer. Additionally, we do not observe a shift of the PTCDA F-LUMO peak upon CuPc adsorption, while in experiments the apparent peak maximum shifts by 0.12 eV at full CuPc coverage.[7]

Here it has to be kept in mind that the coverage we have considered is only *ca.* 40% of full coverage in experiments, for which also in Ref. 7 a much smaller shift is observed. This and the considerations involving the inequivalent PTCDA molecules described in the main manuscript lead us to conclude that capturing the subtle shift observed in the experiments for the F-LUMO and at the same time explaining why no shift of the position of the HOMO is seen would require at least the consideration of the full experimental surface unit cell and an explicit calculation of the photoionization cross-sections. Beyond that, also a much denser k-point grid and the use of harder PAW potentials would be desirable (see preceding section). All that is well beyond the scope of the present manuscript and most of it appears by no means feasible with today's computational resources.

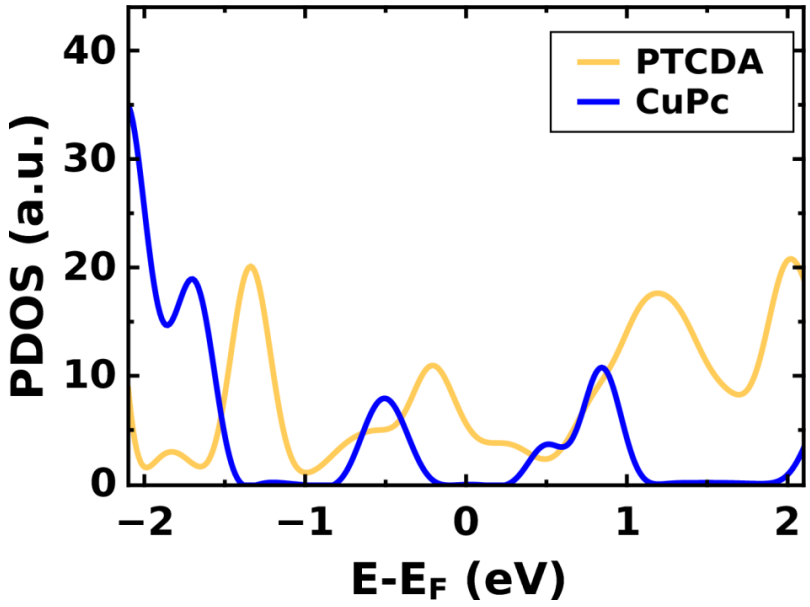

FIGURE S3: Density of states of Ag(111)-PTCDA-CuPc projected onto the PTCDA (yellow) and CuPc (blue) layers in the combined CuPc-PTCDA-Ag(111)system; the Fermi level is set to zero.

References

(1) Kresse, G.; Furthmüller, J. *Phys. Rev. B* **1996**, *54*, 11169–11186.
(2) Monkhorst, H. J.; Pack, J. D. *Phys. Rev. B* **1976**, *13*, 5188–5192.
(3) Methfessel, M.; Paxton, A. T. Phys. Rev. *B* **1989**, *40*, 3616–3621.
(4) Ruiz, V.; Liu, W.; Zojer, E.; Scheffler, M.; Tkatchenko, A. *Phys. Rev. Lett.* **2012**, *108*, 146103.
(5) Tkatchenko, A.; Scheffler, M. *Phys. Rev. Lett.* **2009**, *102*, 073005.
(6) Bučko, T.; Hafner, J.; Ángyán, J. G. *J. Chem. Phys.* **2005**, *122*, 124508.
(7) Stadtmüller, B.; Sueyoshi, T.; Kichin, G.; Kröger, I.; Soubatch, S.; Temirov, R.; Tautz, F.; Kumpf, C. *Phys. Rev. Lett.* **2012**, *108*, 106103.
(8) Rohlfing, M.; Temirov, R.; Tautz, F. *Phys. Rev. B* **2007**, *76*, 115421.
(9) Marom, N.; Hod, O.; Scuseria, G. E.; Kronik, L. *J. Chem. Phys.* **2008**, *128*, 164107.
(10) Körzdörfer, T.; Kümmel, S.; Marom, N.; Kronik, L. *Phys. Rev. B* **2009**, *79*, 201205.
(11) Kümmel, S.; Kronik, L. *Rev. Mod. Phys.* **2008**, *80*, 3.

6. Publication IV

6.1. Current draft of the publication

Outer-valence electron spectra of prototypical organic molecules from an optimally-tuned range-separated hybrid functional: A quantitative analysis

David A. Egger,[1,2,†] Shira Weissman,[2,†] Sivan Refaely-Abramson,[2,*]

Sahar Sharifzadeh,[3] Matthias Dauth,[4] Roi Baer,[5] Stephan Kümmel,[4]

Jeffrey B. Neaton,[3] Egbert Zojer,[1] and Leeor Kronik[2,*]

[1] Institute of Solid State Physics, Graz University of Technology, 8010 Graz, Austria.

[2] Department of Materials and Interfaces, Weizmann Institute of Science, 76100 Rehovoth, Israel.

[3] Molecular Foundry, Lawrence Berkeley National Laboratory, Berkeley, 94720 California, USA.

[4] Theoretical Physics IV, University of Bayreuth, 95440 Bayreuth, Germany.

[5] Fritz Haber Center for Molecular Dynamics, Institute of Chemistry, Hebrew University, 91904 Jerusalem, Israel.

[†] These authors contributed equally to this work.

*Corresponding authors: leeor.kronik@weizmann.ac.il; sivan.abramson@weizmann.ac.il

Abstract

Density functional theory with optimally-tuned range-separated hybrid (OT-RSH) functionals has been recently suggested [Refaely-Abramson et al., *Phys. Rev. Lett.* **109**, 226405 (2012)] as a non-empirical approach to predict outer-valence electronic structure with the same accuracy as many-body perturbation theory. Here, we provide a quantitative evaluation of the OT-RSH approach by examining its performance in predicting the outer-valence electron spectra of several prototypical gas-phase molecules, from aromatic rings (benzene, pyridine and pyrimidine) to more complex organic systems (terpyrimidinethiol and copper phthalocyanine). For a range up to several eV away from the frontier orbital energies, we find that the outer-valence electronic structure obtained from the OT-RSH method agrees very well (typically within ~0.1-0.2 eV) with both experimental photoemission and theoretical many-body perturbation theory data in the GW approximation. In particular, the OT-RSH approach offers a balanced description of localized and delocalized states. We discuss in detail the sole exception found - a high-symmetry orbital, particular to small aromatic rings, which is relatively deep inside the valence state manifold. Overall the OT-RSH method is the most accurate DFT method for outer-valence electronic structure prediction for such systems and of essentially the same level of accuracy as GW at a reduced computational cost.

I. Introduction

Many electronic properties of molecules and materials are determined by and understood through the energetics of the valence electrons, which are often probed experimentally using photoemission spectroscopy (PES).[1] Via measurement of the kinetic energy of photo-emitted electrons, PES provides direct experimental access to the electron ejection energies, the smallest of which is the ionization potential (IP). Calculating PES data from first principles is a long-standing challenge to modern electronic structure methods.[2,3] A state-of-the-art method for obtaining ionization spectra theoretically is many-body perturbation theory (MBPT), which calculates quasi-particle excitation energies via solving the Dyson equation, typically within the GW approximation (where G is the Green function and W is the dynamically screened Coulomb potential).[4–7] Unfortunately, GW calculations can be computationally demanding. Moreover, in particular for gas-phase computations that are at the center of this work, results are frequently sensitive to details of the specific GW scheme[8–13] employed and can also be difficult to converge.[11,14]

Density functional theory (DFT),[15,16] in which the ground-state electron density, rather than the many-electron wave-function, is the fundamental quantity,[17] is a computationally efficient first principles method for calculating the electronic structure of many-electron systems. DFT is often made practical via the Kohn-Sham (KS) scheme,[18] in which the original many-electron problem is mapped uniquely into a fictitious non-interacting electron system yielding the same electron density. This mapping leads to effective single-particle equations that provide a significant conceptual and computational simplification of the original many-electron problem. However, due to the fictitious nature of the non-interacting particles, the correspondence of KS eigenvalues with ionization energies measured in an experiment is not at all straightforward.[3,19] It can be shown that for the exact KS potential the energy of the

highest occupied molecular orbital (HOMO) equals the negative of the IP, a result known as the IP theorem.[20–23] Lower-lying eigenvalues do not strictly correspond to electron removal energies.[19] For outer-valence electrons, however, exact DFT eigenvalues may still serve as a useful and even quantitative approximation to electron removal energies.[3,24]

The KS mapping scheme relies on an exchange-correlation energy-functional of the density, the exact form of which is generally unknown and must be approximated. Common approximate exchange-correlation functionals used within the KS scheme are the local density approximation (LDA) and the generalized gradient approximation (GGA).[15,16] In the former, one assumes that at each point in space the exchange-correlation energy per particle is given by its value for a homogeneous electron gas. In the latter, information on deviations from homogeneity is partly accounted for by considering gradients of the charge density. Unfortunately, for gas-phase molecules, KS eigenvalues obtained through the use of these approximations are not in good agreement with experimental ionization spectra.[3,25] First, the IP theorem is grossly disobeyed and the negative of the HOMO energy usually underestimates the IP severely.[26–29] Even if this difference is accounted for by rigidly shifting the theoretical eigenvalue spectrum,[30,31] the calculated eigenvalue spectrum may still exhibit qualitative failures, notably an erroneous ordering of the electronic levels (see, e.g., Refs.32–40).

These two drawbacks can be traced back to two different (yet not unrelated) deficiencies of the above-described approximations: lack of a derivative discontinuity (DD) and self-interaction-errors (SIE).[3,25,27,41] The DD is a uniform ‘‘jump’’ in the KS potential, when approaching the integer electron number either from above or from below. The DD accounts for the discontinuity of the chemical potential, i.e., for the fact that the electron removal energy is not the same as the electron insertion energy. Part of this discontinuity is accounted for by the KS kinetic energy term.[23,42] But the kinetic energy contribution to the discontinuity

is generally insufficient and the remaining discontinuity must be provided by the KS potential. Because the electron-ion and Hartree energies are continuous in the electron density, the remaining discontinuity can only be attained by a "jump" in the exchange-correlation potential. However, in standard LDA or GGA functionals the exchange-correlation potential explicitly depends on the electron density and does not incorporate any orbital dependence (in contrast to, e.g., Fock exchange). As a result, calculations based on these approximations cannot exhibit any DD in the exchange-correlation part of the potential.[43] Instead, they approximately average over it and as a consequence the KS-HOMO energy is strongly underbinding with respect to the true ionization potential.[30,44,45]

The SIE[46] arises from the fact that the classical electron-electron repulsion term (Hartree potential) in the KS equation means that each electron is repelled from the total charge in the system, including a spurious repulsion from itself. Because KS theory is, in principle, exact, then whatever error one makes in the Hartree term must be completely canceled out by the exact exchange-correlation term. Unfortunately, only partial error cancellation is obtained in either LDA or GGA. For strongly localized orbitals, self-interaction may be significant and spuriously destabilize electron energies.

The situation can be improved, if one uses "hybrid" DFT, i.e., functionals that contain exact exchange based expressions employed using a non-local Fock operator.[25] We emphasize that while such functionals do not fall within the KS scheme, they are still very much within the DFT framework[3,25,47] through the *generalized* Kohn-Sham (GKS) scheme.[48] In the KS scheme, many-body effects are incorporated entirely in a multiplicative potential (which is the sum of the Hartree and exchange-correlation potentials). In contrast, in the GKS scheme many-body effects are incorporated in a combination of a multiplicative potential and a non-local operator (non-multiplicative potential). This is achieved via mapping to a partially

interacting electron gas. An improved description of ionization energies using "hybrid" DFT can be obtained because the additional non-local operator can mitigate the need for a DD in the multiplicative potential,[25] and, furthermore, because expressions based on Fock exchange mitigate self-interaction errors. Most hybrid functionals in everyday use are of the global type, i.e., they contain a fixed fraction of Fock exchange.[49–51] In practice, one typically observes that HOMO energies extracted from such hybrid functionals are closer to experimental ionization energies than those obtained from LDA or GGA, but still significantly underestimate those obervables.[9,31,52] Spectral distortions (including the possibility of an erroneous ordering of the electronic levels) are often mitigated, as the fraction of Fock exchange reduces the SIE.[3,25,32,33] However, the quantitative details of the eigenvalue spectrum still typically depend on the specific choice of the approximate hybrid functional.[53]

One reason for the failure of conventional hybrid functionals to obey the IP theorem is the presence of only a fraction of exact exchange. Because of this, they do not yield the correct ~1/r asymptotic potential that should be "felt" by an electron at large distances from the molecule, especially in the ionization process. However, when using the full Fock exchange to correct for that, the delicate balance between exchange and correlation is disrupted, which is highly detrimental – especially for short-range electron interaction that governs chemical bonding.[25] A promising strategy for tackling that problem is offered by the more recent class of range-separated hybrid (RSH) DFT functionals,[54] pioneered by Savin and co-workers.[55] In these functionals, the inter-electron Coulomb repulsion term is separated into long-range (LR) and short range (SR) components via a range-separation parameter γ. The LR term is mapped using full Fock exchange, thereby establishing the correct asymptotic potential. The SR termed is (typically) mapped using a GGA approach, thereby maintaining the compatibility between the exchange and correlation expressions. In this approach, one still needs to determine the range-separation parameter, γ.

Both formal considerations[56] and practical simulations show that aiming at accurate results for a broad range of systems, one typically needs significantly different values of γ. This is taken care of by using optimally-tuned RSH (OT-RSH) functionals.[31,47] There, instead of using one and the same range-separation parameter for all systems, γ is tuned for each system such that physically-motivated tuning conditions are fulfilled without introducing any empirical parameters. In particular, it has been shown for gas phase molecules that insisting on the HOMO energy being equal to the negative of the IP (i.e. fulfilling the IP theorem) for the neutral and anion species yields highly accurate HOMO energies and HOMO-LUMO gaps when compared to experimental fundamental gaps or GW calculations.[52,57] More recently, some of us have shown that in addition to the IP and the fundamental gap, the entire higher-lying part of the valence-electron spectrum of gas-phase molecules and molecular solids can be accurately described by the eigenvalues of OT-RSH ground-state DFT calculations.[58,59] In particular, it was suggested that a more general OT-RSH functional that introduces a fraction of Fock exchange in the SR and simultaneously maintains the full Fock exchange in the LR[60] allows for a more flexible treatment of differently localized molecular orbitals, resulting in an accurate description of more complex organic molecules relevant for applications in organic electronics.[58]

In the present contribution, we further investigate the capabilities of OT-RSH functionals for predicting outer-valence electron spectra of organic molecules in the gas phase. First, we study the prototypical aromatic molecules benzene, pyridine and pyrimidine (see Fig. 1a). This choice is motivated by the fact that for such simple systems, existing high-level experimental reference data can serve as useful benchmarks for the theory. Moreover, the nitrogen heteroatoms in the azabenzenes can be expected to result in differently localized molecular orbitals in the higher-lying part of the valence electron system and, in particular,

close-lying σ- and π-states.[29] Therefore, the OT-RSH description would need to attain a quantitatively satisfactory balance of self-interaction errors for both.[58] Moreover, these prototypical systems were recently identified as a challenge for both the GW[61] and the OT-RSH[62] methods. Here, we perform both OT-RSH and GW calculations for these systems and find that they are of similar (~0.2 eV) overall accuracy. We suggest that a simultaneously reliable prediction of both π and σ orbital energies is indeed within the realm of the OT-RSH functional applied here. Still, we identify one specific molecular orbital that is peculiar to ring-type molecules, which in the OT-RSH calculations displays a significant deviation from experiment and GW calculations. We analyze the origin of this discrepancy by further computing the same spectra using conventional hybrid calculations, as well as explicitly self-interaction corrected (SIC) calculations.

With the obtained overall very encouraging results at hand, we proceed towards larger and more complex systems, here chosen to be terpyrimidinethiol and copper phthalocyanine (3N-thiol and CuPc, see Fig. 1b). These molecules are interesting for novel applications in organic electronics,[63–68] but at the same time challenging to assess theoretically due to pronounced differences in SIE among the high-lying orbitals in the valence electron spectrum.[33,68,69] Through a comparison to GW calculations and/or PES experiments, we show that OT-RSH can provide accurate valence-electron spectra also for these more complex organic molecules. Our results clearly demonstrate that OT-RSH functionals are a highly promising, state-of-the-art approach for predicting ionization spectra of gas-phase organic molecules.

II. Theoretical and Methodological Details

A. Formalism

As mentioned in the introduction, we examine a generalized RSH form, which allows for different amounts of Fock exchange in the short-range and in the long-range.[70] We use the range-partitioning expression of Yanai et al., given by[71]

$$\frac{1}{r} = \underbrace{\frac{\alpha+\beta erf(\gamma r)}{r}}_{"HF"} + \underbrace{\frac{1-[\alpha+\beta erf(\gamma r)]}{r}}_{"GGA"}. \qquad (1)$$

Here, r is the inter-electron coordinate and α, β, and γ are adjustable parameters. Naturally, this partition is not unique, but the choice of the error function is computationally convenient when using a Gaussian basis for expanding the wave-functions of finite systems.[55] Eq. (1) defines the range-separation procedure, where the Coulomb operator, $1/\mathrm{r}$, in the exchange-part of the xc-potential is replaced by two complementary terms, which are treated differently. As suggested by the "HF" and "GGA" delimiters in the equation, the first term is treated using Hartree-Fock exchange, the second term is treated using GGA semi-local exchange. Specifically, using the Perdew-Burke-Ernzerhof (PBE)[72] form for the GGA exchange-correlation leads to the following expression for the exchange-correlation energy[73]

$$E_{xc}^{RSH} = \alpha E_{x,HF}^{SR,\gamma} + (1-\alpha)E_{x,PBE}^{SR,\gamma} + (\alpha+\beta)E_{x,HF}^{LR,\gamma} + (1-\alpha-\beta)E_{x,PBE}^{LR,\gamma} + E_{c,PBE}, \qquad (2)$$

where the superscripts LR and SR denote that the full Coulomb repulsion, $1/\mathrm{r}$, has been substituted by the LR and SR Coulomb repulsions, $\mathrm{erf}(\gamma r)/r$ and $\mathrm{erfc}(\gamma r)/r$, respectively. PBE correlation is used for the entire range. Yanai et al. viewed α, β, and γ as semi-empirical parameters and determined "universal" values for them based on benchmark thermochemistry data. Here, we wish to determine these parameters based on the satisfaction of inherent

constraints on the exchange-correlation density functional, without recourse to experimental data.

From Eq. (2) it is clear that for full long-range Fock exchange, which guarantees the correct asymptotic potential, one condition is that $\alpha + \beta = 1$ (note that the fit to thermochemistry data performed by Yanai et al. lead to $\alpha + \beta = 0.65$, i.e., to a potential that is not asymptotically correct and will, therefore, run into problems when trying to associate eigenvalues with ionization energies or electron affinities). Eq. (2) further shows that α controls the fraction of SR Fock exchange. We, therefore, restrict the current investigation to α values between 0 and 0.2. This is because in the former limit, the SR behavior is expected to be GGA-like; in the latter limit, the SR behavior is expected to resemble that of a conventional hybrid functional.[58,74] For example, in the PBE0 hybrid functional, which is based on the PBE semi-local functional, a global exact-exchange fraction of 25% is used.[51] The remaining parameter, γ, controls the range-separation. As mentioned in the introduction, we do not seek a universal value for γ. Instead, we rely on a non-empirical tuning procedure, where γ is adjusted on a per-system basis. One possibility to determine the optimum gamma, γ^{opt}, is to choose it such that the IP theorem is satisfied:[31,75]

$$\varepsilon_H^{\gamma^{opt}}(N) = -IP^{\gamma^{opt}}(N). \quad (3)$$

$\varepsilon_H(N)$ is the HOMO energy of the *N*-electron system, and IP is the ionization potential of the *N*-electron system, determined from total energy difference of the *N*- and *N*-1-electron systems. In general, both $\varepsilon_H(N)$ and IP display a strong γ-dependence.

It is often useful to invoke the IP theorem not only for the molecule in its neutral state, but also in certain charged states. The condition that then needs to be fulfilled is that the target function J^2, given by[31]

$$J^2(\gamma;\alpha) = \sum_i \left(\varepsilon_H^{\gamma;\alpha}(N+i) + IP^{\gamma;\alpha}(N+i)\right)^2 \quad , \tag{4}$$

is minimized. In Eq. (4), i can in principle adopt any integer number and one can observe the effect of adding further terms on the residual J value (*vide infra*). In practice, only values of i that are close to zero are of interest to avoid information from highly charged radical species – a point elaborated below. In particular, including the anion has been found to be highly beneficial for the prediction of fundamental gaps and the energies of charge-transfer excited states.[52,76,77] Note that when restricting i to 0 in Eq. (4), which we do here if the electron affinity is negative and the molecule does not bind an extra electron, then Eq. (3) is recovered. Interestingly, it was repeatedly found that the optimal γ strongly changes from one system to the other, showing that our "per system" tuning approach is indeed necessary.[31,60,78–80]

The inclusion of various charged states in the tuning poses another advantage, as it, in principle, allows the simultaneous optimization of γ and α, for example by minimizing J^2 with respect to both parameters. This approach has, indeed, been successfully applied in Ref. 58 and is discussed further below, where we analyze the dependence of J^2 on the amount of SR Fock exchange α and tune γ as a function of different pre-selected values of α.

B. Computational Details

All PBE calculations (within the KS scheme) and PBE0 and RSH calculations (within the GKS scheme) presented in this article were obtained within the QChem[81] and NWChem[82] codes, using cc-PVTZ[83] basis functions. All geometries were optimized using the PBE functional. As the above-described tuning scheme is based on components taken from well-

established density functionals (cf. Eq. (2)) and range-separation is available in many different electronic structure codes, optimal tuning of γ via Eq. (4) is straightforward to perform. Moreover, the tuning strategy is computationally efficient, as it relies on a series of standard total-energy DFT calculations. We note, however, that when charging the gas-phase molecule as part of the above-explained tuning procedure, the configuration of the cation and/or anion must be identified carefully, as it may affect the results of the computation.[84]

We illustrate the possible complications associated with ion configuration issue by considering pyridine - one of the molecules of Fig. 1, which is discussed extensively in the results section. When tuning γ using the above-described approach, it is important to ensure that the character of the HOMO (related to the left-hand term in Eq. (3)) corresponds to the "hole density", defined as the charge-density difference of the neutral and charged states (and, consequently, related to the right-hand term in Eq. (3)). For pyridine, the self-consistent solution of GKS equation with the RSH functional was found to lead to two different doublet configurations of the cation, depending on the initial guess used in the iterations. These two configurations correspond to two qualitatively different hole densities (see Fig. 2, left part). As shown in the right part of Fig. 2, the reason for the different "hole densities" is that the two cation configurations possess two different LUMO orbitals, i.e., the two cationic ground states represent two different ionization processes. The main difference is that in one case the electron "loss" is from a π-orbital and in the other case from a σ-orbital. These two cationic configurations are energetically close, which is consistent with the observation that the HOMO and the HOMO-1 of pyridine are very close in energy. Importantly, however, only the "hole density" depicted in Fig. 2b - which is associated with the configuration lower in energy, i.e., the true ground state predicted for the cation - corresponds to the HOMO of pyridine (see Fig. 2c). Therefore, we have to ensure that the cationic state shown in Fig. 2b is

indeed the one entering the tuning procedure, in order to retain consistency for the orbital energies and total energies required in Eq. (3).

For our analysis of the OT-RSH results, we also performed comparative GW calculations, as well as self-interaction-corrected calculations and KS-PBE0 calculations (the latter are defined and explained below). Our GW calculations are based on a standard G_0W_0,[14] where quasi-particle energies are computed via a first-order correction to DFT, with no self-consistent update of the starting wavefunctions. The starting quasi-particle wavefunction for the G_0W_0 corrections were obtained from the PBE functional.[72] The static dielectric function is computed within the random-phase approximation and extended to finite frequency via the generalized Plasmon-pole model of Hybertsen and Louie.[5]

GW calculations were performed using the BerkeleyGW package,[85] which employs a plane-wave basis set to compute the dielectric function and self-energy. DFT-PBE calculations for the starting-point were performed within the Quantum Espresso package,[86] which is compatible with BerkeleyGW. The nuclei and core electrons of atoms were described by Troullier-Martins relativistic norm-conserving pseudopotentials,[87] which are part of the Quantum Espresso pseudopotential library version 0.2.5. Here, 1, 4, 5, and 6 electrons were explicitly considered as valence electrons for H, C, N, and S, respectively, with cutoff radii (in Bohr) of 1.3, 0.5, 1.0, and 1.7, respectively. The plane-wave basis cutoff was 80 Ry for benzene, and 120 Ry for pyridine, pyrimidine, and 3N-thiol. These values lead to a convergence of the total DFT energy to < 1 meV/atom. To avoid spurious interactions with periodic images, the molecules were contained in a box whose lattice vectors are twice the size necessary to contain 99% of the charge density and the Coulomb interaction was truncated at distances larger than half of the unit cell size. The box size, in atomic units, was

35 x 39 x 24; 30 x 20 x 32, 19 x 30 x 30; and 64 x 26 x 15.5 for benzene, pyridine, pyrimidine, and 3N-thiol, respectively.

The number of states that build the GW dielectric function and self-energy were 4914, 5515, 5071, and 3598 for benzene, pyridinie, pyrimidine, and 3N-thiol, respectively. For the former three prototypical small molecules, this energy range corresponds to 90 eV above the vacuum energy, while for 3N-thiol, it corresponds to 50 eV above vacuum energy. Fewer number of states were included for 3N-thiol due to the greater computational expense associated with this rather large system. A static remainder approach was applied to the self-energy to estimate the correction to complete the unoccupied subspace.[88] The plane-wave cutoff for the dielectric function was 30 Ry for pyridine and pyrimidine, and 24 Ry for 3N-thiol and benzene. We find that these parameters converge the HOMO energies of the prototypical small molecules to less than 0.1 eV. Based on the convergence behavior of these molecules and the residual differences that we find for GW and OT-RSH HOMO energies (vide infra), we extrapolate the errors associated with eigenvalues of the 3N-thiol calculation to be less than 0.2 eV.

All SIC calculations were based on the seminal SIC functional of Perdew and Zunger.[46] However, we constructed a spatially local, multiplicative exchange-correlation potential, identical for all orbitals in the system, which ensures that the SIC remains within the KS realm.[89,90] This is based on the generalized optimized effective potential (OEP) equation, which extends the original OEP equation to the case of unitarily variant functionals.[91] It is solved using the generalized Krieger-Li-Iafrate (KLI) approximation.[91] Unlike the original KLI approximation to the standard OEP equation, which can introduce significant deviations for the SIC,[92] the generalized KLI approximation used here has been shown to be an excellent approximation to the generalized OEP. [91] The additional degree of freedom arising from the

variance inherent to our procedure can be used to construct a set of orbitals that minimize the total SIC energy of the system, where we applied a complex-valued energy minimizing unitary orbital transformation.[90] For additional insights, we also used the PBE0 functional in conjunction with a local multiplicative potential, constructed – in contrast to traditional GKS-schemes – via the KLI[89] approximation for the exact exchange part of the functional. We refer to these calculations as KS-PBE0.

All SIC and KS-PBE0 calculations were performed with the Bayreuth version[93] of the PARSEC real-space code,[94] where we employed a grid-spacing of 0.2 Bohr and Troullier-Martins norm-conserving pseudopotentials.[87]

Finally, for a meaningful comparison between the results of different functionals and/or computational approaches, we verified explicitly by visual inspection that compared eigenvalues calculated from different methods correspond to the same molecular orbitals.[95,96]

III. Prototypical Aromatic Rings - Results and Discussion

We start our analysis by considering the prototypical aromatic gas-phase molecules of Fig. 1a. The computed peaks in the eigenvalue spectra - neglecting differences of the photoionization cross-sections – should correspond to those in the photoemission spectra (in arbitrary units), and are shown in Fig. 3. The computed spectra are obtained from OT-RSH eigenvalues with SR Fock exchange fractions of α=0 and α=0.2 for (a) benzene, (b) pyridine, and (c) pyrimidine. The results are compared to gas-phase PES spectra from Refs. 97–99 and to the results of GW calculations. Importantly, the spectra are plotted on an absolute energy scale, i.e., the calculated eigenvalue spectra shown in Fig. 3 have *not* been shifted so as to align the theoretical data with experiment. To facilitate a visual comparison with the experimental

spectra, we broadened the calculated eigenvalue spectra via convolutions with a Gaussian (with a standard deviation of 0.4 eV for benzene and 0.2 eV for pyridine and pyrimidine). For all three systems we find an overall excellent agreement between OT-RSH, GW, and experiment. In particular, the HOMO energies calculated from the OT-RSH approach correspond very well to the first peak in the experimental spectrum, indicating the success of the tuning procedure. In addition, the shape of the experimental spectra at higher binding energies is very well reproduced by the OT-RSH spectra. Note that the comparison extends over a relatively large energy range of ~8 eV below the first IP (much more than the ~3 eV in previous work on somewhat larger aromatic-based organic molecules)[58]. This is remarkable, considering that the agreement between DFT eigenvalues and photoemission energies is expected, on general theoretical grounds, to deteriorate for lower-lying states.[3,24,100] Interestingly, the shape of the OT-RSH spectrum for these molecules is only mildly sensitive to the choice of α.

Despite the overall agreement, there is one particular feature which does not agree with experiment for each of the three molecules: For benzene, the pronounced intensity in the OT-RSH spectra around -13 eV is in contrast to the very low intensity seen in the experiment. For pyridine and pyrimidine, mismatches occur around -13 eV and -15 eV, respectively. These discrepancies, discussed in more detail below, are observed for both considered SR choices (α=0 and α=0.2). The main deviation between GW calculations and experiments is found for the benzene molecule, where the feature that in the experiment occurs around -11.5 eV is shifted to higher binding energies. A similar discrepancy (as well as some additional ones for the other rings) have previously been pointed out by Marom *et al.*[61]

A precise quantitative comparison between theory and experiment beyond the above statements is complicated by several aspects: (i) The peaks in the experiments are not well separated; i.e., to determine peak maxima and, correspondingly, vertical ionization energies,

one would need to perform extensive fitting. (ii) To the best of our knowledge, there has never been an experimental study reporting the *orbital ordering* of these prototypical organic cycles in the gas phase. Rather, it is common practice to use simulations for that purpose, as was done in, e.g., Ref. 97. Moreover, there are also deviations in experimental reports, e.g., for pyrimidine, where the two experimental spectra from Refs. 98 and 99, shown in Fig. 3c, appear to be shifted with respect to each other by ~0.2 eV. Therefore, in the following we prefer to compare theoretical data only to the original experimental spectra and typically avoid the extraction of vertical ionization series from the experiments. Nevertheless, in the interest of putting our OT-RSH results for these prototypical systems into perspective with previous literature findings[62], we adopt the extracted experimental values for the ionization energies reported by Marom et al.[61] We can then perform a straightforward statistical analysis of mean absolute differences (MADs) between theory and experiment. This yields MADs of ~0.1 eV for the GW calculations and MADs of ~0.2 eV for the OT-RSH(α=0.2) calculations. In contrast to the claim of Ref. 62, the MAD of the OT-RSH calculation differs from that of the GW calculation by an extent which is marginal and on par with the experimental resolution. Furthermore, the MAD between the RSH and GW results is ~0.2 eV, i.e., in the same range.

For a deeper analysis of the remaining differences between theory and experiment and their origin, we turn to a detailed comparison between the OT-RSH and GW eigenvalues, given in Fig. 4. For each eigenvalue, the figure also provides the corresponding single-electron orbital. Körzdörfer et al.[62] have argued that the excellent agreement between OT-RSH and GW, reported in Ref. 58, was partly due to the comparison with a GW scheme based on a PBE DFT starting point. They argued that a GW calculation based on hybrid-functional DFT starting point, with a global exact exchange fraction close to that of the PBE0[51] functional (25%), yields quantitatively more accurate GW results and worsens the agreement between

OT-RSH and GW. To examine whether this argument is pertinent, the first two columns in Fig. 4 show PBE- and PBE0-based GW valence-electron energies computed by Marom et al.[61] Our PBE-based GW calculations, already shown in Fig. 3, are given in the third column in Fig. 4, followed by our two (α=0 and α=0.2) OT-RSH results. As in Fig. 3, all eigenvalues are shown on an absolute energy scale, with no shifting of the computed data. Surprisingly, for all three prototypical rings our PBE-based GW calculations are in much better agreement with the PBE0-based GW calculations of Marom et al.[61] than with their PBE-based ones. These two non-self-consistent, "one-shot" GW results are, however, calculated using different approximations within the GW scheme itself: here, we use a plasmon-pole approximation, pseudopotentials, and a plane-wave basis; Ref. 61 reports all-electron calculations, with a fully frequency-dependent dielectric function and a finite localized basis. In our opinion, this illustrates very clearly that the outcome of a GW calculation depends on much more than the starting point alone. Other physical and numerical approximations, e.g. use of pseudopotentials, plasmon-pole approximations, choice of basis set, and degree of self-consistency and convergence, can influence the precise result to a similar degree .[9,12,14,101,102] This does underscore, however, that residual differences of ~0.1 - 0.2 eV between different calculations are not physically meaningful and that any single theoretical dataset should not be interpreted beyond this level. In previous work,[14] some of us have shown that for a plane-wave basis and pseudopotentials, a converged G_0W_0 scheme based on a PBE starting point yields excellent agreement with the IP of gas-phase molecules, and thus we proceed with comparing our results to this approach – referred to as simply GW hereafter – for the remainder of the work.

Turning to the detailed comparison between OT-RSH and our GW calculation, given in Fig. 4, the following picture emerges. First, the OT-RSH HOMO energies for all three systems are in very good (<0.15 eV) agreement with the respective lowest quasi-hole energy computed

from GW. Excellent agreement of OT-RSH HOMO values with reference theoretical or experimental IPs has been previously reported for a variety of systems – see, e.g., Refs.52,57,78. Nevertheless, this finding is still not trivial, because the HOMO of benzene consists of degenerate π-orbitals, whereas the HOMO of pyridine and pyrimidine is of σ character (*n*, to be precise). We emphasize the importance of the tuning procedure for obtaining this level of accuracy for the HOMO energy. For comparison, consider the LC-ωPBE[103] or LC-ωPBE0[74] functionals. Both are PBE-based RSH functionals just like the one used here, with (α=0, γ=0.4 Bohr^{-1}) and (α=0.2, γ=0.2 Bohr^{-1}) respectively, but with a fixed non-tuned value of γ. Using these functionals for these molecules results in HOMO energies that deviate by 0.3 eV to 0.6 eV from the corresponding GW energy. Furthermore, with the optimally-tuned functional the predicted deeper-lying parts of the spectra (with one exception, mentioned previously and discussed in more detail below) are in an overall excellent agreement with our GW data in spite of the large energy range and the fact that for both systems σ- and π-orbitals are present. Increasing α from 0 to 0.2 slightly improves the agreement between OT-RSH and GW, but the effect is overall minor. In contrast to Körzdörfer *et al.*,[62] we, thus, conclude that OT-RSH schemes do indeed provide us with means for predicting accurate outer-valence ionization-spectra, irrespectively of the π or σ nature of the involved orbitals.

We note that the theoretical grounds, used in Ref. 62 to question the accuracy of the OT-RSH functional for describing states with higher binding-energies, were based on the absence of piecewise-linearity (discussed in more detail below) for highly charged species of the studied system. While such piecewise-linearity is, indeed, something to be obtained with the exact DFT functional, it has little bearing on excited states of the singly-charged cation. These are, however, essential for theoretically describing the photoemission process[3,104–106] and hence

directly relevant for many physical and chemical properties. Moreover, it should be kept in mind that a highly charged radical is much less stable and undergoes considerable charge density relaxation and orbital reordering with respect to the neutral or cationic molecule. In fact, as shown above for the case of the pyridine molecule, even for the (only singly-charged) cation it can be difficult to obtain a meaningful ground state - we expect this issue to be much more severe for more highly charged molecules.

The one discrepancy between the GW and OT-RSH data (vide supra) involves a particular ring-shaped π orbital (orange-colored in Fig. 4), which is specific to cyclic compounds. In the OT-RSH, this orbital appears significantly below its GW position (by ~0.4 eV for benzene and pyridine and an even worse ~0.6 eV for pyrimidine, almost independently of α). For all three molecules, this orbital is primarily responsible for the remaining disagreement between the OT-RSH calculations and the experimental spectra in Fig. 3.

To understand the OT-RSH results in more detail, and to explore the possible origins of this discrepancy, we performed additional DFT calculations with several different functionals. Of all DFT functionals studied here, the OT-RSH one is the only one capable of obeying the ionization potential theorem of Eq. (3) and, consequently, to provide HOMO energies that are close to the experimental IP.[3] Therefore, in the following comparison all energies are reported relative to the HOMO energy of the respective calculation (which is set to zero). The resulting shifted eigenvalue spectra for the three prototypical aromatic molecules are shown in Fig. 5, with the original (G)KS-HOMO energies shown on top.

First, we compare our OT-RSH results to those obtained with their "parent" semi-local functional – PBE – and those obtained from PBE0, the most popular "conventional" hybrid functional based on PBE. In the latter functional, semi-local PBE exchange is mixed with

25% non-local Fock exchange for the entire interaction range. This leads to an orbital-dependent functional for the exchange-correlation energy,[25] which can then be used within DFT in two different ways. If one wishes to remain within the KS framework, one must take the variational derivative of the exchange-correlation energy with respect to the density, so as to determine the *multiplicative* KS potential. This can be achieved for an implicit density-functional by solving the (integro-differential) optimized effective potential (OEP) equation.[25,107–109] Here, we solve this equation within the KLI approximation[91] (for details see "Computational details") and refer to the result as PBE0^{KS}. Alternatively, one can minimize the total energy with respect to the orbitals. This is the almost universal practice with hybrid functionals, which (as explained in the introduction) is rigorously justified within the generalized Kohn-Sham scheme. We refer to this result as PBE0^{GKS}.

A first observation is that the shifted PBE0^{KS} eigenvalues are virtually identical to the shifted PBE ones for all systems, in agreement with similar observations reported in Ref. 53 for other systems. One notable difference between the PBE and PBE0^{KS} results is that the shift needed to align the PBE0^{KS} HOMO energy to its experimental value is substantially smaller than in PBE, albeit still significant. More profound differences occur between the PBE0^{GKS} and the PBE0^{KS} data. While the amount of shift needed for alignment of the HOMO with experiment is essentially the same for PBE0^{GKS} and PBE0^{KS}, the PBE0^{GKS} eigenvalues are overall "stretched" (=energy rescaled) with respect to the PBE0^{KS} data – as seen most clearly for the case of benzene. For pyridine and pyrimidine some additional orbital reordering is found, especially in the upper part of the valence band, due to mitigation of self-interaction errors, as discussed below). Such a "stretching" of the energy scale has been observed previously (see, e.g., Refs. 53,110,111): Körzdörfer and Kümmel[53] have rationalized it by arguing that, if the differences in the shapes of the KS and GKS orbitals are ignored, then the difference between

GKS and corresponding KS eigenvalue can be viewed in terms of first-order perturbation theory involving the difference between Fock and semi-local exchange. They suggested that this first-order correction mimics successfully the first-order correction between KS values and ionization energies, which is known to dominate for outer-valence electrons.[3,24,100] Indeed, the shifted PBE0^{GKS} eigenvalues are in much better agreement with GW than the PBE0^{KS} ones. This underscores the beneficial effect of the non-local potential operator that is inherent to the GKS scheme, but absent in the KS schemes.

As a next step, the role played by the self-interaction error (SIE) shall be assessed: Körzdörfer et al.[62] have suggested that orbital-energy discrepancies between OT-RSH and GW arise because the orbital SIEs for π and σ orbitals are substantially different and the OT-RSH functional does not correct these to the same degree. We have already seen above that in fact most π and σ orbitals are equally well-described by OT-RSH. However, one still needs to examine whether orbital SIE considerations may explain the discrepancy found above for the ring-shaped π orbital. In order to examine that, we have performed SIC calculations within the KS scheme (for details see the "Computational details" section) which results in SIE-free orbitals and eigenvalues. Generally speaking, the shifted SIC spectra are quite similar to the shifted PBE0^{KS} spectra for all systems, although some eigenvalue differences between the two spectra (up to ~0.3 eV for benzene and ~0.4 eV for pyridine and pyrimidine) are found. We furthermore find that SIC modifies PBE eigenvalues differently for π and σ orbitals, by an average of 0.2 eV, which in particular leads to reordering of the close-lying HOMO-1 and HOMO-2 of pyrimidine. Notably, these differences in the SIC-corrections for π and σ PBE orbital-energies are rather similar for all three systems, meaning that the relative differences of SIEs in the σ and π orbitals of benzene are similar to the ones in pyridine and pyrimidine. We note that, for these systems, the magnitude of the SIC modifications is not sizeable

compared to the typical energy spacing of the eigenvalues, which is usually of the order of an eV or more.

Comparison of the SIC data to the GW data reveals immediately that, just like the $PBE0^{KS}$ data, they would benefit from further "stretching". This is fully consistent with the fact that both SIC and $PBE0^{KS}$ spectra arise from a KS, rather than a GKS, calculation. We can simulate the effect of such "stretching" on the SIC spectrum by multiplying the shifted SIC eigenvalues with a constant (a procedure that is, in fact, often performed heuristically in the comparison of KS data with experimental spectra – see, e.g., Refs. 112,113). For each SIC spectrum, we chose this stretching factor such that the lowest-energy $PBE0^{GKS}$ and SIC eigenvalues agree. For all three prototypical systems, the resulting stretched SIC eigenvalue spectra are in overall better agreement with the $PBE0^{GKS}$ spectra than the regular SIC spectra and, furthermore, are in very good agreement with the OT-RSH data and with GW. For a few of the pyridine and pyrimidine orbitals, we find some remaining deviations of the stretched SIC from the $PBE0^{GKS}$ and OT-RSH results, which is, however, expected as the three approaches are very different. This agreement shows that a (range-separated or conventional) hybrid can be highly effective in the quantitative mitigation of SIEs, even though it is not rigorously self-interaction free because only a fraction of exact exchange is employed in the short range. Indeed, similar observations have been made for many other molecular systems,[32–34,38,53,58,61,110,114] often by comparison to experiment, but also by comparison to SIC.[35,68] This rules out that the poor description of the "ring-shaped" (orange-colored) π orbital by OT-RSH is due to a general lack of balance in the description of π and σ orbitals owing to the SIE.

Instead, we attribute the incorrect description of the highly delocalized orbital to the absence of beyond-PBE (and possibly non-local) correlation. This is supported by the observation that this π orbital is also overbound in the shifted PBE0^{GKS} data, albeit by a lesser amount of ~0.2 to ~0.35 eV. As semi-local exchange is known to mimic static correlation,[115,116] it stands to reason that further removal of some of it, as in the OT-RSH scheme, would worsen the situation. From this point of view, the error in this orbital is then yet one more issue of compatibility between exact exchange and correlation, especially static one.[25] However, one cannot rule out that even if the correlation issue is overcome, an error would still remain, owing to further dynamic relaxation which is not captured in any eigenvalue-based and thus static description. Indications for such effects have been reported in the literature for small metal clusters[117] and the response of a very delocalized orbital may be "metallic like". Overcoming this drawback, e.g., by examining more advanced correlation functionals is, therefore, a challenge for future work.

IV. More Complex Organic Molecules - Results and Discussion

Encouraged by the overall success of the OT-RSH approach for the prototypical aromatic rings we now turn to examining the performance of the OT-RSH method for more complex organic molecules: terpyrimidinethiol (3N-thiol) and copper phthalocyanine (CuPc) - see Fig. 1b.

Pyrimdinethiols such as 3N-thiol are known to form self-assembled monolayers (SAMs),[118] and they were shown to display a number of interesting phenomena, e.g. they exhibit diode-type current-voltage characteristics in molecular-scale electronic devices.[66,119] In the context of 3N-thiol SAMs, some of us have predicted theoretically that the electronic structure is significantly altered due to collective electrostatic effects in the SAM, leading to a

localization of the frontier molecular orbitals and a concomitant pronounced reduction in the HOMO-LUMO gap.[68] 3N-thiols were also suggested as SAMs to strongly reduce or enhance the work function of an underlying metal.[67]. These appealing findings render 3N-thiol an interesting candidate for applications in organic and molecular electronics. 3N-thiols are also interesting from a methodological perspective, as they poses a serious challenge to semi-local KS schemes:[68] By means of SIC calculations analogous to the ones performed here, it was shown that close-lying π and σ orbitals in the outer-valence region of 3N-thiol have markedly different SIEs and, as a consequence, are wrongly ordered in (semi-)local DFT functionals such as PBE. Moreover, it was found that the Heyd-Scuseria-Ernezerhof (HSE) SR hybrid functional[120,121] to a large extent reproduces the SIC corrections to the PBE outer-valence eigenvalues. In HSE, the SR components are the same as in PBE0 but in the LR there is no non-local exchange. From the photoemission spectroscopy point of view, the behavior of HSE is known to be similar to that of conventional hybrid functionals.[33,122–126]

The above findings are supported by the data in Fig. 6, which shows the shifted eigenvalue spectrum of 3N-thiol, aligning all HOMO levels to zero starting with the literature data[68] for PBE, SIC, and HSE. Here, we focus on the range of ~3 eV below the HOMO, which we have previously identified for molecules of a similar size as a useful range of accuracy for the RSH-derived eigenvalues.[58] Generally, PBE tends to produce σ orbitals that are underbound owing to significant SIE.[33,58,68] Because the HOMO obtained from PBE is of σ nature, shifting according to its energy results in π orbitals that appear to be overbound. The SIC calculations (as above, the spectrum is shown both "as calculated" and "stretched") correct the SIE and, as discussed above, strongly shift the σ orbitals down in energy with respect to the π ones, leading to extensive reordering of the eigenvalue spectrum. As mentioned above, the same phenomenon is manifested in the HSE spectrum, which needs no stretching as it

originates from a GKS calculation. We additionally performed PBE0^{GKS} calculations, also shown in Fig. 6,[127] and found an overall very good agreement with the HSE spectrum and with the "stretched" SIC with an average deviation of the eigenvalues around ~0.1 eV. This agrees well with the above-mentioned previous findings as to HSE being comparable to conventional hybrid functionals as far as photoemission spectra are concerned.

To the best of our knowledge, an experimental PES spectrum of 3N-thiol is not available in the literature. Therefore, we performed reference GW calculations for which the (shifted) eigenvalue spectrum is also given in Fig. 6. As seen above for the prototypical aromatic rings, the agreement of the shifted GW spectrum with the shifted hybrid functional (PBE0 or HSE) spectrum is very good. Some discrepancy is observed between ~-2.0 to ~-2.5 eV, but in this context it should be kept in mind that here the plotted energy range is much smaller than for the aromatic rings above. In fact, in the present case the errors do not exceed 0.2 eV, which is within the expected level of agreement between the two methods (*vide supra*). This confirms the conclusion drawn already from the data of the "prototypical" molecules, i.e., that the partial correction of SIE and a "stretching" of the spectrum are the essential effects of a hybrid functional.

Results from the OT-RSH functional, again with two different choices of SR exact exchange - α=0 and α=0.15 - are also shown in Fig. 6 (the motivation for this particular choice of α is discussed below). As with the simpler systems, the IPs deduced from the OT-RSH and GW leading eigenvalue are very close in energy (~0.2 eV) for both choices of α. Consequently, the OT-RSH scheme produces quantitatively meaningful spectra also on an *absolute* energy scale as shown in Fig. 7. This is in sharp contrast to all other DFT methods presented in Fig. 6. However, in contrast to the case of the small aromatic rings (where the spatial extent within the plane of the rings is quite similar for σ and π orbitals, i.e. differences between the

localization of the orbitals are rather small), here the differences between the OT-RSH spectra for the two choices of α are more pronounced. They also include qualitative deviations, e.g., a reordering of the HOMO-3 and HOMO-4 orbitals. In particular, we observe that, while the position of the π orbitals is similar in both spectra, the σ orbitals are systematically underbound in the α=0 calculation. This underscores that, as suggested in Ref. 58 and discussed in the introduction, a fraction of Fock exchange in the SR together with full Fock exchange in the LR allows for a mitigation of SIE and therefore a balanced treatment of differently localized molecular orbitals, while retaining the correct absolute position of the energy levels.

A remaining difficulty is the *a priori* choice of optimal α. Srebro and Autschbach[60] have suggested that this can be achieved by tuning α. Specifically, they sought the value of α that (with the optimal γ per each choice of α obtained from Eq. (4)) minimizes the curvature of the ideally piecewise-linear total energy versus particle number curve, for the addition and removal of one charge from the neutral molecule. This was done while simultaneously determining the optimum γ for each choice of α obtained from Eq. (4) (with *i* restricted to 0 and 1). As discussed in Ref. 58, some of us successfully employed a similar approach, involving additionally the removal of two electrons, to also determine an optimal value of α directly from Eq. (4). (α^{opt} was found to equal 0.2 for 3,4,9,10-perylene-tetracarboxylic-dianhydride (PTCDA) and 1,4,5,8-naphtalene-tetracarboxylic-dianhydride (NTCDA)). Furthermore, Stein et al. established a rigorous quantitative equality between deviations from piecewise linearity and deviations from the IP theorem.[128] Therefore, one can equivalently seek α such that the target function of Eq. (4) is minimized, without explicit consideration of fractional densities.

Indeed, in cases where an optimal α can be clearly identified using the above procedure, several different properties, including the eigenvalue spectrum, have been found to be predicted satisfactorily.[58,60,129] However, in the case of 3N-thiol (with *i* restricted to 0 and 1) a similar minimal value of the target function *J* of Eq. (4) is obtained across a large range of α values: the residual *J* only changed by 0.05 eV from α=0.00 to α=0.60. Therefore, while the above prescription for choosing α does not fail as such (i.e., it does not suggest a wrong value of α), it does not offer any predictive power either. In the absence of viable alternatives, a possible strategy would be to resort to the generally recommended value[74] of α=0.2, which indeed has been shown to yield very good results.[59] This would also be the case here, i.e. the MAD between the absolute eigenenergies from GW and OT-RSH with α=0.2, for the states shown in Fig. 7, is ~0.1 eV. However, as the 3N-thiol results do depend more sensitively on α, it would still be beneficial to determine an optimal α value from other considerations. In this context, a useful observation is that the *shifted* results of the conventional hybrid functional PBE0 are in good agreement with experimental and/or theoretical reference data for the systems discussed here as well as for many other cases.[34,58,59,130] Therefore, one can simply tune α so as to obtain agreement between eigenvalue differences in the OT-RSH spectrum and in the PBE0 spectrum. Here this was done by tuning α with the PBE0 energy difference between the HOMO and HOMO-1 to represent π- and σ-orbitals in this procedure. This allows us to obtain the same useful level of SIE mitigation as in a conventional hybrid functional, without the need for spectral shifting and without any empiricism. It is this approach which has led to the value of α=0.15 for which the data shown in Figs. 6 and 7 have been obtained.

Comparing the unshifted GW and OT-RSH (α=0.15) data of Fig. 7, one, indeed, observes a very good agreement between the two methods. The only clear difference is some orbital

reordering around ~-10.8 eV. However, note that the eigenvalues clustered there are very close in energy and this reordering does not involve deviations greater than ~0.1 eV between corresponding eigenvalues of the two methods. Overall, the MAD between the GW and OT-RSH(α=0.15) data is a satisfying ~0.1 eV, with the largest deviation being ~0.2 eV for the HOMO. For comparison, with OT-RSH(α=0) the MAD is ~0.25 eV, with the largest deviation being ~0.45 eV, where the deterioration of the level of agreement is mostly due to the less accurate description of the σ orbitals.

Encouraged by this further success, we now turn to an even more complex system – copper phthalocyanine (CuPc - see Fig. 1b). In molecular-solid form, CuPc is a highly stable organic semiconductor with a broad range of applications, including light-emitting diodes, solar cells, gas sensors, and thin-film transistors.[131] Owing to these applications, there is considerable interest in investigating its electronic structure (see Ref. 69 and additional references therein). In the present context, CuPc mainly serves as a test casethat poses several additional challenges for the OT-RSH method: First, it is an open shell molecule (s=1/2). Second, the interaction between the *d* orbitals of the copper atom and the *sp* orbitals of the embedding macrocycle result in a highly non-trivial set of localized and delocalized orbitals – an issue elaborated below.

For the CuPc molecule, Marom et al. have previously established that: (1) Semi-local functionals, such as PBE, result in eigenvalue spectra that are strongly distorted by severe SIE;[33] (2) these errors are mitigated substantially, though not completely, by the use of hybrid functionals such as PBE0 or HSE;[33,69] (3) severe SIE distortions at the DFT level are partly carried over to GW calculations based on them.[69]

To better understand the above claims, consider Figure 8a, which provides a scheme of computed frontier eigenvalues and orbitals. We illustrate the severe SIE (claim 1) by considering several selected frontier orbitals. Whereas the a_{1u} orbital and the doubly degenerate e_g orbitals are highly delocalized on the macrocycle, the spin-split b_{1g} orbitals are quite strongly localized around the copper atom. Configuration 1 (left side of Fig. 8a) was obtained from the OT-RSH calculations discussed below, but is equivalent to the one obtained from the GW calculations of Ref. 69. It identifies the delocalized a_{1u} and e_g orbitals as the HOMO and LUMO, respectively, and places the spin-split $b_{1g\uparrow}$ and $b_{1g\downarrow}$ orbitals as HOMO-1 and LUMO+1, respectively. PBE calculations, however, predict configuration 2 (right side of Fig. 8a), in which the spin-split $b_{1g\uparrow}$ and $b_{1g\downarrow}$ are identified as HOMO and LUMO, respectively. Clearly, the localized $b_{1g\uparrow}$ orbital is spuriously pushed to higher energies by the SIE, to the point of becoming the HOMO. This forces the unoccupied $b_{1g\downarrow}$ orbital to be spuriously shifted to lower energies in order to maintain the spin-splitting symmetry, to the point of it becoming the LUMO. PBE0 or HSE strongly mitigate this error (claim 2) and yield configuration (1).

To understand the manifestation of the SIE (and its mitigation) in the simulated photoelectron spectra, computed spectra obtained from the different computational methods are compared to experimental photoemission data in Fig. **9**. Importantly, in this figure we compare occupied-state eigenvalues to the gas-phase photoelectron spectrum as before, but further compare unoccupied-state eigenvalues to experimental *inverse* photoemission spectroscopy (IPES). In IPES, photons are emitted from a sample due to its irradiation with fixed-energy electrons and the energy distribution of the emitted photons is measured, yielding experimental information on virtual states.[1] Because gas-phase inverse photoemission spectroscopy is unavailable, the comparison is to experimental data obtained from thin CuPc films. Due to polarization effects,[59,132,133] the electron affinity of a film is much smaller than that of an isolated molecule

and therefore the computed empty state energies and the measured inverse photoemission spectroscopy data can be compared only up to a rigid shift. To preserve the computational gas-phase data, the experimental IPES spectra were shifted so as to align the lowest-energy peak with the GW spectrum given at the top of Fig. 9.

As discussed above, it is well known that for either PBE or PBE0 the HOMO and LUMO do not correspond to the ionization potential or the electron affinity, respectively (see e.g., Refs. 25 & 31), causing an uncontrolled rigid shift of the simulated photoemission curve. To facilitate a meaningful comparison also for these functionals, which implies the need to overcome this rigid shift, the PBE and PBE0 spectra of Fig. 9 are additionally shown in shifted form, as in Ref.61. In this form, the ionization potential is computed as the total energy difference between the neutral species and the cation, and the filled-state eigenvalue spectrum is rigidly shifted such that the HOMO coincide with the computed ionization potential. Similarly, the electron affinity is computed as the total energy difference between the anion and the neutral species and the unoccupied-state eigenvalue spectrum is rigidly shifted such that the LUMO coincide with the computed electron affinity. Comparison of the PBE- and PBE0-based simulated spectra in Fig. 9, taken from Ref. 69 with the experimental data reveals both the severe SIE in the PBE calculation and its mitigation by the PBE0 calculation – whereas the shifted PBE spectrum is in poor agreement with experiment for both filled and empty states, the shifted PBE0 spectrum provides for a much improved agreement with experiment. Better agreement yet, including an accurate placement of the spin-split filled $b_{1g\uparrow}$ and empty $b_{1g\downarrow}$ orbitals, is afforded by GW calculations of Marom et al., [69] based on a PBE0 starting point. It is in significantly better agreement with experiment than their GW calculations based on a PBE starting point (at least with the particular flavor of GW used in that work, which is different from the one used above in this work; Due to computational

expense, we did not perform further GW calculations for CuPc). This substantiates the third above claim, i.e., the possible carry-over of severe SIE to the GW calculation.

In light of the above results, it is intriguing to determine how well the OT-RSH approach performs in this more complicated scenario. As for the case of pyridine (see Fig. 2), it is important to choose the correct cationic configuration used in the tuning procedure. Two cationic configurations can be obtained from the OT-RSH calculation. One is an "open shell singlet", with a single spin in the b_{1g} orbital and in the a_{1u} orbital, which corresponds to removal of an electron from the a_{1u} HOMO of configuration (1) in Fig. 8a. The other is a "closed-shell singlet" cation, which corresponds to removal of an electron from the b_{1g} HOMO of configuration (2) in Fig. 8a. Importantly, only for the "open-shell singlet" configuration (which is lower in total energy) the LUMO is consistent with the character of the neutral HOMO, and with the "hole density", as shown in Fig. 8b. Just like in the pyridine example of Fig. 2, all tuning must be performed solely with this configuration. We note that multiple stable configurations are well-known to occur in metal-phthalocyanines,[130] which is why we strongly stress the need for correct identification and usage of compatible neutral and ionic configurations in the tuning procedure. We have observed that with a smaller basis set, multiple stable configurations were obtained even for the CuPc neutral. However, this spurious phenomenon vanished when using a sufficiently large basis set.

Having ascertained the validity of our tuning procedure, we turn to the spectra simulated using the OT-RSH method, also shown in Fig. 9. As for the case of 3N-thiol, the obtained spectra (second and fourth theoretical curves in the figure) are strongly α-dependent, but a reliable direct tuning of α solely using equation (4) (including i values beyond 0, 1) was again not useful. Thus, to determine α, we again used the PBE0 spectrum. As discussed above, a crucial aspect in the theoretical description of the CuPc spectrum is the energy separation

between the delocalized a_{1u} orbital and the filled localized b_{1g} orbital of Fig. 8. Therefore, we tune the value of α so as to agree with the PBE0-calculated separation between the eigenvalues for the a_{1u} and b_{1g} orbitals. This yields α=0.17, quite similar to the above-mentioned "default" value of 0.2. This value was then used to calculate the second theoretical curve in Fig. 9. It yields an excellent agreement with the GW@PBE0 and the experimental data in both the top valence (i.e., occupied) states and the bottom conduction (i.e., unoccupied) states. In particular, the OT-RSH alignment of the a_{1u}, b_{1g}, and e_g states of Fig. 8, agrees very well with GW. As orbitals above and below these frontier ones tend to be "clustered" for these larger molecule, we do not discuss them individually. However, it is clear that the agreement between GW and OT-RSH gradually deteriorates as one goes further down or up in the valence or conduction states, respectively. In particular, it appears that agreement of the lower valence states with the GW results could be further assisted by some "stretching" of the energy scale – an observation consistent with the generally expected differences between non-local exchange and self-energy operators,[3] as well as with our general guideline of restricting our attention to states within a few eV of the frontier orbitals. Nevertheless, in the absence of detailed orbital information, at the level of the given experimental resolution the OT-RSH results can be viewed as agreeing with experiment as well as the GW ones, possibly even relatively deep into the valence band.

As an additional observation, we note that the HOMO and LUMO eigenvalues obtained from the OT-RSH(α=0.17) calculation (as is, without any rigid shifting of the data) are in excellent agreement with the lowest quasi-hole and quasi-electron excitations, respectively, obtained from GW@PBE0. This is fully consistent with the work of Stein et al.,[52] who suggested that OT-RSH gaps can be identified with quasi-particle gaps – an observation that has since been confirmed for a large variety of systems by ourselves, as well as by several other groups.[58,59,78,134–137] A related interesting observation is that the OT-RSH(α=0) data are rather

similar to the GW@PBE data: Both are far better than the PBE data, but in both spectra the a_{1u}-b_{1g} and e_g-b_{1g} separation are not large enough. This highlights yet again the positive role of SR exchange in mitigating SIEs where they are significant.[58]

V. Conclusions

In conclusion, we examined the performance of optimally-tuned range-separated hybrid functional for predicting the photoemission spectra of several challenging prototypical and complex organic molecules. Overall, the resulting spectra agree very well (typically within ~0.1-0.2 eV) with experimental and GW reference data, even within a range of several eV away from the frontier orbitals. We performed several additional hybrid DFT calculations in both the KS and GKS scheme, and found that the inclusion of a non-local operator strongly benefits the calculated spectrum. Moreover, our SIC calculations confirmed that self-interaction errors can be efficiently mitigated in OT-RSH functionals, which shows that OT-RSH can offer an excellent balance in the description of localized and delocalized states. The sole exception found in the studied systems is a high-symmetry orbital, particular to small aromatic rings. We conclude that the OT-RSH method is a highly accurate DFT method for outer-valence PES prediction for such systems and is accuracy comparable to GW. This success comes at the price of increased computational and conceptual cost that is inherent to the parameter tuning. While this increase in effort is notable compared to standard, non-tuned DFT calculations, it is not overwhelming and still much lower than the cost of a GW calculation.

Acknowledgments

D.A.E. is a recipient of a DOC fellowship by the Austrian Academy of Sciences. S.R.A. acknowledges support by an Adams fellowship by Mr. Marcel Adams of Canada and the Israel Academy of Sciences and Humanities. Portions of this work were supported by the European Research Council, the Israel Science Foundation, the United States-Israel Binational Science Foundation, the Germany-Israel Foundation, the Wolfson Foundation, the Hemlsley Foundation, the Austrian Science Fund (FWF), P24666-N20, the German Science Foundation (DFG/GRK 1640) and the Molecular Foundry. J.B.N was supported by the U.S. Department of Energy, Office of Basic Energy Sciences, Division of Materials Sciences and Engineering (Theory FWP) under Contract No. DE-AC02-05CH11231. S.S. was partially supported by the Scientific Discovery through Advanced Computing (SciDAC) Partnership program funded by U.S. Department of Energy, Office of Science, Advanced Scientific Computing Research and Basic Energy Sciences. Work performed at the Molecular Foundry was also supported by the Office of Science, Office of Basic Energy Sciences, of the U.S. Department of Energy. We thank the National Energy Research Scientific Computing center for computational resources.

References

(1) Hüfner, S. *Photoelectron spectroscopy: principles and applications*; Advanced texts in physics; 3rd ed.; Springer: Berlin ; New York, 2003.
(2) Martin, R. M. *Electronic structure: basic theory and practical methods*; Cambridge University Press: Cambridge, UK; New York, 2004.
(3) L. Kronik; S. Kümmel *Top. Curr. Chem.* in press.
(4) Hedin, L. *Phys. Rev.* **1965**, *139*, A796–A823.
(5) Hybertsen, M.; Louie, S. *Phys. Rev. B* **1986**, *34*, 5390–5413.
(6) Aulbur, W. G.; Jönsson, L.; Wilkins, J. W. In *Solid State Physics*; Elsevier, 1999; Vol. 54, pp. 1–218.
(7) Onida, G.; Reining, L.; Rubio, A. *Rev. Mod. Phys.* **2002**, *74*, 601–659.
(8) Grossman, J.; Rohlfing, M.; Mitas, L.; Louie, S.; Cohen, M. *Phys. Rev. Lett.* **2001**, *86*, 472–475.
(9) Blase, X.; Attaccalite, C.; Olevano, V. *Phys. Rev. B* **2011**, *83*, 115103.
(10) Blase, X.; Attaccalite, C. *Appl. Phys. Lett.* **2011**, *99*, 171909.
(11) Qian, X.; Umari, P.; Marzari, N. *Phys. Rev. B* **2011**, *84*.
(12) Sharifzadeh, S.; Biller, A.; Kronik, L.; Neaton, J. B. *Phys. Rev. B* **2012**, *85*.
(13) Körzdörfer, T.; Marom, N. *Phys. Rev. B* **2012**, *86*.
(14) Sharifzadeh, S.; Tamblyn, I.; Doak, P.; Darancet, P. T.; Neaton, J. B. *Eur. Phys. J. B* **2012**, *85*.
(15) Parr, R. G.; Yang, W. *Density-functional theory of atoms and molecules*; Oxford University Press ; Clarendon Press: New York; Oxford [England], 1989.
(16) Dreizler, R. M.; Gross, E. K. U. *Density functional theory: an approach to the quantum many-body problem*; Springer-Verlag: Berlin; New York, 1990.
(17) Hohenberg, P.; Kohn, W. *Phys. Rev.* **1964**, *136*, B864–B871.
(18) Kohn, W.; Sham, L. J. *Phys. Rev.* **1965**, *140*, A1133–A1138.
(19) Sham, L.; Kohn, W. *Phys. Rev.* **1966**, *145*, 561–567.
(20) Perdew, J. P.; Parr, R. G.; Levy, M.; Balduz, J. L. *Phys. Rev. Lett.* **1982**, *49*, 1691–1694.
(21) Levy, M.; Perdew, J.; Sahni, V. *Phys. Rev.* **1984**, *30*, 2745–2748.
(22) Almbladh, C.-O.; von Barth, U. *Phys. Rev. B* **1985**, *31*, 3231–3244.
(23) Perdew, J.; Levy, M. *Phys. Rev. B* **1997**, *56*, 16021–16028.
(24) Chong, D. P.; Gritsenko, O. V.; Baerends, E. J. *J. Chem. Phys.* **2002**, *116*, 1760.
(25) Kümmel, S.; Kronik, L. *Rev. Mod. Phys.* **2008**, *80*, 3.
(26) Baerends, E. J.; Ros, P. *Chem. Phys.* **1973**, *2*, 52–59.
(27) Perdew, J. P. *Chem. Phys. Lett.* **1979**, *64*, 127–130.
(28) Salzner, U.; Baer, R. *J. Chem. Phys.* **2009**, *131*, 231101.
(29) Faber, C.; Attaccalite, C.; Olevano, V.; Runge, E.; Blase, X. *Phys. Rev. B* **2011**, *83*.
(30) Teale, A. M.; De Proft, F.; Tozer, D. J. *J. Chem. Phys.* **2008**, *129*, 044110.
(31) Kronik, L.; Stein, T.; Refaely-Abramson, S.; Baer, R. *J. Chem. Theory Comput.* **2012**, *8*, 1515–1531.
(32) Dori, N.; Menon, M.; Kilian, L.; Sokolowski, M.; Kronik, L.; Umbach, E. *Phys. Rev. B* **2006**, *73*.
(33) Marom, N.; Hod, O.; Scuseria, G. E.; Kronik, L. *J. Chem. Phys.* **2008**, *128*, 164107.
(34) Marom, N.; Kronik, L. *Appl. Phys.* **2008**, *95*, 159–163.
(35) Körzdörfer, T.; Kümmel, S.; Marom, N.; Kronik, L. *Phys. Rev. B* **2009**, *79*, 201205.
(36) Körzdörfer, T.; Kümmel, S.; Marom, N.; Kronik, L. *Phys. Rev. B* **2010**, *82*, 129903.
(37) Puschnig, P.; Reinisch, E.-M.; Ules, T.; Koller, G.; Soubatch, S.; Ostler, M.; Romaner, L.; Tautz, F. S.; Ambrosch-Draxl, C.; Ramsey, M. G. *Phys. Rev. B* **2011**, *84*.

(38) Brena, B.; Puglia, C.; de Simone, M.; Coreno, M.; Tarafder, K.; Feyer, V.; Banerjee, R.; Göthelid, E.; Sanyal, B.; Oppeneer, P. M.; Eriksson, O. *J. Chem. Phys.* **2011**, *134*, 074312.
(39) Vogel, M.; Schmitt, F.; Sauther, J.; Baumann, B.; Altenhof, A.; Lach, S.; Ziegler, C. *Anal. Bioanal. Chem.* **2011**, *400*, 673–678.
(40) Dauth, M.; Körzdörfer, T.; Kümmel, S.; Ziroff, J.; Wiessner, M.; Schöll, A.; Reinert, F.; Arita, M.; Shimada, K. *Phys. Rev. Lett.* **2011**, *107*.
(41) Cohen, A. J.; Mori-Sanchez, P.; Yang, W. *Science* **2008**, *321*, 792–794.
(42) Perdew, J. P.; Levy, M.; Balduz, J. L. *Phys. Rev. Lett.* **1982**, *49*, 1691–1694.
(43) But note recent work on non-standard LDA and GGA expressions that allows a DD to emerge naturally even within these approximations: Kraisler E, Kronik L (2013) Phys Rev Lett 110:126403 118; Armiento R, Kümmel S (2013) Phys Rev Lett 111:036402.
(44) Perdew, J.; Levy, M. *Phys. Rev. Lett.* **1983**, *51*, 1884–1887.
(45) Borgoo, A.; Teale, A. M.; Tozer, D. J. *J. Chem. Phys.* **2012**, *136*, 034101.
(46) Perdew, J. P.; Zunger, A. *Phys. Rev. B* **1981**, *23*, 5048–5079.
(47) Baer, R.; Livshits, E.; Salzner, U. *Annu. Rev. Phys. Chem.* **2010**, *61*, 85–109.
(48) Seidl, A.; Görling, A.; Vogl, P.; Majewski, J.; Levy, M. *Phys. Rev. B* **1996**, *53*, 3764–3774.
(49) Becke, A. D. *J. Chem. Phys.* **1993**, *98*, 1372.
(50) Stephens, P. J.; Devlin, F. J.; Chabalowski, C. F.; Frisch, M. J. *J. Phys. Chem.* **1994**, *98*, 11623–11627.
(51) Perdew, J. P.; Ernzerhof, M.; Burke, K. *J. Chem. Phys.* **1996**, *105*, 9982.
(52) Stein, T.; Eisenberg, H.; Kronik, L.; Baer, R. *Phys. Rev. Lett.* **2010**, *105*.
(53) Körzdörfer, T.; Kümmel, S. *Phys. Rev. B* **2010**, *82*, 155206.
(54) Iikura, H.; Tsuneda, T.; Yanai, T.; Hirao, K. *J. Chem. Phys.* **2001**, *115*, 3540.
(55) Leininger, T.; Stoll, H.; Werner, H.-J.; Savin, A. *Chem. Phys. Lett.* **1997**, *275*, 151–160.
(56) Baer, R.; Neuhauser, D. *Phys. Rev. Lett.* **2005**, *94*.
(57) Refaely-Abramson, S.; Baer, R.; Kronik, L. *Phys. Rev. B* **2011**, *84*, 075144.
(58) Refaely-Abramson, S.; Sharifzadeh, S.; Govind, N.; Autschbach, J.; Neaton, J. B.; Baer, R.; Kronik, L. *Phys. Rev. Lett.* **2012**, *109*, 226405.
(59) Refaely-Abramson, S.; Sharifzadeh, S.; Jain, M.; Baer, R.; Neaton, J. B.; Kronik, L. *Phys. Rev. B* **2013**, *88*, 081204(R).
(60) Srebro, M.; Autschbach, J. *J. Phys. Chem. Lett.* **2012**, *3*, 576–581.
(61) Marom, N.; Caruso, F.; Ren, X.; Hofmann, O. T.; Körzdörfer, T.; Chelikowsky, J. R.; Rubio, A.; Scheffler, M.; Rinke, P. *Phys. Rev. B* **2012**, *86*, 245127.
(62) Körzdörfer, T.; Parrish, R. M.; Marom, N.; Sears, J. S.; Sherrill, C. D.; Brédas, J.-L. *Phys. Rev. B* **2012**, *86*, 205110.
(63) Van den Brink, J.; Morpurgo, A. F. *Nature* **2007**, *450*, 177–178.
(64) Heutz, S.; Mitra, C.; Wu, W.; Fisher, A. J.; Kerridge, A.; Stoneham, M.; Harker, A. H.; Gardener, J.; Tseng, H.-H.; Jones, T. S.; Renner, C.; Aeppli, G. *Adv. Mater.* **2007**, *19*, 3618–3622.
(65) Mugarza, A.; Lorente, N.; Ordejón, P.; Krull, C.; Stepanow, S.; Bocquet, M.-L.; Fraxedas, J.; Ceballos, G.; Gambardella, P. *Phys. Rev. Lett.* **2010**, *105*.
(66) Díez-Pérez, I.; Hihath, J.; Lee, Y.; Yu, L.; Adamska, L.; Kozhushner, M. A.; Oleynik, I. I.; Tao, N. *Nat. Chem.* **2009**, *1*, 635–641.
(67) Egger, D. A.; Rissner, F.; Rangger, G. M.; Hofmann, O. T.; Wittwer, L.; Heimel, G.; Zojer, E. *Phys. Chem. Chem. Phys.* **2010**, *12*, 4291.
(68) Rissner, F.; Egger, D. A.; Natan, A.; Körzdörfer, T.; Kümmel, S.; Kronik, L.; Zojer, E. *J. Am. Chem. Soc.* **2011**, *133*, 18634–18645.

(69) Marom, N.; Ren, X.; Moussa, J. E.; Chelikowsky, J. R.; Kronik, L. *Phys. Rev. B* **2011**, *84*.
(70) Even more general range-separation schemes can be devised, e.g., to include a middle-range as well. See, e.g., Lucero MJ, Henderson TM, Scuseria GE (2012). J Phys: Condens Matter 24:145504 .
(71) Yanai, T.; Tew, D. P.; Handy, N. C. *Chem. Phys. Lett.* **2004**, *393*, 51–57.
(72) Perdew, J. P.; Burke, K.; Ernzerhof, M. *Phys. Rev. Lett.* **1996**, *77*, 3865–3868.
(73) This is obtained by replacing the 1/r terms in the exchange-part of the potential according to Eq. (1) and using the identity erf(γr) + erfc(γr) = 1.
(74) Rohrdanz, M. A.; Martins, K. M.; Herbert, J. M. *J. Chem. Phys.* **2009**, *130*, 054112.
(75) Livshits, E.; Baer, R. *Phys. Chem. Chem. Phys.* **2007**, *9*, 2932.
(76) Stein, T.; Kronik, L.; Baer, R. *J. Am. Chem. Soc.* **2009**, *131*, 2818–2820.
(77) Stein, T.; Kronik, L.; Baer, R. *J. Chem. Phys.* **2009**, *131*, 244119.
(78) Körzdörfer, T.; Sears, J. S.; Sutton, C.; Brédas, J.-L. *J. Chem. Phys.* **2011**, *135*, 204107.
(79) Pandey, L.; Doiron, C.; Sears, J. S.; Brédas, J.-L. *Phys. Chem. Chem. Phys.* **2012**, *14*, 14243.
(80) Sun, H.; Autschbach, J. *ChemPhysChem* **2013**, *14*, 2450–2461.
(81) Shao, Y.; Molnar, L. F.; Jung, Y.; Kussmann, J.; Ochsenfeld, C.; Brown, S. T.; Gilbert, A. T. B.; Slipchenko, L. V.; Levchenko, S. V.; O?Neill, D. P.; DiStasio Jr, R. A.; Lochan, R. C.; Wang, T.; Beran, G. J. O.; Besley, N. A.; Herbert, J. M.; Yeh Lin, C.; Van Voorhis, T.; Hung Chien, S.; Sodt, A.; Steele, R. P.; Rassolov, V. A.; Maslen, P. E.; Korambath, P. P.; Adamson, R. D.; Austin, B.; Baker, J.; Byrd, E. F. C.; Dachsel, H.; Doerksen, R. J.; Dreuw, A.; Dunietz, B. D.; Dutoi, A. D.; Furlani, T. R.; Gwaltney, S. R.; Heyden, A.; Hirata, S.; Hsu, C.-P.; Kedziora, G.; Khalliulin, R. Z.; Klunzinger, P.; Lee, A. M.; Lee, M. S.; Liang, W.; Lotan, I.; Nair, N.; Peters, B.; Proynov, E. I.; Pieniazek, P. A.; Min Rhee, Y.; Ritchie, J.; Rosta, E.; David Sherrill, C.; Simmonett, A. C.; Subotnik, J. E.; Lee Woodcock III, H.; Zhang, W.; Bell, A. T.; Chakraborty, A. K.; Chipman, D. M.; Keil, F. J.; Warshel, A.; Hehre, W. J.; Schaefer III, H. F.; Kong, J.; Krylov, A. I.; Gill, P. M. W.; Head-Gordon, M. *Phys. Chem. Chem. Phys.* **2006**, *8*, 3172.
(82) Valiev, M.; Bylaska, E. J.; Govind, N.; Kowalski, K.; Straatsma, T. P.; Van Dam, H. J. J.; Wang, D.; Nieplocha, J.; Apra, E.; Windus, T. L.; de Jong, W. A. *Comput. Phys. Commun.* **2010**, *181*, 1477–1489.
(83) Dunning, T. H. *J. Chem. Phys.* **1989**, *90*, 1007.
(84) Karolewski, A.; Kronik, L.; Kümmel, S. *J. Chem. Phys.* **2013**, *138*, 204115.
(85) Deslippe, J.; Samsonidze, G.; Strubbe, D. A.; Jain, M.; Cohen, M. L.; Louie, S. G. *Comput. Phys. Commun.* **2012**, *183*, 1269–1289.
(86) Giannozzi, P.; Baroni, S.; Bonini, N.; Calandra, M.; Car, R.; Cavazzoni, C.; Ceresoli, D.; Chiarotti, G. L.; Cococcioni, M.; Dabo, I.; Dal Corso, A.; de Gironcoli, S.; Fabris, S.; Fratesi, G.; Gebauer, R.; Gerstmann, U.; Gougoussis, C.; Kokalj, A.; Lazzeri, M.; Martin-Samos, L.; Marzari, N.; Mauri, F.; Mazzarello, R.; Paolini, S.; Pasquarello, A.; Paulatto, L.; Sbraccia, C.; Scandolo, S.; Sclauzero, G.; Seitsonen, A. P.; Smogunov, A.; Umari, P.; Wentzcovitch, R. M. *J. Phys. Condens. Matter* **2009**, *21*, 395502.
(87) Troullier, N.; Martins, J. L. *Phys. Rev. B* **1991**, *43*, 1993–2006.
(88) Deslippe, J.; Samsonidze, G.; Jain, M.; Cohen, M. L.; Louie, S. G. *Phys. Rev. B* **2013**, *87*.
(89) Körzdörfer, T.; Kümmel, S.; Mundt, M. *J. Chem. Phys.* **2008**, *129*, 014110.
(90) Hofmann, D.; Klüpfel, S.; Klüpfel, P.; Kümmel, S. *Phys. Rev.* **2012**, *85*, 062514.
(91) Krieger, J. B.; Li, Y.; Iafrate, G. J. *Phys. Lett.* **1990**, *146*, 256–260.
(92) Körzdörfer, T.; Mundt, M.; Kümmel, S. *Phys. Rev. Lett.* **2008**, *100*, 133004.
(93) Mundt, M.; Kümmel, S. *Phys. Rev. B* **2007**, *76*, 035413.

(94) Kronik, L.; Makmal, A.; Tiago, M. L.; Alemany, M. M. G.; Jain, M.; Huang, X.; Saad, Y.; Chelikowsky, J. R. *Phys. Status Solidi B* **2006**, *243*, 1063–1079.
(95) Humphrey, W.; Dalke, A.; Schulten, K. *J. Mol. Graph.* **1996**, *14*, 33–38.
(96) Kokalj, A. *J. Mol. Graph. Model.* **1999**, *17*, 176–179.
(97) Liu, S.-Y.; Alnama, K.; Matsumoto, J.; Nishizawa, K.; Kohguchi, H.; Lee, Y.-P.; Suzuki, T. *J. Phys. Chem. A* **2011**, *115*, 2953–2965.
(98) Kishimoto, N.; Ohno, K. *J. Phys. Chem. A* **2000**, *104*, 6940–6950.
(99) Potts, A. W.; Holland, D. M. P.; Trofimov, A. B.; Schirmer, J.; Karlsson, L.; Siegbahn, K. *J. Phys. B At. Mol. Opt. Phys.* **2003**, *36*, 3129–3143.
(100) Jones, R. O.; Gunnarsson, O. *Rev. Mod. Phys.* **1989**, *61*, 689–746.
(101) Bruneval, F.; Marques, M. A. L. *J. Chem. Theory Comput.* **2013**, *9*, 324–329.
(102) Caruso, F.; Rinke, P.; Ren, X.; Scheffler, M.; Rubio, A. *Phys. Rev. B* **2012**, *86*.
(103) Vydrov, O. A.; Scuseria, G. E. *J. Chem. Phys.* **2006**, *125*, 234109.
(104) Ehrler, O.; Weber, J.; Furche, F.; Kappes, M. *Phys. Rev. Lett.* **2003**, *91*, 113006.
(105) Mundt, M.; Kümmel, S. *Phys. Rev. B* **2007**, *76*.
(106) Walter, M.; Häkkinen, H. *New J. Phys.* **2008**, *10*, 043018.
(107) Sharp, R.; Horton, G. *Phys. Rev.* **1953**, *90*, 317–317.
(108) Talman, J.; Shadwick, W. *Phys. Rev.* **1976**, *14*, 36–40.
(109) Sahni, V.; Gruenebaum, J.; Perdew, J. *Phys. Rev. B* **1982**, *26*, 4371–4377.
(110) Marom, N.; Tkatchenko, A.; Scheffler, M.; Kronik, L. *J. Chem. Theory Comput.* **2010**, *6*, 81–90.
(111) Stowasser, R.; Hoffmann, R. *J. Am. Chem. Soc.* **1999**, *121*, 3414–3420.
(112) Segev, L.; Salomon, A.; Natan, A.; Cahen, D.; Kronik, L.; Amy, F.; Chan, C.; Kahn, A. *Phys. Rev. B* **2006**, *74*.
(113) Hwang, J.; Kim, E.-G.; Liu, J.; Bredas, J.-L.; Duggal, A.; Kahn, A. *J. Phys. Chem. C* **2007**, *111*, 1378–1384.
(114) Palummo, M.; Hogan, C.; Sottile, F.; Bagalá, P.; Rubio, A. *J. Chem. Phys.* **2009**, *131*, 084102.
(115) Mok, D. K. W.; Neumann, R.; Handy, N. C. *J. Phys. Chem.* **1996**, *100*, 6225–6230.
(116) Gritsenko, O. V.; Schipper, P. R. T.; Baerends, E. J. *J. Chem. Phys.* **1997**, *107*, 5007.
(117) Mundt, M.; Kümmel, S.; Huber, B.; Moseler, M. *Phys. Rev. B* **2006**, *73*, 205407.
(118) Sek, S. *Langmuir* **2009**, *25*, 13488–13492.
(119) Lörtscher, E.; Gotsmann, B.; Lee, Y.; Yu, L.; Rettner, C.; Riel, H. *ACS Nano* **2012**, *6*, 4931–4939.
(120) Heyd, J.; Scuseria, G. E.; Ernzerhof, M. *J. Chem. Phys.* **2003**, *118*, 8207–8215.
(121) Heyd, J.; Scuseria, G. E.; Ernzerhof, M. *J. Chem. Phys.* **2006**, *124*, 219906.
(122) Janesko, B. G.; Henderson, T. M.; Scuseria, G. E. *Phys. Chem. Chem. Phys.* **2009**, *11*, 443.
(123) Ren, J.; Meng, S.; Wang, Y.-L.; Ma, X.-C.; Xue, Q.-K.; Kaxiras, E. *J. Chem. Phys.* **2011**, *134*, 194706.
(124) Bisti, F.; Stroppa, A.; Picozzi, S.; Ottaviano, L. *J. Chem. Phys.* **2011**, *134*, 174505.
(125) Bisti, F.; Stroppa, A.; Donarelli, M.; Picozzi, S.; Ottaviano, L. *Phys. Rev. B* **2011**, *84*.
(126) Bisti, F.; Stroppa, A.; Perrozzi, F.; Donarelli, M.; Picozzi, S.; Coreno, M.; de Simone, M.; Prince, K. C.; Ottaviano, L. *J. Chem. Phys.* **2013**, *138*, 014308.
(127) The HOMO-10 and HOMO-11 are degenerate in the case of the $PBE0^{GKS}$ calculation. We do not show both orbital energies for clarity.
(128) Stein, T.; Autschbach, J.; Govind, N.; Kronik, L.; Baer, R. *J. Phys. Chem. Lett.* **2012**, *3*, 3740–3744.
(129) Moore, B.; Srebro, M.; Autschbach, J. *J. Chem. Theory Comput.* **2012**, *8*, 4336–4346.
(130) Marom, N.; Kronik, L. *Appl. Phys.* **2008**, *95*, 165–172.

(131) *The porphyrin handbook, Vol 19: Applications of Phthalocyanines*; Academic Press: San Diego, 2000.
(132) Sato, N.; Seki, K.; Inokuchi, H. *J. Chem. Soc. Faraday Trans. 2* **1981**, *77*, 1621.
(133) Neaton, J. B.; Hybertsen, M. S.; Louie, S. G. *Phys. Rev. Lett.* **2006**, *97*, 216405.
(134) Risko, C.; Brédas, J.-L. *Top. Curr. Chem.* in press.
(135) Sini, G.; Sears, J. S.; Brédas, J.-L. *J. Chem. Theory Comput.* **2011**, *7*, 602–609.
(136) Phillips, H.; Zheng, S.; Hyla, A.; Laine, R.; Goodson, T.; Geva, E.; Dunietz, B. D. *J. Phys. Chem. A* **2012**, *116*, 1137–1145.
(137) Foster, M. E.; Wong, B. M. *J. Chem. Theory Comput.* **2012**, *8*, 2682–2687.
(138) Evangelista, F.; Carravetta, V.; Stefani, G.; Jansik, B.; Alagia, M.; Stranges, S.; Ruocco, A. *J. Chem. Phys.* **2007**, *126*, 124709.
(139) Murdey, R.; Sato, N.; Bouvet, M. *Mol. Cryst. Liq. Cryst.* **2006**, *455*, 211–218.
(140) Hill, I. G.; Kahn, A.; Soos, Z. G.; Pascal, Jr, R. A. *Chem. Phys. Lett.* **2000**, *327*, 181–188.

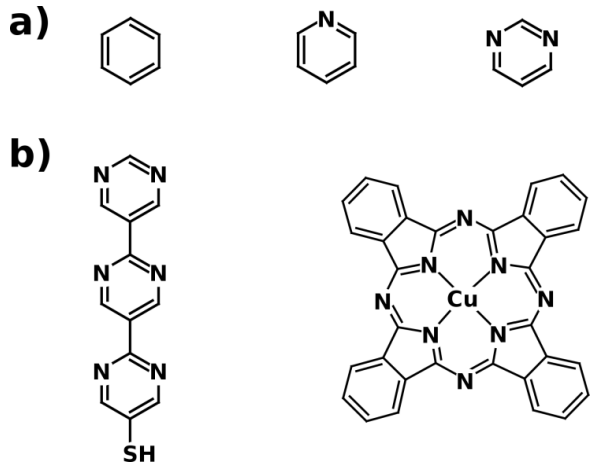

Figure 1: Molecules studied in this article: (a) Prototypical aromatic rings - benzene, pyridine, and pyrimidine. (b) More complex representative systems - terpyrimidinethiol and copper phthalocyanine.

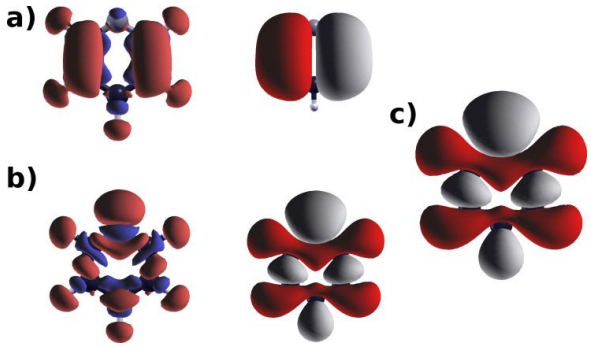

Figure 2: Charge-density difference between neutral and cation (left) and LUMO of cation (right), obtained using two different doublet configurations (a and b) of the pyridine cation. The configuration denoted by (b) is the energetically more stable one. In the charge-density difference plots, red (blue) regions denote areas of electron density depletion (accumulation) as a consequence of the ionization process. (c) HOMO of the neutral pyridine molecule.

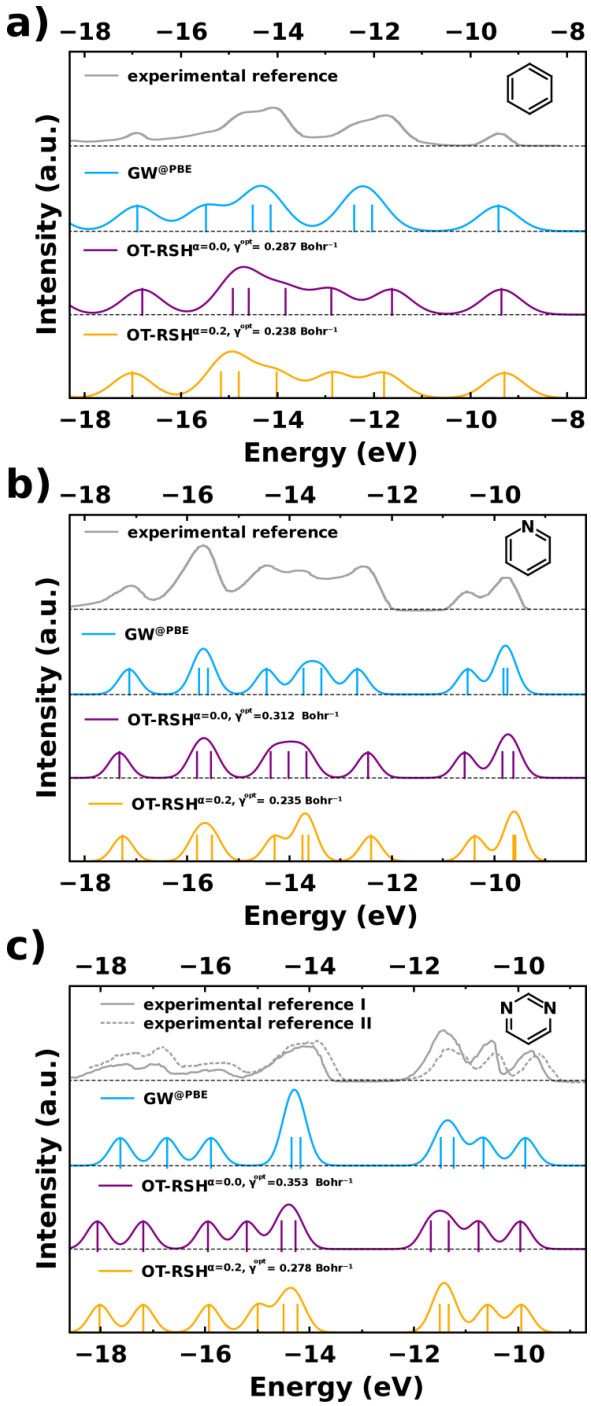

Figure 3: Valence electron spectra for: (a) benzene; (b) pyridine; (c) pyrimidine, as obtained from experiment (benzene and pyridine: Ref. 97; pyrimidine: Refs. 99 and 98 - reference I and II, respectively, on the figure), compared with simulated data obtained from GW calculations and OT-RSH calculations (with two different amounts of SR Fock exchange, α), broadened with Gaussians of widths 0.4 eV, 0.2 eV and 0.2 eV, respectively, to facilitate comparison with experiment.

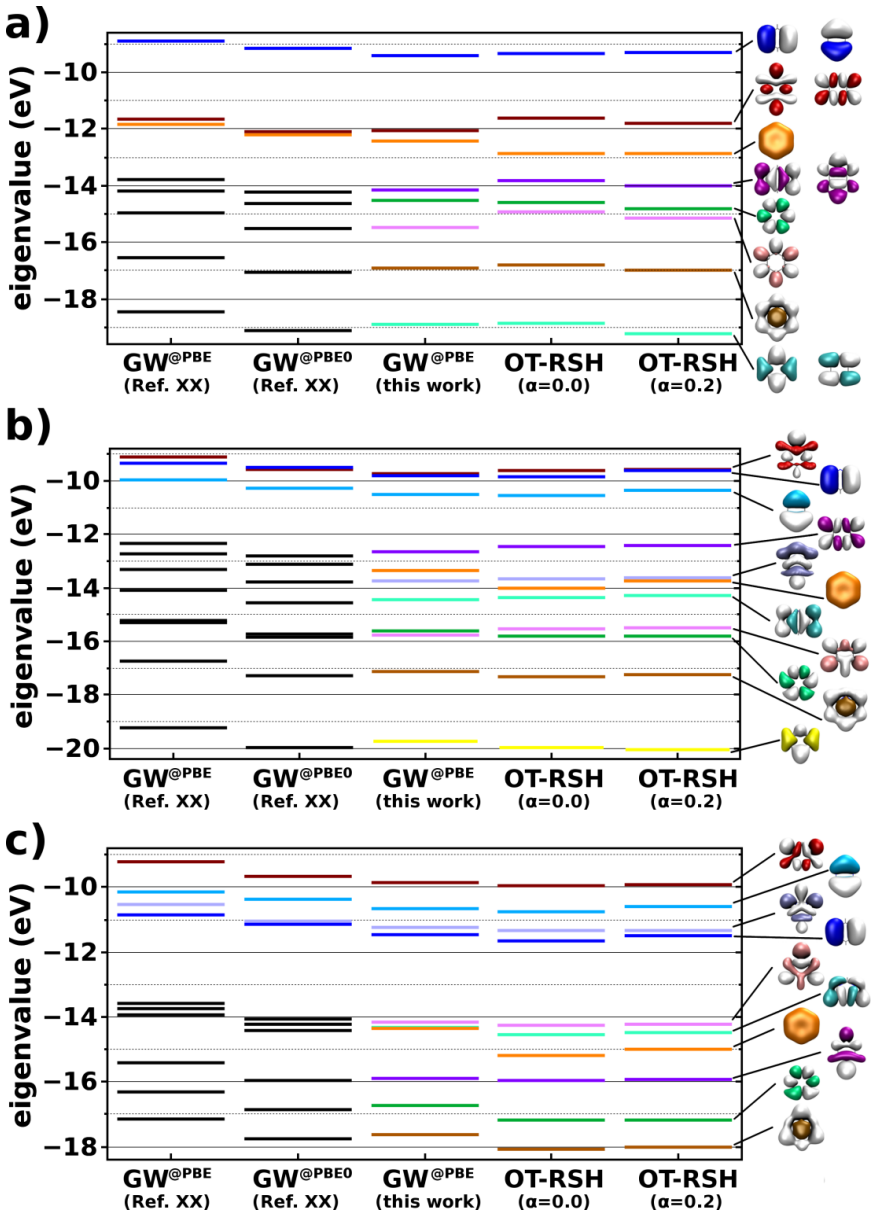

Figure 4: Eigenvalue spectra of: (a) benzene; (b) pyridine; and (c) pyrimidine, obtained from GW and OT-RSH. The GW spectra shown were obtained from literature data (scanned in from Ref. 61) with two different starting points, and from our own work. The OT-RSH data was obtained from two different choices for the amount of SR Fock exchange, α.

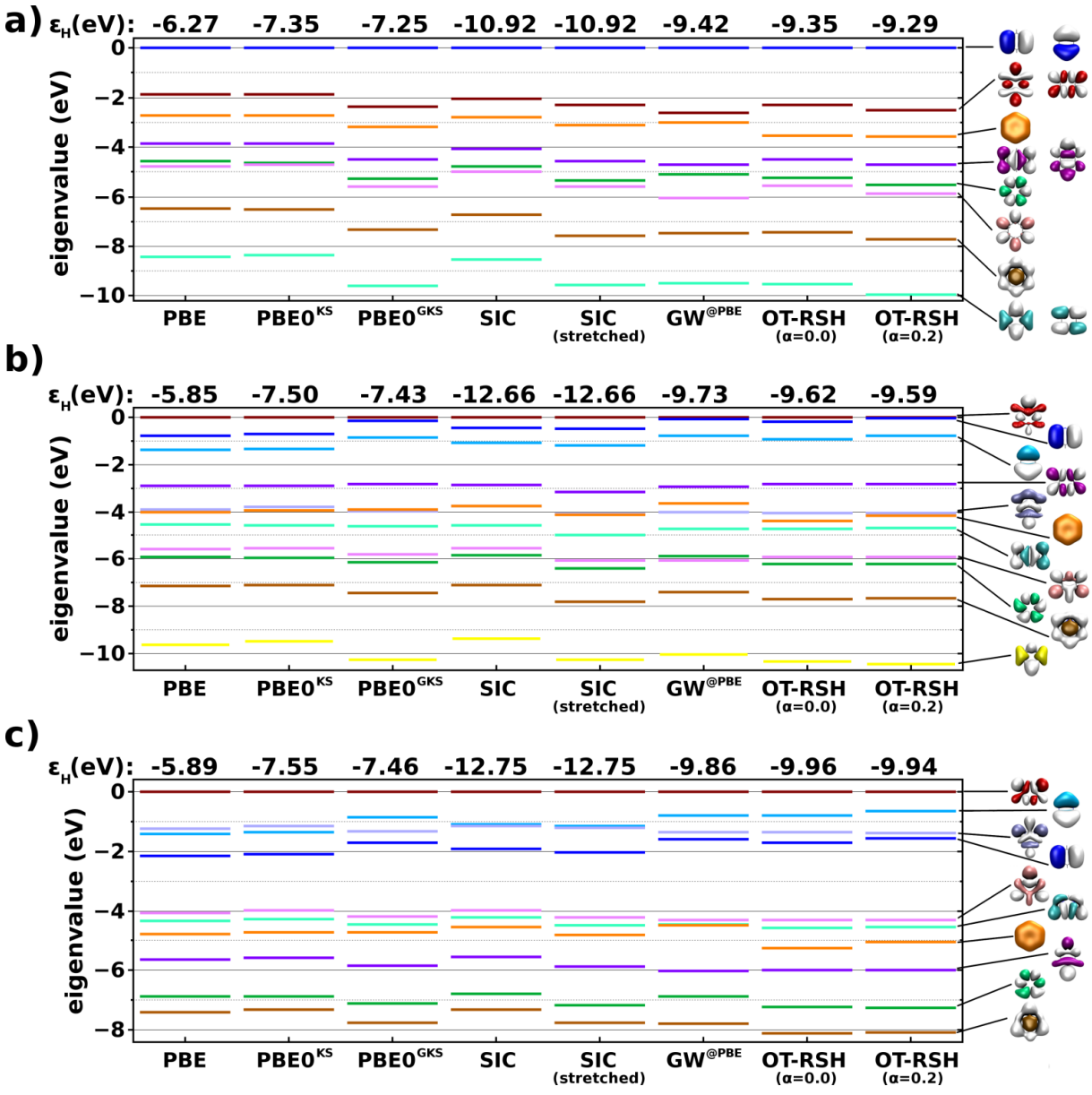

Figure 5: Shifted eigenvalue spectrum of: (a) benzene; (b) pyridine; and (c) pyrimidine obtained from different theoretical schemes. : A semi-local functional (PBE); A conventional hybrid functional (PBE0) in both the Kohn-Sham (KS) and generalized Kohn-Sham (GKS) scheme; A self-interaction-corrected (SIC) calculation, with and without additional "stretching" of the energy axis; GW calculations based on a PBE starting point, and optimally-tuned range-separated hybrid (OT-RSH) calculations with two different short-range exchange parameters, α=0 and α=0.2. See text for further details on the computational approaches.

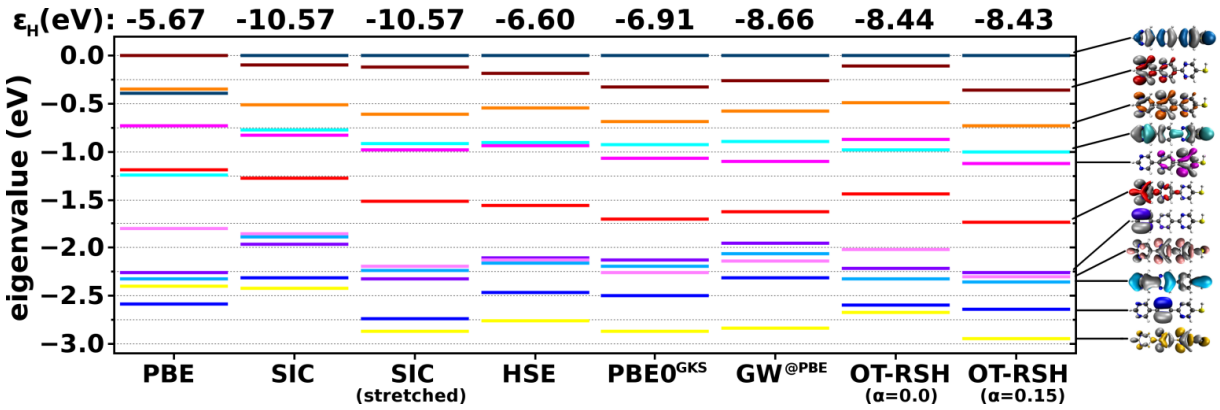

Figure 6: Shifted eigenvalue spectra of 3N-thiol as obtained from different theoretical schemes (see text for details). PBE, SIC, and HSE values were taken from Ref. 68. For the OT-RSH calculations, the optimal γ value was 0.217 and 0.187 for α=0 and α=0.15, respectively.

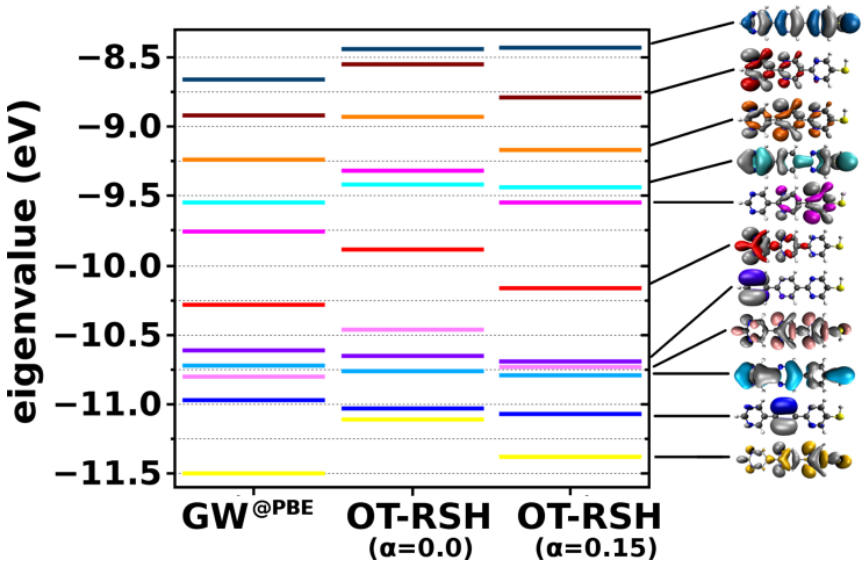

Figure 7: Unshifted eigenvalue spectra of 3N-thiol as calculated from GW and optimally-tuned range-separated hybrid (OT-RSH) calculations with two different short-range exchange parameters, α=0 and α=0.15.

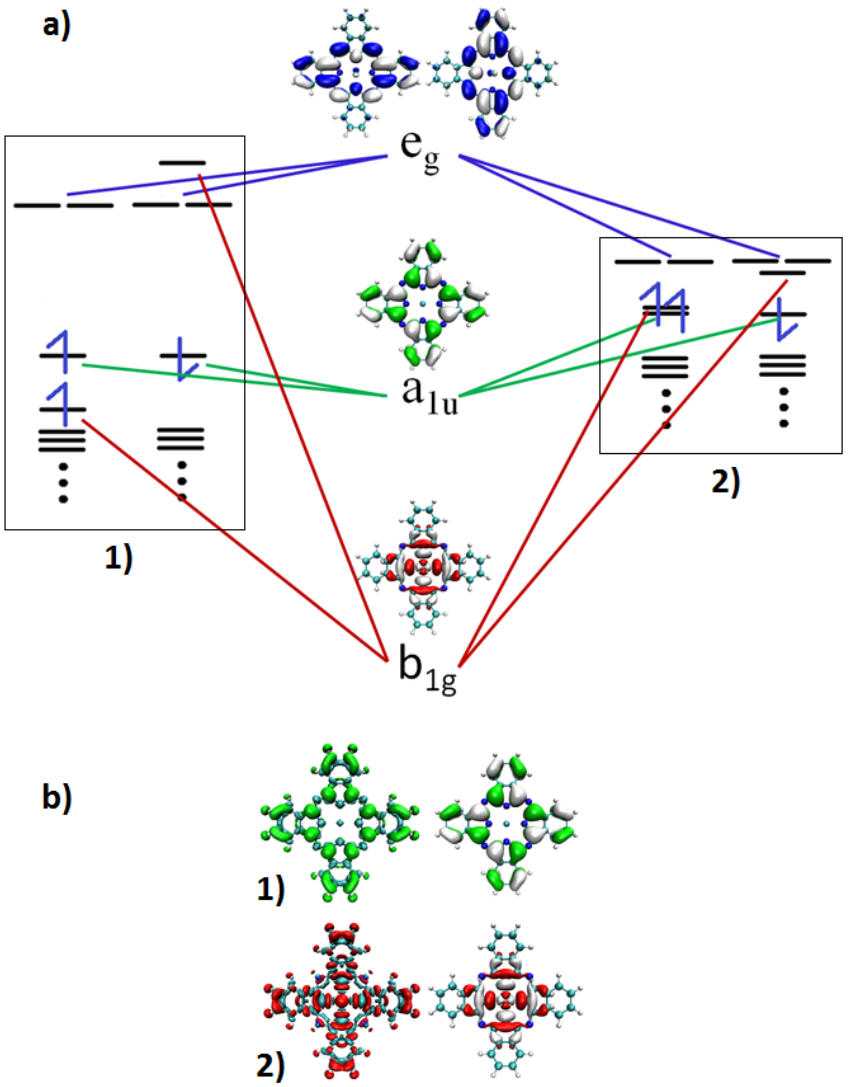

Figure 8: (a) Schematic diagram of selected frontier eigenvalues and orbitals for the CuPc molecule, as obtained from an OT-RSH calculation (configuration 1, left) and from a PBE calculation (configuration 2, right). (b) OT-RSH charge-density differences between neutral and cation (left) and LUMO of cation (right), obtained from the "open-shell singlet" configuration of the CuPc cation, corresponding to ionization of netrual configuration 1 (in green), and from the "closed- shell singlet" configuration of the CuPc cation, corresponding to ionization of configuration 2 (in red). In the charge density difference plots, green or red (blue) regions denote areas of electron density depletion (accumulation) as a consequence of the ionization process.

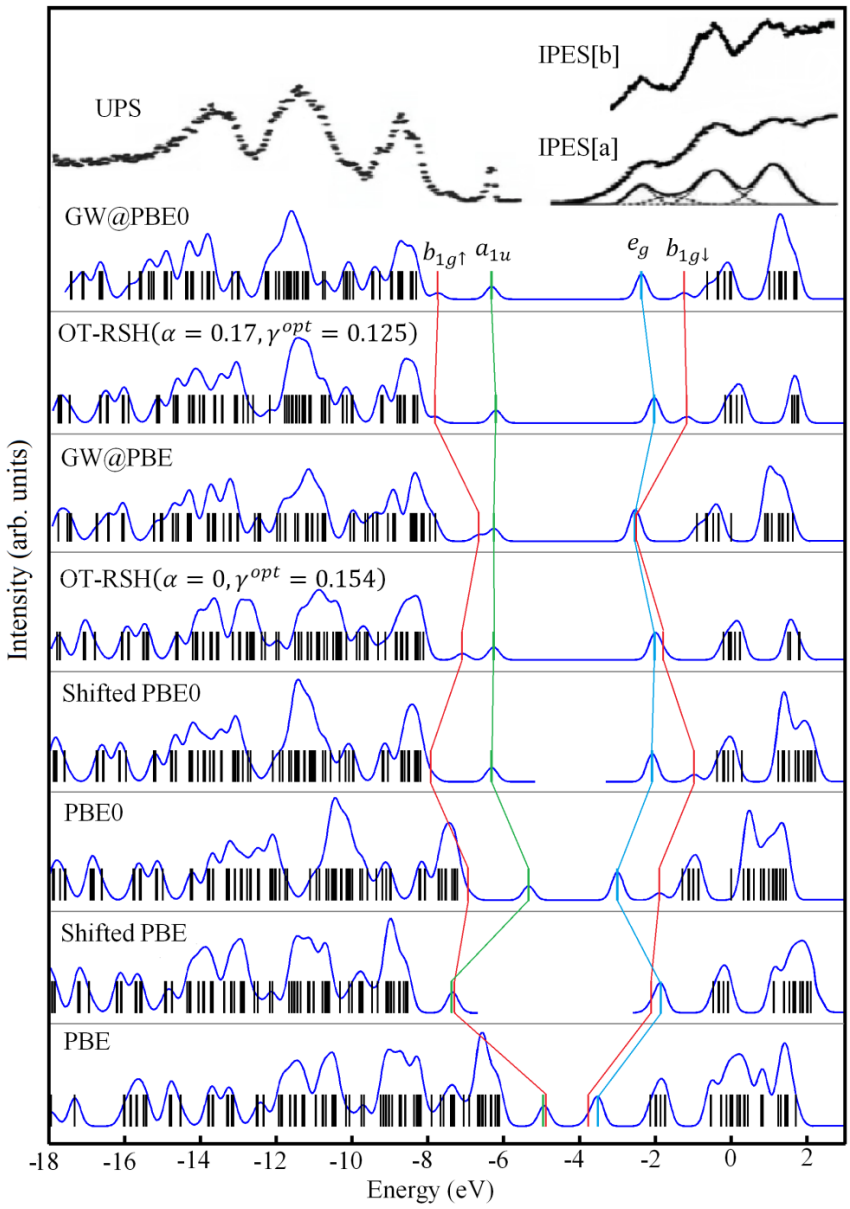

Figure 9: Simulated DFT and GW spectra (see text for details), obtained from computed energy levels (shown as sticks) by broadening via convolution with a 0.15-eV-wide Gaussian. PBE, PBE0, and GW data were taken from Ref. 69. Theoretical data are compared to the experimental gas phase photoemission data of Evangelista et al.138 and to the thin film inverse photoemission data of (a) Murdey et al.139 (shown with curve fitting results) and (b) Hill et al.140 The experimental inverse photoemission spectra were shifted so as to align the LUMO peak with the computed GW@PBE0 LUMO peak. Eigenvalues corresponding to the e_g, a_{1u}, and b_{1g} orbitals are designated by the same color scheme as in Fig. 8.

Part III.

Summary and Outlook

In this thesis, materials relevant in the context of organic electronics have been studied using atomistic simulations based on density-functional theory (DFT). In the following, I will summarize the results and give an outlook for potential future efforts.

For self-assembled monolayers (SAMs) of oligopyrimidinethiols, which are molecules that contain dipoles distributed along their backbone, together with others I showed already during my Master's thesis that a gradient in electrostatic energy along the backbone of the monolayer occurs.[132] This gradient in the potential energy landscape is different to the effect induced by polar substitution at the tail of the monolayer, because the latter results in a change in energy that is spatially localized to the tail of the SAM.[132] In the work[i] by Rissner *et al.*,[133] we emphasized the importance and implications of such a gradient in electrostatic energy (see Figure 7.1), which, of course, represents an electric field.[133] This is intriguing, as the electric field is not external to the SAM, but arises exclusively from the interactions within the densely-packed monolayer of distributed dipoles.[133] For the case of terpyrimidinethiol (3N-thiol), we showed on the basis of conventional hybrid band-structure calculations that the occurrence of the electric field has important implications for the electronic structure of the SAMs: In analogy to the Quantum-Confined Stark effect in the context of inorganic semiconductor quantum-wells,[134] the frontier electronic states localize on opposite ends of the SAM and the band gap is strongly reduced.[133] As the electric field is generated by the ensemble of molecules present in the 3N-thiol SAM, it depends on the packing density of the molecules and, of course, vanishes in the limit of the isolated gas phase molecule.[133] Therefore, the electronic properties of 3N-thiol as an isolated molecule and as monolayer are different (see densities of states in Figure 7.1). As these differences arise from the ensemble of molecules that form a SAM, the responsible electrostatic effect was termed to be a *collective effect*.[84,133] We have later also shown[ii] that these collective effects lead to a linear dependence of the global band gap on the length of a 2D-extended SAM.[135]

As discussed in the introduction, the importance of collective electrostatic effects was earlier emphasized by Heimel *et al.* for substituted thiols on gold.[73] They showed that due to the electrostatics associated with a 2D-extended sheet of dipoles,[85] molecules with a very different *molecular IP* can result in metal-SAM systems with nearly identical level alignment.[73] In ref. 1, which is the first article enclosed in this thesis, we have now shown that the two molecules N_{in} and N_{out} (see Figure 7.2) have a very *similar* molecular *IP*, but in metal-SAM-metal systems (see sketch in Figure 7.2) exhibit very different level alignment.[1] On the basis of DFT and Green's function techniques,[27,136,137] we have also calculated the charge-transport characteristics of the associated SAM-devices.[1] The resulting *IV* curves shown in the left part of Figure 7.3 are entirely different for N_{in} and N_{out} SAMs: although N_{in} and N_{out} are very similar as isolated molecules, in the respective SAMs the total current differs by a factor of 9 (at $V = 1.4\,\mathrm{V}$) and the polarity of

[i] an article to which I have contributed in the course of this thesis: F. Rissner, D. A. Egger, A. Natan, T. Körzdörfer, S. Kümmel, L. Kronik, E. Zojer: J. Am. Chem. Soc. **2011**, 133, 18634.

[ii] an article to which I have contributed in the course of this thesis: F. Rissner, A. Natan, D. A. Egger, O. T. Hofmann, L. Kronik, E. Zojer: Org. Elect. **2012**, 13, 3165.

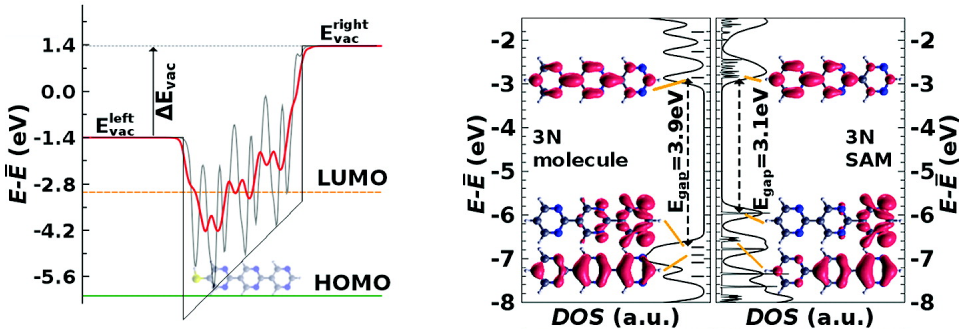

Figure 7.1.: Plane-averaged electron potential energy along a 3N-thiol-SAM (left) and comparison of the density of states for 3N-thiol in the gas phase and as a densely-packed SAM (right). Adapted with permission from ref. 133. Copyright 2011 American Chemical Society.

charge transport switches.[1] The latter effect also implies a change in the thermoelectric properties of the two SAM-devices.[138] Accordingly, the sign of the calculated Seebeck coefficient for N_{in} and N_{out} monolayers is different.[1]

We have rationalized this observation with an electrostatic interplay of the polar bonds present in N_{in} and N_{out}.[1] While the overall dipole moment of these two molecules is zero, local dipoles occur in the pyrimidine rings of N_{in} and N_{out} due to the polar carbon-nitrogen bonds (see Figure 7.2). Importantly, these local dipoles point in opposite directions for the two molecules. We have explicitly calculated the impact of arranging the molecules (as sketched in Figure 7.2) on the electrostatic energy, and the result is reproduced in Figure 7.3. Clearly, the collective electrostatic effect modifying the energy landscape when the molecules are arranged to a SAM is different for N_{in} and N_{out}, *i.e.*, the potential energy in the region of the molecular backbone is shifted more towards the vacuum energy by ≈1 eV in the case of N_{in}.[1] When arranging the local dipoles of the molecules into SAM-devices (see sketch in Figure 7.2), this collective effect

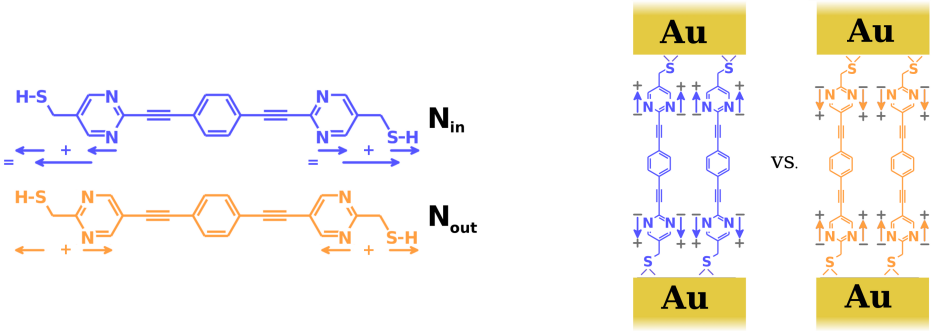

Figure 7.2.: N_{in} and N_{out} molecule with local dipoles indicated (left) and a sketch of N_{in} and N_{out} SAM-devices. Reproduced with permission from ref. 1, ©2012 WILEY-VCH Verlag GmbH & Co. KGaA, Weinheim.

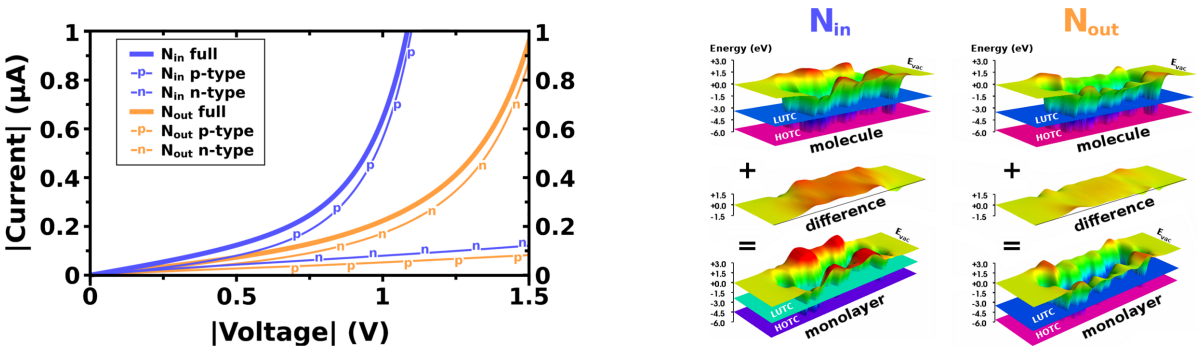

Figure 7.3.: (left) Calculated charge-transport characteristics of N_{in} and N_{out} SAM-devices. (right) DFT-calculated potential wells of N_{in} and N_{out} molecules (top) and monolayers (bottom), and the respective collective electrostatic effect on the energy landscape (middle). Reproduced with permission from ref. 1, ©2012 WILEY-VCH Verlag GmbH & Co. KGaA, Weinheim.

together with the interface dipole was shown[1] to be responsible for the entirely different charge-transport characteristics of N_{in} and N_{out} SAMs.

For such molecular-scale electronic devices, it was repeatedly seen that a chemical functionalization of the molecules allows tuning the charge-transport characteristics of the associated devices. For example, attaching polar groups to the central ring of the so-called "Tour Wire" molecule led to the experimental observation of negative differential resistance[139] and rectification.[140] Moreover, as the energy difference between the Fermi energy of the electrodes and the transport channels in the molecules has emerged as an important parameter governing charge transport,[26] tuning the molecular electronic structure through appropriate chemical design at the single-molecule level evolved as an appealing strategy to control the electrical properties of molecular devices. However, at the same time the fundamental difference between charge transport through a single molecule and a monolayer has been stressed as well, *e.g.*, by Selzer and co-authors.[141] More recently, Ratner and co-workers have emphasized the importance of interwire coupling (*e.g.*, through π-π interactions) and substrate-mediated coupling in molecular layers.[142] Here, our work aids to the understanding that the collectivity in multi-molecule system matters, and it shows that for engineering the electrical properties of the associated devices one needs to think beyond the "single molecule picture". As the physical origin of the observed collective effects – the Coulomb interaction of local dipoles – is long range in nature, these effects are expected to play a significant role also for molecular arrangements that are not as densely-packed as was initially assumed in our work. Here, we currently continue our investigations (under the lead of my colleague V. Obersteiner), and study the coverage dependence of collective electrostatic effects and their implications for the charge-transport properties of molecular systems. One might, however, also envision to exploit the energetic shifting and localization of molecular electronic states towards a controlled tuning of wave functions in molecular ensembles. With my colleague B. Kretz leading the efforts, we currently explore the

promising strategy to use specifically designed polar elements in molecular wires, adopt their mutual collective interactions and by that control the energetics and spatial localization of appearing molecular electronic states.

The importance of the spatial localization and energetics of electronic states in the organic semiconductor was also emphasized in the context of metal-organic interfaces that comprise flat-lying charge-transfer monolayers.[iii] There, we have shown for the relevant Fermi-level pinning regime (see Section 1.3) that whether a work-function modification "*beyond Pinning*" is feasible or not depends on the spatial position of the pinning level in the organic monolayer.[143] In publication II enclosed in this thesis, we now explore the limits of modifying the substrate work-function using SAMs of molecules with large extended dipoles.[2] For metal-SAM systems, it was found experimentally that the attained adsorption-induced work-function modification, $\Delta\Phi$, is correlated with the dipole moment of the SAM-molecules, see, *e.g.*, refs. 19, 23, 24. However, it was also shown that this direct correlation between the dipole moments of the SAM molecules and $\Delta\Phi$ can be weakened by collective electrostatic effects, *i.e.*, the mutual depolarization of the polar molecules.[85,144] In fact, under the assumption of dielectric breakdown,[82] it was argued that Φ of the combined metal-organic system would even saturate. In publication II, we explored the limits of work-function modification further,[2] and for this task chose merocyanine-type molecules (see Figure 7.4), as they exhibit a large dipole moment extended along the molecular backbone.[2] Moreover, these merocyanines are archetype donor-acceptor systems that have been synthesized and studied in the context of nonlinear optics.[145,146] These molecules also allow for a convenient way to tune the dipole moment (see top part in Figure 7.4) by twisting the inter-ring carbon-carbon double bond, which can be realized in practice by attaching bulky groups to the periphery of the backbone.[146] Alternatively, the molecular dipole moment can be enlarged by increasing the donor-acceptor charge-transfer distance through insertion of -C_2H_2- spacers. We have calculated the step in the electrostatic energy induced by the collective interplay of the molecular dipoles present in the free-standing SAM, ΔE_{vac}, and found that it is *increased* by *ca.* 0.7 eV when the inter-ring twist angle is varied from 0 ° to 90 ° (see bottom part in Figure 7.4).[2] Intriguingly, however, when the SAM is calculated in contact with gold, the work-function modification, $\Delta\Phi$, is found to follow the opposite trend and calculated to *decrease* by 0.3 eV.[2] As these findings are entirely unexpected from purely electrostatic considerations that presage a saturation of $\Delta\Phi$, one apparently needs to dig deeper and study the details of the associated interfacial level alignment. There, we have calculated that the merocyanine-SAMs are in a Fermi-level pinning situation, where the charge density associated with this "pinned" molecular electronic state is shifted away from the immediate interface region and rather localized towards the vacuum-oriented side of the combined metal-SAM system.[2] This intramolecular charge-transfer occurs already for the molcules in the gas phase, but is found to withstand the collective effect of depolarization in the SAM. In fact, upon twisting the merocyanine SAM, the

[iii] an article to which I have contributed in the course of this thesis: O. T. Hofmann, D. A. Egger, E. Zojer: Nano Lett. **2010**, 10, 4369.

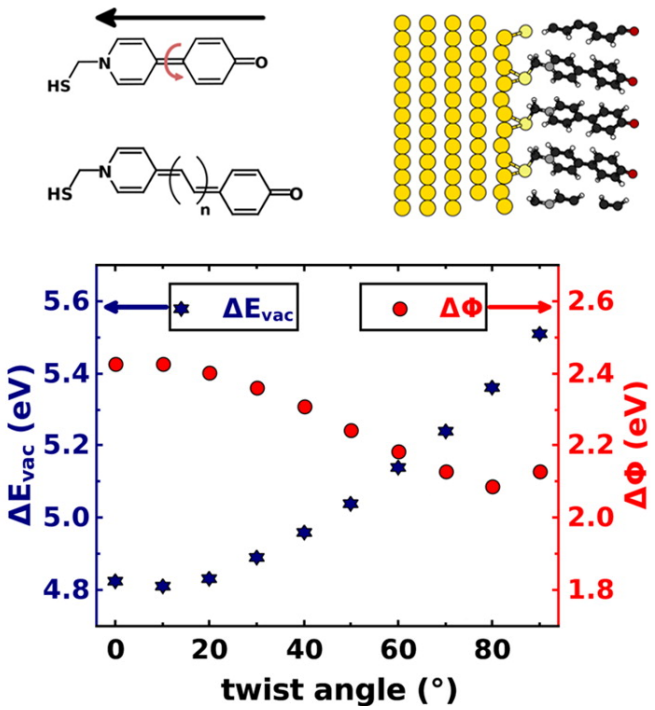

Figure 7.4.: (top left) Chemical structures of the merocyanine-type molecules. The molecular dipole moments can be increased by twisting or elongating these molecules. (top right) Side view of the Au(111)/SAM interface. (bottom) Calculated step in the electrostatic energy for the free-standing SAM, ΔE_{vac}, and induced work function-modification, $\Delta\Phi$, for the SAM adsorbed on gold, both as a function of the inter-ring twist angle. Adapted with permission from ref. 2. Copyright 2013 American Chemical Society.

HOMO-derived band is even slightly more localized, and also strongly shifted in energy.[2] The latter effect drives the HOMO further up in energy, which triggers additional equilibrating charge rearrangements necessary to maintain thermodynamic equilibrium at the interface. This process in total energetically overshoots the effect of increasing the dipole and causes the observed anticorrelation.[2] Furthermore, we argued that the orbital localization and energy shifting is expected to occur quite generally for large extended molecular dipoles, which will, therefore, likely provoke a Fermi-level pinning situation upon adsorption, beyond which Φ cannot be further modified.

One of the most thoroughly studied metal-organic systems, which also involves interfacial Fermi-level pinning processes, is PTCDA on Ag(111). Using scanning tunneling spectroscopy experiments, Kraft *et al.*[147] have shown that the bonding of PTCDA to Ag(111) involves a chemical interaction channeled through the former LUMO of the PTCDA molecule in the gas phase (see ref. 16 for a detailed discussion of the chemisorptive binding mechanism of PTCDA on Ag(111)). At the same time, however, it was

established theoretically[148] that a proper treatment of long-range VDW interactions is imperative for accurately predicting the structure of PTCDA on Ag(111): Using popular GGA-DFT functionals such as the celebrated PBE,[149] no binding is predicted for PTCDA on Ag(111),[148] which is inconsistent with the experiment (see refs. 59, 60 for details). These findings were seen as a manifestation of the important long-range VDW interactions present at the Ag(111)-PTCDA interface, since such interactions are absent in (semi-) local DFT functionals.[43] However, recent theoretical progress in the efficient description of VDW interactions for metal-organic interfaces[43,44] was shown to allow for an accurate description of the structural properties for the prototypical PTCDA molecule on the noble metals.[44] Stimulated by extensive experimental information recently reported by Stadtmüller *et al.*,[48] we have taken the simulation of metal-organic hybrid systems one step further and investigated the rather complex metal-organic-organic three-layer stack Ag(111)-PTCDA-CuPc in publication III included in this thesis.[3] Figure 7.5 (part a) shows the relaxed structure of Ag(111)-PTCDA-CuPc as calculated with PBE+vdW$^{\text{surf}}$. The calculated interlayer distances are in excellent agreement with the experimentally measured distances, which underlines the reliability of the applied theoretical approach for predicting the structural properties also of rather complex metal-organic hybrid systems. In part b of Figure 7.5, the calculated binding-energy profile between CuPc and Ag(111)-PTCDA as a function of the CuPc-PTCDA layer distance is shown.[3] In absence of long-range VDW interactions (curve PBE in Figure 7.5), no visible minimum is calculated for the CuPc layer on Ag(111)-PTCDA.[3] Importantly, once VDW interactions are switched on in the system, the situation changes drastically:[3] CuPc binds to the rest of the system and the predicted organic-organic interlayer distance is in very good agreement with the experimental data.[48] Furthermore, we have shown that the calculated energy contributions associated with the VDW interactions are quite large (more than 3 eV at the minimum distance, see Figure 7.5). This finding renders the prevalent association of "weak" VDW interactions questionable for the case of large flat-lying organic species on metal substrates. Interestingly, binding energies of similar magnitude due to VDW interactions have recently also been extracted from scanning tunneling and atomic force microscope measurements for PTCDA adsorbed on Au(111).[150]

The importance of VDW interactions has also been stressed in the context of single-molecule transport measurements,[151] and their critical role for the performance of the diode behavior of ferrocene-based SAMs has been additionally acknowledged.[152] Regarding potentially interesting future investigations, it seems natural to explore the significance of VDW interactions for the structural properties of even more complex systems, such as metal-organic interfaces involving SAMs (as is currently conducted by my colleague E. Verwüster). These systems can establish a strong covalent bond to the substrate (*e.g.*, through the use of suitable docking-groups), but at the same time interact rather "weakly" on an intermolecular level (see Section 1.3). The balanced description of this rather involved situation indeed represents a considerable challenge for the theoretical methodology. But also for more "classical" metal-organic systems, the vast amount of high-quality experimental data prevalent in literature allows to theoretically approach the "full spectrum" of interactions that can occur between large organic adsorbates and

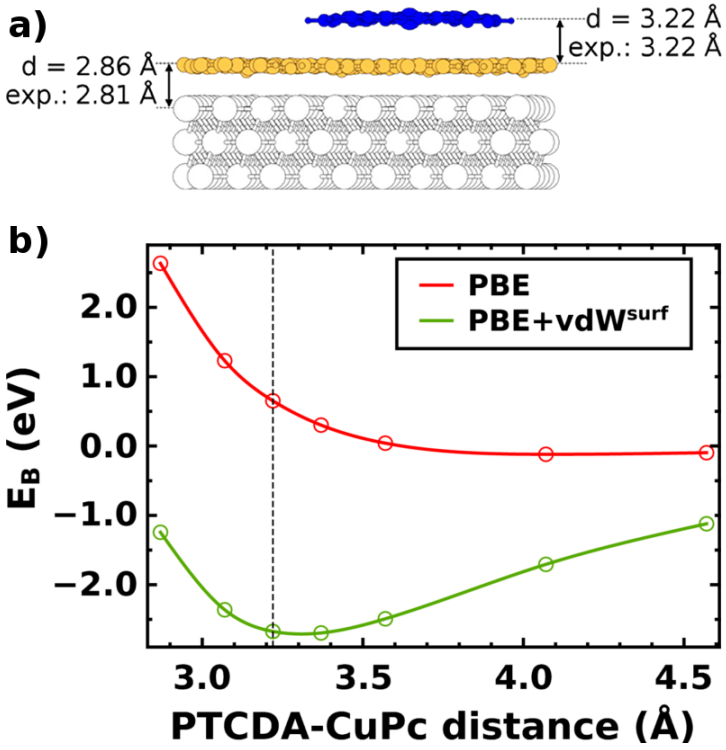

Figure 7.5.: (a) Side view of CuPc (blue) on PTCDA (yellow) on Ag(111) (white), the calculated and experimental[48] average distances are listed as well. (b) Binding energy between CuPc and Ag(111)-PTCDA as a function of the difference between the average vertical positions of the carbon atoms in PTCDA and CuPc calculated with PBE (red) and PBE+vdW^{surf} (green); the dashed vertical line indicates the experimental distance.[48] Adapted with permission from ref. 3. Copyright 2013 American Chemical Society.

metal surfaces. Therefore, it is highly interesting to also continue the detailed comparison of calculated and measured properties of metal-organic interfaces that involve flat-lying molecules, which is currently pursued in our group by E. Wruss.

The latter is especially relevant regarding the observation that minute variances in the electronic structure remained between the experimental results reported by Stadtmüller *et al.*[48] and publication III enclosed in this thesis.[3] Experimentally, it was seen that features in the UPS spectrum associated with the PTCDA monolayer shifted energetically upon the additional adsorption of the CuPc layer,[48] an effect that we could not reproduce in our simulations. At this stage, the most probable reason for this remaining discrepancy between experiment and theory are the inherent technical limitations of the simulations that are necessary simply due to the immense size of the Ag(111)-PTCDA-CuPc system: The unit cell considered in the simulations contains already more than 400 atoms, and yet the experimentally reported surface unit-cell is still by a factor of 2.5 larger.[3] This structural constraint additionally resulted in the considered packing

density of CuPc being smaller than the one obtained experimentally.[3] Furthermore, our simulations cannot account for PES cross-section redistributions that might occur in the experiment due to the adsorption of CuPc. Such effects could explain the remaining discrepancy,[3] because the two inequivalent PTCDA molecules were experimentally seen to be associated with two peak maxima split by 0.16 eV,[147] which might manifest itself differently in the measured spectrum of PTCDA on Ag(111) once it is covered by CuPc.[3] These inherent limitations of the calculations might very well be responsible for the observed differences, which is why it is absolutely crucial to further test the capabilities of the applied theoretical methodology on various metal-organic systems and by that determine its limits.

In this context, it is also worth recalling that a (semi-)local DFT-based theoretical description of the electronic structure at the Ag(111)-PTCDA-CuPc interface, especially regarding the molecular density of states of the PTCDA and CuPc layer, can be expected to deviate from the experiment on even fundamental grounds. First and foremost, for the organic molecules CuPc and PCTDA in the gas-phase, it is well-established in the theoretical literature that their valence-electronic structure as calculated from (semi-)local DFT functionals is distorted by significant orbital-SIE (see refs. 119–121). Secondly, the violation of the IP theorem by common (semi-)local DFT functionals results in gas-phase HOMO energies that are too shallow with respect to experimental gas-phase IPs (see Section 2.3). Last but not least, common approximations in DFT cannot account for long-range correlation effects (such as the above discussed long-range VDW interactions) and, as a consequence, neglect the renormalization of energy levels due to polarization effects: When molecules are assembled into a monolayer, the IP of the system changes due to the polarization induced *via* the neighboring molecules.[130,153–155] Similarly, the gas-phase ionization energies of an organic molecule are altered once the molecule is in the vicinity of a metal substrate, see, *e.g.*, refs. 130, 156. The underestimation of the HOMO energy and the error in energy due to the absence of screening-induced renormalization of the energy levels are opposite in sign. Notably, however, Biller *et al.* have shown for benzene on graphite and benzene diamine on gold that their magnitude is not the same and that a systematic error cancellation is not obtained.[157]

This unsatisfying situation calls for improving current electronic structure techniques towards efficient and accurate *first-principles* simulations that also allow for a quantitative agreement with the experiment. In this context, an efficient DFT-based electronic structure method that allows for an accurate theoretical treatment of the gas-phase molecular electronic structure – namely optimally-tuned range-separated hybrid functionals – was applied and tested in publication IV enclosed in this thesis. In Figure 7.6 I reproduce one of the many results from this study, where eigenvalues calculated from the OT-RSH scheme (using two different amounts of short-range Fock exchange α) and from the GW approximation are compared to experimental PES spectra for the outer-valence spectrum of the prototypical gas-phase molecules benzene, pyridine and pyrimidine; note that all spectra are shown on an absolute energy scale, *i.e.*, without imposing an additional artificial energy shift. It can be seen that the agreement of the OT-RSH scheme

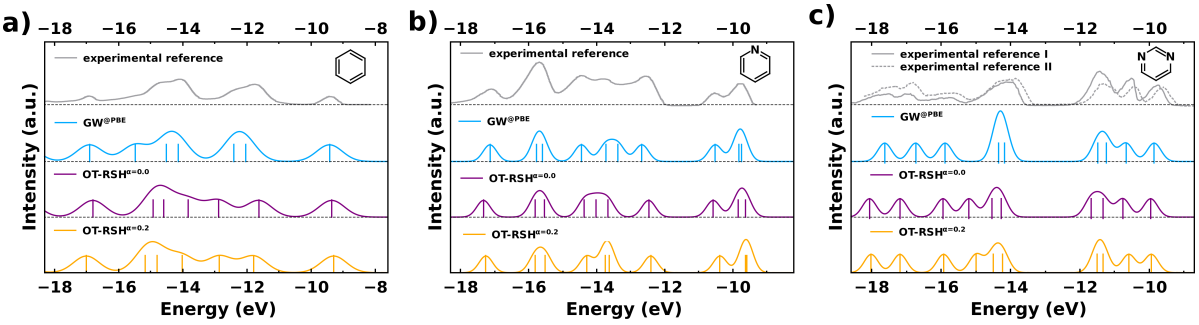

Figure 7.6.: Valence electron spectra for: (a) benzene; (b) pyridine; (c) pyrimidine, as obtained from experiment (benzene and pyridine: ref. 158; pyrimidine: ref. 159 and ref. 160 - reference I and II, respectively, on the figure), compared with simulated data as obtained from the *GW* approximation based on a PBE starting point, and OT-RSH calculations with two different amounts of short-range Fock exchange, α. Note that the calculated data was additionally broadened with Gaussians to facilitate comparison with experiment.

with the experimental spectra and the *GW* calculations – for a wide energy range of several eVs – is very good (with one exception, which is a high-symmetry orbital distinct to cyclic compounds). In particular, our quantitative study performed in publication IV showed that the mean absolute difference between the orbital energies calculated from OT-RSH (with α=0.2) and *GW* is ≈0.2 eV for these organic molecules, which likely is at the limit of resolution for both considered theoretical techniques. Encouraged by this success, we pursued to investigate the more complex molecules 3N-thiol and CuPc. For 3N-thiol, we have shown in ref. 133 that differently localized molecular orbitals occur in the outer-valence region. As discussed in Section 2.3, this causes a significant distortion of the GGA-calculated eigenvalue energy spectrum due to the different orbital-SIEs, which was shown to be satisfactorily corrected by using a conventional hybrid DFT functional.[133] In the context of orbital-SIE, even more severe distortions of the outer-valence electron energies are known to occur upon the use of (semi-)local DFT functionals for the rather complex molecule CuPc.[120] Recently, Refaely-Abramson *et al.*[128] suggested the additional use of short-range Fock exchange in the OT-RSH scheme to efficiently mitigate this problem, and they demonstrated the power of such an approach for several organic molecules such as NTCDA and PTCDA.[128] Our work contained in publication IV takes this approach to the next level for the more complex molecules 3N-thiol and CuPc. We found that a value of $\alpha \approx 0.2$ for the short-range Fock exchange efficiently reduces the SIE in the orbital energies and results in valence-electron spectra that are *on par* with the ones obtained from the much more computationally demanding *GW* calculations, even for the rather complex molecules 3N-thiol and CuPc. Note that the computational complexity associated with *GW* calculations and their convergence[161,162] so far prevents their widespread use for the simulation of metal-organic interfaces.

Therefore, significant efforts in the direction of establishing alternative improvements in the theoretical description of metal-organic interfaces lie ahead. I believe[iv] that one potentially interesting avenue to correct the electronic structure of metal-organic interfaces as obtained from (semi-)local DFT functionals is a "step-by-step" scheme that consecutively corrects the above-outlined errors: (i) in the electronic structure of the gas-phase molecule ; (ii) as a consequence of neglecting the polarization-effect due to the surrounding molecules in a monolayer; and (iii) due to the missing renormalization of the molecular levels in the vicinity of a metal surface. As was shown by Neaton and co-workers (see, *e.g.*, ref. 131), such a scheme can result in a much more accurate description of the electronic properties of metal-organic systems.

In summary, this Ph.D. thesis investigated the interactions that occur at metal-organic interfaces and discussed the theoretical possibilities of how to explore them. Various materials that are relevant in the broader context of organic and molecular electronics have been studied, from gas-phase organic molecules to molecular assemblies and complex three-layer metal-organic systems. It was shown that atomistic simulations based on DFT allow for establishing microscopic insight into the relevant processes at metal-organic interfaces, and that there are promising novel theoretical schemes that provide an efficient correction for some of the well-known drawbacks of common DFT functionals. With the continuously growing demand for developing novel materials, I believe that computer simulation will further strengthen its role as a vital tool in science and technology.

[iv] Numerous discussions with G. Heimel and further supporting discussions with E. Zojer are acknowledged.

Bibliography

(1) Egger, D. A.; Rissner, F.; Zojer, E.; Heimel, G. *Adv. Mater.* **2012**, *24*, 4403–4407, DOI: 10.1002/adma.201200872 (cit. on pp. vi, 27, 128–130).

(2) Egger, D. A.; Zojer, E. *J. Phys. Chem. Lett.* **2013**, 3521–3526, DOI: 10.1021/jz401721r (cit. on pp. vi, 41, 131, 132).

(3) Egger, D. A.; Ruiz, V. G.; Saidi, W. A.; Bučko, T.; Tkatchenko, A.; Zojer, E. *J. Phys. Chem. C* **2013**, *117*, 3055–3061, DOI: 10.1021/jp309943k (cit. on pp. vi, 61, 133–135).

(4) *The Molecule-Metal Interface*; Koch, N., Ueno, N., Wee, A. T. S., Eds.; Wiley-VCH Verlag GmbH & Co. KGaA: Weinheim, Germany, 2013 (cit. on pp. 3, 8).

(5) Oura, K.; Lifshits, V.; Saranin, A.; Zotov, A.; Katayama, M., *Surface Science: An Introduction*; Springer: Berlin ; New York, 2003 (cit. on pp. 3, 4, 6, 8).

(6) Lüth, H., *Solid Surfaces, Interfaces and Thin Films*; Springer: Heidelberg ; New York, 2010 (cit. on pp. 3, 9).

(7) Gross, A., *Theoretical Surface Science: A Microscopic Perspective*; Springer: Berlin ; London, 2009 (cit. on pp. 3, 6).

(8) Ashcroft, N. W., *Solid State Physics*; Holt, Rinehart and Winston: New York, 1976 (cit. on pp. 3, 5, 6).

(9) Groß, R.; Marx, A., *Festkörperphysik*; Oldenbourg: München, 2012 (cit. on p. 3).

(10) Heeger, A. *Rev. Mod. Phys.* **2001**, *73*, 681–700, DOI: 10.1103/RevModPhys.73.681 (cit. on p. 3).

(11) Cuevas, J. C.; Scheer, E., *Molecular Electronics: An Introduction to Theory and Experiment*; World Scientific: Singapore, 2010 (cit. on pp. 3, 7).

(12) Koch, N. *ChemPhysChem* **2007**, *8*, 1438–1455, DOI: 10.1002/cphc.200700177 (cit. on pp. 3, 8).

(13) Kroemer, H. *Rev. Mod. Phys.* **2001**, *73*, 783–793, DOI: 10.1103/RevModPhys.73.783 (cit. on p. 3).

(14) Love, J. C.; Estroff, L. A.; Kriebel, J. K.; Nuzzo, R. G.; Whitesides, G. M. *Chem. Rev.* **2005**, *105*, 1103–1170, DOI: 10.1021/cr0300789 (cit. on pp. 3, 12).

(15) Heimel, G.; Romaner, L.; Zojer, E.; Bredas, J.-L. *Acc. Chem. Res.* **2008**, *41*, 721–729, DOI: 10.1021/ar700284q (cit. on pp. 3, 8, 10).

(16) Tautz, F. *Prog. Surf. Sci.* **2007**, *82*, 479–520, DOI: 10.1016/j.progsurf.2007.09.001 (cit. on pp. 3, 8, 11, 132).

(17) Lang, N. D.; Kohn, W. *Phys. Rev. B* **1971**, *3*, 1215, DOI: 10.1103/PhysRevB.3.1215 (cit. on pp. 4–6).

(18) Cahen, D.; Kahn, A. *Adv. Mater.* **2003**, *15*, 271–277, DOI: 10.1002/adma.200390065 (cit. on pp. 5, 6).

(19) Ishii, H.; Sugiyama, K.; Ito, E.; Seki, K. *Adv. Mater.* **1999**, *11*, 605–625, DOI: 10.1002/(SICI)1521-4095(199906)11:8<605::AID-ADMA605>3.0.CO;2-Q (cit. on pp. 5, 6, 8, 9, 131).

(20) Hüfner, S., *Photoelectron Spectroscopy: Principles and Applications*; Springer: Berlin ; New York, 2003 (cit. on p. 5).

(21) Helander, M.; Greiner, M.; Wang, Z.; Lu, Z. *Appl. Surf. Sci.* **2010**, *256*, 2602–2605, DOI: 10.1016/j.apsusc.2009.11.002 (cit. on p. 6).

(22) Greiner, M. T.; Chai, L.; Helander, M. G.; Tang, W.-M.; Lu, Z.-H. *Adv. Func. Mater.* **2012**, *22*, 4557–4568, DOI: 10.1002/adfm.201200615 (cit. on p. 6).

(23) Campbell, I. H.; Rubin, S.; Zawodzinski, T. A.; Kress, J. D.; Martin, R. L.; Smith, D. L.; Barashkov, N. N.; Ferraris, J. P. *Phys. Rev. B* **1996**, *54*, R14321, DOI: 10.1103/PhysRevB.54.R14321 (cit. on pp. 6, 131).

(24) Boer, B. de; Hadipour, A.; Mandoc, M. M.; Woudenbergh, T. van; Blom, P. W. M. *Adv. Mater.* **2005**, *17*, 621–625, DOI: 10.1002/adma.200401216 (cit. on pp. 6, 131).

(25) Braun, S.; Salaneck, W. R.; Fahlman, M. *Adv. Mater.* **2009**, *21*, 1450–1472, DOI: 10.1002/adma.200802893 (cit. on pp. 6, 9, 11, 12).

(26) Xue, Y.; Datta, S.; Ratner, M. A. *J. Chem. Phys.* **2001**, *115*, 4292, DOI: 10.1063/1.1391253 (cit. on pp. 7, 130).

(27) Datta, S., *Quantum Transport: Atom to Transistor*; Cambridge University Press: Cambridge, UK ; New York, 2005 (cit. on pp. 7, 128).

(28) Kahn, A.; Koch, N. in: *The Molecule-Metal Interface*, Koch, N., Ueno, N., Wee, A. T. S., Eds.; Wiley-VCH Verlag GmbH & Co. KGaA: Weinheim, Germany, 2013 (cit. on p. 7).

(29) Damascelli, A.; Hussain, Z.; Shen, Z.-X. *Rev. Mod. Phys.* **2003**, *75*, 473, DOI: 10.1103/RevModPhys.75.473 (cit. on p. 7).

(30) Walter, M.; Häkkinen, H. *New J. Phys.* **2008**, *10*, 043018, DOI: 10.1088/1367-2630/10/4/043018 (cit. on p. 7).

(31) Kronik, L.; Kümmel, S. *Topics in Current Chemistry* **2013**, in press (cit. on pp. 7, 18, 20, 23, 24).

(32) Hwang, J.; Wan, A.; Kahn, A. *Mater. Sci. Eng. R* **2009**, *64*, 1–31, DOI: 10.1016/j.mser.2008.12.001 (cit. on p. 7).

(33) Kümmel, S.; Kronik, L. *Rev. Mod. Phys.* **2008**, *80*, 3–60, DOI: 10.1103/RevModPhys.80.3 (cit. on pp. 7, 16, 17, 20–24).

(34) Kronik, L.; Stein, T.; Refaely-Abramson, S.; Baer, R. *J. Chem. Theory Comput.* **2012**, *8*, 1515–1531, DOI: 10.1021/ct2009363 (cit. on pp. 7, 19, 22, 24, 25).

(35) Zharnikov, M. *J. Electron. Spectrosc. Relat. Phenom.* **2010**, *178-179*, 380–393, DOI: 10.1016/j.elspec.2009.05.008 (cit. on pp. 8, 12).

(36) Ballav, N.; Schüpbach, B.; Dethloff, O.; Feulner, P.; Terfort, A.; Zharnikov, M. *J. Am. Chem. Soc.* **2007**, *129*, 15416–15417, DOI: 10.1021/ja0751882 (cit. on p. 8).

(37) Heimel, G.; Rissner, F.; Zojer, E. *Adv. Mater.* **2010**, *22*, 2494–2513, DOI: 10.1002/adma.200903855 (cit. on pp. 8, 12–14).

(38) Koch, N. *Phys. Status Solidi - RRL* **2012**, *6*, 277–293, DOI: 10.1002/pssr.201206208 (cit. on pp. 8, 10, 11).

(39) Tung, R. T. *Mater. Sci. Eng. R* **2001**, *35*, 1–138, DOI: 10.1016/S0927-796X(01)00037-7 (cit. on pp. 8, 9).

(40) Narioka, S.; Ishii, H.; Yoshimura, D.; Sei, M.; Ouchi, Y.; Seki, K.; Hasegawa, S.; Miyazaki, T.; Harima, Y.; Yamashita, K. *Appl. Phys. Lett.* **1995**, *67*, 1899, DOI: 10.1063/1.114370 (cit. on pp. 9, 10).

(41) Ishii, H.; Seki, K. *IEEE Trans. Electron Dev.* **1997**, *44*, 1295–1301, DOI: 10.1109/16.605471 (cit. on pp. 9, 11).

(42) Hill, I. G.; Rajagopal, A.; Kahn, A.; Hu, Y. *Appl. Phys. Lett.* **1998**, *73*, 662, DOI: 10.1063/1.121940 (cit. on pp. 9, 11).

(43) Tkatchenko, A.; Romaner, L.; Hofmann, O. T.; Zojer, E.; Ambrosch-Draxl, C.; Scheffler, M. *MRS Bulletin* **2010**, *35*, 435–442, DOI: 10.1557/mrs2010.581 (cit. on pp. 9, 12, 133).

(44) Ruiz, V. G.; Liu, W.; Zojer, E.; Scheffler, M.; Tkatchenko, A. *Phys. Rev. Lett.* **2012**, *108*, 146103, DOI: 10.1103/PhysRevLett.108.146103 (cit. on pp. 10, 133).

(45) Tkatchenko, A.; Scheffler, M. *Phys. Rev. Lett.* **2009**, *102*, 073005, DOI: 10.1103/PhysRevLett.102.073005 (cit. on p. 10).

(46) Lifshits, E. M. *Sov. Phys. JETP* **1956**, *2*, 73 (cit. on p. 10).

(47) Zaremba, E.; Kohn, W. *Phys. Rev. B* **1976**, *13*, 2270, DOI: 10.1103/PhysRevB.13.2270 (cit. on p. 10).

(48) Stadtmüller, B.; Sueyoshi, T.; Kichin, G.; Kröger, I.; Soubatch, S.; Temirov, R.; Tautz, F. S.; Kumpf, C. *Phys. Rev. Lett.* **2012**, *108*, 106103, DOI: 10.1103/PhysRevLett.108.106103 (cit. on pp. 10, 133, 134).

(49) Mignolet, J. C. P. *Disc. Faraday Soc.* **1950**, *8*, 105, DOI: 10.1039/df9500800105 (cit. on p. 10).

(50) Mignolet, J. C. P. *J. Chem. Phys.* **1953**, *21*, 1298, DOI: 10.1063/1.1699190 (cit. on p. 10).

(51) Flynn, C.; Chen, Y. *Phys. Rev. Lett.* **1981**, *46*, 447–449, DOI: 10.1103/PhysRevLett.46.447 (cit. on p. 10).

(52) Chen, Y.; Cunningham, J.; Flynn, C. *Phys. Rev. B* **1984**, *30*, 7317–7319, DOI: 10.1103/PhysRevB.30.7317 (cit. on p. 10).

(53) Bagus, P.; Staemmler, V.; Wöll, C. *Phys. Rev. Lett.* **2002**, *89*, 096104, DOI: 10.1103/PhysRevLett.89.096104 (cit. on p. 10).

(54) Lang, N. D. *Phys. Rev. Lett.* **1981**, *46*, 842, DOI: 10.1103/PhysRevLett.46.842 (cit. on p. 10).

(55) Witte, G.; Lukas, S.; Bagus, P. S.; Wöll, C. *Appl. Phys. Lett.* **2005**, *87*, 263502, DOI: 10.1063/1.2151253 (cit. on p. 10).

(56) Hofmann, O. T.; Rangger, G. M.; Zojer, E. *J. Phys. Chem. C* **2008**, *112*, 20357–20365, DOI: 10.1021/jp806834g (cit. on p. 11).

(57) Heimel, G. et al. *Nat. Chem.* **2013**, *5*, 187–194, DOI: 10.1038/nchem.1572 (cit. on p. 11).

(58) Hauschild, A.; Karki, K.; Cowie, B.; Rohlfing, M.; Tautz, F.; Sokolowski, M. *Phys. Rev. Lett.* **2005**, *94*, 036106, DOI: 10.1103/PhysRevLett.94.036106 (cit. on p. 11).

(59) Rohlfing, M.; Temirov, R.; Tautz, F. *Phys. Rev. B* **2007**, *76*, 115421, DOI: 10.1103/PhysRevB.76.115421 (cit. on pp. 11, 133).

(60) Romaner, L; Nabok, D; Puschnig, P; Zojer, E; Ambrosch-Draxl, C *New J. Phys.* **2009**, *11*, 053010, DOI: 10.1088/1367-2630/11/5/053010 (cit. on pp. 11, 133).

(61) Hauschild, A.; Temirov, R.; Soubatch, S.; Bauer, O.; Schöll, A.; Cowie, B. C. C.; Lee, T.-L.; Tautz, F. S.; Sokolowski, M. *Phys. Rev. B* **2010**, *81*, 125432, DOI: 10.1103/PhysRevB.81.125432 (cit. on p. 11).

(62) Koch, N.; Duhm, S.; Rabe, J.; Vollmer, A.; Johnson, R. *Phys. Rev. Lett.* **2005**, *95*, 237601, DOI: 10.1103/PhysRevLett.95.237601 (cit. on p. 11).

(63) Romaner, L.; Heimel, G.; Brédas, J.-L.; Gerlach, A.; Schreiber, F.; Johnson, R.; Zegenhagen, J.; Duhm, S.; Koch, N.; Zojer, E. *Phys. Rev. Lett.* **2007**, *99*, 256801, DOI: 10.1103/PhysRevLett.99.256801 (cit. on p. 11).

(64) Fernandez-Torrente, I.; Monturet, S.; Franke, K.; Fraxedas, J.; Lorente, N.; Pascual, J. *Phys. Rev. Lett.* **2007**, *99*, 176103, DOI: 10.1103/PhysRevLett.99.176103 (cit. on p. 11).

(65) Bröker, B.; Blum, R.-P.; Frisch, J.; Vollmer, A.; Hofmann, O. T.; Rieger, R.; Müllen, K.; Rabe, J. P.; Zojer, E.; Koch, N. *Appl. Phys. Lett.* **2008**, *93*, 243303, DOI: 10.1063/1.3049616 (cit. on p. 11).

(66) Koch, N.; Gerlach, A.; Duhm, S.; Glowatzki, H.; Heimel, G.; Vollmer, A.; Sakamoto, Y.; Suzuki, T.; Zegenhagen, J.; Rabe, J. P.; Schreiber, F. *J. Am. Chem. Soc.* **2008**, *130*, 7300–7304, DOI: 10.1021/ja800286k (cit. on p. 11).

(67) Greiner, M. T.; Helander, M. G.; Tang, W.-M.; Wang, Z.-B.; Qiu, J.; Lu, Z.-H. *Nat. Mater.* **2011**, *11*, 76–81, DOI: 10.1038/nmat3159 (cit. on p. 11).

(68) Hill, I. G.; Milliron, D.; Schwartz, J.; Kahn, A. *Appl. Surf. Sci.* **2000**, *166*, 354–362, DOI: 10.1016/S0169-4332(00)00449-9 (cit. on p. 12).

(69) Ulman, A. *Chem. Rev.* **1996**, *96*, 1533–1554, DOI: 10.1021/cr9502357 (cit. on p. 12).

(70) Vilan, A.; Yaffe, O.; Biller, A.; Salomon, A.; Kahn, A.; Cahen, D. *Adv. Mater.* **2010**, *22*, 140–159, DOI: 10.1002/adma.200901834 (cit. on p. 12).

(71) Li, Y.; Calder, S.; Yaffe, O.; Cahen, D.; Haick, H.; Kronik, L.; Zuilhof, H. *Langmuir* **2012**, *28*, 9920–9929, DOI: 10.1021/la3010568 (cit. on p. 12).

(72) Vericat, C.; Vela, M. E.; Benitez, G.; Carro, P.; Salvarezza, R. C. *Chem. Soc. Rev.* **2010**, *39*, 1805, DOI: 10.1039/b907301a (cit. on p. 12).

(73) Heimel, G.; Romaner, L.; Brédas, J.-L.; Zojer, E. *Phys. Rev. Lett.* **2006**, *96*, 196806, DOI: 10.1103/PhysRevLett.96.196806 (cit. on pp. 12–14, 128).

(74) Schreiber, F. *Prog. Surf. Sci.* **2000**, *65*, 151–257, DOI: 10.1016/S0079-6816(00)00024-1 (cit. on p. 12).

(75) Häkkinen, H. *Nat. Chem.* **2012**, *4*, 443–455, DOI: 10.1038/nchem.1352 (cit. on p. 12).

(76) Woodruff, D. *Appl. Surf. Sci.* **2007**, *254*, 76–81, DOI: 10.1016/j.apsusc.2007.07.081 (cit. on p. 12).

(77) Pensa, E.; Cortés, E.; Corthey, G.; Carro, P.; Vericat, C.; Fonticelli, M. H.; Benítez, G.; Rubert, A. A.; Salvarezza, R. C. *Acc. Chem. Res.* **2012**, *45*, 1183–1192, DOI: 10.1021/ar200260p (cit. on p. 12).

(78) Heimel, G.; Romaner, L.; Zojer, E.; Brédas, J.-L. *Nano Lett.* **2007**, *7*, 932–940, DOI: 10.1021/nl0629106 (cit. on pp. 13, 14).

(79) Baheti, K.; Malen, J. A.; Doak, P.; Reddy, P.; Jang, S.-Y.; Tilley, T. D.; Majumdar, A.; Segalman, R. A. *Nano Lett.* **2008**, *8*, 715–719, DOI: 10.1021/nl0727381 (cit. on p. 13).

(80) Zangmeister, C. D.; Beebe, J. M.; Naciri, J.; Kushmerick, J. G.; Zee, R. D. van *Small* **2008**, *4*, 1143–1147, DOI: 10.1002/smll.200800359 (cit. on p. 13).

(81) Tan, A.; Balachandran, J.; Sadat, S.; Gavini, V.; Dunietz, B. D.; Jang, S.-Y.; Reddy, P. *J. Am. Chem. Soc.* **2011**, *133*, 8838–8841, DOI: 10.1021/ja202178k (cit. on p. 13).

(82) Vager, Z.; Naaman, R. *Chem. Phys.* **2002**, *281*, 305–309, DOI: 10.1016/S0301-0104(02)00374-9 (cit. on pp. 13, 14, 131).

(83) L'vov, V. S.; Naaman, R.; Tiberkevich, V.; Vager, Z. *Chem. Phys. Lett.* **2003**, *381*, 650–653, DOI: 10.1016/j.cplett.2003.09.158 (cit. on p. 13).

(84) Cahen, D.; Naaman, R.; Vager, Z. *Adv. Func. Mater.* **2005**, *15*, 1571–1578, DOI: 10.1002/adfm.200500187 (cit. on pp. 13, 14, 128).

(85) Natan, A.; Kronik, L.; Haick, H.; Tung, R. *Adv. Mater.* **2007**, *19*, 4103–4117, DOI: 10.1002/adma.200701681 (cit. on pp. 13, 14, 128, 131).

(86) Malicki, M.; Heimel, G.; Guan, Z.-L.; Ha, S. D.; Barlow, S.; Kahn, A.; Marder, S. R. *J. Phys. Chem. C* **2011**, *115*, 7487–7495, DOI: 10.1021/jp111900g (cit. on p. 14).

(87) Monti, O. L. A. *J. Phys. Chem. Lett.* **2012**, *3*, 2342–2351, DOI: 10.1021/jz300850x (cit. on p. 14).

(88) Fukagawa, H.; Yamane, H.; Kera, S.; Okudaira, K.; Ueno, N. *Phys. Rev. B* **2006**, *73*, 041302(R), DOI: 10.1103/PhysRevB.73.041302 (cit. on p. 14).

(89) Cornil, D.; Olivier, Y.; Geskin, V.; Cornil, J. *Adv. Func. Mater.* **2007**, *17*, 1143–1148, DOI: 10.1002/adfm.200601116 (cit. on p. 14).

(90) Romaner, L.; Heimel, G.; Ambrosch-Draxl, C.; Zojer, E. *Adv. Func. Mater.* **2008**, *18*, 3999–4006, DOI: 10.1002/adfm.200800876 (cit. on p. 14).

(91) Natan, A.; Kuritz, N.; Kronik, L. *Adv. Func. Mater.* **2010**, *20*, 2077–2084, DOI: 10.1002/adfm.200902162 (cit. on p. 14).

(92) Duhm, S.; Heimel, G.; Salzmann, I.; Glowatzki, H.; Johnson, R. L.; Vollmer, A.; Rabe, J. P.; Koch, N. *Nat. Mater.* **2008**, *7*, 326–332, DOI: 10.1038/nmat2119 (cit. on p. 15).

(93) Salzmann, I.; Duhm, S.; Heimel, G.; Oehzelt, M.; Kniprath, R.; Johnson, R. L.; Rabe, J. P.; Koch, N. *J. Am. Chem. Soc.* **2008**, *130*, 12870–12871, DOI: 10.1021/ja804793a (cit. on p. 15).

(94) Heimel, G.; Salzmann, I.; Duhm, S.; Koch, N. *Chem. Mater.* **2011**, *23*, 359–377, DOI: 10.1021/cm1021257 (cit. on p. 15).

(95) Mattuck, R. D., *A Guide to Feynman Diagrams in the Many-Body Problem*; McGraw-Hill: New York, 1976 (cit. on p. 16).

(96) Martin, R. M., *Electronic Structure: Basic Theory and Practical Methods*; Cambridge University Press: Cambridge, UK ; New York, 2008 (cit. on p. 16).

(97) Perdew, J.; Kurth, S. in: *A Primer in Density Functional Theory*, Fiolhais, C., Nogueira, F., Marques, M. A., Eds.; Springer: 2003 (cit. on pp. 16, 22).

(98) Jones, R. O.; Gunnarsson, O. *Rev. Mod. Phys.* **1989**, *61*, 689, DOI: 10.1103/RevModPhys.61.68 (cit. on pp. 16, 20, 21).

(99) Dreizler, R. M.; Gross, E. K. U., *Density Functional Theory: An Approach to the Quantum Many-Body Problem*; Springer-Verlag: Berlin ; New York, 1990 (cit. on p. 16).

(100) Kohn, W. *Rev. Mod. Phys.* **1999**, *71*, 1253–1266, DOI: 10.1103/RevModPhys.71.1253 (cit. on pp. 16, 21).

(101) Hohenberg, P.; Kohn, W. *Phys. Rev.* **1964**, *136*, B864, DOI: 10.1103/PhysRev.136.B864 (cit. on p. 17).

(102) Kohn, W.; Sham, L. J. *Phys. Rev.* **1965**, *140*, A1133–A1138, DOI: 10.1103/PhysRev.140.A1133 (cit. on pp. 17, 18).

(103) Stowasser, R.; Hoffmann, R. *J. Am. Chem. Soc.* **1999**, *121*, 3414–3420, DOI: 10.1021/ja9826892 (cit. on p. 18).

(104) Almbladh, C.-O.; Barth, U. von *Phys. Rev. B* **1985**, *31*, 3231–3244, DOI: 10.1103/PhysRevB.31.3231 (cit. on pp. 18, 24).

(105) Perdew, J. P.; Levy, M.; Balduz, J. L. *Phys. Rev. Lett.* **1982**, *49*, 1691–1694, DOI: 10.1103/PhysRevLett.49.1691 (cit. on pp. 18, 19).

(106) Mori-Sánchez, P.; Cohen, A. J.; Yang, W. *J. Chem. Phys.* **2006**, *125*, 201102, DOI: 10.1063/1.2403848 (cit. on p. 19).

(107) Mori-Sánchez, P.; Cohen, A.; Yang, W. *Phys. Rev. Lett.* **2008**, *100*, 146401, DOI: 10.1103/PhysRevLett.100.146401 (cit. on p. 19).

(108) Cohen, A. J.; Mori-Sanchez, P.; Yang, W. *Science* **2008**, *321*, 792–794, DOI: 10.1126/science.1158722 (cit. on p. 19).

(109) Cohen, A. J.; Mori-Sánchez, P.; Yang, W. *Chem. Rev.* **2012**, *112*, 289–320, DOI: 10.1021/cr200107z (cit. on p. 19).

(110) Perdew, J. P.; Levy, M. *Phys. Rev. B* **1997**, *56*, 16021, DOI: 10.1103/PhysRevB.56.16021 (cit. on p. 19).

(111) Stein, T.; Autschbach, J.; Govind, N.; Kronik, L.; Baer, R. *J. Phys. Chem. Lett.* **2012**, *3*, 3740–3744, DOI: 10.1021/jz3015937 (cit. on p. 19).

(112) Janak, J. *Phys. Rev. B* **1978**, *18*, 7165–7168, DOI: 10.1103/PhysRevB.18.7165 (cit. on p. 19).

(113) Perdew, J. P.; Levy, M. *Phys. Rev. Lett.* **1983**, *51*, 1884, DOI: 10.1103/PhysRevLett.51.1884 (cit. on p. 20).

(114) Sham, L.; Schlüter, M. *Phys. Rev. Lett.* **1983**, *51*, 1888–1891, DOI: 10.1103/PhysRevLett.51.1888 (cit. on p. 20).

(115) Chong, D. P.; Gritsenko, O. V.; Baerends, E. J. *J. Chem. Phys.* **2002**, *116*, 1760, DOI: 10.1063/1.1430255 (cit. on p. 21).

(116) Dori, N.; Menon, M.; Kilian, L.; Sokolowski, M.; Kronik, L.; Umbach, E. *Phys. Rev. B* **2006**, *73*, 195208, DOI: 10.1103/PhysRevB.73.195208 (cit. on pp. 22, 23).

(117) Perdew, J. *Chem. Phys. Lett.* **1979**, *64*, 127–130, DOI: 10.1016/0009-2614(79)87292-9 (cit. on p. 22).

(118) Perdew, J. P.; Zunger, A. *Phys. Rev. B* **1981**, *23*, 5048–5079, DOI: 10.1103/PhysRevB.23.5048 (cit. on p. 22).

(119) Körzdörfer, T.; Kümmel, S.; Marom, N.; Kronik, L. *Phys. Rev. B* **2009**, *79*, 201205(R), DOI: 10.1103/PhysRevB.79.201205 (cit. on pp. 23, 135).

(120) Marom, N.; Hod, O.; Scuseria, G. E.; Kronik, L. *J. Chem. Phys.* **2008**, *128*, 164107, DOI: 10.1063/1.2898540 (cit. on pp. 23, 135, 136).

(121) Marom, N.; Kronik, L. *Appl. Phys. A* **2008**, *95*, 159–163, DOI: 10.1007/s00339-008-5007-z (cit. on pp. 23, 135).

(122) Nogueira, F.; Castro, A.; Marques, M. A. in: *A Primer in Density Functional Theory*, Fiolhais, C., Nogueira, F., Marques, M. A., Eds.; Springer: 2003 (cit. on p. 23).

(123) Baer, R.; Livshits, E.; Salzner, U. *Ann. Rev. of Phys. Chem* **2010**, *61*, 85–109, DOI: 10.1146/annurev.physchem.012809.103321 (cit. on pp. 23, 24).

(124) Leininger, T.; Stoll, H.; Werner, H.-J.; Savin, A. *Chem. Phys. Lett.* **1997**, *275*, 151–160, DOI: 10.1016/S0009-2614(97)00758-6 (cit. on p. 24).

(125) Baer, R.; Neuhauser, D. *Phys. Rev. Lett.* **2005**, *94*, 043002, DOI: 10.1103/PhysRevLett.94.043002 (cit. on p. 24).

(126) Stein, T.; Eisenberg, H.; Kronik, L.; Baer, R. *Phys. Rev. Lett.* **2010**, *105*, 266802, DOI: 10.1103/PhysRevLett.105.266802 (cit. on pp. 24, 25).

(127) Refaely-Abramson, S.; Baer, R.; Kronik, L. *Phys. Rev. B* **2011**, *84*, 075144, DOI: 10.1103/PhysRevB.84.075144 (cit. on p. 24).

(128) Refaely-Abramson, S.; Sharifzadeh, S.; Govind, N.; Autschbach, J.; Neaton, J. B.; Baer, R.; Kronik, L. *Phys. Rev. Lett.* **2012**, *109*, 226405, DOI: 10.1103/PhysRevLett.109.226405 (cit. on pp. 24, 136).

(129) Seidl, A.; Görling, A.; Vogl, P.; Majewski, J. A.; Levy, M. *Phys. Rev. B* **1996**, *53*, 3764, DOI: 10.1103/PhysRevB.53.3764 (cit. on p. 24).

(130) Neaton, J.; Hybertsen, M.; Louie, S. *Phys. Rev. Lett.* **2006**, *97*, 216405, DOI: 10.1103/PhysRevLett.97.216405 (cit. on pp. 25, 135).

(131) Quek, S. Y.; Venkataraman, L.; Choi, H. J.; Louie, S. G.; Hybertsen, M. S.; Neaton, J. B. *Nano Lett.* **2007**, *7*, 3477–3482, DOI: 10.1021/nl072058i (cit. on pp. 25, 137).

(132) Egger, D. A.; Rissner, F.; Rangger, G. M.; Hofmann, O. T.; Wittwer, L.; Heimel, G.; Zojer, E. *Phys. Chem. Chem. Phys.* **2010**, *12*, 4291, DOI: 10.1039/b924238b (cit. on p. 128).

(133) Rissner, F.; Egger, D. A.; Natan, A.; Körzdörfer, T.; Kümmel, S.; Kronik, L.; Zojer, E. *J. Am. Chem. Soc.* **2011**, *133*, 18634–18645, DOI: 10.1021/ja203579c (cit. on pp. 128, 129, 136).

(134) Miller, D. A. B.; Chemla, D. S.; Damen, T. C.; Gossard, A. C.; Wiegmann, W.; Wood, T. H.; Burrus, C. A. *Phys. Rev. Lett.* **1984**, *53*, 2173 (cit. on p. 128).

(135) Rissner, F.; Natan, A.; Egger, D. A.; Hofmann, O. T.; Kronik, L.; Zojer, E. *Org. Elecr.* **2012**, *13*, 3165–3176, DOI: 10.1016/j.orgel.2012.09.003 (cit. on p. 128).

(136) Sancho, M. L.; Sancho, J. L.; Rubio, J. *J. Phys. F: Met. Phys.* **1985**, *15*, 851, DOI: 10.1088/0305-4608/15/4/009 (cit. on p. 128).

(137) Nardelli, M. B. *Phys. Rev. B* **1999**, *60*, 7828 (cit. on p. 128).

(138) Paulsson, M.; Datta, S. *Phys. Rev. B* **2003**, *67*, 241403(R), DOI: 10.1103/PhysRevB.67.241403 (cit. on p. 129).

(139) Chen, J.; Reed, M. A.; Rawlett, A. M.; Tour, J. M. *Science* **1999**, *286*, 1550–1552, DOI: 10.1126/science.286.5444.1550 (cit. on p. 130).

(140) Fan, F.-R. F.; Yao, Y.; Cai, L.; Cheng, L.; Tour, J. M.; Bard, A. J. *J. Am. Chem. Soc.* **2004**, *126*, 4035–4042, DOI: 10.1021/ja0359815 (cit. on p. 130).

(141) Selzer, Y.; Cai, L.; Cabassi, M. A.; Yao, Y.; Tour, J. M.; Mayer, T. S.; Allara, D. L. *Nano Lett.* **2005**, *5*, 61–65, DOI: 10.1021/nl048372j (cit. on p. 130).

(142) Reuter, M. G.; Seideman, T.; Ratner, M. A. *Nano Lett.* **2011**, *11*, 4693–4696, DOI: 10.1021/nl202342a (cit. on p. 130).

(143) Hofmann, O. T.; Egger, D. A.; Zojer, E. *Nano Lett.* **2010**, *10*, 4369–4374, DOI: 10.1021/nl101874k (cit. on p. 131).

(144) Natan, A.; Zidon, Y.; Shapira, Y.; Kronik, L. *Phys. Rev. B* **2006**, *73*, 193310, DOI: 10.1103/PhysRevB.73.193310 (cit. on p. 131).

(145) Albert, I. D.; Marks, T. J.; Ratner, M. A. *J. Am. Chem. Soc.* **1997**, *119*, 3155–3156, DOI: 10.1021/ja964389v (cit. on p. 131).

(146) Kang, H.; Facchetti, A.; Zhu, P.; Jiang, H.; Yang, Y.; Cariati, E.; Righetto, S.; Ugo, R.; Zuccaccia, C.; Macchioni, A.; Stern, C. L.; Liu, Z.; Ho, S.-T.; Marks, T. J. *Angew. Chem. Int. Ed.* **2005**, *44*, 7922–7925, DOI: 10.1002/anie.200501581 (cit. on p. 131).

(147) Kraft, A.; Temirov, R.; Henze, S.; Soubatch, S.; Rohlfing, M.; Tautz, F. *Phys. Rev. B* **2006**, *74*, 041402(R), DOI: 10.1103/PhysRevB.74.041402 (cit. on pp. 132, 135).

(148) Picozzi, S.; Pecchia, A.; Gheorghe, M.; Di Carlo, A.; Lugli, P.; Delley, B.; Elstner, M. *Phys. Rev. B* **2003**, *68*, 195309, DOI: 10.1103/PhysRevB.68.195309 (cit. on p. 133).

(149) Perdew, J. P.; Burke, K.; Ernzerhof, M. *Phys. Rev. Lett.* **1996**, *77*, 3865 (cit. on p. 133).

(150) Wagner, C.; Fournier, N.; Tautz, F. S.; Temirov, R. *Phys. Rev. Lett.* **2012**, *109*, 076102, DOI: 10.1103/PhysRevLett.109.076102 (cit. on p. 133).

(151) Aradhya, S. V.; Frei, M.; Hybertsen, M. S.; Venkataraman, L. *Nat. Mater.* **2012**, *11*, 872–876, DOI: 10.1038/nmat3403 (cit. on p. 133).

(152) Nerngchamnong, N.; Yuan, L.; Qi, D.-C.; Li, J.; Thompson, D.; Nijhuis, C. A. *Nat. Nanotechnol.* **2013**, *8*, 113–118, DOI: 10.1038/nnano.2012.238 (cit. on p. 133).

(153) Sato, N.; Seki, K.; Inokuchi, H. *J. Chem. Soc., Faraday Trans. 2* **1981**, *77*, 1621, DOI: 10.1039/f29817701621 (cit. on p. 135).

(154) Sharifzadeh, S.; Biller, A.; Kronik, L.; Neaton, J. B. *Phys. Rev. B* **2012**, *85*, 125307, DOI: 10.1103/PhysRevB.85.125307 (cit. on p. 135).

(155) Refaely-Abramson, S.; Sharifzadeh, S.; Jain, M.; Baer, R.; Neaton, J. B.; Kronik, L. *Phys. Rev. B* **2013**, *88*, 081204(R), DOI: 10.1103/PhysRevB.88.081204 (cit. on p. 135).

(156) Garcia-Lastra, J. M.; Rostgaard, C.; Rubio, A.; Thygesen, K. S. *Phys. Rev. B* **2009**, *80*, 245427, DOI: 10.1103/PhysRevB.80.245427 (cit. on p. 135).

(157) Biller, A.; Tamblyn, I.; Neaton, J. B.; Kronik, L. *J. Chem. Phys.* **2011**, *135*, 164706, DOI: 10.1063/1.3655357 (cit. on p. 135).

(158) Liu, S.-Y.; Alnama, K.; Matsumoto, J.; Nishizawa, K.; Kohguchi, H.; Lee, Y.-P.; Suzuki, T. *J. Phys. Chem. A* **2011**, *115*, 2953–2965, DOI: 10.1021/jp1098574 (cit. on p. 136).

(159) Potts, A. W.; Holland, D. M. P.; Trofimov, A. B.; Schirmer, J.; Karlsson, L.; Siegbahn, K. *J. Phys. B: At. Mol. Opt. Phys.* **2003**, *36*, 3129, DOI: 10.1088/0953-4075/36/14/314 (cit. on p. 136).

(160) Kishimoto, N.; Ohno, K. *J. Phys. Chem. A* **2000**, *104*, 6940–6950, DOI: 10.1021/jp0009731 (cit. on p. 136).

(161) Tamblyn, I.; Darancet, P.; Quek, S. Y.; Bonev, S. A.; Neaton, J. B. *Phys. Rev. B* **2011**, *84*, 201402(R), DOI: 10.1103/PhysRevB.84.201402 (cit. on p. 136).

(162) Sharifzadeh, S.; Tamblyn, I.; Doak, P.; Darancet, P. T.; Neaton, J. B. *Eur. Phys. J. B* **2012**, *85*, 323, DOI: 10.1140/epjb/e2012-30206-0 (cit. on p. 136).